JAERI-Research
95-010

CONSISTENT CALCULATIONS OF FAST NEUTRON INDUCED FISSION, (n,2n) and (n,3n) CROSS-SECTIONS FOR 71 ISOTOPES OF Th, Pa, U, Np, Pu, Am, Cm, Bk and Cf

February 1995

Valentin A. KONSHIN*

日本原子力研究所
Japan Atomic Energy Research Institute

本レポートは，日本原子力研究所が不定期に公刊している研究報告書です。
入手の問合わせは，日本原子力研究所技術情報部情報資料課（〒319-11 茨城県那珂郡東海村）あて，お申し越しください。なお，このほかに財団法人原子力弘済会資料センター（〒319-11 茨城県那珂郡東海村日本原子力研究所内）で複写による実費頒布をおこなっております。

This report is issued irregularly.
Inquiries about availability of the reports should be addressed to Information Division, Department of Technical Information, Japan Atomic Energy Research Institute, Tokai-mura, Naka-gun, Ibaraki-ken 319-11, Japan.

© Japan Atomic Energy Research Institute, 1995

編集兼発行　日本原子力研究所
印　　刷　㈱原子力資料サービス

Consistent Calculations of Fast Neutron Induced Fission, (n,2n) and (n,3n) Cross-sections for 71 Isotopes of Th, Pa, U, Np, Pu, Am, Cm, Bk and Cf

Valentin A. KONSHIN*

Department of Reactor Engineering
Tokai Research Establishment
Japan Atomic Energy Research Institute
Tokai-mura, Naka-gun, Ibaraki-ken

(Received January 26, 1995)

The neutron cross-sections for fission, (n,2n) and (n,3n) reactions have been calculated consistently for $^{227-234}$Th, $^{229-233}$Pa, $^{230-240}$U, $^{235-239}$Np, $^{236-247}$Pu, $^{239-245}$Am, $^{238-251}$Cm, $^{245-249}$Bk and $^{249-252}$Cf using the Hauser－Feshbach statistical model code STAPRE. The main parameter of the pre-equilibrium exciton model was tested against the experimental data for the secondary neutron spectra for ^{238}U. Shell, superfluid and collective effects in nuclear level density have been taken into account. Neutron transmission coefficients were calculated using the coupled-channel code ECIS. All experimental data available for fission and (n,2n) reactions for the above isotopes have been used for model testing. Due to a lack of experimental data for the majority of the nuclei considered theoretical prediction of neutron cross-sections has been made.

Keywords: Fission Cross Section, (n,2n) , (n,3n) Cross Sections, Fission Barriers, Fast Neutron Energy Region, Actinides, Transactinides, Calculations.

---

* Research Fellow

Th, Pa, U, Np, Pu, Am, Cm, Bk及びCfの同位体71核種に対する高速中性子入射による核分裂断面積と（n,2n）及び（n,3n）反応断面積の統一的計算

日本原子力研究所東海研究所原子炉工学部
Valentin A. KONSHIN*

（1995年1月26日受理）

Hauser-Feshbach統計模型に基づくSTAPREコードを用いて，$^{227\sim234}$Th，$^{229\sim233}$Pa，$^{230\sim240}$U，$^{235\sim239}$Np，$^{236\sim247}$Pu，$^{239\sim245}$Am，$^{238\sim251}$Cm，$^{245\sim249}$Bk及び$^{249\sim252}$Cfの核分裂断面積，（n,2n）及び（n,3n）反応断面積の計算を統一的に行った。前平衡励起子モデルの主なパラメータは，^{238}Uの非弾性散乱中性子スペクトルの実験データで検証された。レベル密度には，殻効果，超流動効果及び集団運動効果を考慮した。中性子透過係数は，チャンネル結合理論に基づくECISコードで計算した。上記核種のうち核分裂断面積と（n,2n）反応断面積の実験データがあるものはそれを計算モデルの検証に使用した。今回考慮した核種のほとんどは実験データが無いために，理論計算を行った。

東海研究所：〒319－11　茨城県那珂郡東海村白方字白根2－4
＊　リサーチフェロー

Contents

目　　次

1. Introduction

In order to evaluate the accumulation of transactinides in spent fuel and for handling of nuclear waste, it is necessary to have a fairly accurate nuclear data base. Of particular importance are the cross-sections for the fission and (n,xn) reactions.

The present paper describes the results of the first phase of the work on the actinide nuclear data generation for transmutation purposes and covers the energy region of the incoming neutrons from 1 to 20 MeV. The second part of the work will be devoted to the energy region from 10 MeV to 1 GeV.

For the majority of transactinides the experimental data base available is not sufficient for practical applications. There are only 3 nuclei for which experimental data are available for fission, (n,2n) and (n,3n) reaction cross-sections – ^{232}Th, ^{238}U and ^{235}U, and 2 nuclei with fission and (n,2n) experimental data – ^{239}Pu and ^{237}Np. These nuclei provide a possibility for a consistent analysis of the fission process and neutron emission.

For a second group of nuclei consisting of 14 nuclei – ^{231}Pa, ^{233}U, ^{234}U, ^{236}U, ^{238}Pu, ^{240}Pu, ^{241}Pu, ^{242}Pu, ^{244}Pu, ^{241}Am, ^{242m}Am, ^{243}Am, ^{245}Cm and ^{249}Cf – extensive measurements of fission cross-sections exist which can be used for a consistent analysis of the energy dependence of fission cross-sections for different isotopes. In this case fission cross-sections provide a constraint for (n,2n) reaction cross-section calculations.

The third group of nuclei considered here consisting of 52 isotopes for Th, Pa, U, Np, Pu, Am, Cm, Bk and Cf has practically no experimental data and the theoretical model was needed for the prediction of necessary data.

The extensive calculations of fission, (n,2n) and (n,3n) reaction cross-sections for 71 transactinide isotopes from Th to Cf were done in the present work. A consistent analysis of all relevant experimental data in the International Database EXFOR was made and the theoretical prediction of neutron cross-sections for nuclei with no experimental data available was completed.

2. Model and Parameters Used

In the present work the statistical model code STAPRE[1] taking into account conservation of spin and parity for all nuclear reaction cascades was used for the calculation of the fission and (n,xn)-reaction cross-sections. The statistical model had been extensively used for a consistent analysis of the fission and (n,2n)-reaction cross-sections for isotopes of U, Pu, Am and Cm[2]. The approach used by Ignatyuk et al[2],[3] was taken in the present work.

There are three major factors which should be considered carefully in any statistical model, namely, neutron transmission coefficients, preequilibrium model parameters and level density parameters. This is particularly true for calculations of the fission cross-sections.

1. Introduction

In order to evaluate the accumulation of transactinides in spent fuel and for handling of nuclear waste, it is necessary to have a fairly accurate nuclear data base. Of particular importance are the cross-sections for the fission and (n,xn) reactions.

The present paper describes the results of the first phase of the work on the actinide nuclear data generation for transmutation purposes and covers the energy region of the incoming neutrons from 1 to 20 MeV. The second part of the work will be devoted to the energy region from 10 MeV to 1 GeV.

For the majority of transactinides the experimental data base available is not sufficient for practical applications. There are only 3 nuclei for which experimental data are available for fission, (n,2n) and (n,3n) reaction cross-sections – ^{232}Th, ^{238}U and ^{235}U, and 2 nuclei with fission and (n,2n) experimental data – ^{239}Pu and ^{237}Np. These nuclei provide a possibility for a consistent analysis of the fission process and neutron emission.

For a second group of nuclei consisting of 14 nuclei – ^{231}Pa, ^{233}U, ^{234}U, ^{236}U, ^{238}Pu, ^{240}Pu, ^{241}Pu, ^{242}Pu, ^{244}Pu, ^{241}Am, ^{242m}Am, ^{243}Am, ^{245}Cm and ^{249}Cf – extensive measurements of fission cross-sections exist which can be used for a consistent analysis of the energy dependence of fission cross-sections for different isotopes. In this case fission cross-sections provide a constraint for (n,2n) reaction cross-section calculations.

The third group of nuclei considered here consisting of 52 isotopes for Th, Pa, U, Np, Pu, Am, Cm, Bk and Cf has practically no experimental data and the theoretical model was needed for the prediction of necessary data.

The extensive calculations of fission, (n,2n) and (n,3n) reaction cross-sections for 71 transactinide isotopes from Th to Cf were done in the present work. A consistent analysis of all relevant experimental data in the International Database EXFOR was made and the theoretical prediction of neutron cross-sections for nuclei with no experimental data available was completed.

2. Model and Parameters Used

In the present work the statistical model code STAPRE[1] taking into account conservation of spin and parity for all nuclear reaction cascades was used for the calculation of the fission and (n,xn)-reaction cross-sections. The statistical model had been extensively used for a consistent analysis of the fission and (n,2n)-reaction cross-sections for isotopes of U, Pu, Am and Cm[2]. The approach used by Ignatyuk et al[2],[3] was taken in the present work.

There are three major factors which should be considered carefully in any statistical model, namely, neutron transmission coefficients, preequilibrium model parameters and level density parameters. This is particularly true for calculations of the fission cross-sections.

In the present work neutron transmission coefficients were calculated using the coupled-channel code ECIS[4] with the potential parameters obtained by Haouat et al[5] (Table 1). As the highest neutron energy in the present analysis is limited to 20 MeV, only a surface absorption term of the imaginary potential was taken into account. The potential parameters [5] reproduce the experimental data for the total cross-section of ^{238}U quite well in the energy region up to 18 MeV, but above 20 MeV they give too high values of the total cross-section[6]. The use of correct neutron transmission coefficients plays an essential role in the transactinide data analysis, as it is well known that the use of deformed optical model neutron transmission coefficients leads to decrease of the compound nucleus formation cross-section by 7-15% compared to the traditional spherical optical model.

The second important factor of the model used is the main parameter of the exciton model, the matrix element $M^2 = 10/A^3$ MeV^2 that was fixed by fitting the experimental data by Kornilov et al[7] for the neutron secondary spectra for ^{238}U at 6-14.3 MeV, as was done by Ignatyuk et al[3].

For the calculation of the level density for residual and fissioning nuclei a generalized superfluid phenomenological model proposed by Ignatyuk et al[8] was used in the present work. This model takes into account pairing correlations, odd-even, collective and shell effects, in contrast to the traditional Fermi-gas model. Recent testing of the Fermi-gas and generalized superfluid models based on the analysis of the experimental data on neutron resonance density, evaporation neutron spectra and nuclear fissility made by Rastopchin et al[9] showed that the Fermi-gas model was too inaccurate at low excitation energies and the standard version of this model was in contradiction to the experimental information on the asymptotic parameter $\tilde{a}(A)$. These shortcomings of the Fermi-gas model are eliminated in the superfluid model and the most favorable nuclei to be dealt within the framework of the superfluid model are those with $A \geq 220$ and also with $A \leq 60$, $A \approx 90$. As a result of the analysis done by Rastopchin et al[9] it was concluded that the transactinide nuclei were the ideal object for application of the superfluid nuclear level density model.

According to the superfluid model[8],

$$\rho(U,J,\pi) = \rho_{qp}(U,J,\pi)K_{rot}(U,J)K_{vib}(U),$$

where $\rho_{qp}(U,J,\pi)$ is the quasi-particle level density at the excitation energy U, and $K_{rot}(U,J)$ and $K_{vib}(U)$ factors of rotational and vibrational enhancement of level density. For axially symmetric equilibrium deformations $K_{rot} \cong \sigma_\perp^2$; for saddle deformations, at the inner saddle $K_{rot}(U,J) \cong 2\sqrt{2\pi}\sigma_\perp^2\sigma_\parallel$, and at the outer saddle $K_{rot}(U) \cong 2\sigma_\perp^2$[2], where $\sigma_\perp$ and $\sigma_\parallel$ are spin dispersion parameters.

The factor of vibrational enhancement of level density $K_{vib}(U)$ can be calculated using a liquid-drop model: $K_{vib}(U) \cong \exp U^{2/3}$[8]. For actinides, at equilibrium deformations, $K_{rot} \cong 10$-

100 and $K_{vib} \cong 2$.

One of the basic parameters of the superfluid model is the pairing correlation function Δ_0, which is directly related to the critical temperature t_{cr} of the phase transition from the superconducting to the normal state by $t_{cr}=0.567\Delta_0$. Above the temperature t_{cr} the energy dependence of the level density differs from the Fermi-gas model only by a shift of the excitation energy denoted E_{cond}. Below t_{cr} this energy dependence changes and becomes similar to that of the constant temperature model.

The level density parameter is given by

$$a(U,Z,A) = \begin{cases} \tilde{a}(A)\left\{1+\delta W(Z,A)\,\dfrac{f(U-E_{cond})}{(U-E_{cond})}\right\} & \text{for } U \geq U_{cr}\ , \\ a_{cr} & \text{for } U < U_{cr}\ , \text{ where } a_{cr} \text{ is the a-value at } t = t_{cr}\ . \end{cases}$$

Here $\tilde{a}(A)$ is the asymptotic value of the level density parameter at high excitation energy, and the function f(U) determines the energy behavior of the a-parameter at lower energies:

$$\begin{aligned} f(U) &= 1 - \exp(-\gamma U), \text{ where } \gamma = 0.40A^{-1/3}, \\ E_{cond} &= 0.152\, a_{cr}\Delta_0^2 - n\Delta_0, \\ U_{cr} &= 0.472\, a_{cr}\Delta_0^2 - n\Delta_0, \end{aligned}$$

where n=0,1,2 for even-even, odd-A, odd-odd nuclei, respectively,

$$\begin{aligned} \Delta_0 &= 12/\sqrt{A}, \\ \tilde{a}(A) &= 0.073A + 0.115A^{2/3}\ . \end{aligned}$$

It should be noted that the generalized superfluid model is formulated for even-even nuclei, that is quite opposite to the Fermi-gas model, where the initial equations are related to odd-odd nuclei.

In the actinide region the above superfluid model underestimates the level density at low energies. This shortcoming was observed at the comparison of the calculated and experimental data for low-lying level densities for equilibrium-shape nuclei[10],[11].

Therefore the level density of low-lying levels was modelled by a constant temperature dependence, in the Gilbert-Cameron approach, with T_n=0.385 MeV[11] for excitation energies below $U_c=10.7-0.028A-n\Delta_0$, where n=0, 1, 2 for even-even, odd-A and odd-odd nuclei, respectively.

Nuclear level density parameters for nuclei where experimental data are available are given in Table 2.

For the fission channel the temperature value T_f was determined by

$$T_f = \left\{ \frac{d}{dU} \ln \rho_f(U)_{U=Uc} \right\}^{-1} ,$$

where $\rho_f(U)$ was expressed by the equation

$$\rho_f(U) = \frac{\sigma_{\perp f}^2 \ \rho_f^{in}(U)}{\sqrt{2\pi} \ \sigma_{\parallel f}}$$

with $\rho_f^{in}(U)$ is density of intrinsic and noncollective levels.

The above equation leads to

$$\frac{1}{T_f} \exp\left(\frac{U_c - E_0}{T_f} \right) = \frac{K_{rot} \ K_{vib} \ \rho_f^{in}(U)}{\sqrt{2\pi} \ \sigma_{\parallel f}} ,$$

where $E_0=-n\Delta_f$, Δ_f the correlation function for saddle-point deformations: $\Delta_f=14/\sqrt{A}$ and $\sigma_\parallel$ and $\sigma_\perp$ are spin dispersion parameters.

It is essential that the level densities of the fissioning nucleus at saddle deformations and of the relevant residual nucleus at equilibrium deformations were calculated by introducing the odd-even excitation energy shift: $U^*=U+\Delta_f$. The former governs the fission cross-section and the latter governs the (n,2n) cross-section.

For the fission channel it is essential in description of transition level densities to take into account axial and mirror asymmetry of saddle configurations of the fissile nucleus on the internal hump A and mirror asymmetry of configurations on the external hump B. For the internal hump with axial and mirror asymmetry the level density is increased by a factor $2\sqrt{2\pi}\sigma_\parallel$, and for the external hump with the mirror asymmetry by a factor 2, where $\sigma_\parallel$ is the spin dispersion parameter related to the moments of inertia for transition states of the fissile nucleus[8].

Shell corrections $\delta W_{n(f)}(Z,A)$ are calculated taking into account quadrupole deformations ε[12]: $\delta W_{n(f)}(Z,A,\varepsilon)=M_{exp}(Z,A)-\tilde{M}(Z,A,\varepsilon)$, where $\tilde{M}(Z,A,\varepsilon)$ is liquid drop mass for a respective value of ε. Shell corrections δW_f^A and δW_f^B for the saddle points are defined relative to the liquid drop component of the fission barrier[13] and for all isotopes considered, except for Th and Pa isotopes, were taken to be δW_f^A=2.5 MeV and δW_f^B=0.6 MeV[14], and δW_n was calculated using the liquid drop model[12]. Uncertainties in theoretical calculations of shell corrections may be about 1 MeV, but they do not have an essential impact on

calculated fission cross-section values.

The fission barrier parameters E_f^A and E_f^B were obtained by analyzing the experimental data for fission cross sections within the framework of the level density model used. For those nuclei, whose experimental data are not virtually available, the systematics proposed by Kuprijanov et al[15] and Smirenkin[16] for the first plateau region, as well as indirect experimental data, were used. This systematics was also used, with certain caution, to extrapolate $E_f^A(Z,A)$ and $E_f^B(Z,A)$ within small limits, beyond the experimentally investigated region of nuclei, and the accuracy of the fission cross-sections calculated in this case may be not higher than 20 – 30 %.

3. Comparison of theoretical and experimental data

3.1 Neutron Cross-Sections

In Figs. 1-213 calculated and experimental data, for σ_f, $\sigma_{n,2n}$ and $\sigma_{n,3n}$ for Th, Pa, U, Np, Pu, Am, Cm, Bk and Cf isotopes are given. The validity of the model used can be demonstrated by a consistent description of all the experimental data on the fission and (n,2n) cross-sections. The parameter systematics adopted makes it possible to describe satisfactorily the neutron and fission channels of nuclear decay and enables the (n,2n) reaction cross-sections to be predicted rather reliably.

$^{227-234}$Th: The triple-humped barrier conception should be used for analysis of neutron data for Th-isotopes, but as we are interested in high energies, a double-humped fission barrier model was used. Some experimental data for the fission, (n,2n) and (n,3n) reaction cross-sections of ^{232}Th and for the fission cross-section of ^{230}Th are available. The same model parameters, as mentioned earlier, was used for the analysis of Th data, except for the shell corrections δW_f^A and δW_f^B. The experimental data were fitted with δW_f^A=2.5 MeV and δW_f^B=0.1 MeV, and δW_n was taken from liquid drop model calculations. The calculated curve for the ^{232}Th (n,2n) reaction cross-section is lying rather high and in agreement with the old data by Butler and Santry[19] in the energy region up to 10 MeV (Fig.17). The experimental data by Raics et al[20] which are not compiled in the EXFOR Data Library fully confirm the present calculations in the entire energy region.

$^{229-233}$Pa: The analysis of neutron data for these isotopes was made with the same approach as for Th isotopes. The only experimental data available, the fission cross-section for ^{231}Pa, were described satisfactorily within the framework of the model used (Fig.31). It should be noted that the calculated fission cross-section values for Pa isotopes practically do not depend on the first barrier height E_f^A. Actually it was confirmed that E_f^A is much lower E_f^B in this case. Due to a complete lack of experimental data for the (n,2n) and (n,3n) reaction cross-sections they were theoretically predicted (Figs.26-39).

$^{230-240}$U: The calculated values agree rather well with experimental data for the fission cross section of $^{232-236}$U, ^{238}U, and for the (n,2n) and (n,3n) reaction cross-sections of ^{235}U and

calculated fission cross−section values.

The fission barrier parameters E_f^A and E_f^B were obtained by analyzing the experimental data for fission cross sections within the framework of the level density model used. For those nuclei, whose experimental data are not virtually available, the systematics proposed by Kuprijanov et al[15] and Smirenkin[16] for the first plateau region, as well as indirect experimental data, were used. This systematics was also used, with certain caution, to extrapolate $E_f^A(Z,A)$ and $E_f^B(Z,A)$ within small limits, beyond the experimentally investigated region of nuclei, and the accuracy of the fission cross−sections calculated in this case may be not higher than 20 − 30 %.

3. Comparison of theoretical and experimental data

3.1 Neutron Cross−Sections

In Figs. 1−213 calculated and experimental data, for σ_f, $\sigma_{n,2n}$ and $\sigma_{n,3n}$ for Th, Pa, U, Np, Pu, Am, Cm, Bk and Cf isotopes are given. The validity of the model used can be demonstrated by a consistent description of all the experimental data on the fission and (n,2n) cross−sections. The parameter systematics adopted makes it possible to describe satisfactorily the neutron and fission channels of nuclear decay and enables the (n,2n) reaction cross−sections to be predicted rather reliably.

$^{227-234}$Th: The triple−humped barrier conception should be used for analysis of neutron data for Th−isotopes, but as we are interested in high energies, a double−humped fission barrier model was used. Some experimental data for the fission, (n,2n) and (n,3n) reaction cross−sections of ^{232}Th and for the fission cross−section of ^{230}Th are available. The same model parameters, as mentioned earlier, was used for the analysis of Th data, except for the shell corrections δW_f^A and δW_f^B. The experimental data were fitted with δW_f^A=2.5 MeV and δW_f^B=0.1 MeV, and δW_n was taken from liquid drop model calculations. The calculated curve for the ^{232}Th (n,2n) reaction cross−section is lying rather high and in agreement with the old data by Butler and Santry[19] in the energy region up to 10 MeV (Fig.17). The experimental data by Raics et al[20] which are not compiled in the EXFOR Data Library fully confirm the present calculations in the entire energy region.

$^{229-233}$Pa: The analysis of neutron data for these isotopes was made with the same approach as for Th isotopes. The only experimental data available, the fission cross−section for ^{231}Pa, were described satisfactorily within the framework of the model used (Fig.31). It should be noted that the calculated fission cross−section values for Pa isotopes practically do not depend on the first barrier height E_f^A. Actually it was confirmed that E_f^A is much lower E_f^B in this case. Due to a complete lack of experimental data for the (n,2n) and (n,3n) reaction cross−sections they were theoretically predicted (Figs.26−39).

$^{230-240}$U: The calculated values agree rather well with experimental data for the fission cross section of $^{232-236}$U, ^{238}U, and for the (n,2n) and (n,3n) reaction cross−sections of ^{235}U and

and ^{238}U. For the (n,2n) cross section of ^{238}U the calculated values are in agreement with the data on the upper boundary of the scatter among experimental data confirming the data of Kornilov et al[17] and lying above the data of Frehaut et al[18] by 15% (Fig.65). For other U isotopes from ^{230}U to ^{240}U theoretical prediction of the (n,2n) and (n,3n) reaction cross−sections was made.

$^{235-239}$Np: Only experimental data available are those for the fission and (n,2n) reaction cross−sections for ^{237}Np (Figs.79,80). The experimental data for the fission cross−section are in disagreement with each other in particular for the relative data of Pankratov[21], and for the (n,2n) cross section there is no experimental data in the energy region 10−13 MeV. The renormalization of relative measurements by Pankratov[21] did not lead to a better agreement between experimental data. The theoretical curve for the fission cross section of ^{237}Np is lower than the data of Pankratov[21] and agrees in general with the data of Meadows[22] (Fig.79). This leads to the (n,2n) cross−section value of 0.44b at 12 MeV.

For other Np−isotopes theoretical calculations of the (n,2n) cross−sections show their increase with A increasing (Fig.74,77,83,86). Reliability of their prediction, in particular for ^{235}Np, ^{236}Np, ^{239}Np with no experimental data for the fission cross−sections, is lower than for ^{237}Np.

$^{236-247}$Pu: Experimental data for the fission cross−sections of ^{236}Pu, ^{238}Pu, ^{239}Pu, ^{240}Pu, ^{241}Pu, ^{242}Pu and ^{244}Pu can be described consistently within the framework of the model used. For ^{238}Pu the calculated curve for the fission cross−section in the region of the second plateau is lying a little lower than the data of Budtz−Yoergensen et al[23] and for ^{239}Pu the theoretical curve is in agreement with the data of Meadows[22], being higher than the data of Kari and Cierjacks[24] (Figs.94,97). For ^{240}Pu the calculated curve agrees with the data of Kari et al[24] and Meadows[25] (Fig.100), for ^{241}Pu with the data of Behrens et al[26](Fig.103), for ^{242}Pu (Fig.106) and ^{244}Pu(Fig.112) with the data of Behrens et al[27]. Measurements done relative to the fission cross section of ^{235}U were normalized using the JENDL−3 $\sigma_f(^{235}U)$−values.

The calculated fission cross−section for ^{239}Pu provides a constraint for the (n,2n) reaction cross−section. The calculated (n,2n) reaction cross−section values are in general agreement with experimental data[28], although near the threshold energy region (about 7 MeV) the calculated values are higher than experimental data (Fig.98). There appears to be a step−like behaviour of the (n,2n) cross−section, which can be attributed to excitation of two−quasi−particle states in the residual ^{238}Pu nucleus, as pointed out by Maslov[29].

Unfortunately, there is no experimental data for the (n,2n) cross−sections for nuclei heavier than ^{239}Pu for which similar behavior could be more pronounced, in particular for even−odd target nuclei (even−even residual nuclei).

The detailed structure of (n,2n) cross sections can not be interpreted within the framework of the present rather crude model and for this purpose the real shell structure of single−particle states should be incorporated into the model.

$^{239-245}$Am: Experimental data for the fission cross−sections of ^{241}Am by Dabbs et al[31],

^{242m}Am by Browne et al[32] and ^{243}Am by Knitter et al[33] were analyzed consistently (Figs.130,133,136). Theoretically predicted (n,2n) reaction cross-sections for Am isotopes increase with A increasing from 0.03b for ^{239}Am to 0.9b for ^{245}Am at 13 MeV.

$^{238-251}$Cm: Experimental data for the fission cross-sections of Cm isotopes are available only for the first plateau region, except for ^{245}Cm. The data were analyzed and fission barrier height values were obtained. For ^{245}Cm the experimental point at 14 MeV by White[34] is higher than the calculated curve by 8%, although his experimental data at the other energy points are in good agreement with the present calculations (Fig.166).

The results of the calculations by Ignatyuk et al[2] may look too low for the ^{245}Cm fission cross-section above 8 MeV (Fig.166) and subsequently too high for the (n,2n) reaction cross-section. In order to verify the STAPRE results, extensive calculations were made in the energy region from 5 to 100 MeV using the GNASH code[40]. The results of these calculations will be discussed in a further report, but one can mention here that the GNASH calculations agree fairly well with the present STAPRE calculations of the fission cross-sections (Figs.94,97,130,133,157,160,163,166,169,172), somewhat lower for the (n,2n) cross-sections (Figs.95,98,134,158,161,164,167,170,173) and generally higher for (n,3n) cross-sections (Figs.96,99,135,159,162,165,168,171,174).

For odd Cm isotope targets (even-even residual nuclei) some irregularities in the (n,2n) reaction cross-sections can be seen in the energy region 7-8 MeV (Figs.167,179), as well as for odd Pu-isotopes (Figs.104,110,116,122) and even Am-isotopes (Figs.128,134,140). Complete lack of experimental data does not allow to verify whether the effect is real or may be due to residual nuclei level density modeling used.

$^{245-249}$Bk and $^{249-252}$Cf: Experimental data on the fission cross-sections exist only for ^{249}Bk and ^{249}Cf and therefore the results of calculations for other Bk and Cf isotopes can be considered as an intellectual guess (Figs.187-213).

Comparison with the existing evaluated data libraries ENDF/B-VI, JENDL-3, BROND-2 shows general agreement for major fissile nuclei and large discrepancies for minor transactinides (Figs.214-277), in particular for the (n,3n) cross-sections.

3.2 Fission Barrier Parameters

In Table 3 the values of fission barrier parameters are given. These values were obtained from the experimental data on fission cross-sections or from systematics and extrapolation for nuclei where no experimental data are available. The penetrability parameters $\hbar\omega_A$ and $\hbar\omega_B$ were taken from the work of Björnholm and Lynn[37]: for even-even nuclei $\hbar\omega_A$=1.04 MeV, $\hbar\omega_B$=0.6 MeV; for odd-A: $\hbar\omega_A$=0.8 MeV, $\hbar\omega_B$=0.52 MeV; for odd-odd: $\hbar\omega_A$= 0.65 MeV, $\hbar\omega_B$=0.45 MeV.

Fission barrier heights obtained on the basis of the generalized superfluid model expressions with collective effects taken into account are different up to 0.5 MeV from the results of the Fermi-gas model analysis.

In the actinide region the general theoretical approach for fission barrier height calculations based on the shell correction method may have the accuracy of 1–2 MeV[35]. Therefore the structure of the fission barriers for actinides was studied on the basis of the phenomenological approach [15], [36], [37]. Calculations by Larsson and Leander[38] and those of Howard and Möller[39] predict that the inner saddle point of the barrier will be unstable with respect to axial deformation in Th–U nuclei for N≥142–144 and, consequently, the height of the barrier A will decrease. On the other hand, an increase in K_{rot}^{A} leads to an increase of the value of E_f^A, as was shown by Smirenkin[16].

The impact of axial asymmetry on E_f^A increases from U to Cm [38]. This behavior is correlated, as it is noted by Smirenkin[16], with a tendency in the analysis of fission probability: the heavier the nucleus, the higher the sensitivity of description to the magnitude of K_{rot}^{A}(U).

The fission barrier hight parameters given in Table 3 are in general agreement with those obtained by Ignatyuk et al[2], where the analysis was based on the superfluid nuclear level density model, and are different up to 0.5 MeV from the values obtained by Kuprijanov et al[15] where the Fermi–gas model was used. The parameters [2] for U, Np, Pu isotopes agree within 0.1–0.2 MeV, and those for Cm isotopes data [2] are 0.1–0.2 MeV higher and for Am 0.2–0.3 MeV higher than the present results. The fission barrier height parameters [16] for U, Pu, Pa, Am isotopes agree within 0.2–0.3 MeV, for Th, Np 0.2–0.3 MeV lower, and for Cm 0.4–0.6 MeV lower than the present parameters.

The accuracy of the fission barrier height parameters obtained in the present work should be considered not higher than 0.3 MeV (0.5 MeV for some nuclei) and their values depend on the model used, in particular the nuclear level density parametrization. Calculations of the ^{238}U fission cross–section made using the code GNASH showed that, although for some nuclei (^{239}U, ^{236}U) the fission barrier parameters agree with those obtained with the code STAPRE, for nuclei ^{238}U and ^{237}U they differ by 0.5 MeV (STAPRE results are higher), which can be attributed to different level density models used in both codes.

4. Conclusion

The analysis of experimental data for fission and (n,2n) cross–sections available for some nuclei showed that the data can be described in a consistent manner by the model presently used. Based on this model the theoretical prediction of fission, (n,2n), (n,3n) cross–sections was made for 50 isotopes of transactinides for which no experimental data are available. Although some model parameters were fixed using the experimental data, it was felt that the experimental data base was not sufficient for reliable data prediction. Any data on the (n,2n) reaction cross–sections for nuclei heavier than Pu, even at one or two energy points near 14 MeV, would be desirable.

The accuracy of the calculations of the (n,3n) reaction cross–sections is much lower than for (n,2n) due to their larger sensitivity to model parameters.

In the actinide region the general theoretical approach for fission barrier height calculations based on the shell correction method may have the accuracy of 1–2 MeV[35]. Therefore the structure of the fission barriers for actinides was studied on the basis of the phenomenological approach [15], [36], [37]. Calculations by Larsson and Leander[38] and those of Howard and Möller[39] predict that the inner saddle point of the barrier will be unstable with respect to axial deformation in Th–U nuclei for N≥142–144 and, consequently, the height of the barrier A will decrease. On the other hand, an increase in K_{rot}^{A} leads to an increase of the value of E_f^A, as was shown by Smirenkin[16].

The impact of axial asymmetry on E_f^A increases from U to Cm [38]. This behavior is correlated, as it is noted by Smirenkin[16], with a tendency in the analysis of fission probability: the heavier the nucleus, the higher the sensitivity of description to the magnitude of K_{rot}^{A}(U).

The fission barrier hight parameters given in Table 3 are in general agreement with those obtained by Ignatyuk et al[2], where the analysis was based on the superfluid nuclear level density model, and are different up to 0.5 MeV from the values obtained by Kuprijanov et al[15] where the Fermi–gas model was used. The parameters [2] for U, Np, Pu isotopes agree within 0.1–0.2 MeV, and those for Cm isotopes data [2] are 0.1–0.2 MeV higher and for Am 0.2–0.3 MeV higher than the present results. The fission barrier height parameters [16] for U, Pu, Pa, Am isotopes agree within 0.2–0.3 MeV, for Th, Np 0.2–0.3 MeV lower, and for Cm 0.4–0.6 MeV lower than the present parameters.

The accuracy of the fission barrier height parameters obtained in the present work should be considered not higher than 0.3 MeV (0.5 MeV for some nuclei) and their values depend on the model used, in particular the nuclear level density parametrization. Calculations of the ^{238}U fission cross–section made using the code GNASH showed that, although for some nuclei (^{239}U, ^{236}U) the fission barrier parameters agree with those obtained with the code STAPRE, for nuclei ^{238}U and ^{237}U they differ by 0.5 MeV (STAPRE results are higher), which can be attributed to different level density models used in both codes.

4. Conclusion

The analysis of experimental data for fission and (n,2n) cross–sections available for some nuclei showed that the data can be described in a consistent manner by the model presently used. Based on this model the theoretical prediction of fission, (n,2n), (n,3n) cross–sections was made for 50 isotopes of transactinides for which no experimental data are available. Although some model parameters were fixed using the experimental data, it was felt that the experimental data base was not sufficient for reliable data prediction. Any data on the (n,2n) reaction cross–sections for nuclei heavier than Pu, even at one or two energy points near 14 MeV, would be desirable.

The accuracy of the calculations of the (n,3n) reaction cross–sections is much lower than for (n,2n) due to their larger sensitivity to model parameters.

The STAPRE code used in the present work gives the possibility to describe the fission cross-sections in a logical manner taking into account the shell and collective effects in the level density and enhancement coefficients in the fission channel. The weak side of the code may lie in a rather simple version of the exciton model used in STAPRE. At energies above 15 MeV the binary reactions are largely determined by the preequilibrium component and calculations become sensitive to the accuracy of that model. Therefore in the second part of the work for the generation of nuclear data for many transactinide nuclei in the energy region from 10 to 100 MeV the code GNASH will be used where a more advanced version of the preequilibrium model had been incorporated.

Acknowledgement

The author is grateful to Dr. Y. Kikuchi and Mr. T. Nakagawa of the Nuclear Data Center, JAERI, for support of the present work, fruitful discussions and for the help in using the computer FACOM-M780.

References

[1] Uhl M. and Strohmaier B.: IRK-76/01, Vienna (1976).
[2] Ignatyuk A.V. and Maslov V.M. : J. of Nucl. Phys. 51, 1227 (1990).
[3] Ignatyuk A.V., Maslov V.M. and Pashchenko A.B.: J. Nucl. Phys., 47, 355 (1988).
[4] Raynal J.: Optical Model and Coupled-Channel Calculations in Nuclear Physics, SMR-9/8, IAEA, Vienna (1970).
[5] Haouat G., Lachkar J., Lagrange Ch., Jary J., Sigaud J. and Patin Y.: Nucl. Sci. Eng., 81, 491 (1982).
[6] Konshin V.A.: Proc. of the IAEA Workshop on Computation and Analysis of Nuclear Data Relevant to Nuclear Energy and Safety, Trieste, Italy, 1992, World Scientific, p.775 (1993).
[7] Komilov V.N., Baryba V.Ya. and Salnikov O.A.: Neutron Physics, Tcniiatominform, Moscow, v.3, 104 (1980).
[8] Ignatyuk A.V., Istekov K.K. and Smizenkin G.N.: J. Nucl. Phys., 29, 450 (1979).
[9] Rastopchin E.M., Svirin M.I. and Smirenkin G.N.: J. Nucl. Phys., 52, 1258 (1990).
[10] Kudyaev G.A., Ostapenko Yu.B. and Smirenkin G.N.: J. Nucl. Phys., 45, 1534 (1987).
[11] Antsipov G.V., Konshin V.A. and Maslov V.M.: Nuclear Constants, Tcniiatominform, Moscow, v.3, p.25 (1985).
[12] Myers W.O and Swiatecky W.J.: Ark Fysik 36, 343 (1967).
[13] Kuprijanov V.M., Smirenkin G.N. and Fursov B.I.: J. Nucl. Phys., 39, 176 (1984).
[14] Istekov K.K. et al.: J. Nucl. Phys., 29, 1156 (1979).
[15] Kuprijanov V.M., Smirenkin G.N. and Fursov B.I.: J. Nucl. Phys. 39, 281 (1984).

The STAPRE code used in the present work gives the possibility to describe the fission cross-sections in a logical manner taking into account the shell and collective effects in the level density and enhancement coefficients in the fission channel. The weak side of the code may lie in a rather simple version of the exciton model used in STAPRE. At energies above 15 MeV the binary reactions are largely determined by the preequilibrium component and calculations become sensitive to the accuracy of that model. Therefore in the second part of the work for the generation of nuclear data for many transactinide nuclei in the energy region from 10 to 100 MeV the code GNASH will be used where a more advanced version of the preequilibrium model had been incorporated.

Acknowledgement

The author is grateful to Dr. Y. Kikuchi and Mr. T. Nakagawa of the Nuclear Data Center, JAERI, for support of the present work, fruitful discussions and for the help in using the computer FACOM-M780.

References

[1] Uhl M. and Strohmaier B.: IRK-76/01, Vienna (1976).
[2] Ignatyuk A.V. and Maslov V.M. : J. of Nucl. Phys. 51, 1227 (1990).
[3] Ignatyuk A.V., Maslov V.M. and Pashchenko A.B.: J. Nucl. Phys., 47, 355 (1988).
[4] Raynal J.: Optical Model and Coupled-Channel Calculations in Nuclear Physics, SMR-9/8, IAEA, Vienna (1970).
[5] Haouat G., Lachkar J., Lagrange Ch., Jary J., Sigaud J. and Patin Y.: Nucl. Sci. Eng., 81, 491 (1982).
[6] Konshin V.A.: Proc. of the IAEA Workshop on Computation and Analysis of Nuclear Data Relevant to Nuclear Energy and Safety, Trieste, Italy, 1992, World Scientific, p.775 (1993).
[7] Kornilov V.N., Baryba V.Ya. and Salnikov O.A.: Neutron Physics, Tcniiatominform, Moscow, v.3, 104 (1980).
[8] Ignatyuk A.V., Istekov K.K. and Smizenkin G.N.: J. Nucl. Phys., 29, 450 (1979).
[9] Rastopchin E.M., Svirin M.I. and Smirenkin G.N.: J. Nucl. Phys., 52, 1258 (1990).
[10] Kudyaev G.A., Ostapenko Yu.B. and Smirenkin G.N.: J. Nucl. Phys., 45, 1534 (1987).
[11] Antsipov G.V., Konshin V.A. and Maslov V.M.: Nuclear Constants, Tcniiatominform, Moscow, v.3, p.25 (1985).
[12] Myers W.O and Swiatecky W.J.: Ark Fysik 36, 343 (1967).
[13] Kuprijanov V.M., Smirenkin G.N. and Fursov B.I.: J. Nucl. Phys., 39, 176 (1984).
[14] Istekov K.K. et al.: J. Nucl. Phys., 29, 1156 (1979).
[15] Kuprijanov V.M., Smirenkin G.N. and Fursov B.I.: J. Nucl. Phys. 39, 281 (1984).

The STAPRE code used in the present work gives the possibility to describe the fission cross-sections in a logical manner taking into account the shell and collective effects in the level density and enhancement coefficients in the fission channel. The weak side of the code may lie in a rather simple version of the exciton model used in STAPRE. At energies above 15 MeV the binary reactions are largely determined by the preequilibrium component and calculations become sensitive to the accuracy of that model. Therefore in the second part of the work for the generation of nuclear data for many transactinide nuclei in the energy region from 10 to 100 MeV the code GNASH will be used where a more advanced version of the preequilibrium model had been incorporated.

Acknowledgement

The author is grateful to Dr. Y. Kikuchi and Mr. T. Nakagawa of the Nuclear Data Center, JAERI, for support of the present work, fruitful discussions and for the help in using the computer FACOM-M780.

References

[1] Uhl M. and Strohmaier B.: IRK-76/01, Vienna (1976).
[2] Ignatyuk A.V. and Maslov V.M. : J. of Nucl. Phys. 51, 1227 (1990).
[3] Ignatyuk A.V., Maslov V.M. and Pashchenko A.B.: J. Nucl. Phys., 47, 355 (1988).
[4] Raynal J.: Optical Model and Coupled-Channel Calculations in Nuclear Physics, SMR-9/8, IAEA, Vienna (1970).
[5] Haouat G., Lachkar J., Lagrange Ch., Jary J., Sigaud J. and Patin Y.: Nucl. Sci. Eng., 81, 491 (1982).
[6] Konshin V.A.: Proc. of the IAEA Workshop on Computation and Analysis of Nuclear Data Relevant to Nuclear Energy and Safety, Trieste, Italy, 1992, World Scientific, p.775 (1993).
[7] Komilov V.N., Baryba V.Ya. and Salnikov O.A.: Neutron Physics, Tcniiatominform, Moscow, v.3, 104 (1980).
[8] Ignatyuk A.V., Istekov K.K. and Smizenkin G.N.: J. Nucl. Phys., 29, 450 (1979).
[9] Rastopchin E.M., Svirin M.I. and Smirenkin G.N.: J. Nucl. Phys., 52, 1258 (1990).
[10] Kudyaev G.A., Ostapenko Yu.B. and Smirenkin G.N.: J. Nucl. Phys., 45, 1534 (1987).
[11] Antsipov G.V., Konshin V.A. and Maslov V.M.: Nuclear Constants, Tcniiatominform, Moscow, v.3, p.25 (1985).
[12] Myers W.O and Swiatecky W.J.: Ark Fysik 36, 343 (1967).
[13] Kuprijanov V.M., Smirenkin G.N. and Fursov B.I.: J. Nucl. Phys., 39, 176 (1984).
[14] Istekov K.K. et al.: J. Nucl. Phys., 29, 1156 (1979).
[15] Kuprijanov V.M., Smirenkin G.N. and Fursov B.I.: J. Nucl. Phys. 39, 281 (1984).

[16] Smirenkin G.N.: INDC(CCP)-359G, IAEA, Vienna (1993).
[17] Kornilov V.N. et al.: ZFK-410, p.68 (1980).
[18] Frehaut J., Bertin A. and Bois R.: Nucl. Sci. Eng., 74, 29 (1980).
[19] Butler J.P. and Santry D.C.: Can. J. Chem., 39, 689 (1961).
[20] Raics P., Daroczy S., Csikai J., Kornilov N.V., Baryba V.Ya. and Salnikov O.A.: Phys. Rev. C32, 87 (1985).
[21] Pankratov V.M.: At. Energ. 14, 177 (1963).
[22] Meadows J.W.: Nucl. Sci. Eng. 85, 271 (1983).
[23] Budtz-Joergensen C. et al.: Intern. Conf. on Nuclear Data for Sci. and Techn., Antwerp, p.206 (1982).
[24] Kari K. and Cierjacks S.: Intern. Conf. on Neutron Phys. and Nucl. Data for Reactors and Appl. Purposes, Harwell, p.905 (1978).
[25] Meadows J.W.: Nucl. Sci. Eng., 79, 233 (1981).
[26] Behrens J.W. et al.: Nucl. Sci. Eng., 68, 128 (1978).
[27] Behrens J.W. et al.: Nucl. Sci. Eng., 66, 433 (1978).
[28] Frehaut J., Bertin A., Bois R., Gryntakis E. and Philis C.A.: Proc. Intern. Conf. on Nuclear Data for Basic and Applied Science, Santa Fe, p.1561 (1985).
[29] Maslov V.M.: Z. Phys., A347, 211 (1994).
[30] Fu C.Y.: Nucl. Sci. Eng., 86, 344 (1984).
[31] Dabbs J.W.T. et al.: Nucl. Sci. Eng., 83, 22 (1983).
[32] Browne J.C. et al.: Phys. Rev. C29, 2188 (1984).
[33] Knitter H. et al: private communication, EXFOR 22032002 (1987).
[34] White R.M.: Intern. Conf. on Nucl. Data for Sci. and Techn., Antwerp, p.218 (1983).
[35] Brack M.: Intern. Symp. on Physics and Chemistry of Fission, Jülich, 1979, IAEA, Vienna, v.1, p.227 (1980).
[36] Kupriyanov V.M., Istekov K.K., Fursov B.I. and Smirenkin G.N.: J. Nucl. Phys., 32, 355 (1980).
[37] Björnholm S. and Lynn J.E.: Rev. Mod. Phys., 52, 725 (1980).
[38] Larsson S.E. and Leander G.: Symp. on Physics and Chemistry of Fission, Rochester, 1973, IAEA, Vienna, 1, 177 (1974).
[39] Howard W.M. and Möller P.: Atomic Data and Nuclear Data Tables, 15, 219 (1980).
[40] Young P.G. and Arthur E.D.: GNASH; A Preequilibrium Statistical Nuclear Model Code for Calculation of Cross Sections and Emission Spectra, LA-6947 (1977).

Table 1 Deformed Potential Parameters Obtained by Haouat et al [5] and Used in the Present Work

Nucleus	V_R: Real Potential	W_D Surface Imaginary Potential	V_{SO}: Spin-Orbit Potential	Quadrupole Deformation (β_2)	Hexadecapole Deformation (β_4)
	r_R=1.26, a_R=0.63	r_D=1.26, a_D=0.52	r_{SO}=1.12, a_{SO}=0.47		
^{232}Th	46.4 − 0.3E	3.6 + 0.4E	6.2	0.190	0.071
^{235}U	46.4 − 0.3E	3.3 + 0.4E	6.2	0.220	0.080
^{238}U	46.2 − 0.3E	3.6 + 0.4E	6.2	0.198	0.057
^{239}Pu	46.2 − 0.3E	3.6 + 0.4E	6.2	0.220	0.070
^{242}Pu	46.0 − 0.3E	3.5 + 0.4E	6.2	0.204	0.051

Table 2 Nuclear Level Density Parameters

Nuclide	Spin	B_n (MeV)	D_o (eV)	a (MeV^{-1})
^{230}Th	2.5	6.793	0.53	19.00
^{231}Th	0.0	5.117	9.60	20.10
^{233}Th	0.0	4.786	19.00	20.05
^{232}Pa	1.5	5.570	0.45	19.30
^{234}Pa	1.5	5.219	0.59	20.10
^{235}Pa	0.0	6.090	0.69	21.70
^{233}U	0.0	5.743	4.60	19.20
^{234}U	2.5	6.843	0.55	18.85
^{235}U	0.0	5.298	10.60	19.11
^{236}U	3.5	6.545	0.44	19.70
^{237}U	0.0	5.125	15.40	19.10
^{238}U	0.5	6.143	3.50	19.48
^{239}U	0.0	4.804	20.80	19.72
^{238}Np	2.5	5.488	0.52	18.70
^{239}Pu	0.0	5.656	9.00	18.30
^{240}Pu	0.5	6.534	2.30	19.10
^{241}Pu	0.0	5.241	13.60	18.95
^{242}Pu	2.5	6.301	0.90	19.70
^{243}Pu	0.0	5.037	17.50	19.25
^{245}Pu	0.0	4.720	24.00	19.93
^{242}Am	2.5	5.539	0.55	18.45
^{243}Am	1.0	6.363	0.40	19.90
^{244}Am	2.5	5.366	0.60	18.84
^{243}Cm	0.0	5.694	12.80	17.45
^{244}Cm	2.5	6.799	0.81	18.10
^{245}Cm	0.0	5.522	12.00	18.15
^{246}Cm	3.5	6.456	1.90	19.70
^{247}Cm	0.0	5.156	32.00	17.43
^{248}Cm	4.5	6.211	1.40	18.20
^{249}Cm	0.0	4.713	33.00	19.17
^{250}Bk	3.5	4.966	1.00	18.80
^{250}Cf	4.5	6.621	0.70	18.15
^{253}Cf	0.0	4.805	27.00	19.40

Table 3 Fission Barrier Parameters for Transactinides

Fissioning Nucleus	E_f^A(MeV)	E_f^B(MeV)	Fissioning Nucleus	E_f^A(MeV)	E_f^B(MeV)
$^{227}Th_{90}$	6.10	6.60	$^{242}Pu_{94}$	5.60	5.35
$^{228}Th_{90}$	6.20	6.60	$^{243}Pu_{94}$	6.00	5.70
$^{229}Th_{90}$	6.20	6.45	$^{244}Pu_{94}$	5.50	5.20
$^{230}Th_{90}$	6.10	6.35	$^{245}Pu_{94}$	5.75	5.60
$^{231}Th_{90}$	6.35	6.60	$^{246}Pu_{94}$	5.50	5.20
$^{232}Th_{90}$	6.00	6.40	$^{239}Am_{95}$	5.70	4.80
$^{233}Th_{90}$	6.20	6.50	$^{240}Am_{95}$	6.70	5.60
$^{234}Th_{90}$	6.00	6.40	$^{241}Am_{95}$	5.90	5.10
$^{230}Pa_{91}$	5.80	5.90	$^{242}Am_{95}$	6.70	5.70
$^{231}Pa_{91}$	5.70	5.70	$^{243}Am_{95}$	6.05	5.10
$^{232}Pa_{91}$	6.00	6.40	$^{244}Am_{95}$	6.70	5.90
$^{233}Pa_{91}$	5.90	6.00	$^{245}Am_{95}$	6.10	5.00
$^{234}Pa_{91}$	5.90	6.00	$^{246}Am_{95}$	6.30	5.20
$^{231}U_{92}$	6.50	5.80	$^{240}Cm_{96}$	6.9	4.9
$^{232}U_{92}$	6.00	5.60	$^{241}Cm_{96}$	7.2	5.2
$^{233}U_{92}$	6.60	5.70	$^{242}Cm_{96}$	6.7	5.1
$^{234}U_{92}$	6.10	5.70	$^{243}Cm_{96}$	7.0	5.4
$^{235}U_{92}$	6.10	5.90	$^{244}Cm_{96}$	6.7	5.2
$^{236}U_{92}$	6.10	5.80	$^{245}Cm_{96}$	6.8	5.5
$^{237}U_{92}$	6.80	6.00	$^{246}Cm_{96}$	6.3	5.3
$^{238}U_{92}$	6.30	5.60	$^{247}Cm_{96}$	6.5	5.2
$^{239}U_{92}$	6.20	6.00	$^{248}Cm_{96}$	5.8	5.0
$^{240}U_{92}$	6.40	5.50	$^{249}Cm_{96}$	6.2	5.1
$^{233}Np_{93}$	5.50	5.10	$^{250}Cm_{96}$	5.5	4.5
$^{234}Np_{93}$	5.70	5.40	$^{244}Bk_{97}$	6.8	4.6
$^{235}Np_{93}$	5.80	5.40	$^{245}Bk_{97}$	7.0	4.7
$^{236}Np_{93}$	6.10	5.90	$^{246}Bk_{97}$	7.3	5.0
$^{237}Np_{93}$	6.20	5.30	$^{247}Bk_{97}$	6.6	4.7
$^{238}Np_{93}$	6.20	6.00	$^{248}Bk_{97}$	7.1	5.0
$^{239}Np_{93}$	5.90	5.30	$^{249}Bk_{97}$	6.4	4.6
$^{235}Pu_{94}$	5.70	5.20	$^{250}Bk_{97}$	6.7	4.7
$^{236}Pu_{94}$	5.70	5.40	$^{249}Cf_{98}$	6.5	4.1
$^{237}Pu_{94}$	6.10	5.90	$^{250}Cf_{98}$	6.7	4.6
$^{238}Pu_{94}$	5.90	5.50	$^{251}Cf_{98}$	6.7	4.3
$^{239}Pu_{94}$	6.40	5.80	$^{252}Cf_{98}$	6.1	3.9
$^{240}Pu_{94}$	6.15	5.30	$^{253}Cf_{98}$	5.9	4.0
$^{241}Pu_{94}$	6.35	5.65			

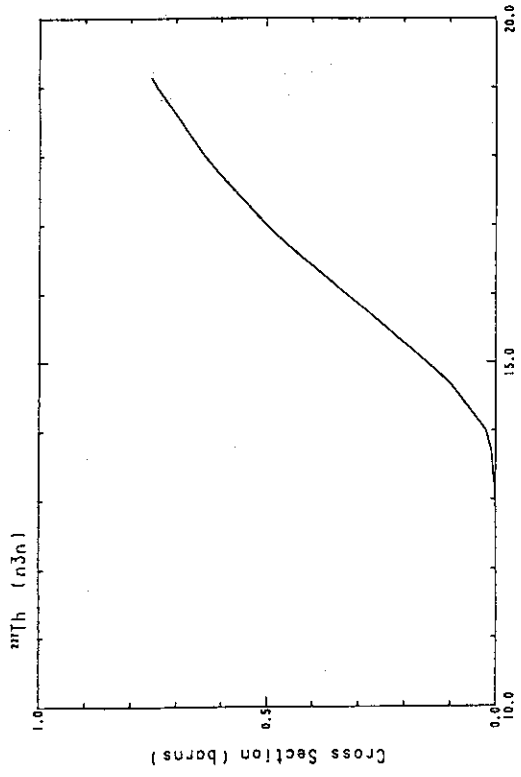

Fig. 3 The (n,3n)-reaction cross-section of ^{227}Th.

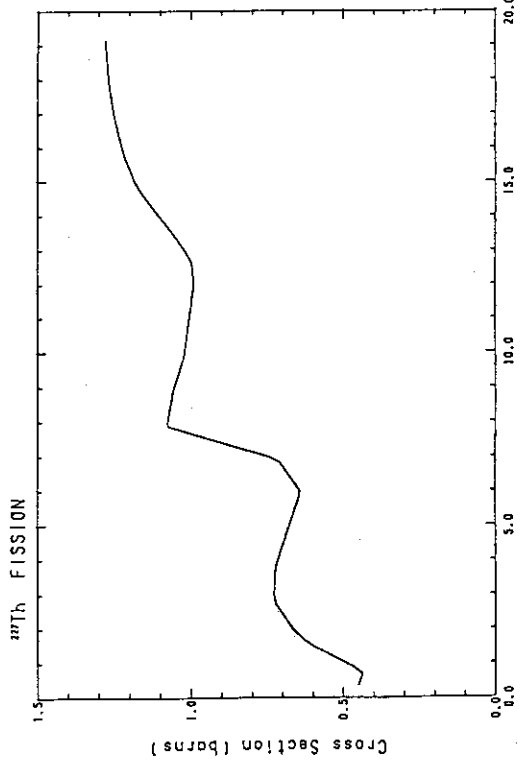

Fig. 1 The fission cross-section of ^{227}Th.

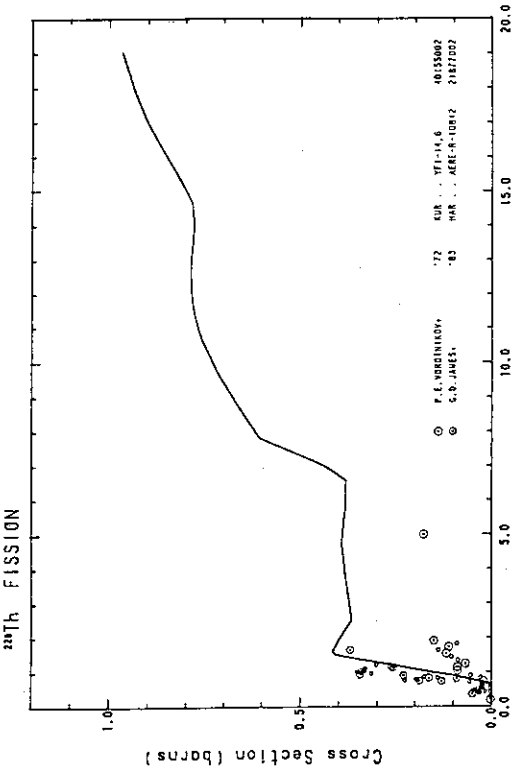

Fig. 4 The fission cross-section of ^{228}Th.

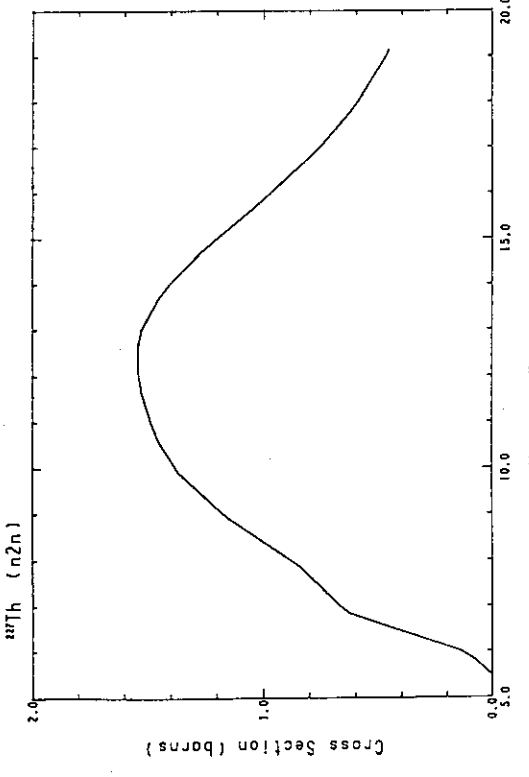

Fig. 2 The (n,2n)-reaction cross-section of ^{227}Th.

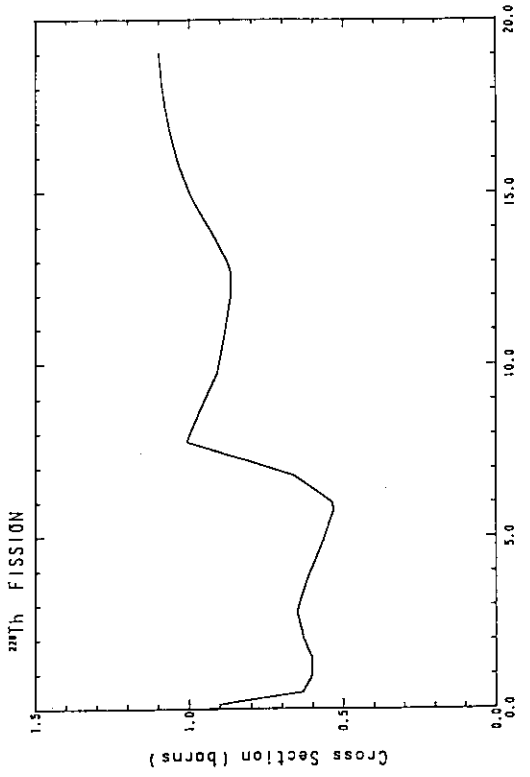

Fig. 7 The fission cross-section of ^{229}Th.

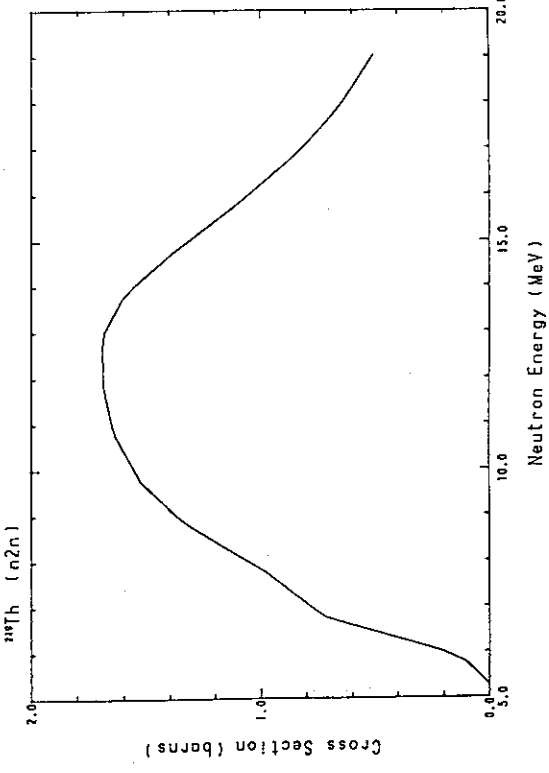

Fig. 8 The (n,2n)-reaction cross-section of ^{229}Th.

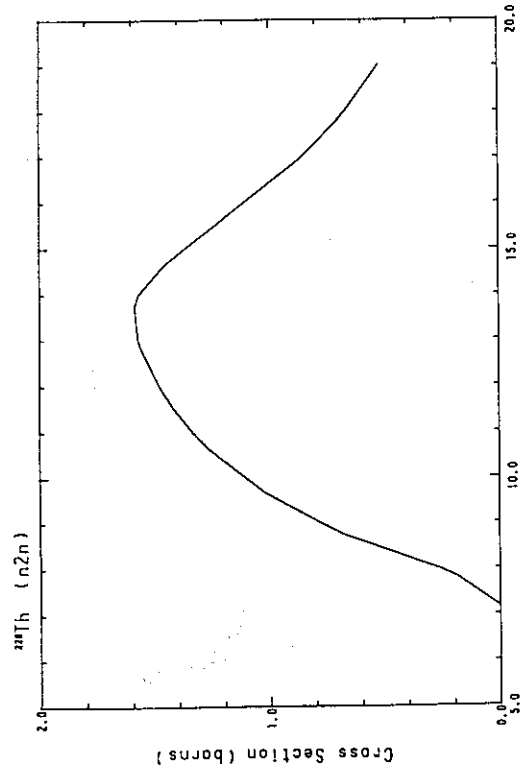

Fig. 5 The (n,2n)-reaction cross-section of ^{228}Th.

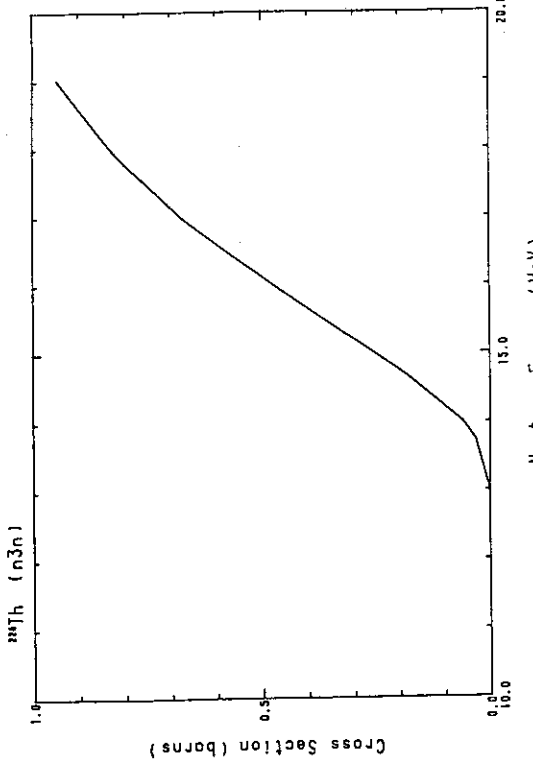

Fig. 6 The (n,3n)-reaction cross-section of ^{228}Th.

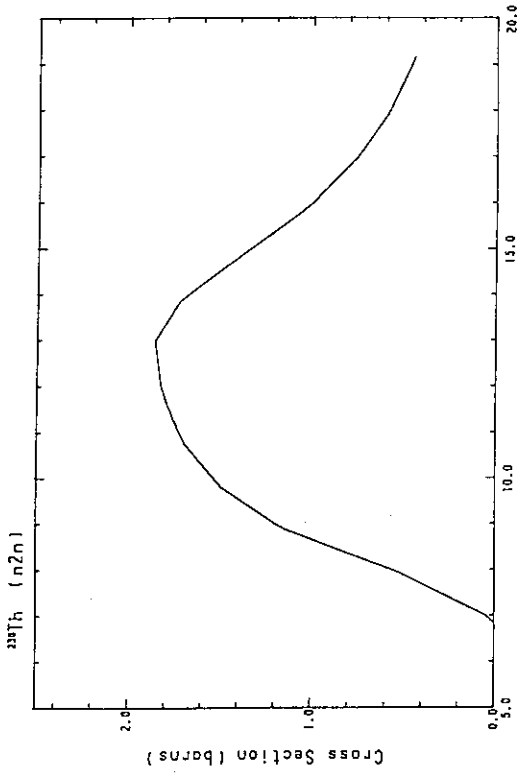

Fig. 11 The (n,2n)-reaction cross-section of ^{230}Th.

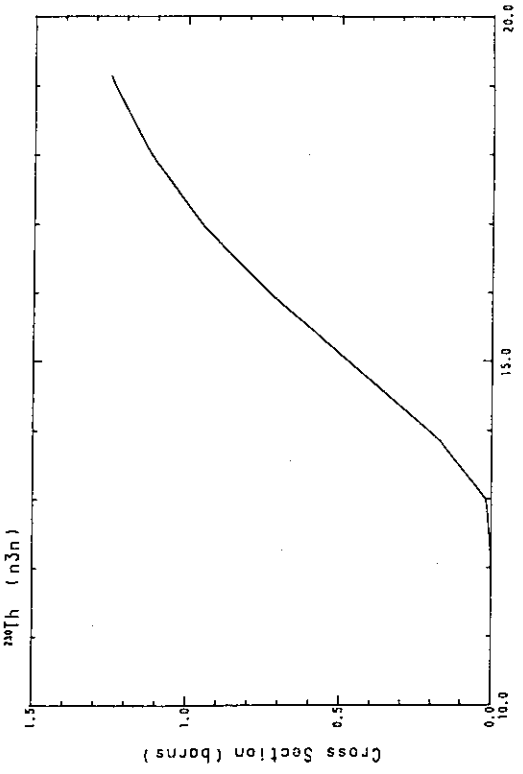

Fig. 12 The (n,3n)-reaction cross-section of ^{230}Th.

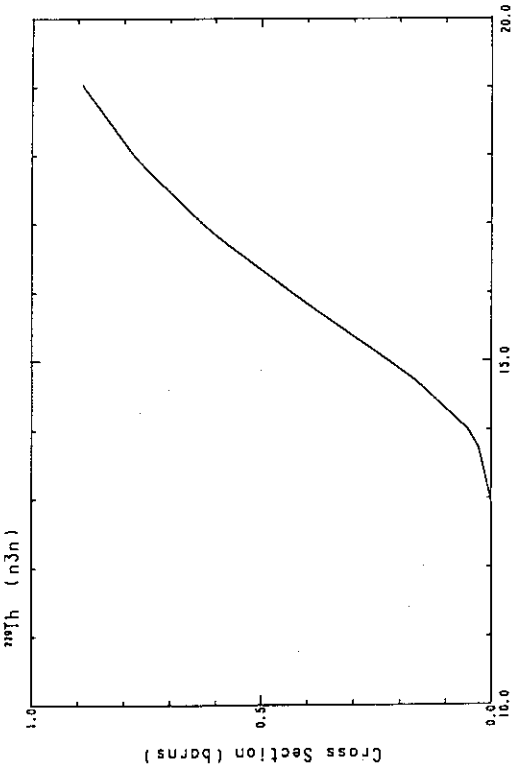

Fig. 9 The (n,3n)-reaction cross-section of ^{229}Th.

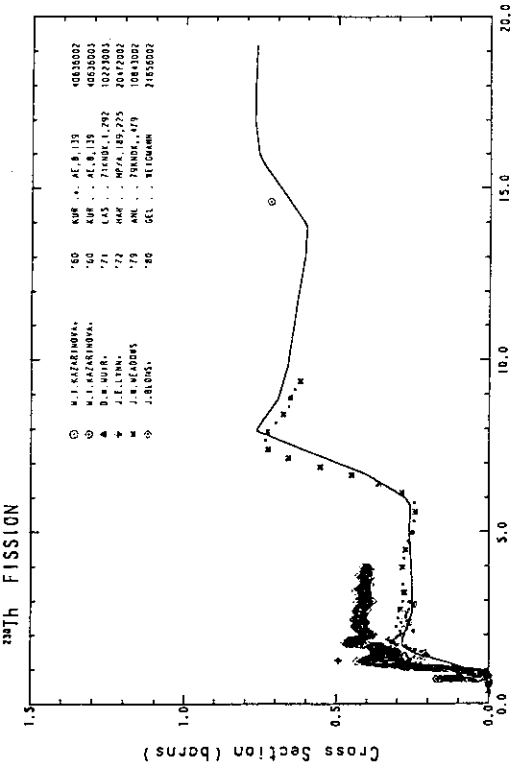

Fig. 10 The fission cross-section of ^{230}Th.

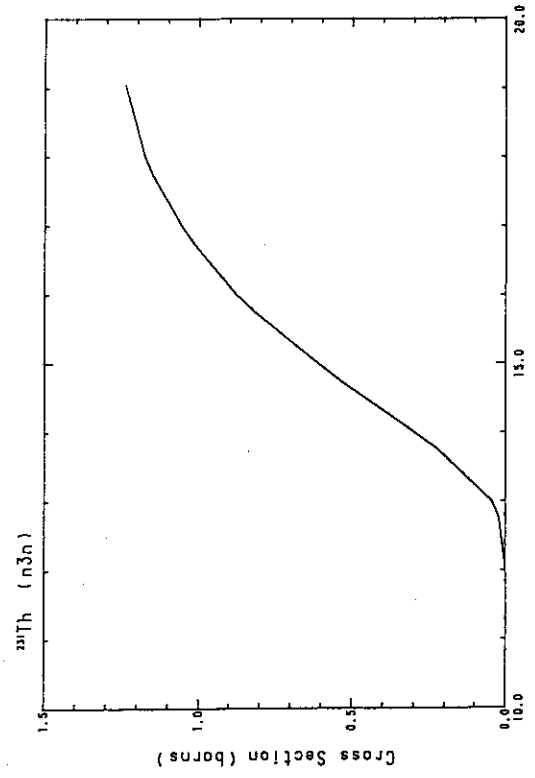

Fig. 15 The (n,3n)-reaction cross-section of ^{231}Th.

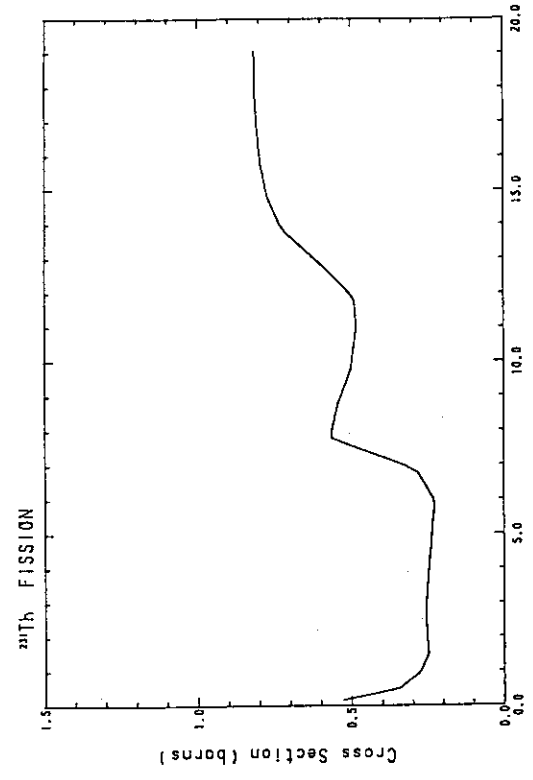

Fig. 13 The fission cross-section of ^{231}Th.

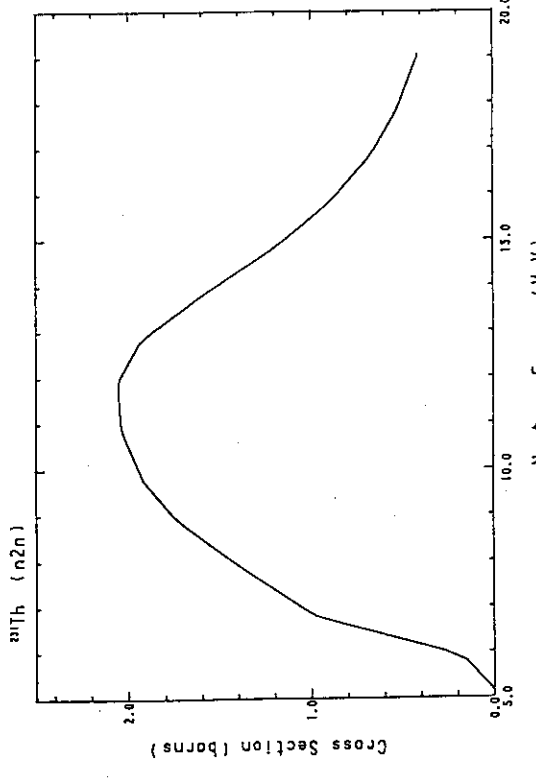

Fig. 14 The (n,2n)-reaction cross-section of ^{231}Th.

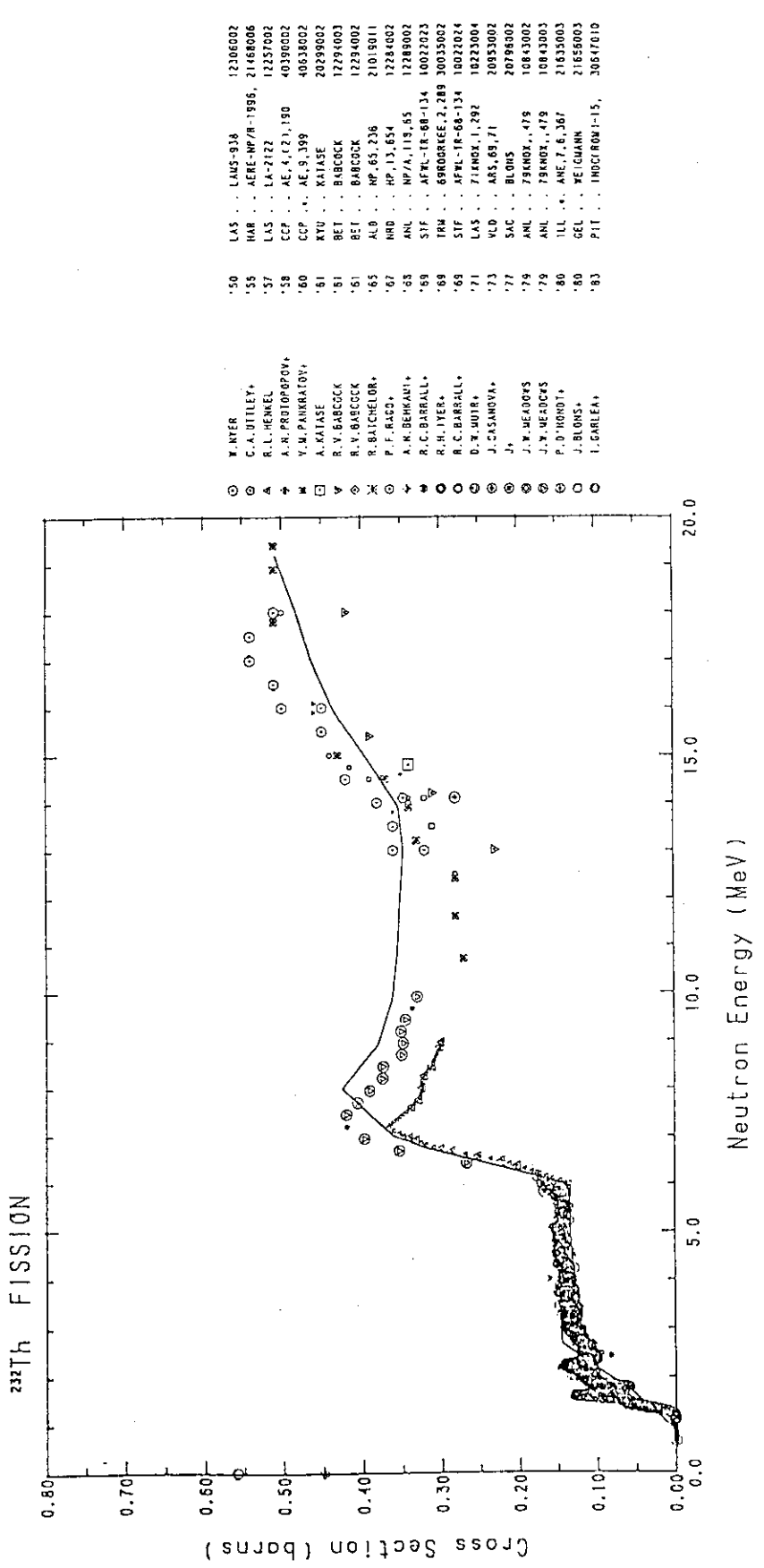

Fig. 16 The fission cross-section of ^{232}Th.

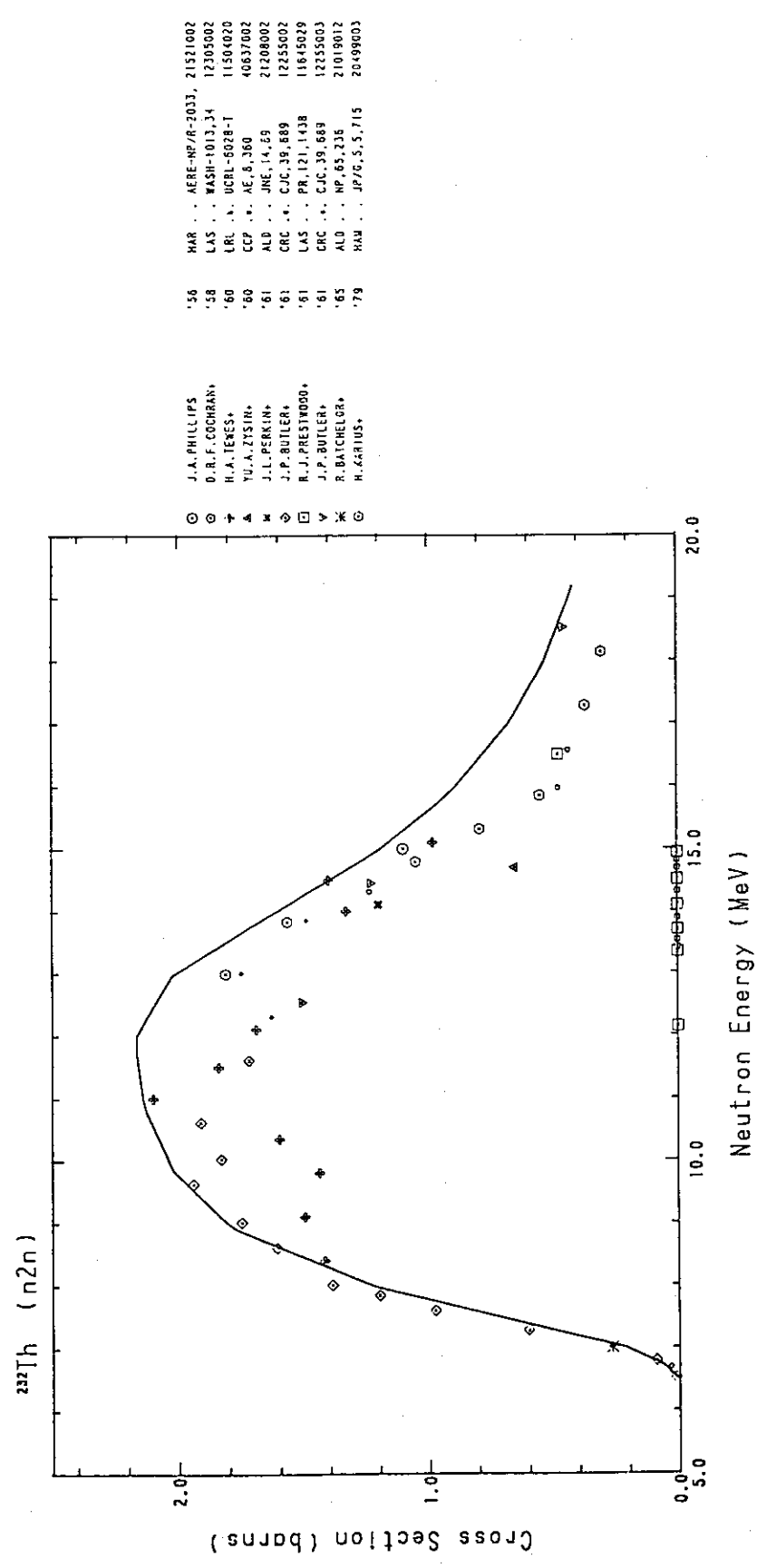

Fig. 17 The (n,2n)-reaction cross-section of ^{232}Th.

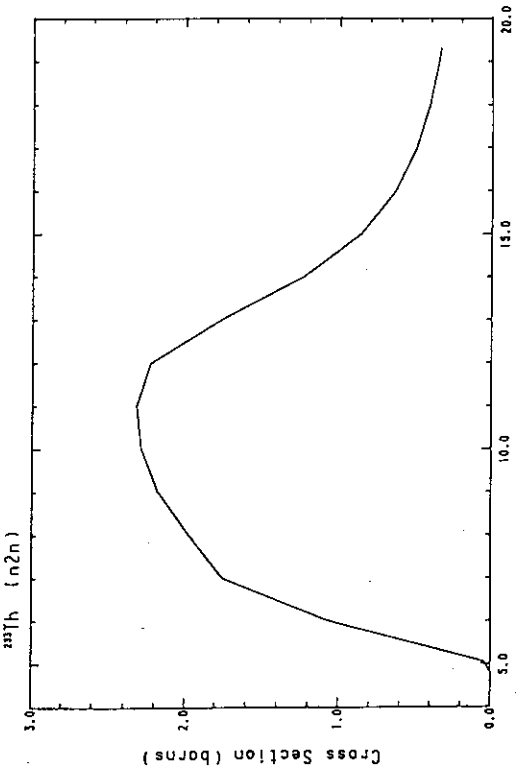

Fig. 20 The (n,2n)-reaction cross-section of ^{233}Th.

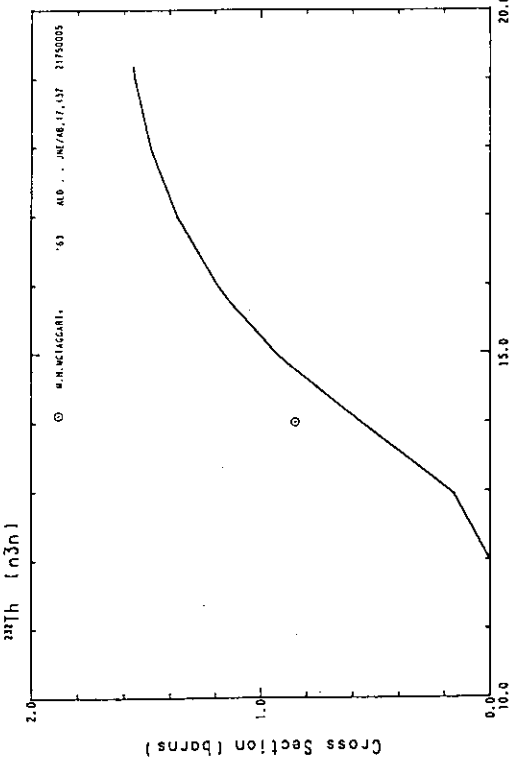

Fig. 18 The (n,3n)-reaction cross-section of ^{232}Th.

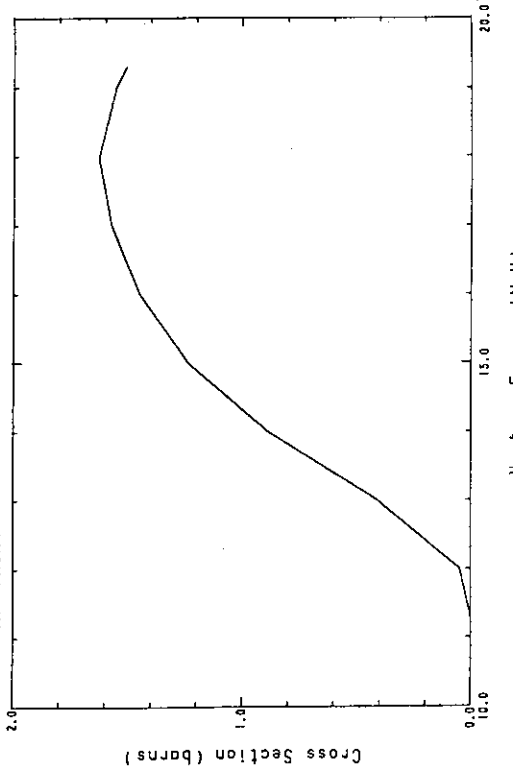

Fig. 21 The (n,3n)-reaction cross-section of ^{233}Th.

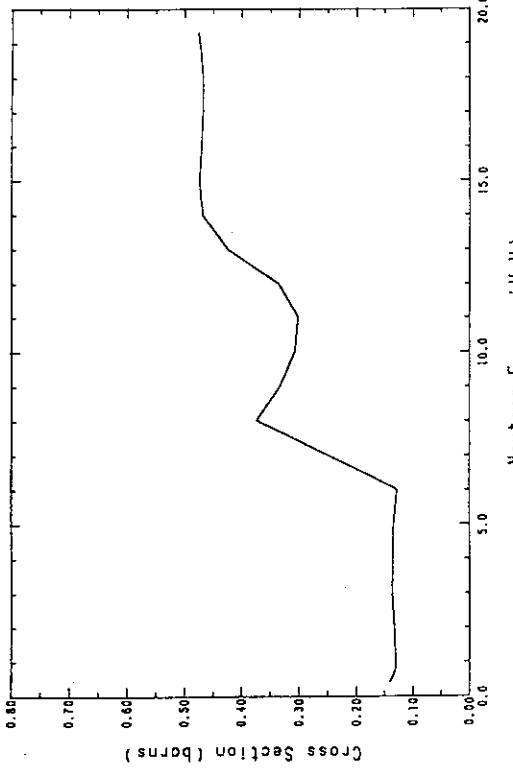

Fig. 19 The fission cross-section of ^{233}Th.

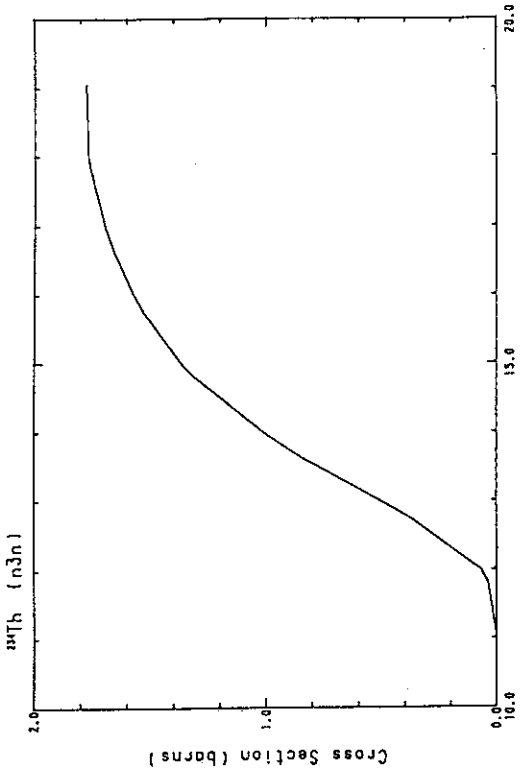

Fig. 24 The (n,3n)-reaction cross-section of ^{234}Th.

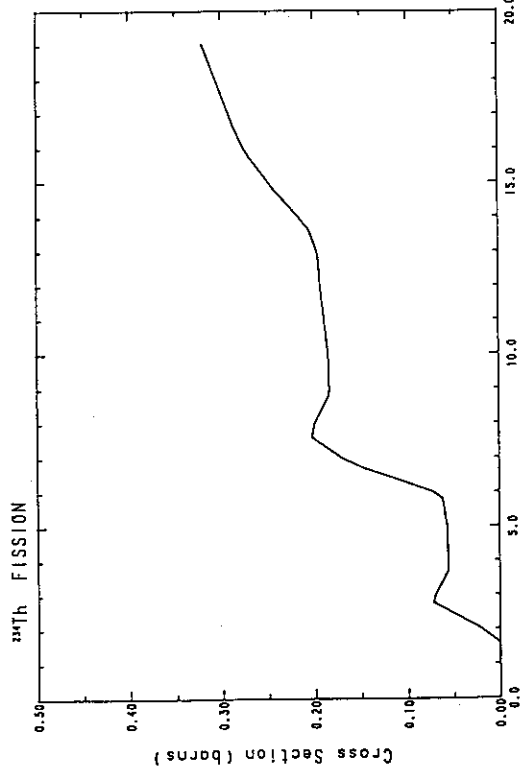

Fig. 22 The fission cross-section of ^{234}Th.

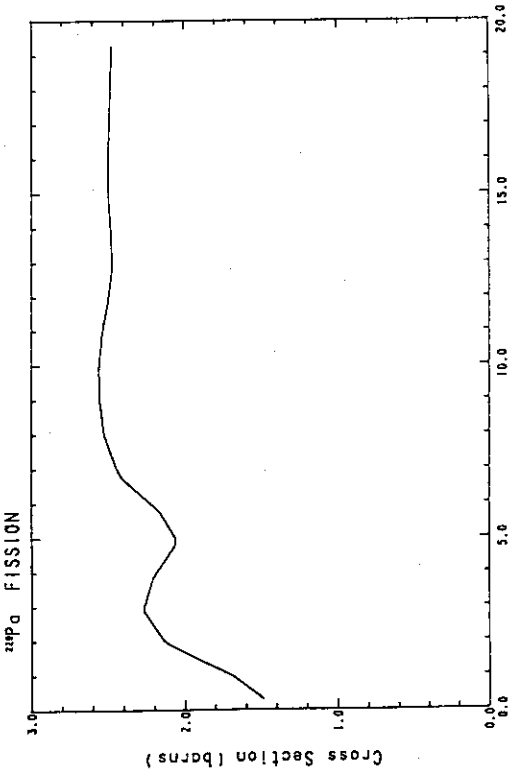

Fig. 25 The fission cross-section of ^{229}Pa.

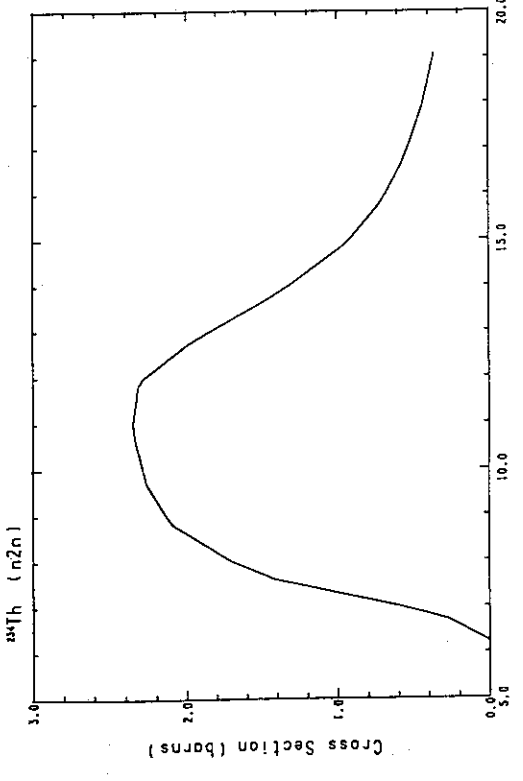

Fig. 23 The (n,2n)-reaction cross-section of ^{234}Th.

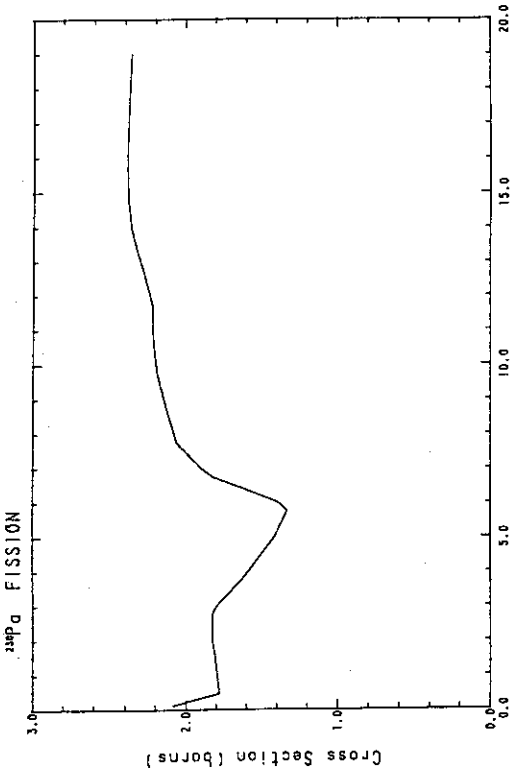

Fig. 28 The fission cross-section of ^{230}Pa.

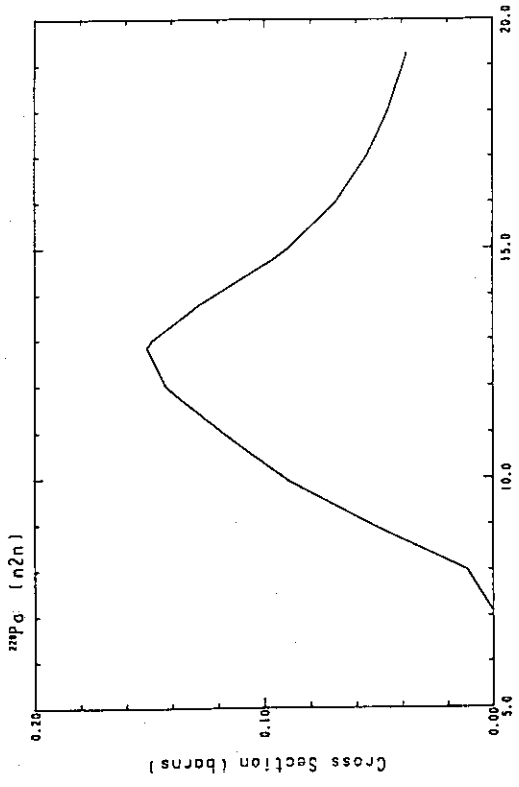

Fig. 26 The (n,2n)-reaction cross-section of ^{229}Pa.

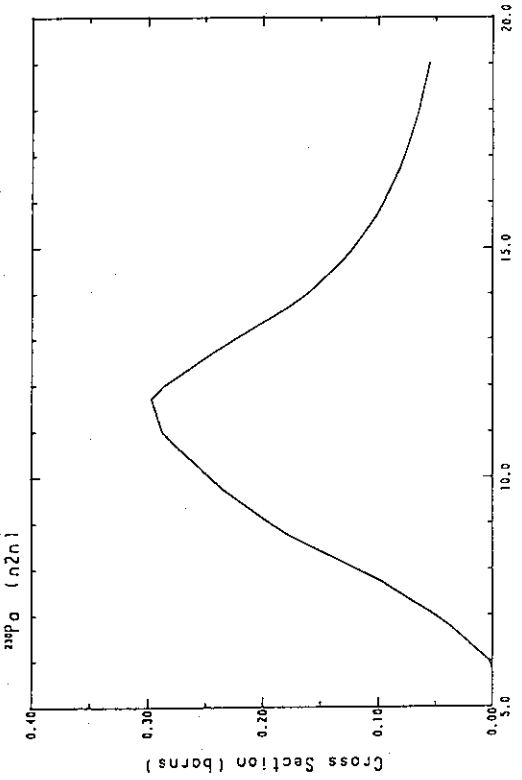

Fig. 29 The (n,2n)-reaction cross-section of ^{230}Pa.

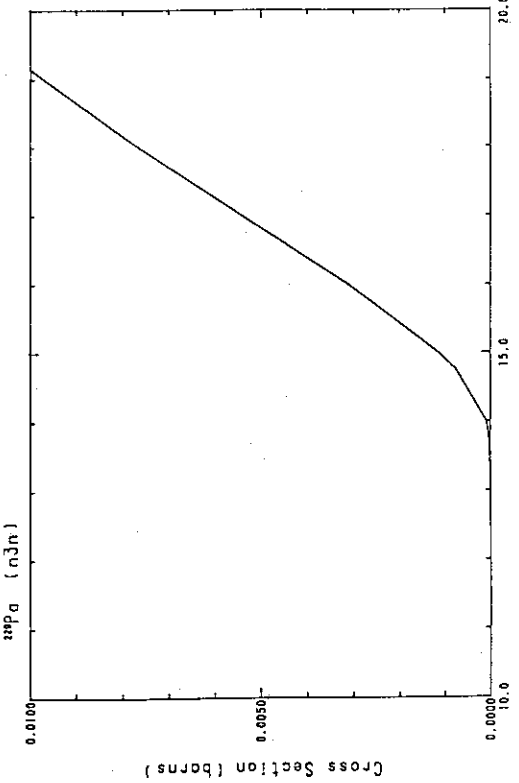

Fig. 27 The (n,3n)-reaction cross-section of ^{229}Pa.

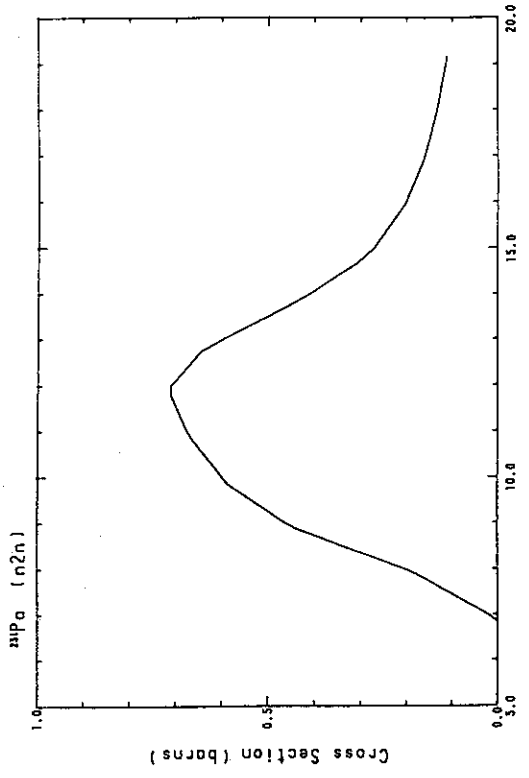

Fig. 32 The (n,2n)-reaction cross-section of ^{231}Pa.

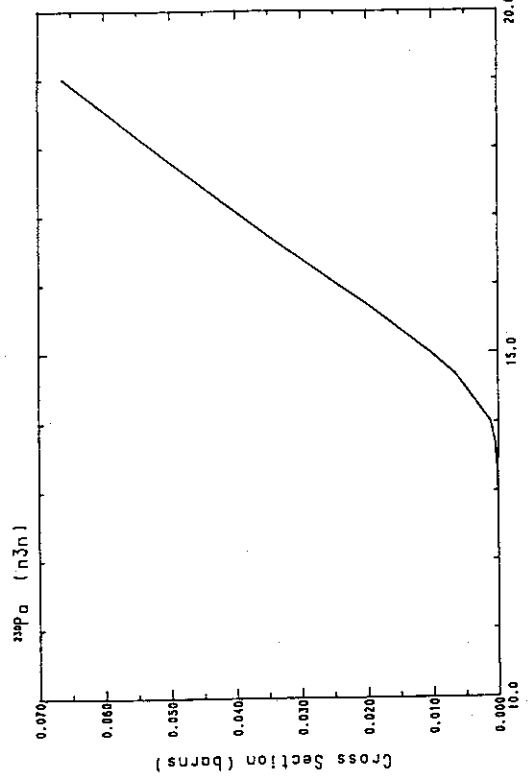

Fig. 30 The (n,3n)-reaction cross-section of ^{230}Pa.

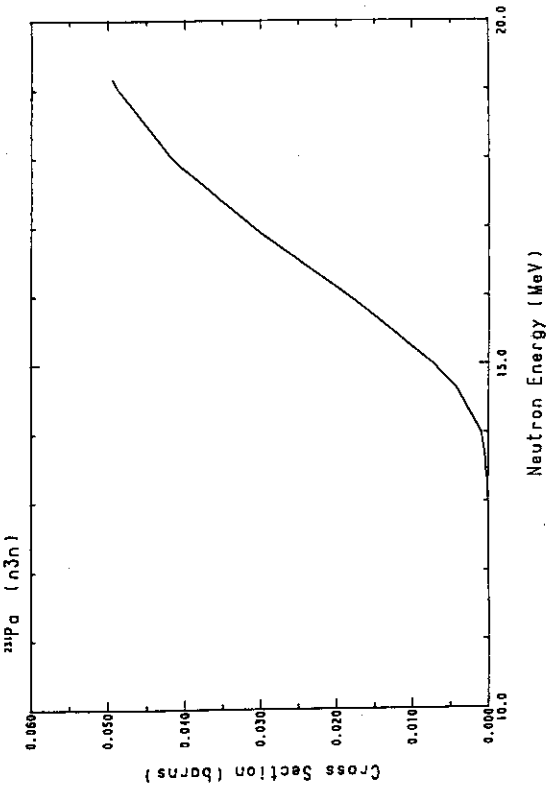

Fig. 33 The (n,3n)-reaction cross-section of ^{231}Pa.

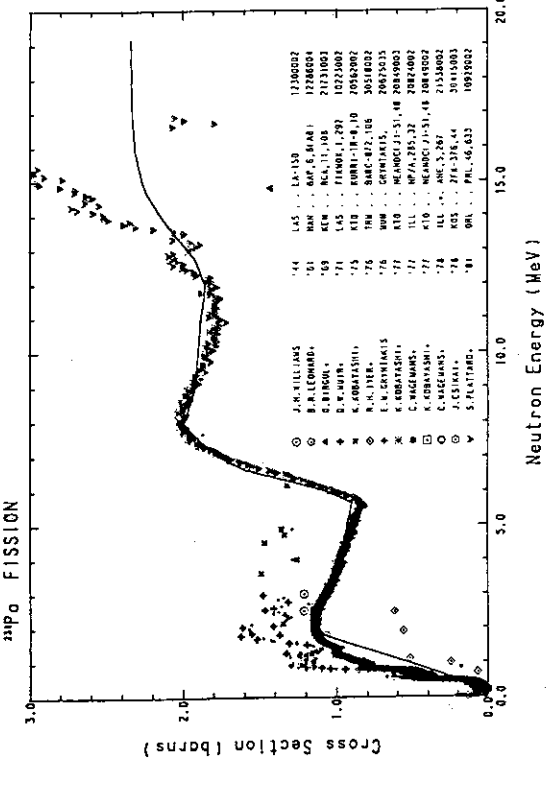

Fig. 31 The fission cross-section of ^{231}Pa.

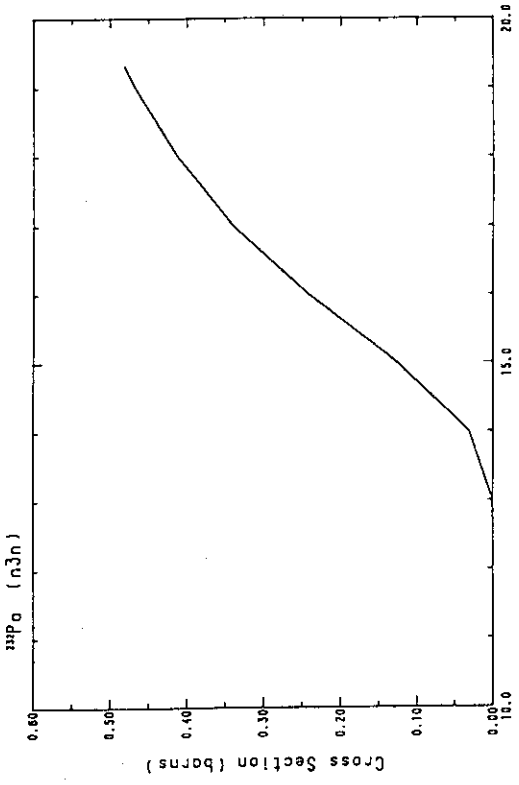

Fig. 36 The (n,3n)-reaction cross-section of ^{232}Pa.

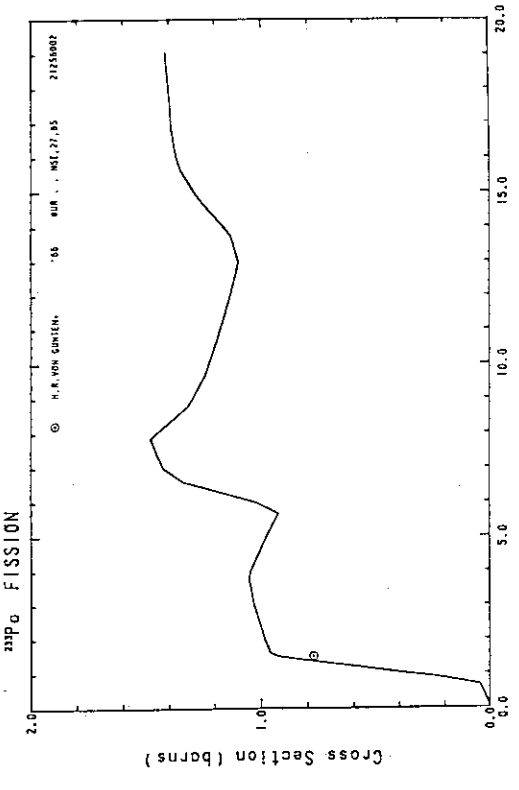

Fig. 37 The fission cross-section of ^{233}Pa.

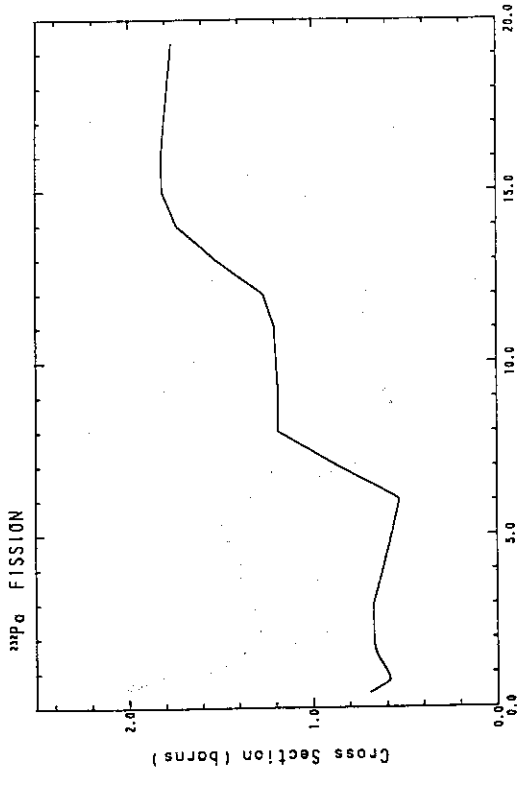

Fig. 34 The fission cross-section of ^{232}Pa.

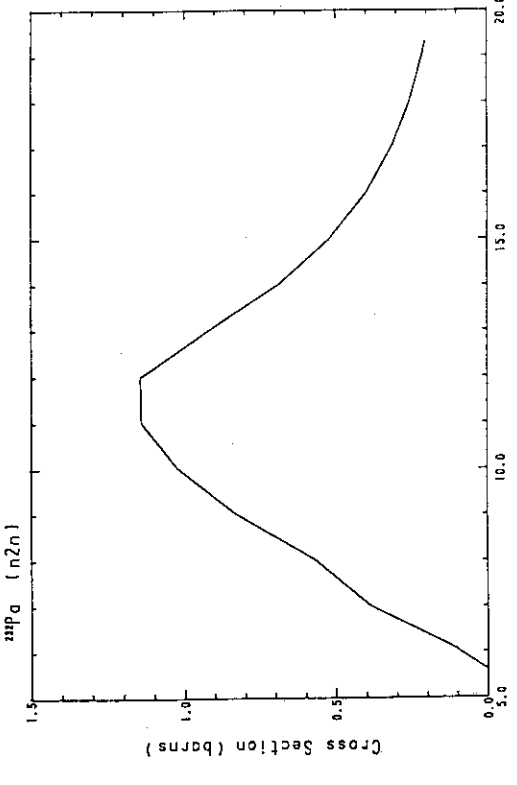

Fig. 35 The (n,2n)-reaction cross-section of ^{232}Pa.

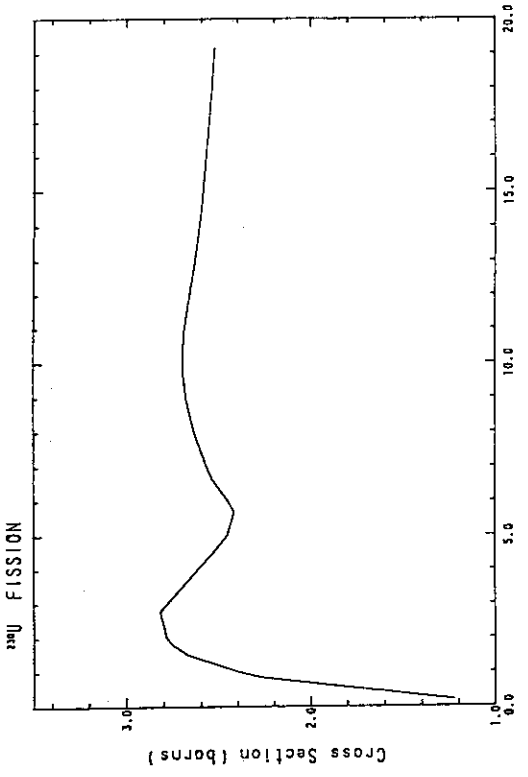

Fig. 40 The fission cross-section of ^{230}U.

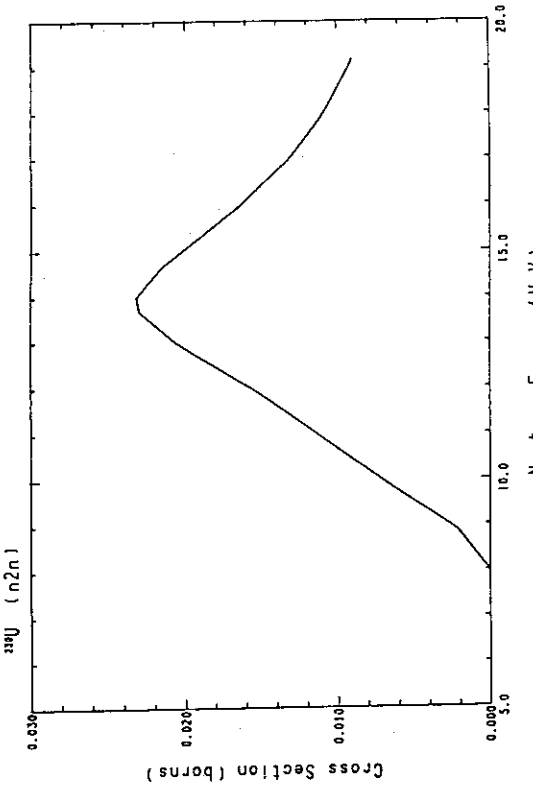

Fig. 41 The (n,2n)-reaction cross-section of ^{230}U.

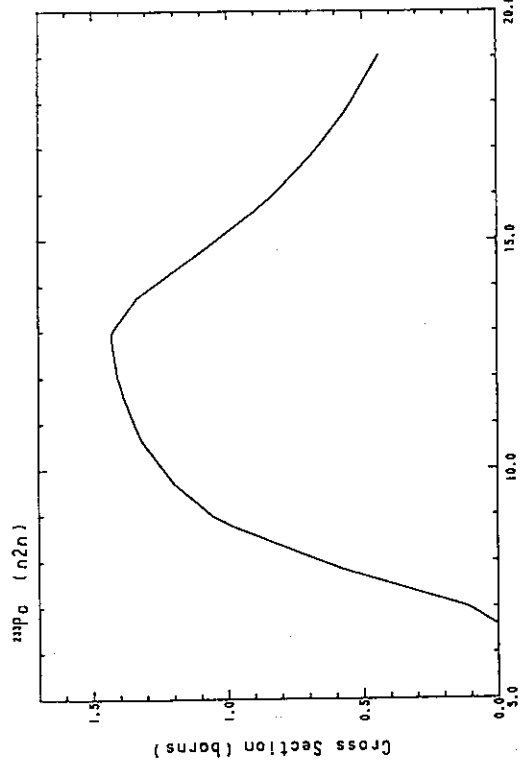

Fig. 38 The (n,2n)-reaction cross-section of ^{233}Pa.

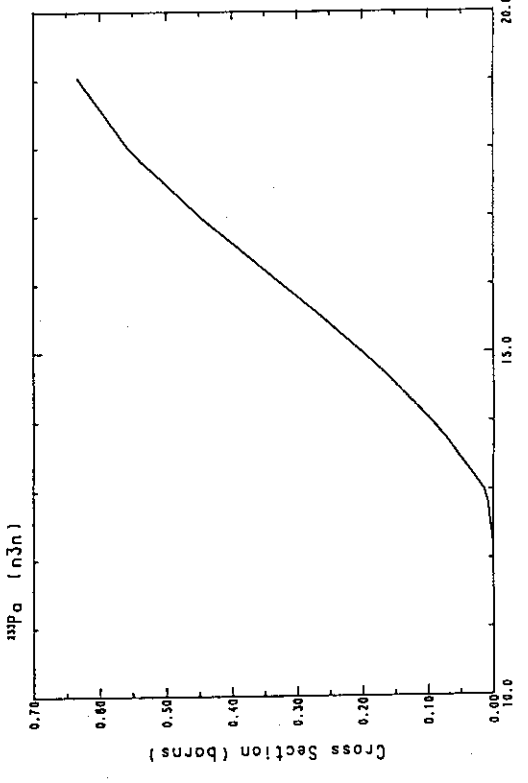

Fig. 39 The (n,3n)-reaction cross-section of ^{233}Pa.

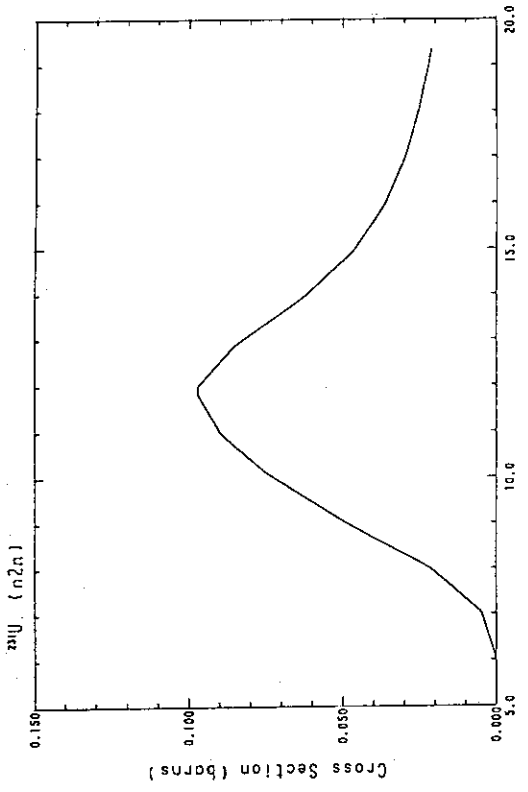

Fig. 44 The (n,2n)-reaction cross-section of ^{231}U.

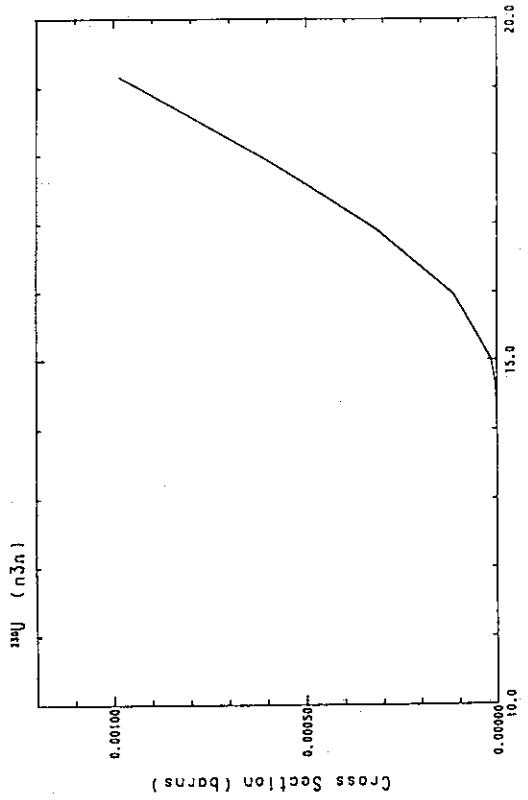

Fig. 42 The (n,3n)-reaction cross-section of ^{230}U.

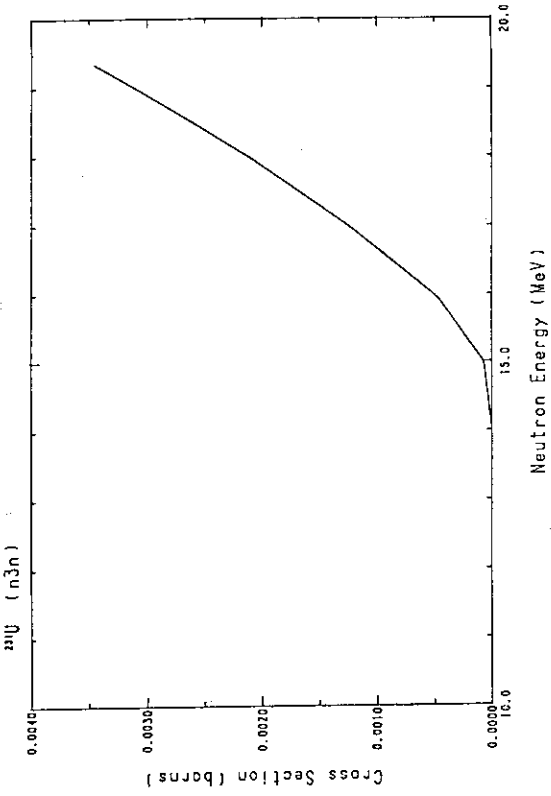

Fig. 45 The (n,3n)-reaction cross-section of ^{231}U.

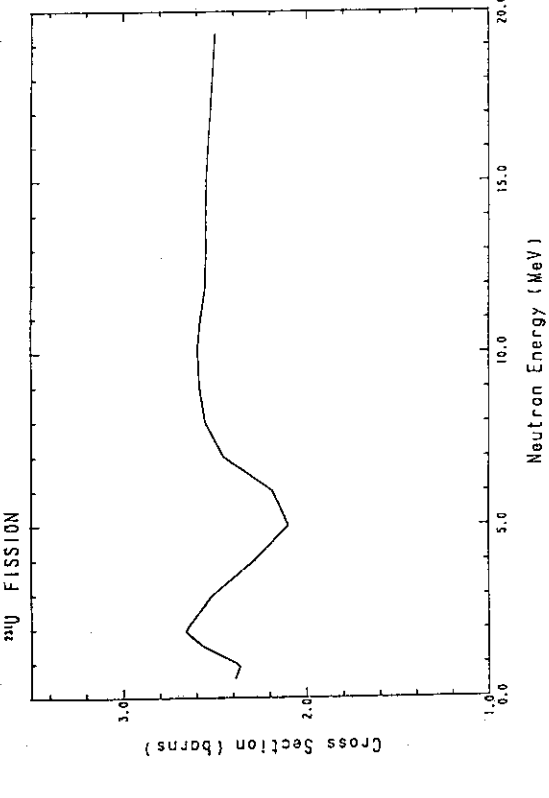

Fig. 43 The fission cross-section of ^{231}U.

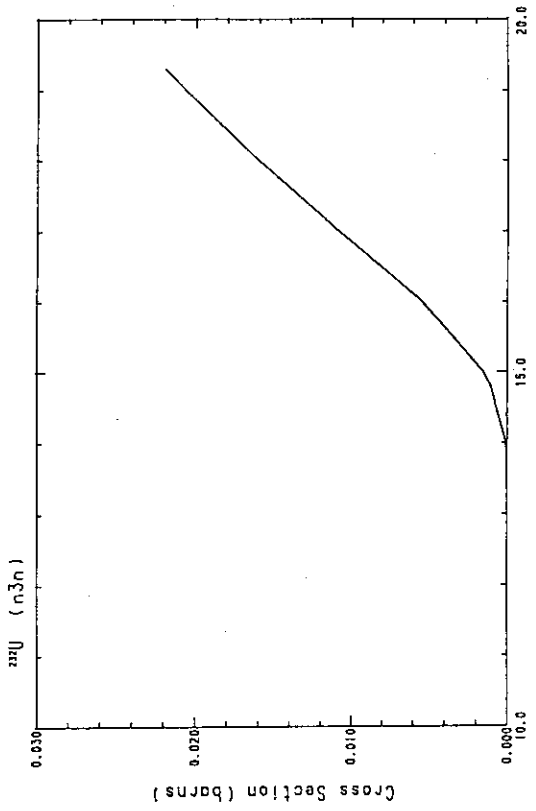

Fig. 48 The (n,3n)-reaction cross-section of ^{232}U.

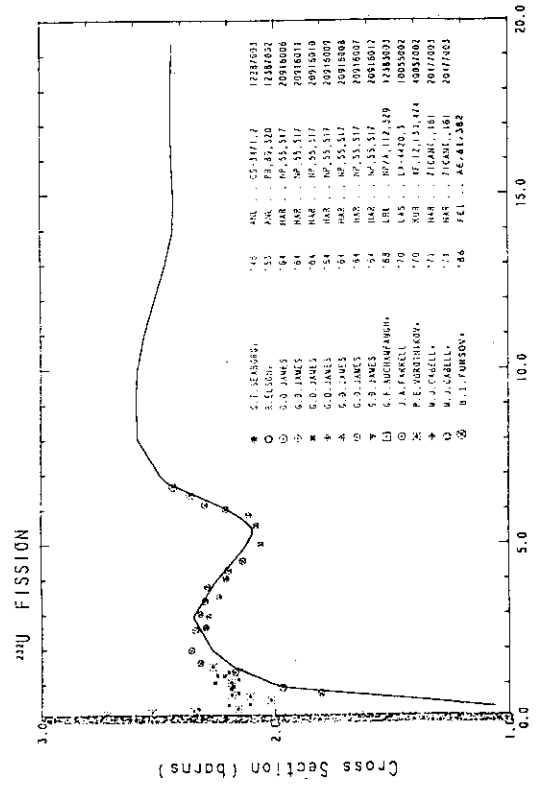

Fig. 46 The fission cross-section of ^{232}U.

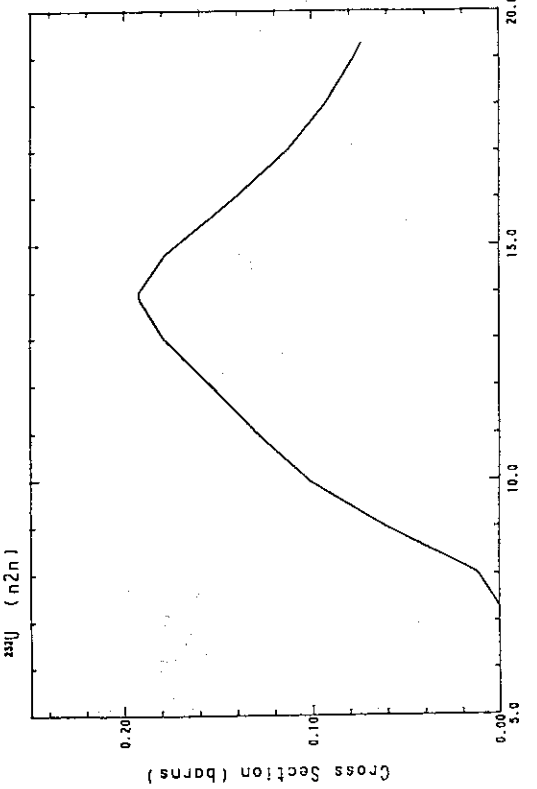

Fig. 47 The (n,2n)-reaction cross-section of ^{232}U.

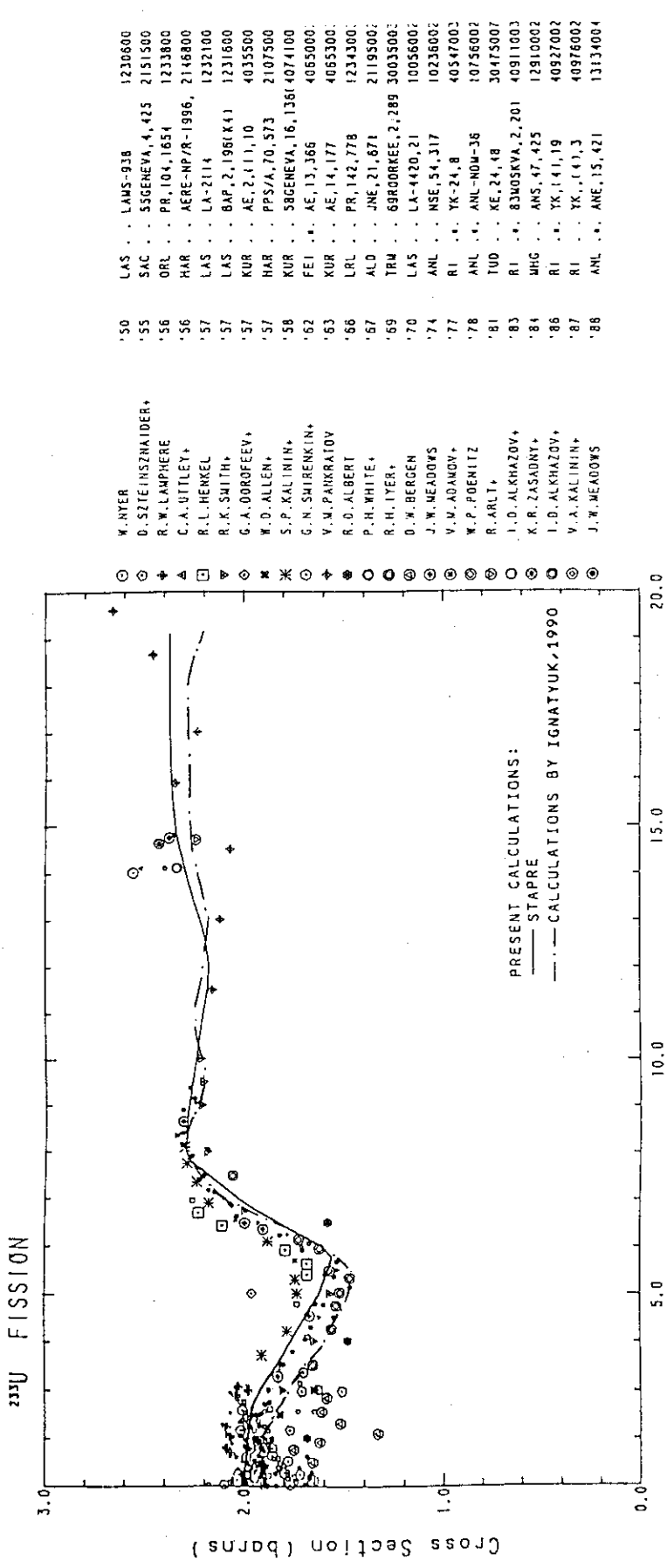

Fig. 49 The fission cross-section of ^{233}U.

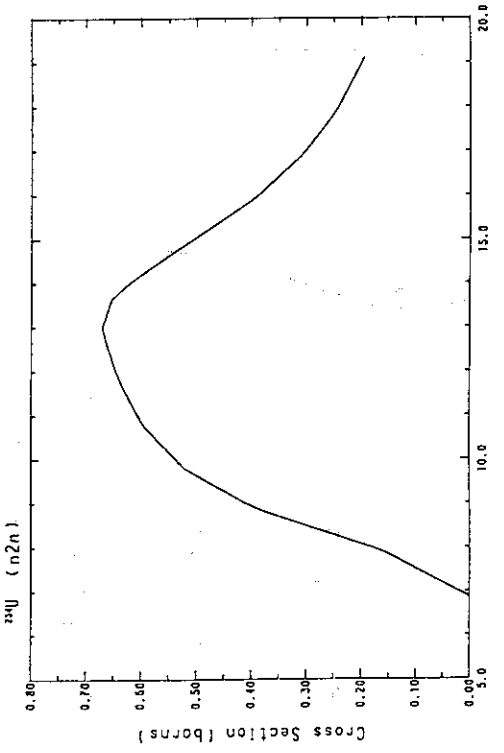

Fig. 52 The (n,2n)-reaction cross-section of ^{234}U.

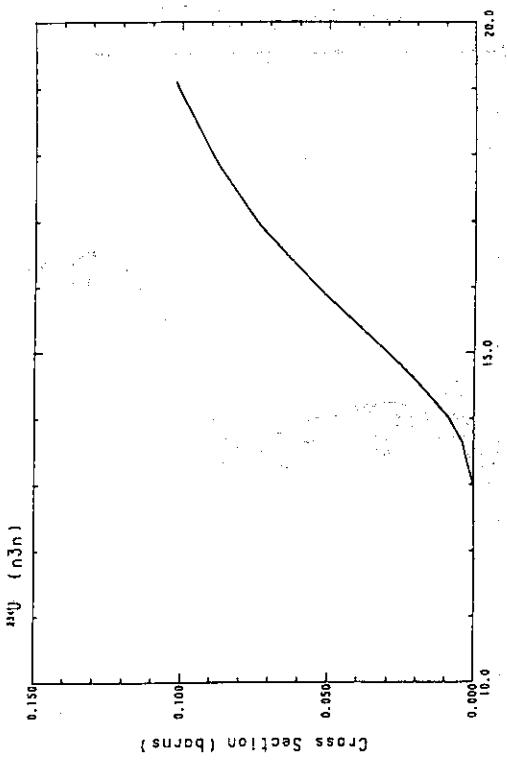

Fig. 53 The (n,3n)-reaction cross-section of ^{234}U.

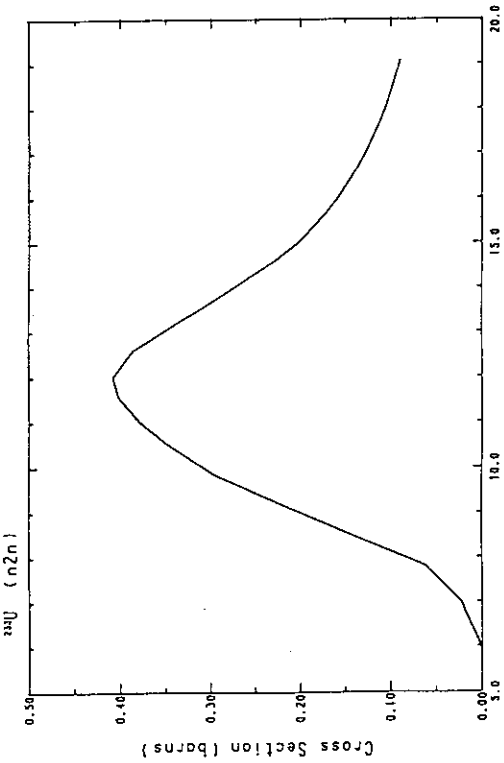

Fig. 50 The (n,2n)-reaction cross-section of ^{233}U.

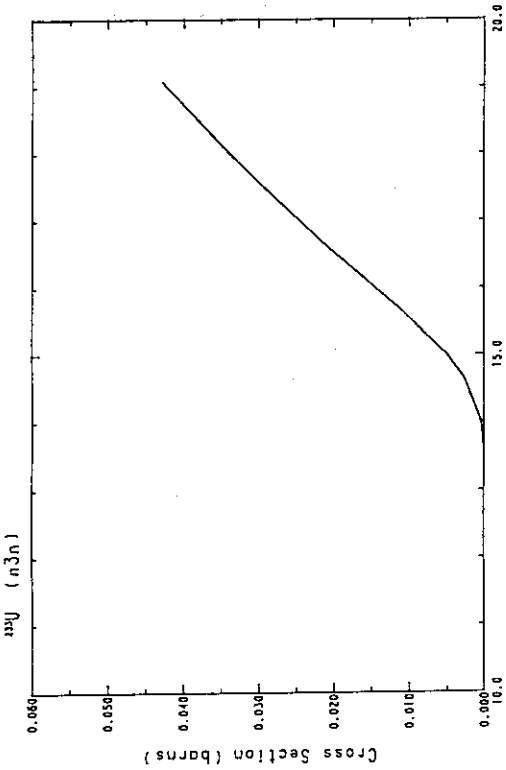

Fig. 51 The (n,3n)-reaction cross-section of ^{233}U.

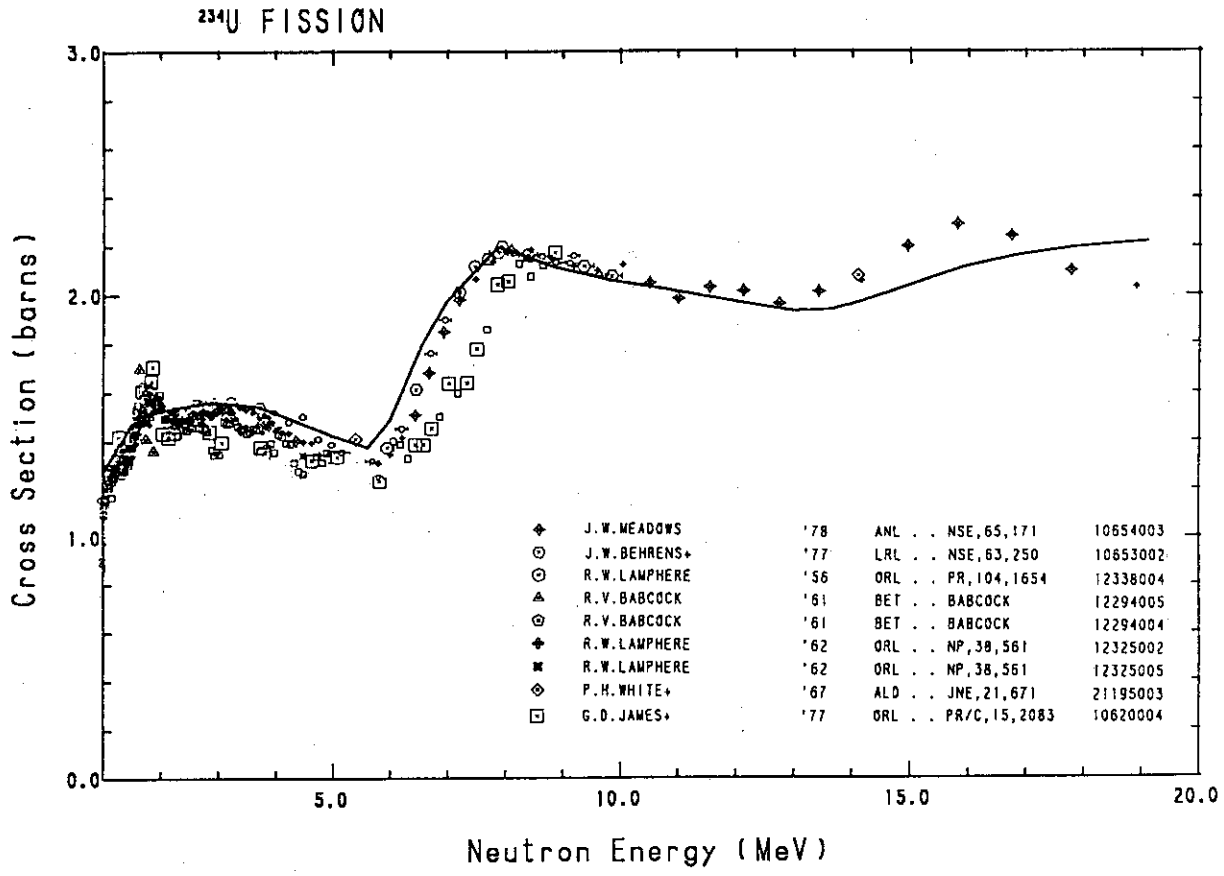

Fig. 54 The fission cross-section of ^{234}U.

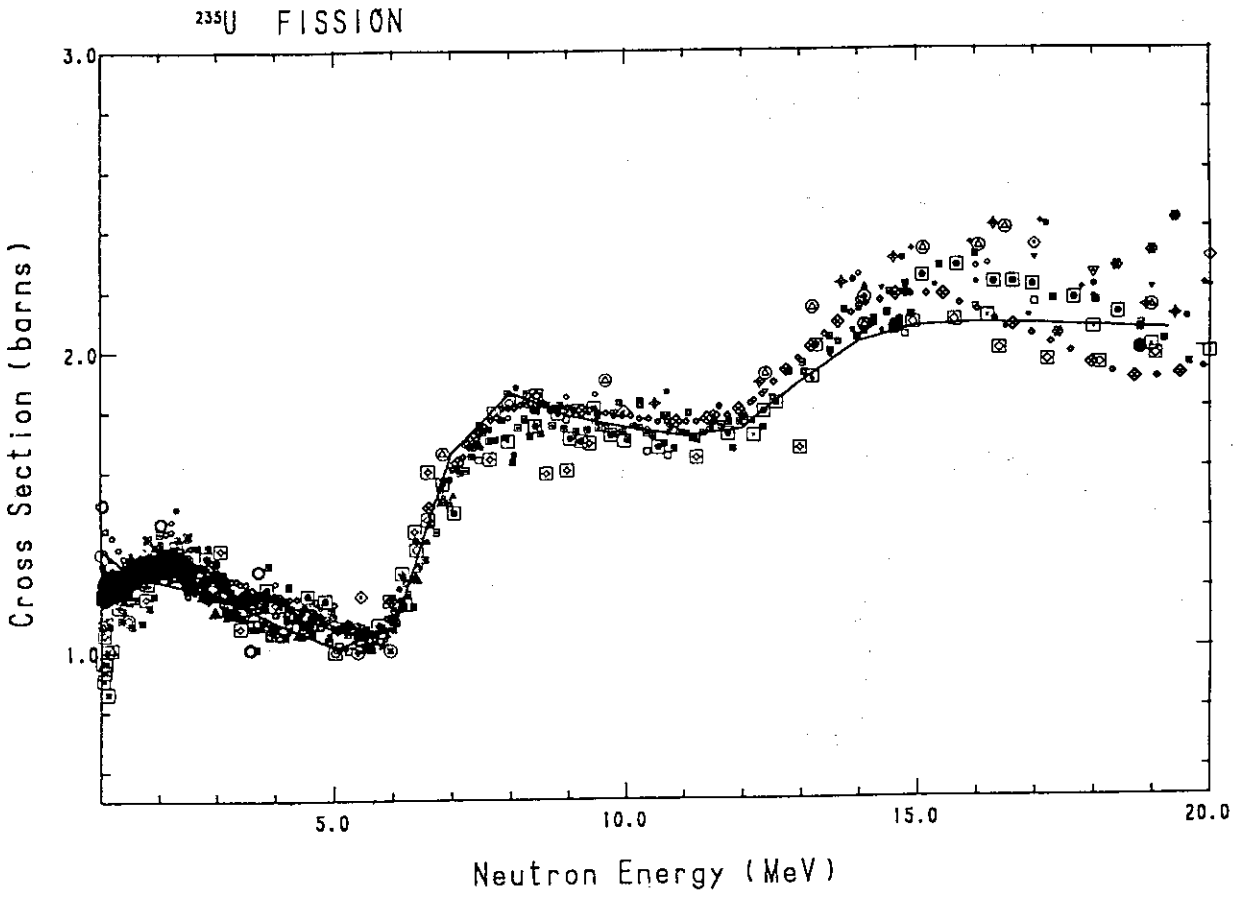

NEUTRON CROSS SECTION
235U FISSION
ENERGY 1.00(MeV) - 20.00(MeV)

						W.P.POENITZ	'74	ANL . .	NSE,53,370	10333005
						W.P.POENITZ	'74	ANL . .	NSE,53,370	10333002
⊙	J.H.WILLIAMS	'44	LAS . .	LA-150	12300003	J.B.CZIRR+	'75	LRL .+.	NSE,58,371	10558002
⊙	W.NYER	'50	LAS . .	LANS-938	12306004	E.MIGNECO+	'75	GEL . .	ISNASH,607	20783002
▲	J.S.WAHL+	'54	LAS . .	LA-1681	12437002	I.SZABO+	'76	CAD . .	76ANL,208	20567002
✚	C.A.UTTLEY+	'56	HAR . .	AERE-NP/R-1995,	21468003	I.SZABO+	'76	CAD . .	76ANL,208	20570002
⊙	B.C.DIVEN	'57	LAS . .	PR,105,1350	12415002	O.M.BARTON+	'76	LAS . .	NSE,60,369	10346003
✳	R.L.HENKEL	'57	LAS . .	LA-2114	12321004	D.M.BARTON+	'76	LAS . .	NSE,60,369	10346002
⊡	R.K.SMITH+	'57	LAS . .	BAP,2,196(K41	12316010	B.LEUGERS+	'76	KFK . .	76ANL,246	20943002
▼	R.K.SMITH+	'57	LAS . .	BAP,2,196(K41	12316005	W.W.OSTERHAGE	'76	GLS . .	OSTERHAGE	20715002
✖	W.D.ALLEN+	'57	HAR . .	PPSA,70,573	21075003	I.SZABO+	'76	CAD . .	76ANL,,	20618002
◈	R.K.SMITH+	'57	LAS . .	BAP,2,196(K41	12316003	V.M.ADAMOV+	'77	RI .+.	YK-24,8	40547005
✦	V.M.PANKRATOV+	'60	KUR .+.	AE,9,399	40638004	W.P.POENITZ	'77	ANL .+.	NSE,64,894	10711002
○	R.BALLINI+	'61	SAC . .	CEA-1913	21093002	W.MEILING+	'78	TUD . .	KE,21,191,292	30461002
●	B.ADAMS+	'61	ALD . .	JNE,14,85	21209003	A.D.CARLSON+	'78	NBS . .	78HARWELL,,880	12848003
○	G.N.SMIRENKIN+	'62	FEI .+.	AE,13,366	40650004	A.D.CARLSON+	'78	NBS . .	78HARWELL,,880	12848002
⊛	V.M.PANKRATOV	'63	KUR . .	AE,14,177	40653005	X.KARI+	'78	KFK . .	78BNL,	20786006
⊛	P.H.WHITE	'65	ALD . .	JNE,19,325	21190002	M.CANCE+	'78	BRC . .	NSE,68,(21,197	20779002
◉	J.A.GRUNOL	'67	LAS .+.	NSE,30,39	10417002	B.M.ALEKSANDROV+	'79	RI . .	AE,46,161,416	40546003
⊛	W.P.POENITZ	'68	ANL . .	68WASH,1,503(	05,12401002	R.ARLT+	'81	TUD . .	KE,24,46	30475002
◉	R.H.IYER+	'69	TRM . .	69ROORKEE,2,289	30035004	M.CANCE+	'81	BRC . .	CEA-N-2194	21620002
○	J.O.CRAMER	'70	LAS . .	LA-4420,45	10057002	O.A.WASSON+	'82	NBS .+.	NSE,80,282	10971002
⊛	D.B.GAYTHER+	'72	HAR . .	72VIENNA,201	20422002	M.MAHDAVI+	'82	WHG . .	82ANTWER,,58	12826002
◉	H.-H.KNITTER+	'72	GEL . .	ZP,257,108	20394006	LI JING-WEN+	'82	AEP . .	82ANTWER,,55	30634002
⊡	I.M.KUKS+	'73	RI . .	73KIEV,4,18	40258002	I.D.ALKHAZOV+	'83	RI .+.	83MOSKVA,2,201	40911002
◉	F.KAEPPELER	'73	KFK . .	KFK-1772	20356003	A.D.CARLSON+	'84	NBS .+.	CARLSON	10987002
⊛	F.KAEPPELER	'73	KFK . .	KFK-1772	20356002	C.M.HERBACH+	'85	TUD .+.	IP,21,344	30706003
⊡	W.P.POENITZ	'74	ANL . .	NSE,53,370	10333007	T.IWASAKI+	'86	TOH . .	86MITO,87	22091002
○	C.M.HERBACH+	'85	TUD .+.	IP,21,344	30706002	I.D.ALKHAZOV+	'86	RI . .	86MITO,,145	41013004
◉	R.ARLT+	'85	TUD . .	IP,21,344	30559002	I.D.ALKHAZOV+	'86	RI .+.	86MITO,,145	41013003
⊛	R.ARLT+	'85	TUD . .	IP,21,344	30558002	Y.A.KALININ+	'86	RI .+.	AE,64,(3),194	40963002
◉	I.D.ALKHAZOV+	'86	RI .+.	YK,(41),19	40927003	R.G.JOHNSON+	'91	MIS .+.	CARLSON	12924002
○	LI JINGWEN+	'86	AEP . .	INDC(CPR)-009/L,	30721002					

Fig. 55 The fission cross-section of ^{235}U.

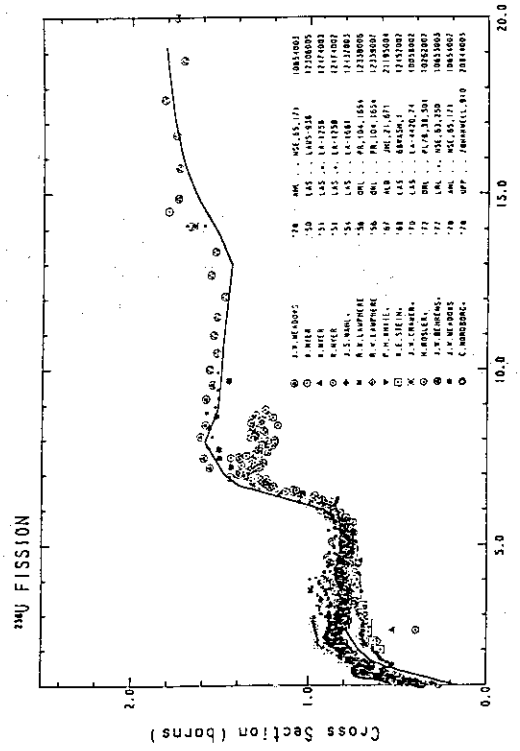

Fig. 58 The fission cross-section of ^{235}U.

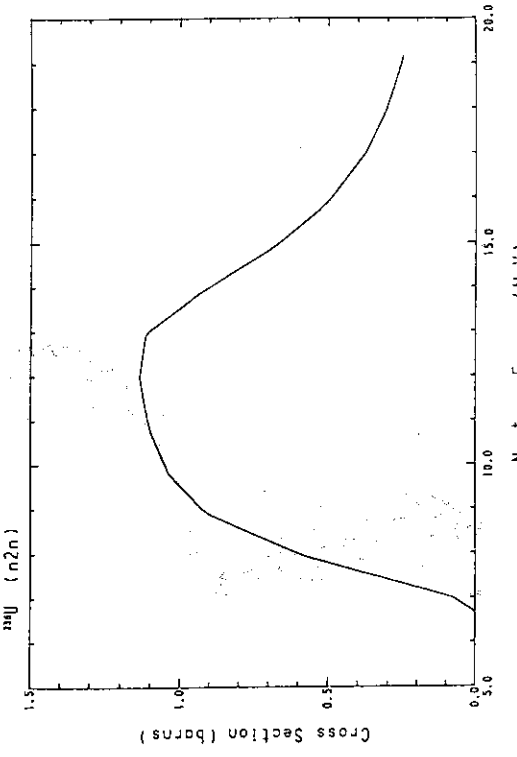

Fig. 59 The (n,2n)-reaction cross-section of ^{235}U.

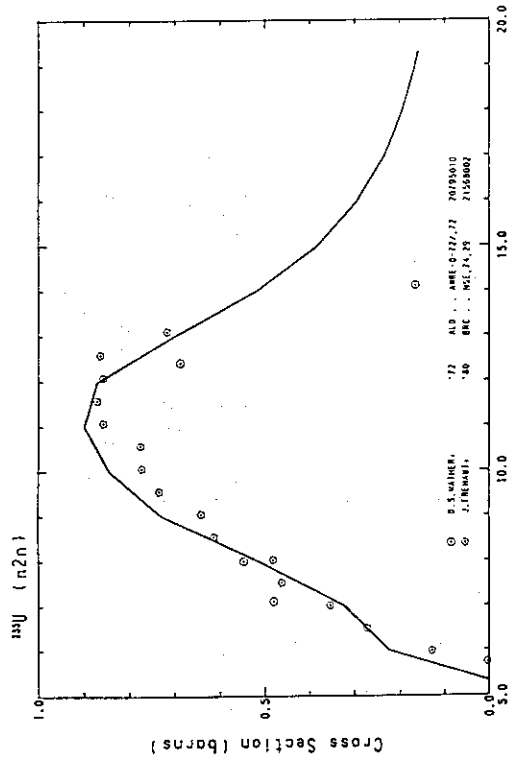

Fig. 56 The (n,2n)-reaction cross-section of ^{235}U.

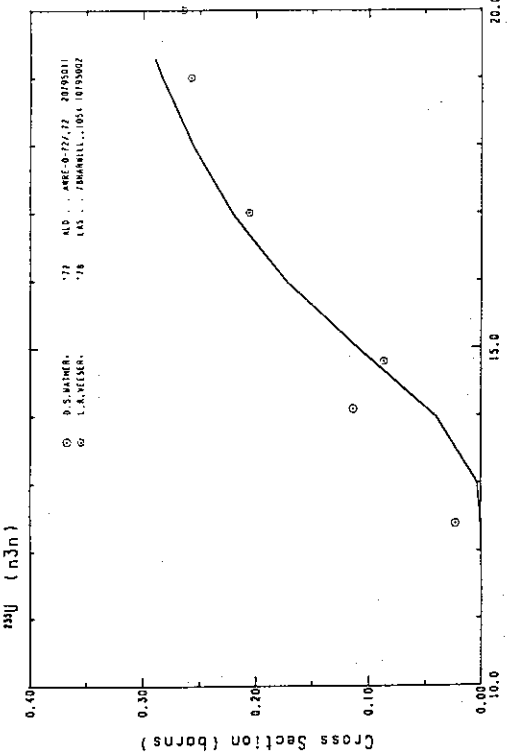

Fig. 57 The (n,3n)-reaction cross-section of ^{235}U.

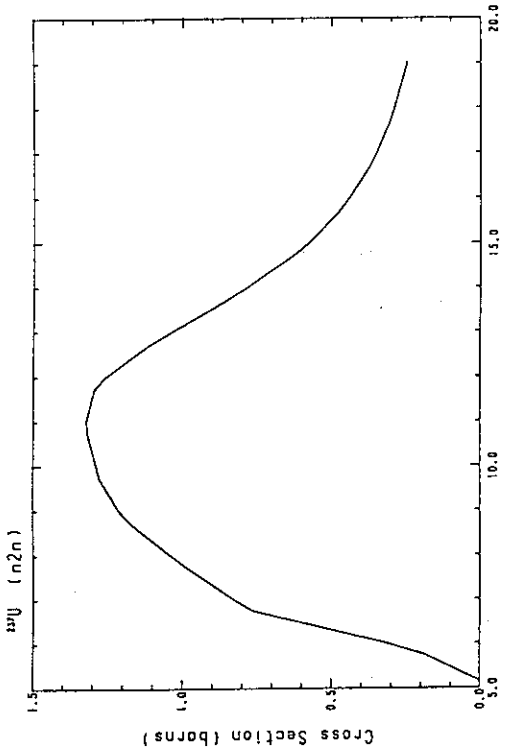

Fig. 62 The (n,2n)-reaction cross-section of ^{238}U.

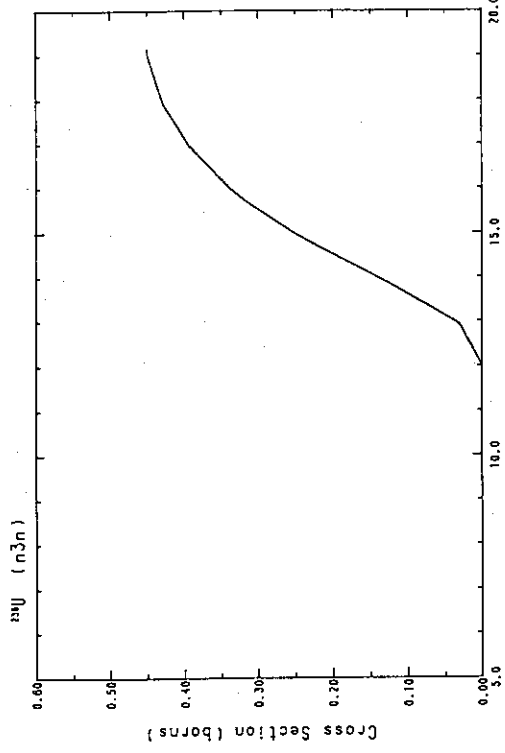

Fig. 60 The (n,3n)-reaction cross-section of ^{238}U.

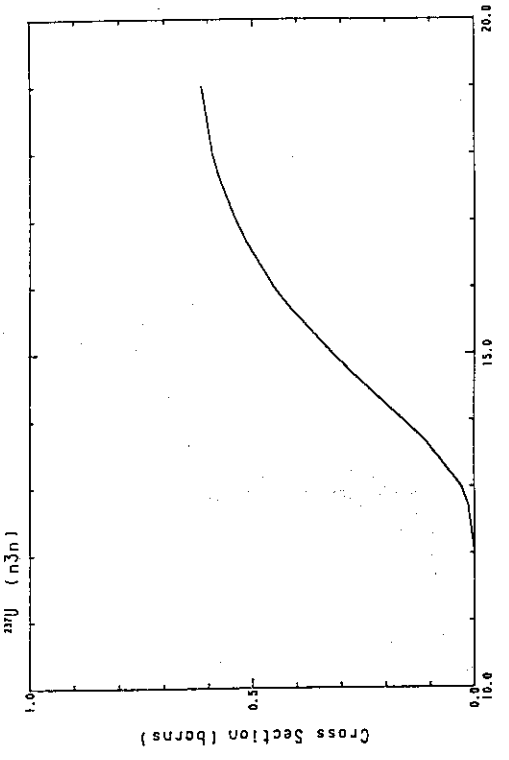

Fig. 63 The (n,3n)-reaction cross-section of ^{237}U.

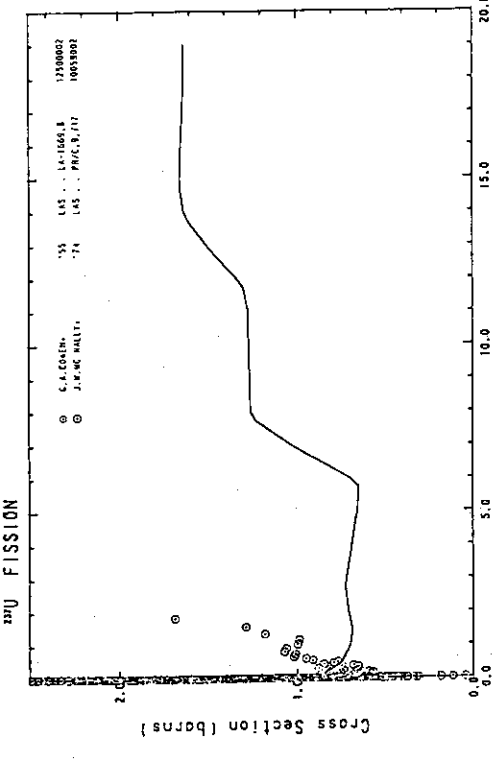

Fig. 61 The fission cross-section of ^{237}U.

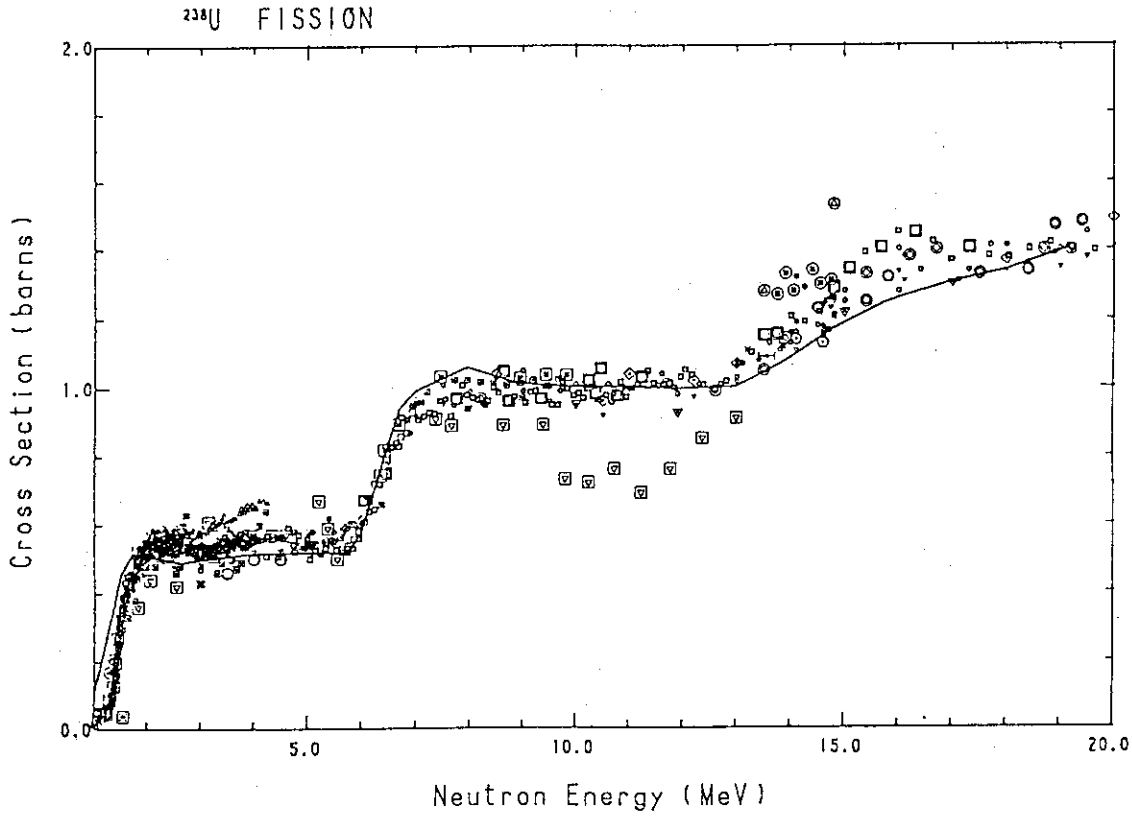

NEUTRON CROSS SECTION
^{238}U FISSION
ENERGY 1.00(MeV) - 20.00(MeV)

					J.W.MEADOWS	'72	ANL . .	NSE,49,310	10237003
					I.O.ALKHAZOV+	'74	RI . .	73KIEV,4,13	40256002
⊙	W.NYER	'48	LAS . .	LA-719	12514002	J+	'75	SAC . .	PRL,35,1749	20795003
+	R.W.LAMPHERE	'56	ORL . .	PR,104,1654	12338008	J.W.MEADOWS	'75	ANL . .	NSE,58,255	10506002
△	R.W.LAMPHERE	'56	ORL . .	PR,104,1654	12338005	B.LEUGERS+	'76	KFK . .	76ANL,246	20943003
✳	M.D.GOLDBERG+	'57	LRL . .	WASH-745,31	12468002	W.W.OSTERHAGE	'76	GLS . .	OSTERHAGE	20715003
⊙	C.A.UTTLEY+	'56	HAR . .	AERE-NP/R-1996,	21468002	P.E.VOROTNIKOV+	'77	KUR .+.	77KIEV,3,239	40483002
⊡	R.L.HENKEL	'57	LAS . .	LA-2114	12321005	V.M.ADAMOV+	'77	RI .+.	YK-24,8	40547007
▽	R.K.SMITH+	'57	LAS . .	BAP,2,195(K4)	12316011	M.CANCE+	'78	BRC . .	NSE,68,(2),197	20779003
◇	R.K.SMITH+	'57	LAS . .	BAP,2,195(K4)	12316006	B.M.ALEKSANDROV+	'79	RI . .	AE,46,(6),416	40546004
✖	W.D.ALLEN+	'57	HAR . .	PPS/A,70,573	21075004	R.ARLT+	'81	TUD . .	KE,24,48	30475003
✱	P.BILLAUD+	'58	SAC . .	58GENEVA,16,106	21452002	I.O.ALKHAZOV+	'83	TUD .+.	83MOSKVA,2,201	40911005
✦	S.P.KALININ+	'58	KUR . .	58GENEVA,16,(36(	40741005	I.O.ALKHAZOV+	'83	RI .+.	83MOSKVA,2,201	40911004
⊙	N.N.FLEROV+	'58	CCP . .	AE,5,(6),657	40424002	I.GARLEA+	'83	PIT . .	INDC(ROM)-15	30647008
○	V.M.PANKRATOV+	'60	KUR .+.	AE,9,399	40638005	WU JING-XIA+	'83	AEP . .	CNP,5,(2),158	30669002
⊛	R.BALLINI+	'61	SAC . .	CEA-1913	21093003	I.GARLEA+	'84	PIT . .	RRP,29,421	30813008
⊛	A.KATASE	'61	KYU . .	KATASE	20299003	I.O.ALKHAZOV+	'88	RI . .	BBWITO,,145	41013002
○	B.ADAMS+	'61	ALD . .	JNE,14,85	21209002	J.W.MEADOWS	'88	ANL .+.	ANE,15,421	13134007
⊛	V.M.PANKRATOV	'63	KUR . .	AE,14,177	40653006	J.W.MEADOWS+	'89	ANL . .	ANE,16,471	13169002
⊛	M.MANGIALAJO+	'63	CIS . .	NP,43,124	21127002	J.W.MEADOWS+	'89	ANL . .	ANE,16,471	13169003
○	V.EMMA+	'65	CAT . .	NP,63,641	21134002					
⊛	R.BATCHELOR+	'65	ALD . .	NP,65,236	21019024					
○	J.A.GRUNOL	'67	LAS .+.	NSE,30,39	10417004					
⊛	P.H.WHITE+	'67	ALD . .	JNE,21,671	21195005					
⊛	R.C.BARRALL+	'69	STF . .	AFWL-TR-68-134	10022025					
⊛	R.C.BARRALL+	'69	STF . .	AFWL-TR-68-134	10022026					
⊠	P.E.VOROTNIKOV+	'71	KUR . .	YFI-12,22	40110002					
⊠	I.M.KUKS+	'71	RI . .	AE,30,55	40081002					

Fig. 64 The fission cross-section of ^{238}U.

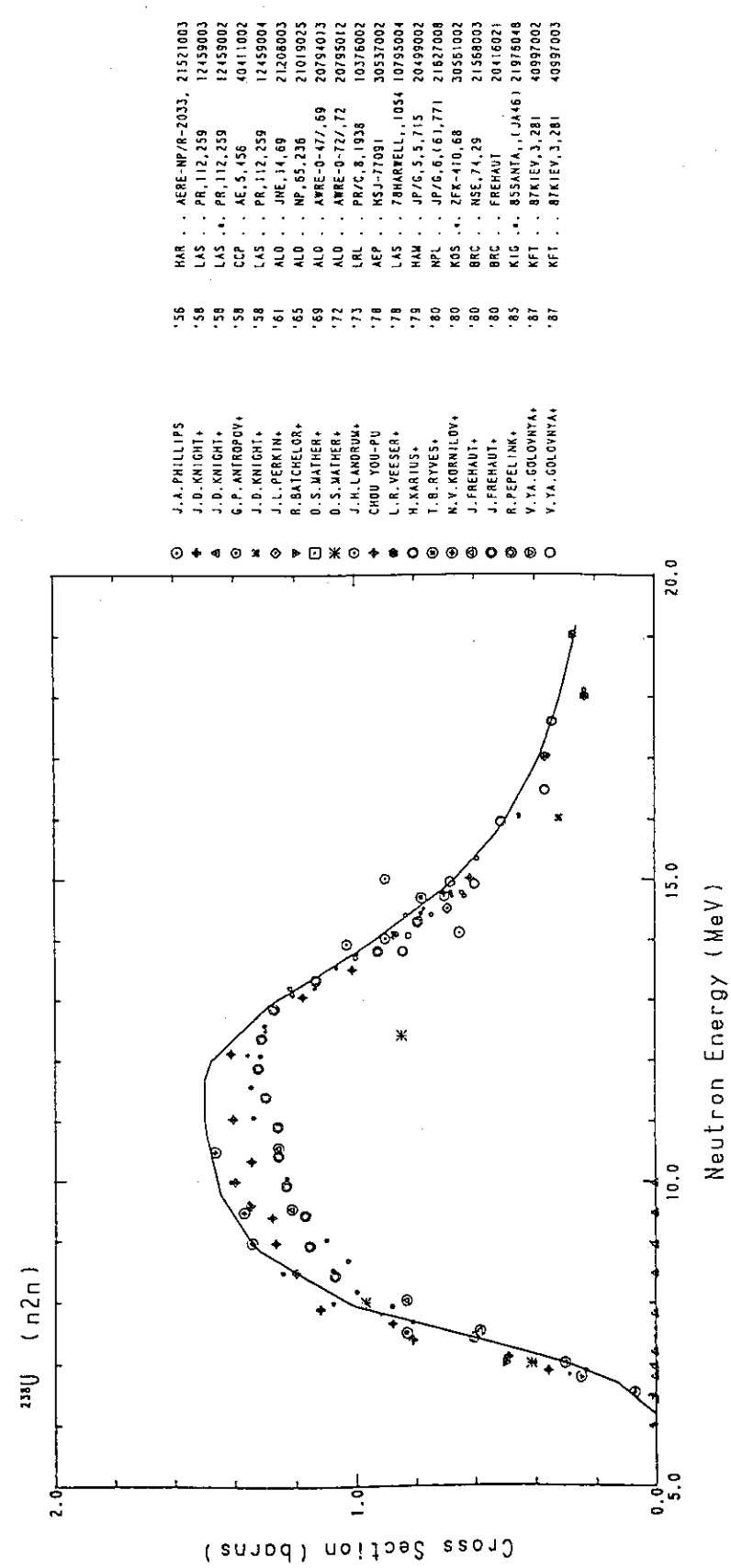

Fig.65 The (n,2n)-reaction cross-section of ^{238}U.

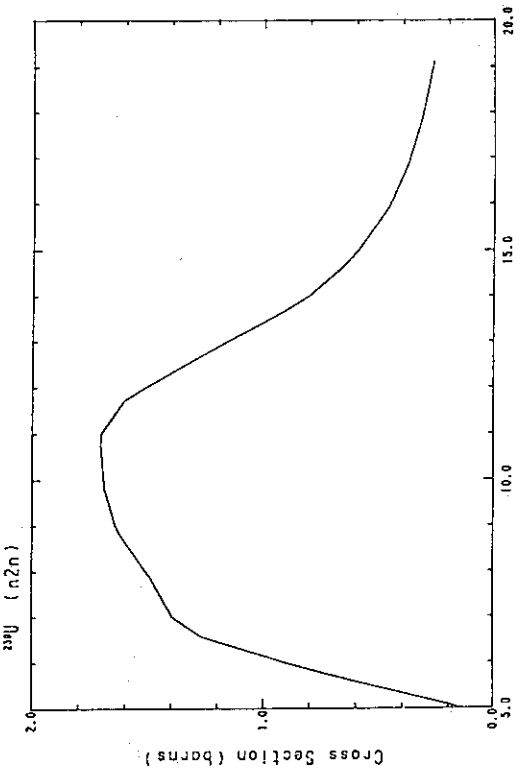

Fig. 68 The (n,2n)-reaction cross-section of ^{238}U.

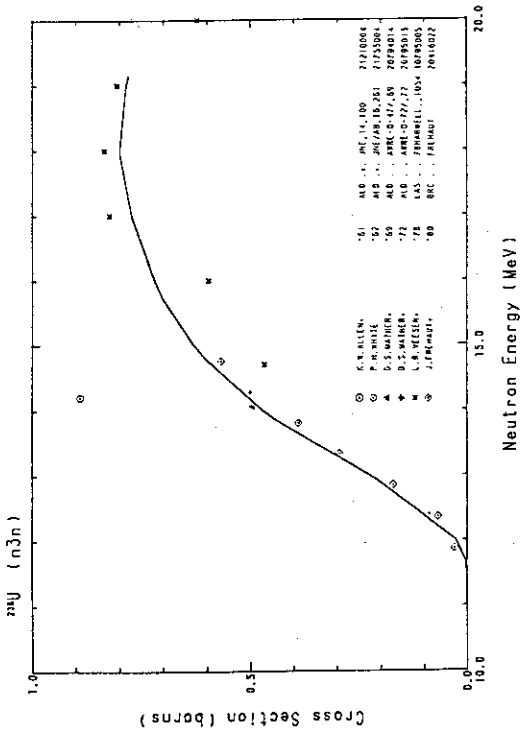

Fig. 66 The (n,3n)-reaction cross-section of ^{238}U.

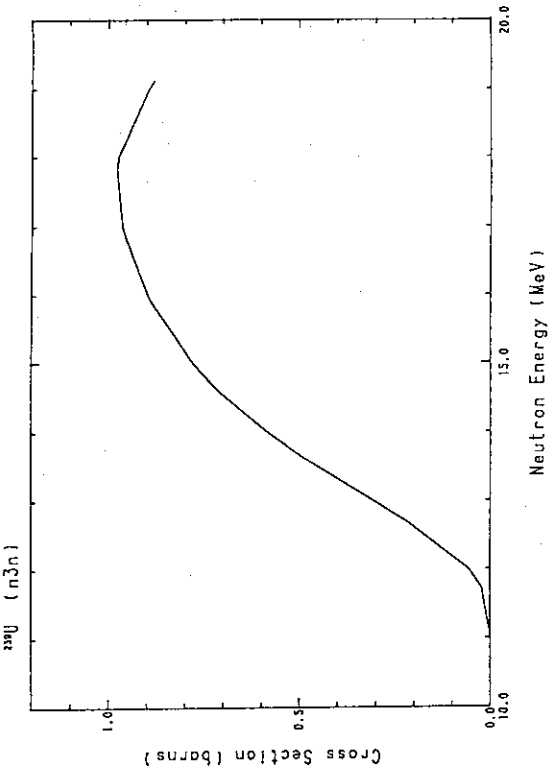

Fig. 69 The (n,3n)-reaction cross-section of ^{239}U.

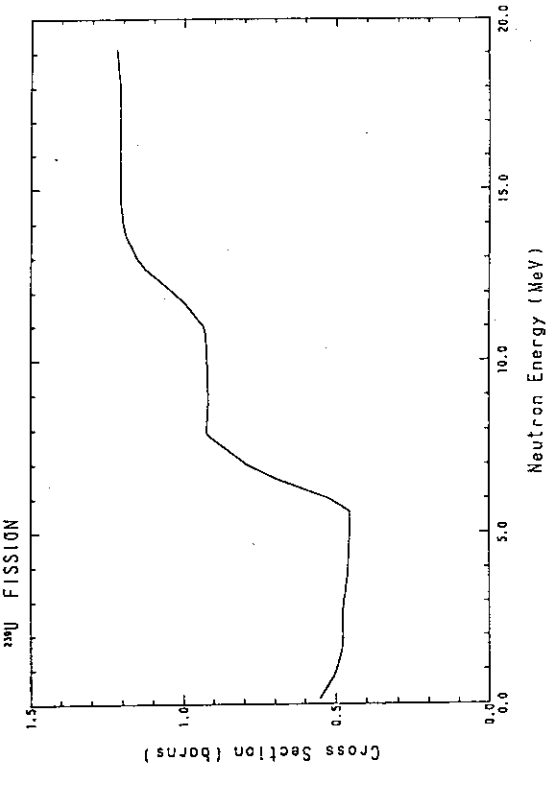

Fig. 67 The fission cross-section of ^{239}U.

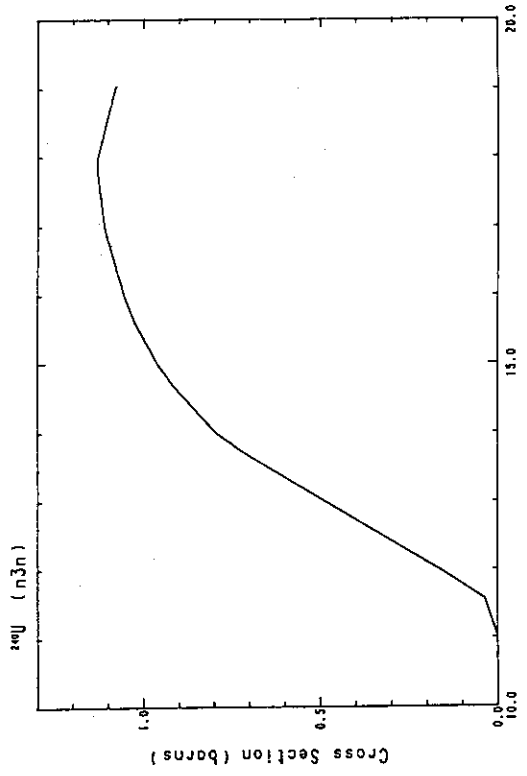

Fig. 72 The (n,3n)-reaction cross-section of ^{240}U.

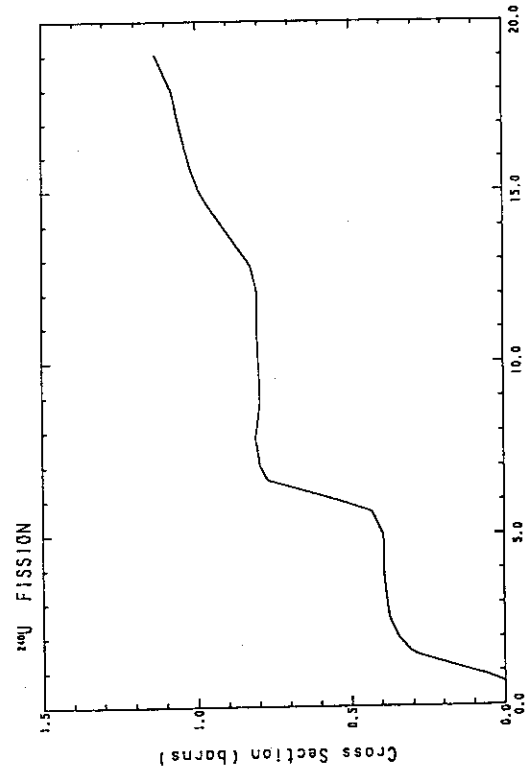

Fig. 70 The fission cross-section of ^{240}U.

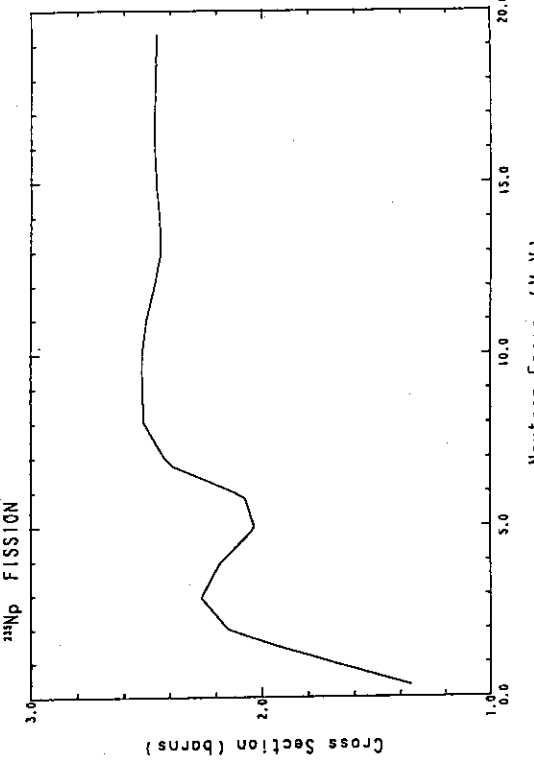

Fig. 73 The fission cross-section of ^{235}Np.

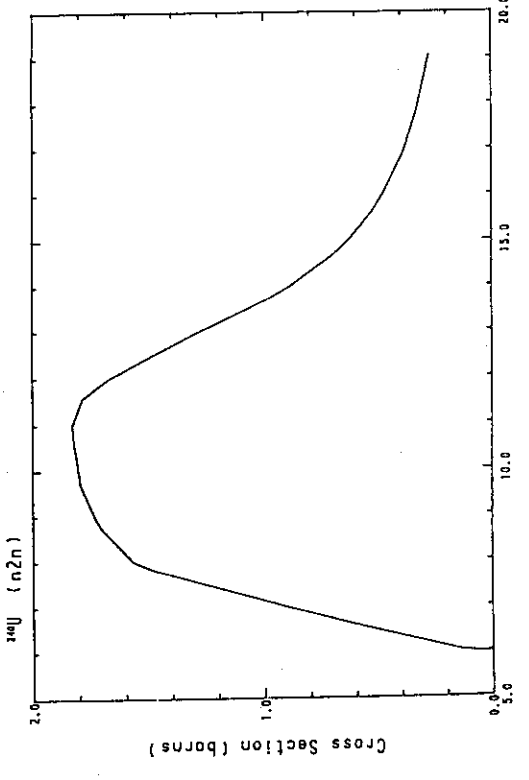

Fig. 71 The (n,2n)-reaction cross-section of ^{240}U.

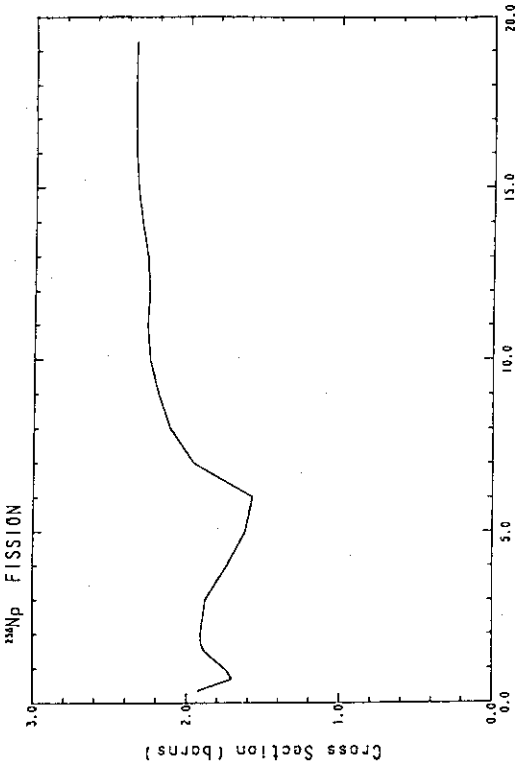

Fig. 76 The fission cross-section of ^{235}Np.

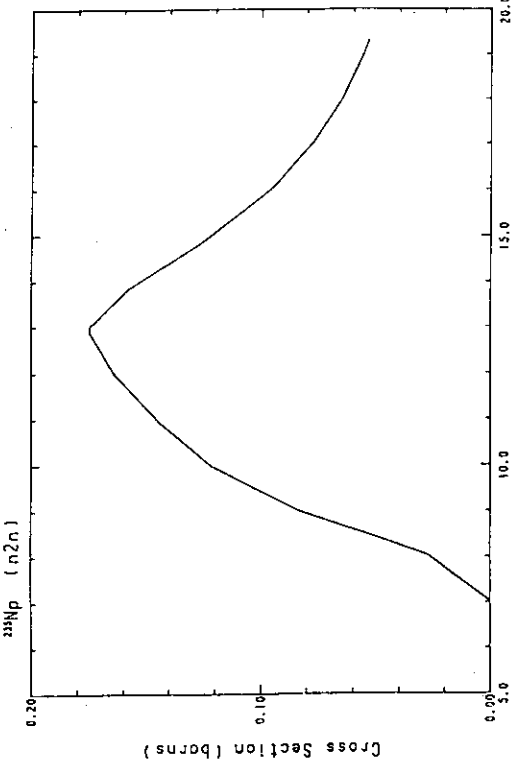

Fig. 74 The (n,2n)-reaction cross-section of ^{235}Np.

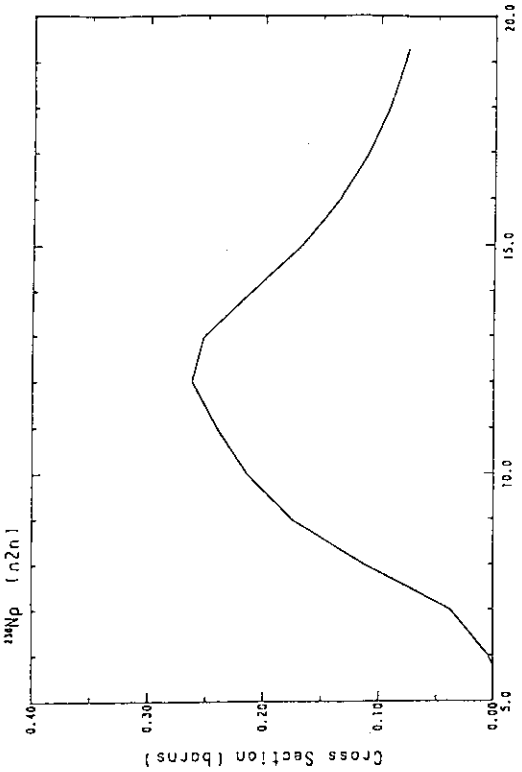

Fig. 77 The (n,2n)-reaction cross-section of ^{236}Np.

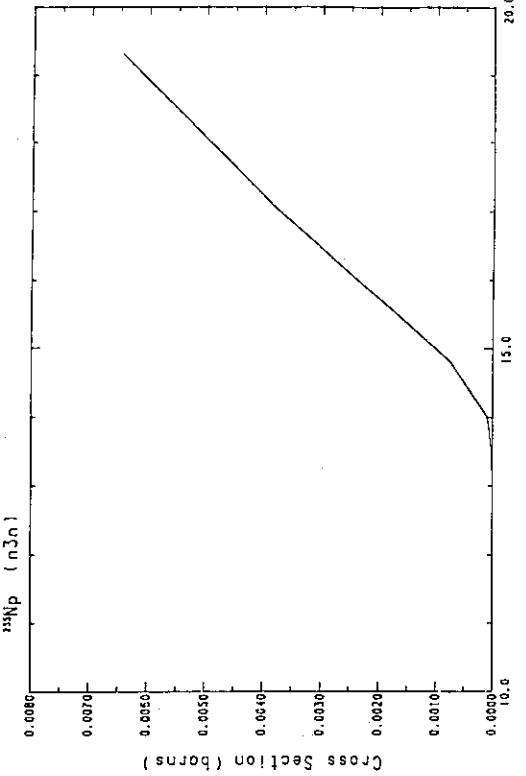

Fig. 75 The (n,3n)-reaction cross-section of ^{235}Np.

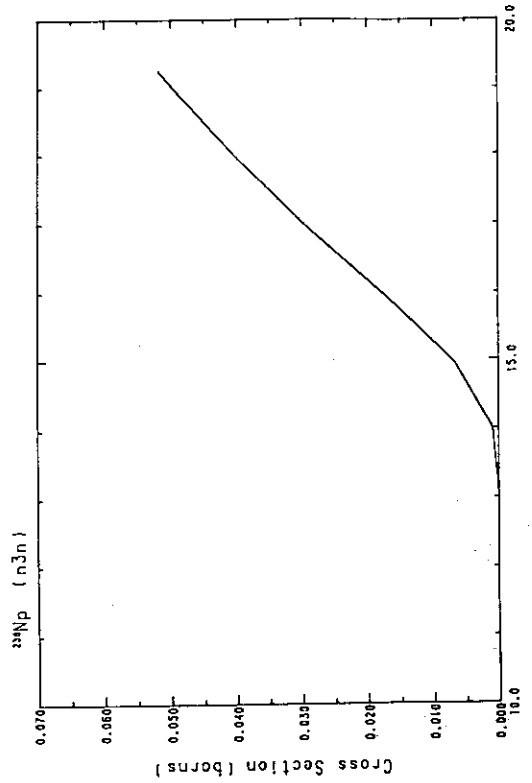

Fig. 78 The (n,3n)-reaction cross-section of ^{236}Np.

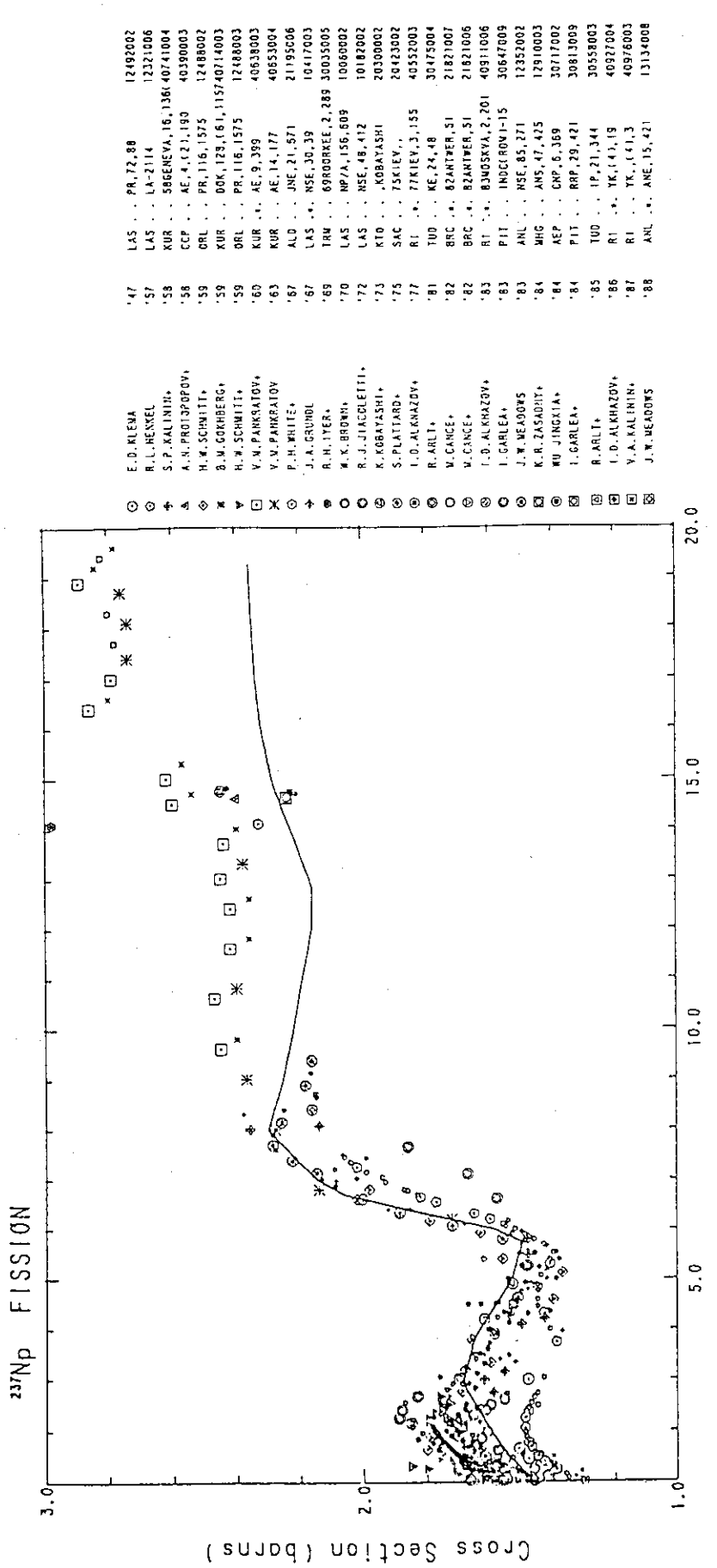

Fig. 79 The fission cross-section of ^{237}Np.

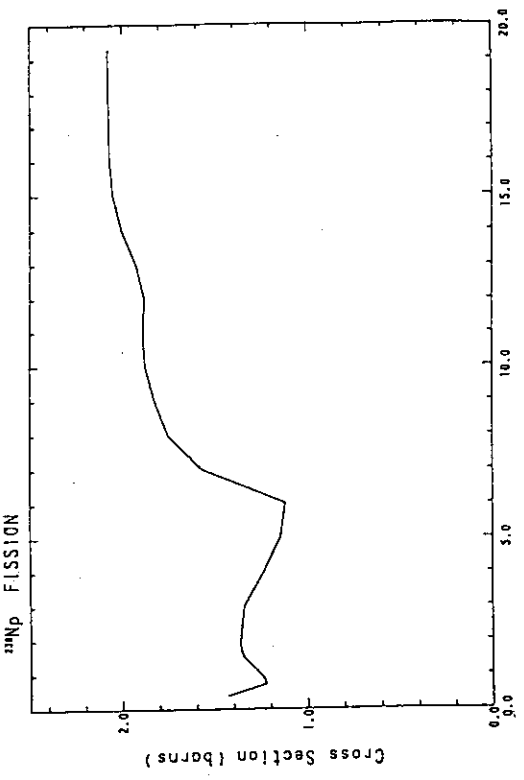

Fig. 82 The fission cross-section of ^{238}Np.

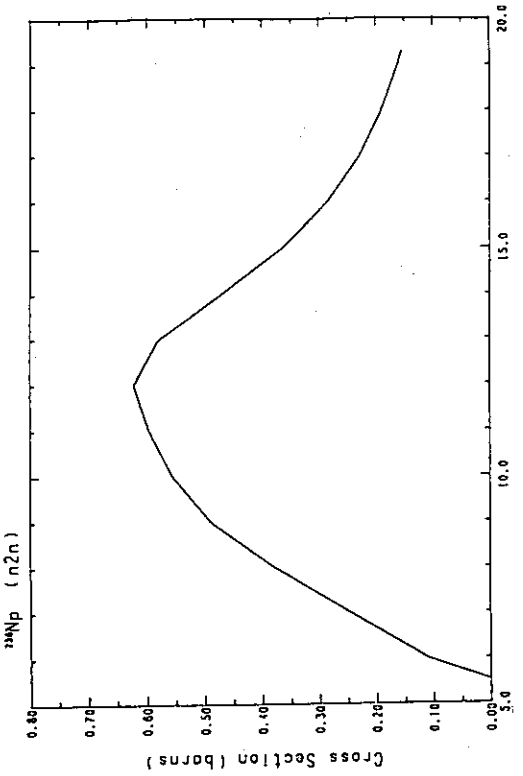

Fig. 83 The (n,2n)-reaction cross-section of ^{238}Np.

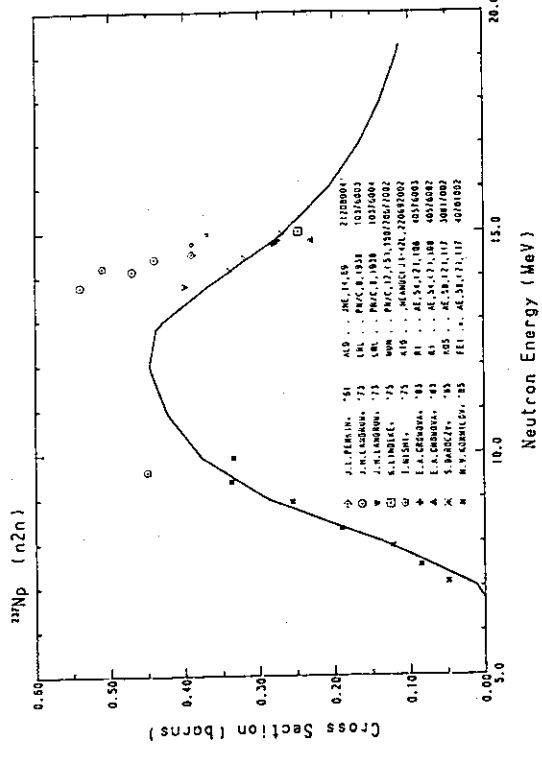

Fig. 80 The (n,2n)-reaction cross-section of ^{237}Np.

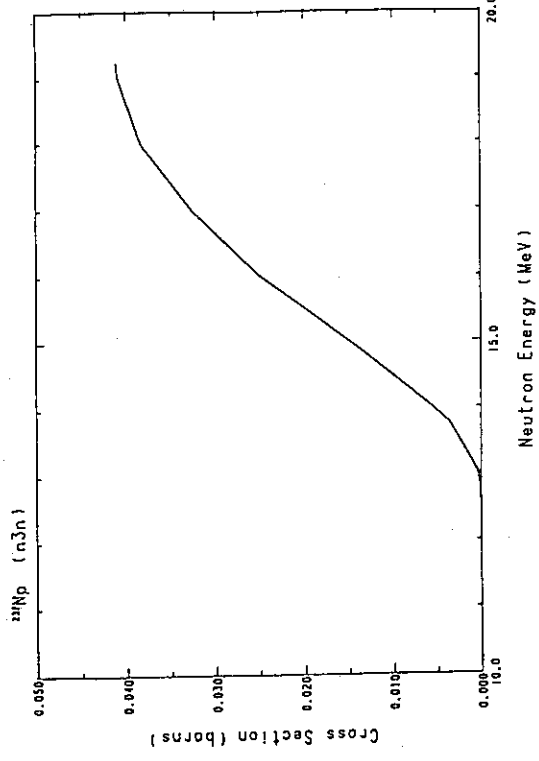

Fig. 81 The (n,3n)-reaction cross-section of ^{237}Np.

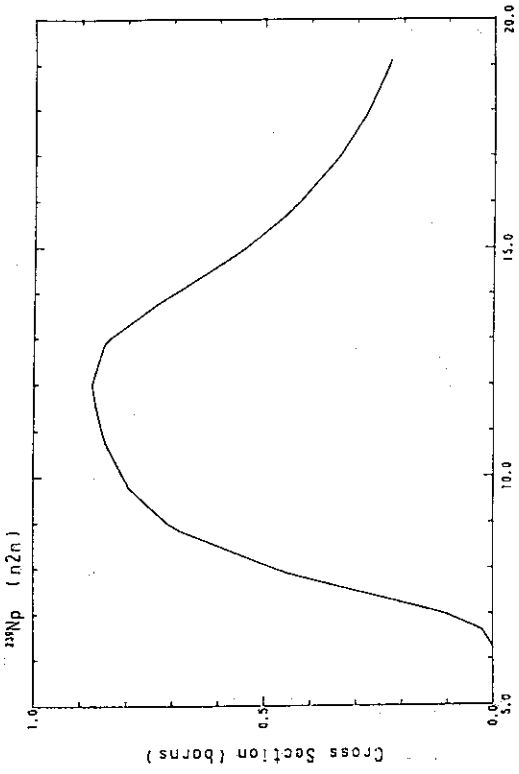

Fig. 86 The (n,2n)-reaction cross-section of ^{239}Np.

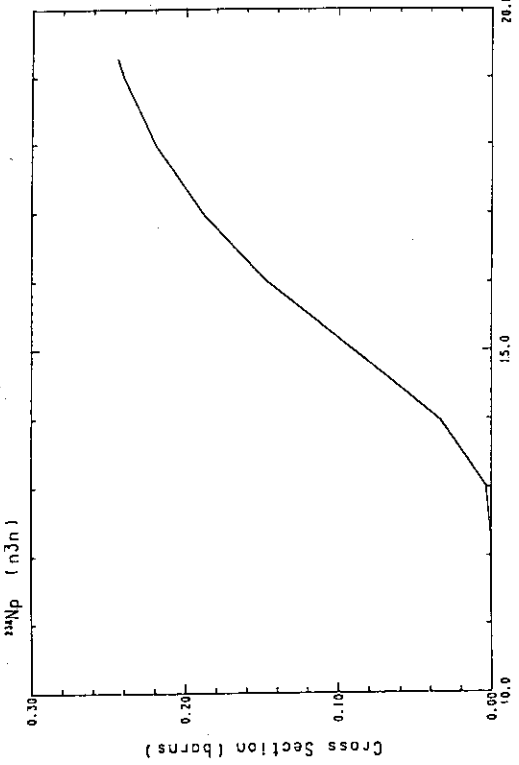

Fig. 84 The (n,3n)-reaction cross-section of ^{238}Np.

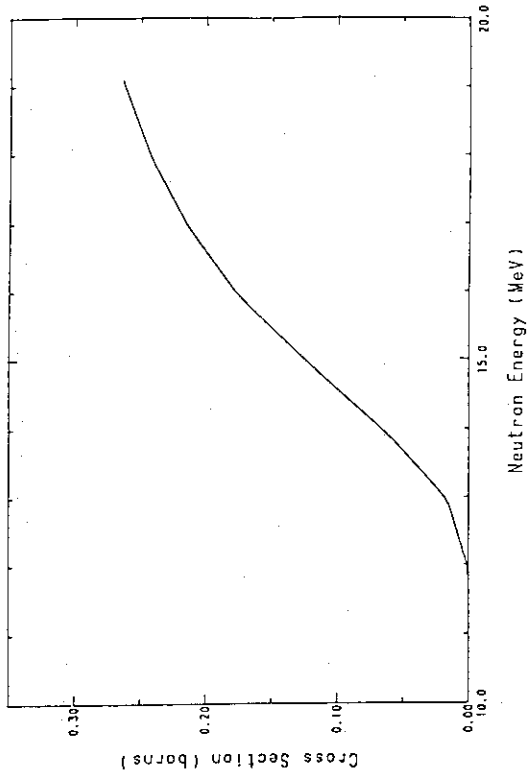

Fig. 87 The (n,3n)-reaction cross-section of ^{239}Np.

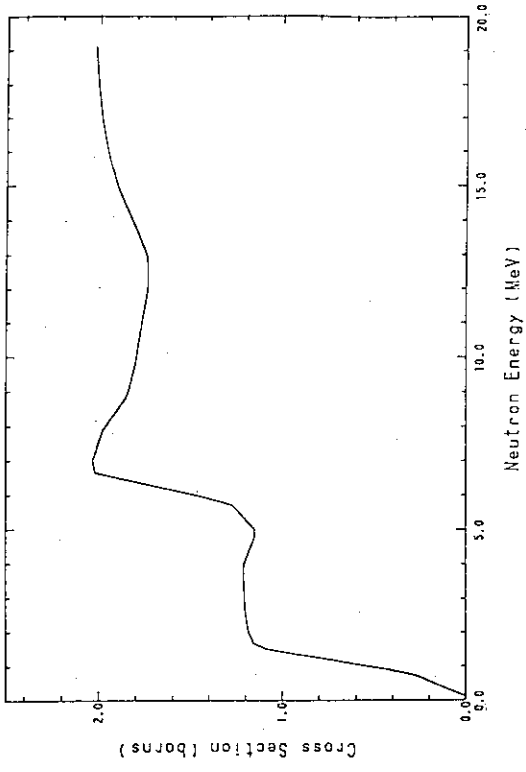

Fig. 85 The fission cross-section of ^{239}Np.

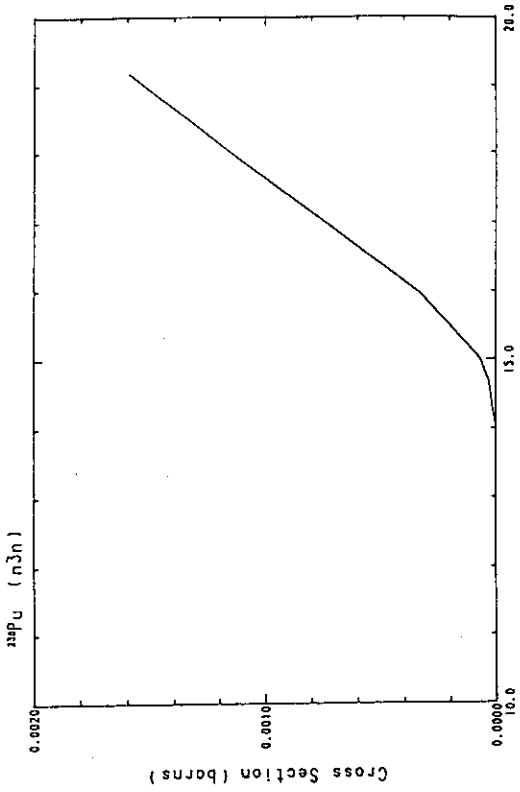

Fig. 90 The (n,3n)-reaction cross-section of ^{236}Pu.

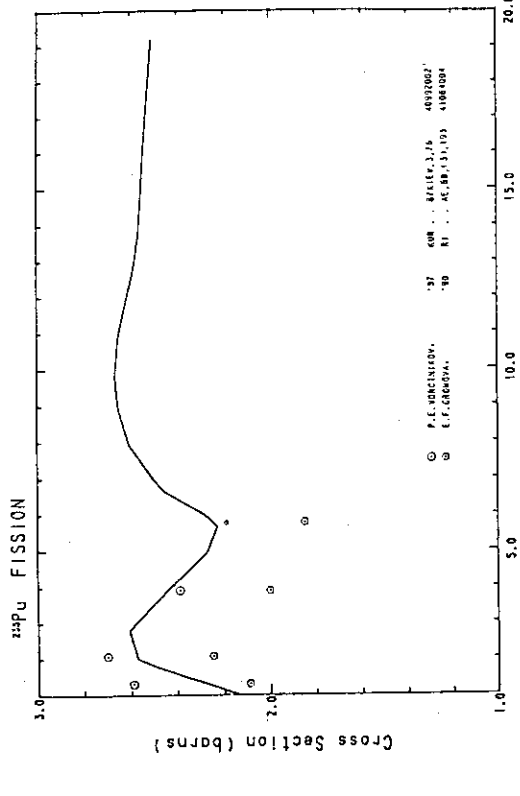

Fig. 88 The fission cross-section of ^{236}Pu.

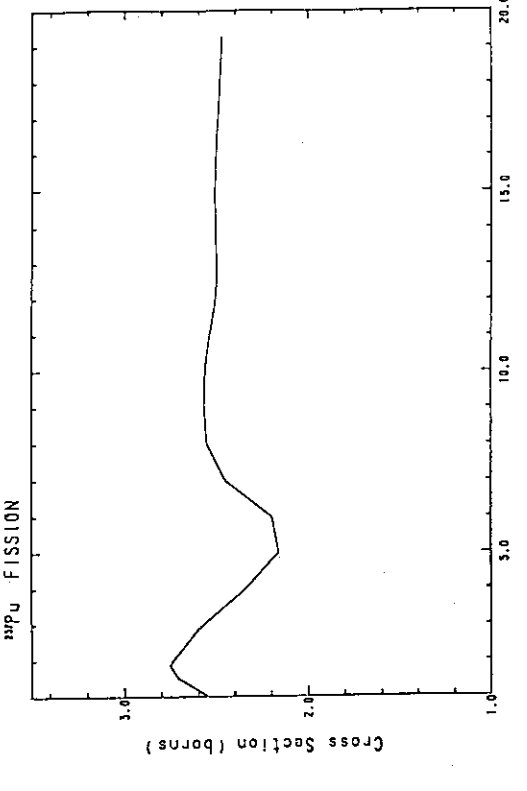

Fig. 91 The fission cross-section of ^{237}Pu.

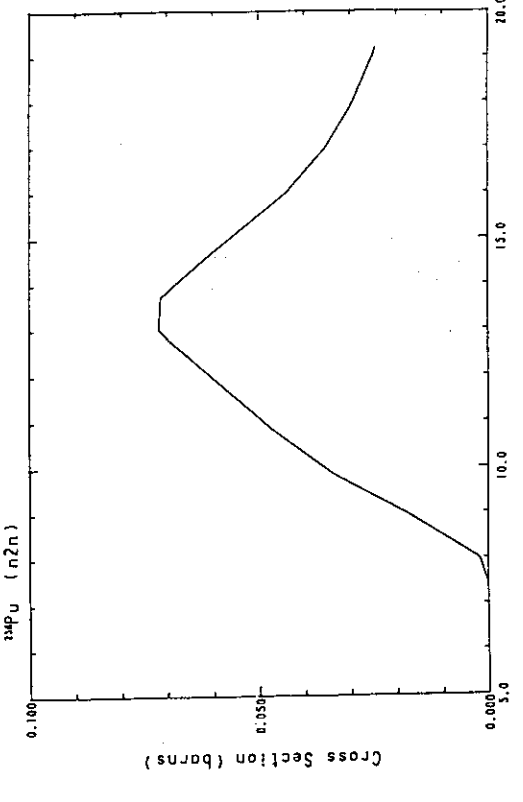

Fig. 89 The (n,2n)-reaction cross-section of ^{236}Pu.

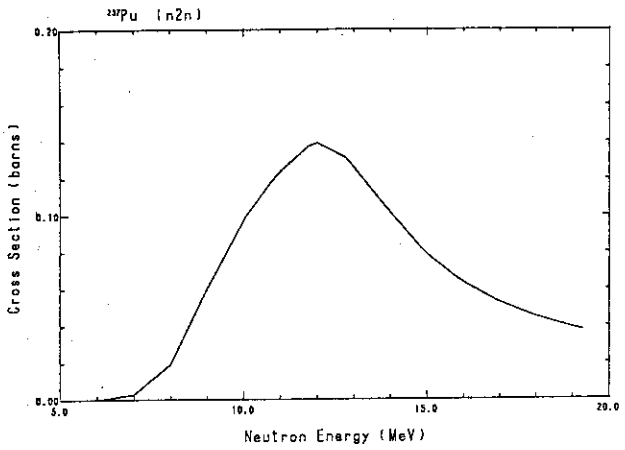

Fig. 92 The (n,2n)-reaction cross-section of ^{237}Pu.

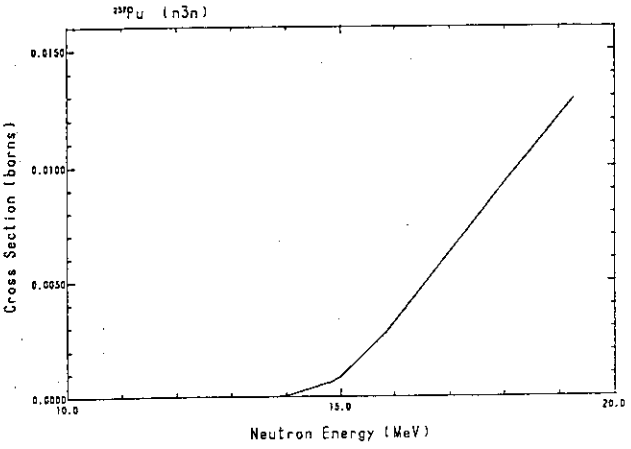

Fig. 93 The (n,3n)-reaction cross-section of ^{237}Pu.

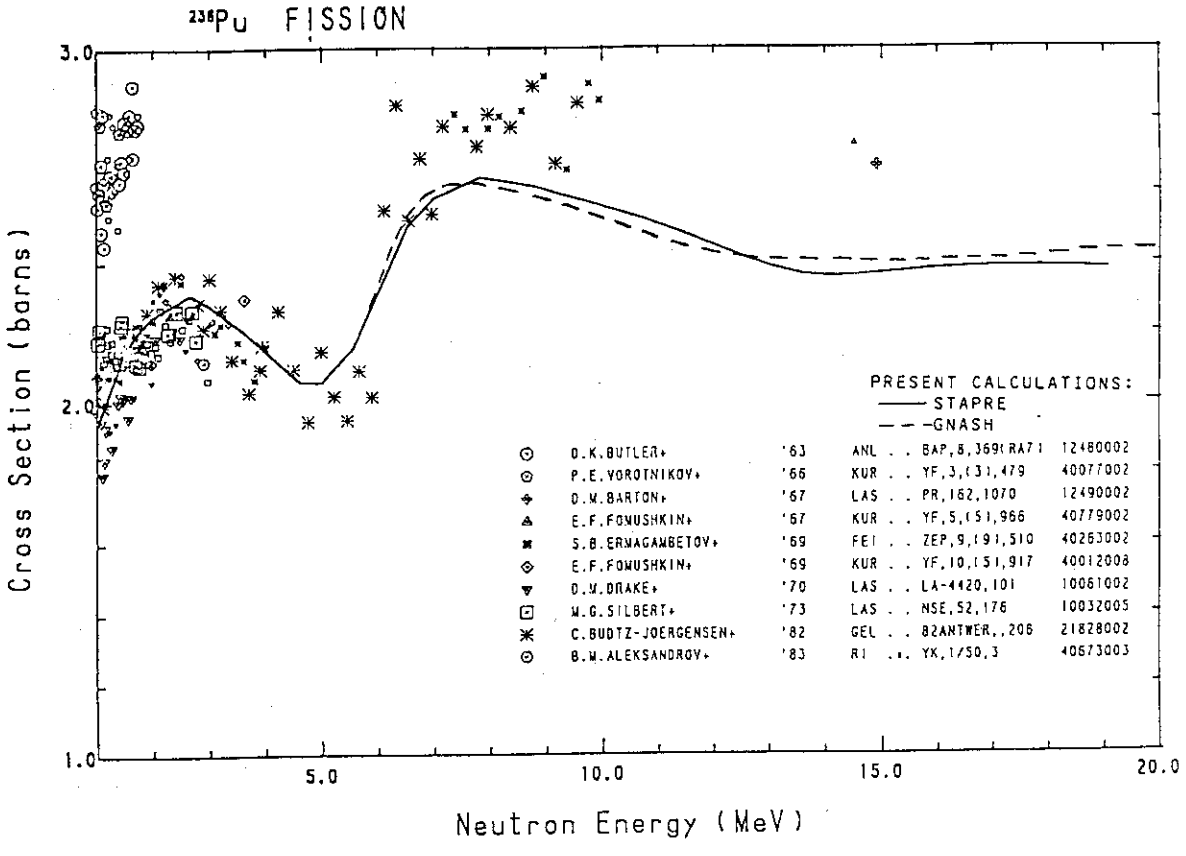

Fig. 94 The fission cross-section of ^{238}Pu.

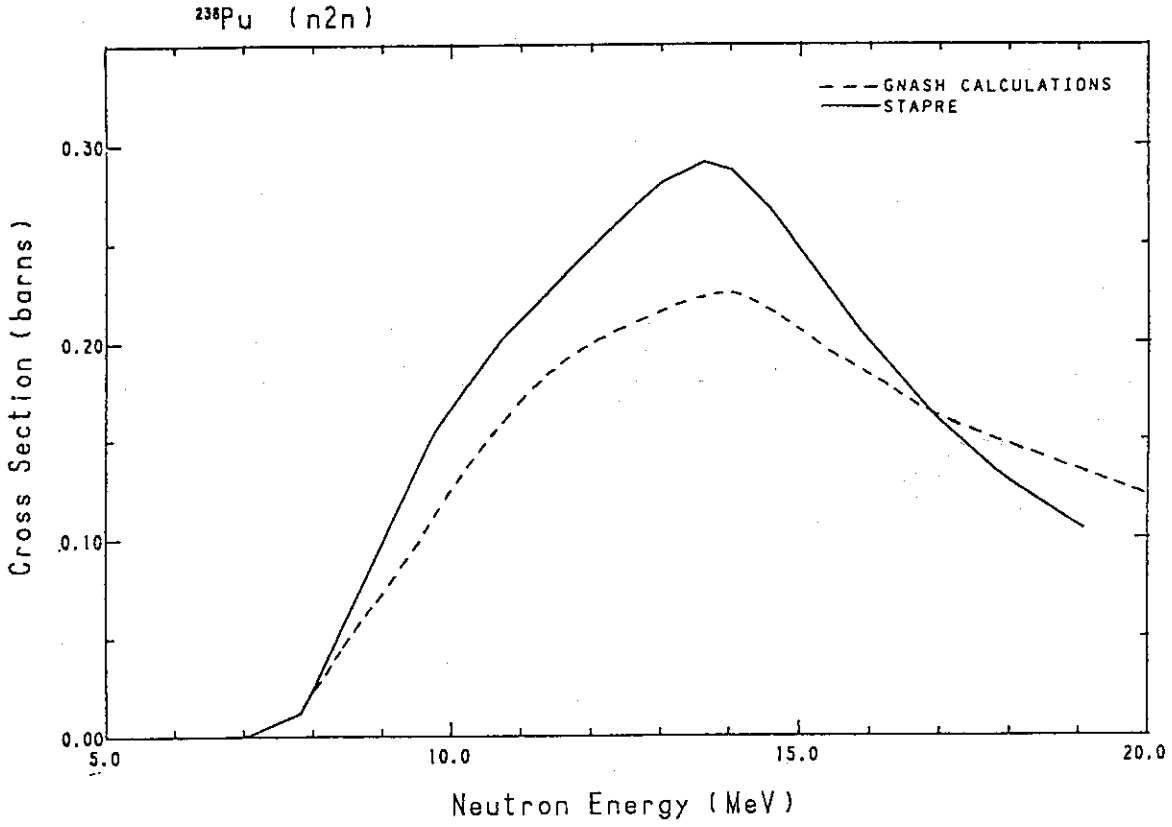

Fig. 95 The (n,2n)-reaction cross-section of ^{238}Pu.

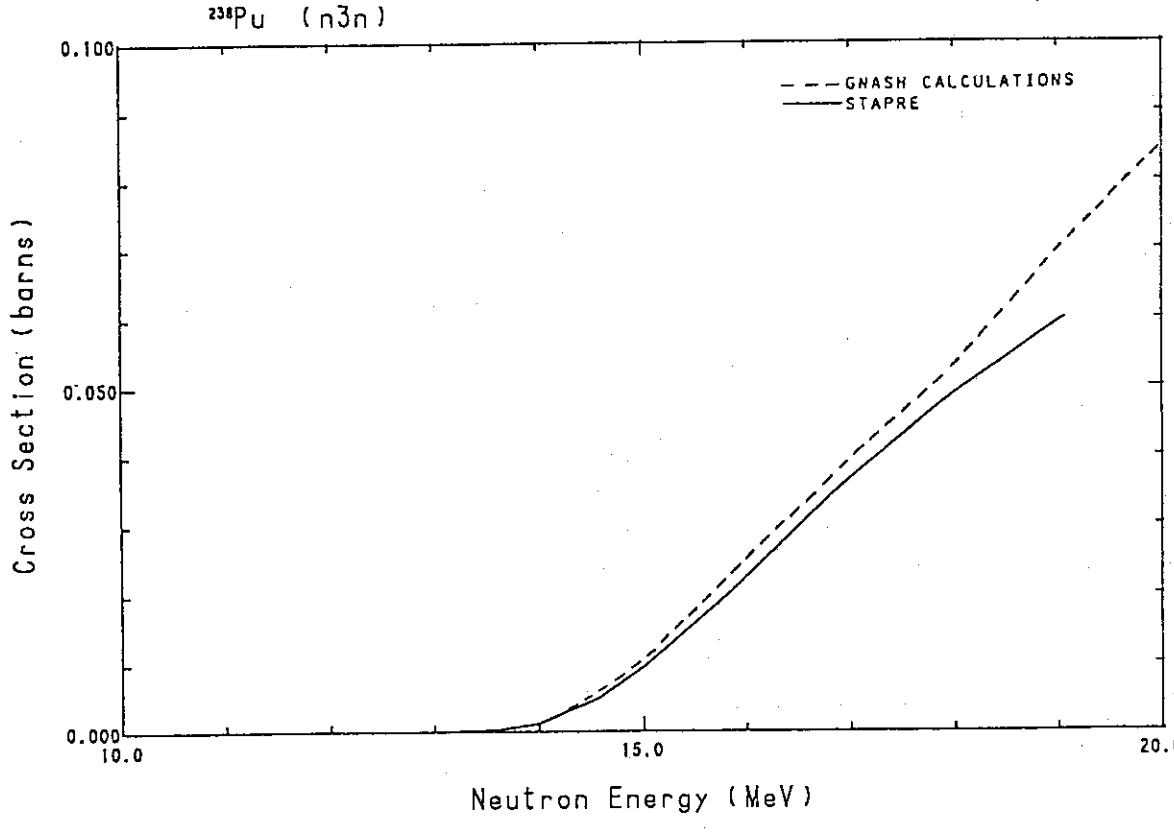

Fig. 96 The (n,3n)-reaction cross-section of ^{238}Pu.

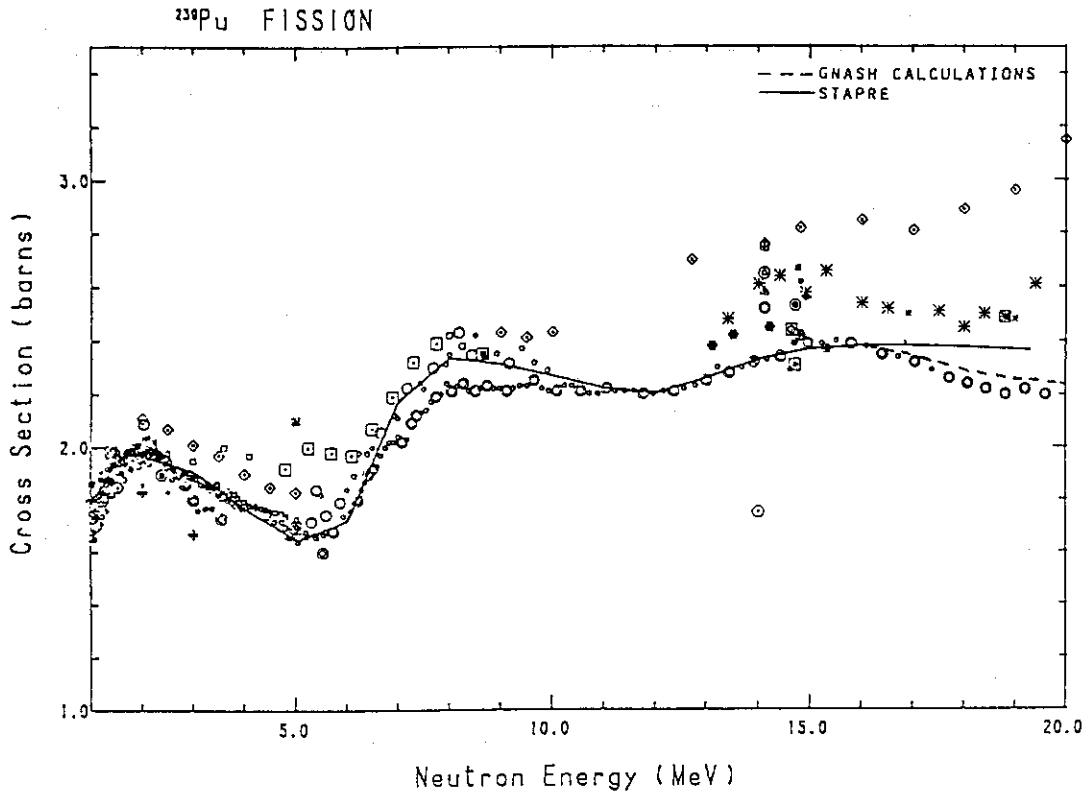

NEUTRON CROSS SECTION
^{239}Pu FISSION
ENERGY 1.00(MeV) - 20.00(MeV)

⊙	W.NYER	'50	LAS . .	LAMS-938	12306006	⊞	I.D.ALKHAZOV+	'83	RI .+. 83MOSKVA,2,20	40911007
⊙	J.S.WAHL+	'54	LAS . .	LA-1681	12437004	⊡	I.GARLEA+	'83	PIT . . INDC(ROM)-15	30647007
▲	C.A.UTTLEY+	'56	HAR . .	AERE-NP/R-1996,	21468005	⊡	I.GARLEA+	'84	PIT . . RRP,29,421	30813010
▼	R.L.HENKEL	'57	LAS . .	LA-2114	12321003	⊠	C.M.HERBACH+	'85	TUD .+. IP,21,344	30706006
◈	R.K.SMITH+	'57	LAS . .	BAP,2,196(K41	12316009	⊠	C.M.HERBACH+	'85	TUD .+. IP,21,344	30706005
✖	G.A.DOROFEEV+	'57	KUR . .	AE,2,(11),10	40355004	⊠	C.M.HERBACH+	'85	TUD .+. IP,21,344	30706004
✚	W.D.ALLEN+	'57	HAR . .	PPS/A,70,573	21075005		I.D.ALKHAZOV+	'86	RI .+. YK,(41),19	40927005
⊡	S.P.KALININ+	'58	KUR . .	58GENEVA,16,136(	40741006		J.W.MEADOWS	'88	ANL .+. ANE,15,421	13134009
✳	B.ADAMS+	'61	ALD . .	JNE,14,85	21209004					
⊙	G.N.SMIRENKIN+	'62	FEI .+.	AE,13,366	40650003					
✦	S.M.DUBROVINA+	'64	KUR .+.	DOK,157,(31,561	40716003					
✸	T.CZYZEWSKI+	'66	IBJ .+.	INR-688	30084002					
○	D.M.BARTON+	'67	LAS . .	PR,162,1070	12490003					
○	P.H.WHITE+	'67	ALD . .	JNE,21,671	21195007					
⊛	R.H.IYER+	'69	TRM . .	69ROORKEE,2,289	30035006					
⊛	D.B.GAYTHER	'75	HAR . .	75WASH,GB-6	20428002					
⊛	I.SZABO+	'76	CAD . .	76ANL,208	20570003					
⊘	I.SZABO+	'76	CAD . .	76ANL,,	20618003					
⊛	V.M.ADAMOV+	'77	RI .+.	YK-24,8	40547009					
○	K.KARI+	'78	KFK . .	78BNL,	20786004					
⊛	M.CANCE+	'78	BRC . .	NSE,68,(21,197	20779005					
○	J.W.MEADOWS	'78	ANL . .	NSE,68,360	10734002					
⊛	R.ARLT+	'81	TUD . .	KE,24,48	30475005					
⊠	M.MAHDAVI+	'82	MHG . .	82ANTWER,,58	12826003					
⊡	ZHOU XIAN-JIAN+	'82	AEP . .	CNP,4,(2),131	30670002					
◉	LI JING-WEN+	'82	AEP . .	82ANTWER,,55	30634003					

Fig. 97 The fission cross-section of ^{239}Pu.

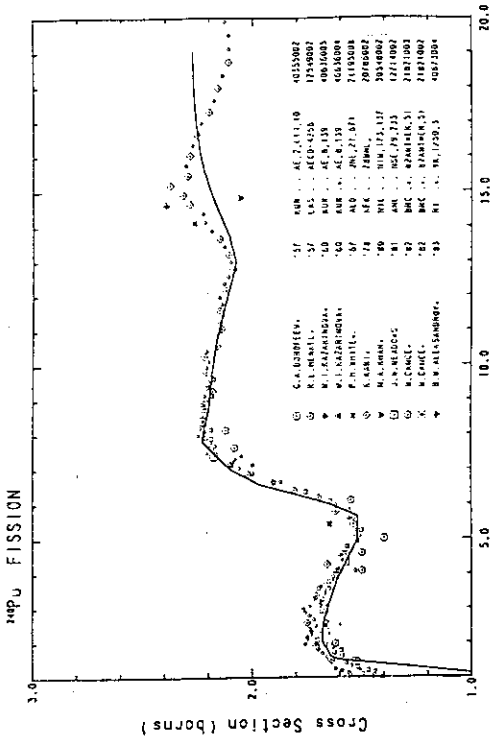

Fig. 100 The fission cross-section of ^{240}Pu.

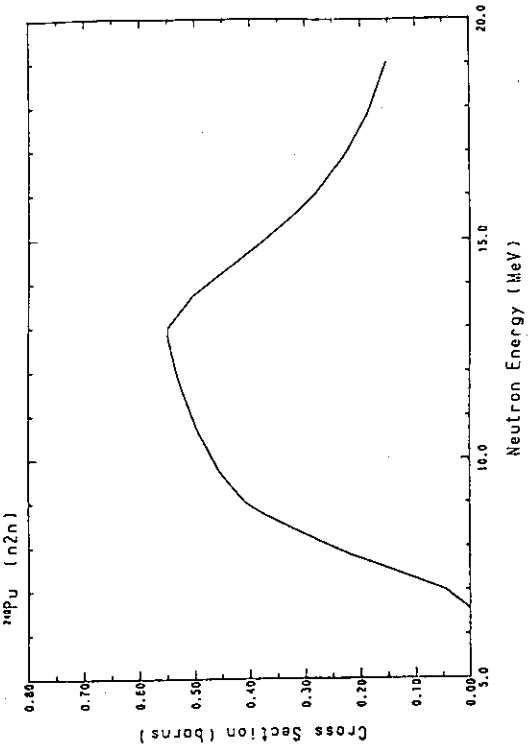

Fig. 101 The (n,2n)-reaction cross-section of ^{240}Pu.

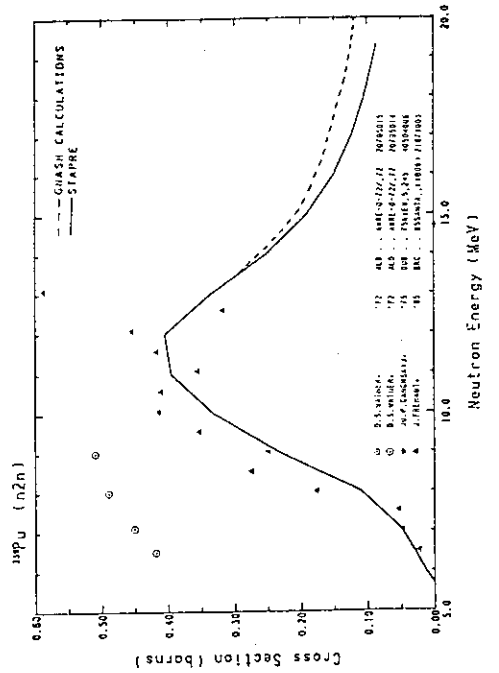

Fig. 98 The (n,2n)-reaction cross-section of ^{239}Pu.

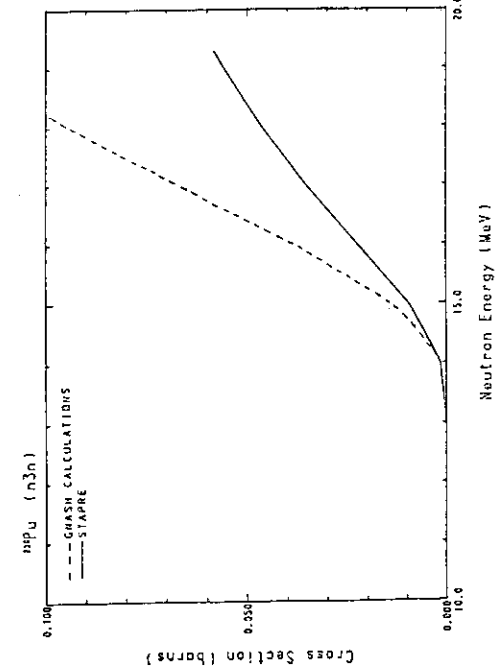

Fig. 99 The (n,3n)-reaction cross-section of ^{239}Pu.

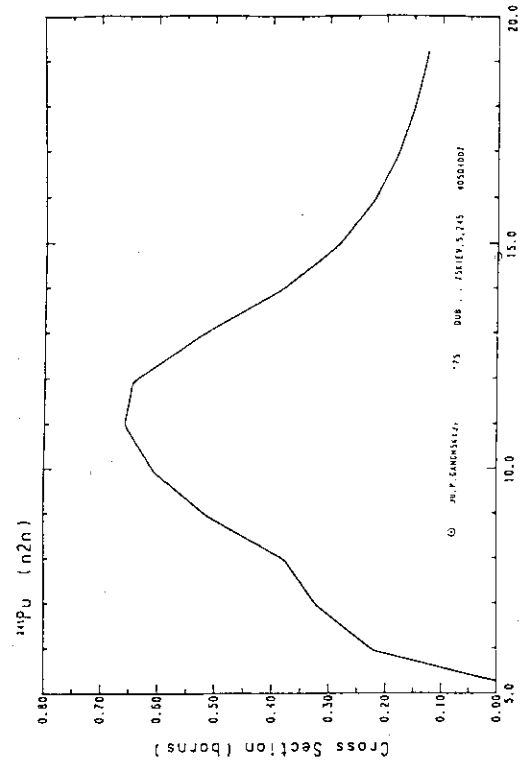

Fig. 104 The (n,2n)-reaction cross-section of ^{241}Pu.

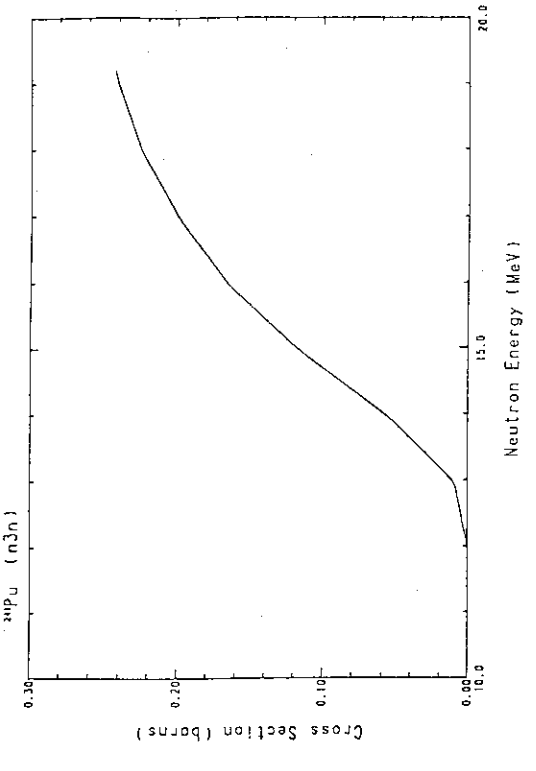

Fig. 105 The (n,3n)-reaction cross-section of ^{241}Pu.

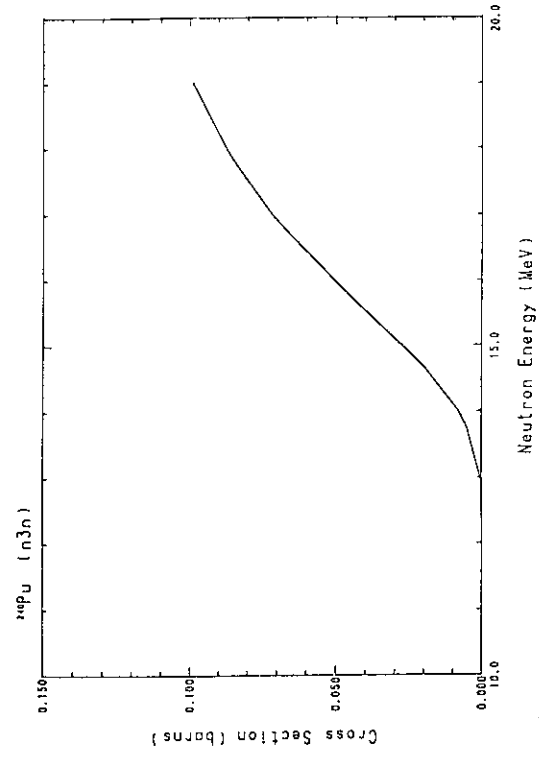

Fig. 102 The (n,3n)-reaction cross-section of ^{240}Pu.

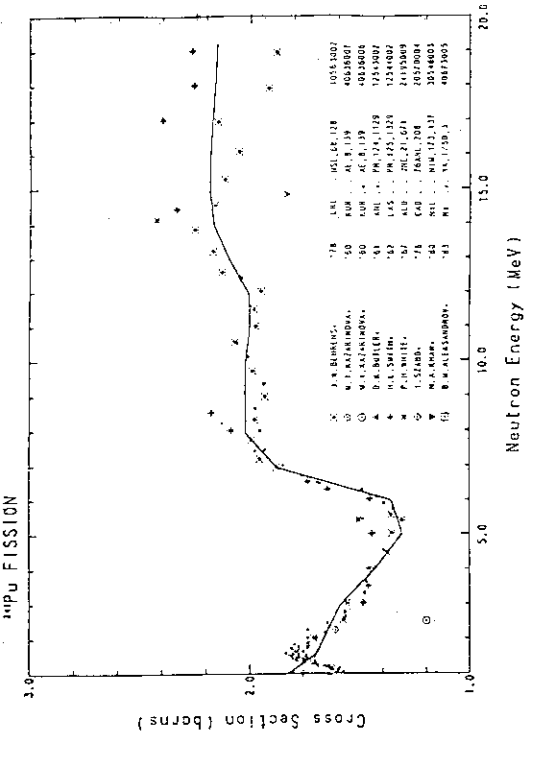

Fig. 103 The fission cross-section of ^{241}Pu.

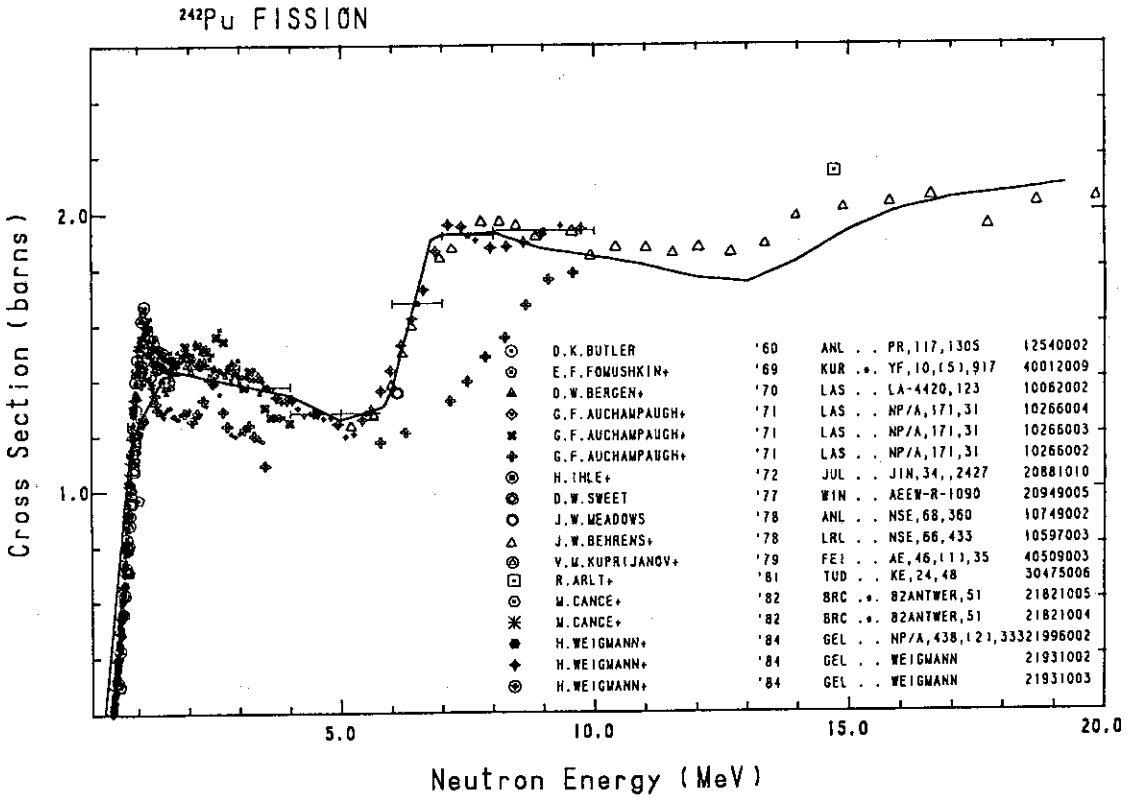

Fig. 106 The fission cross-section of ^{242}Pu.

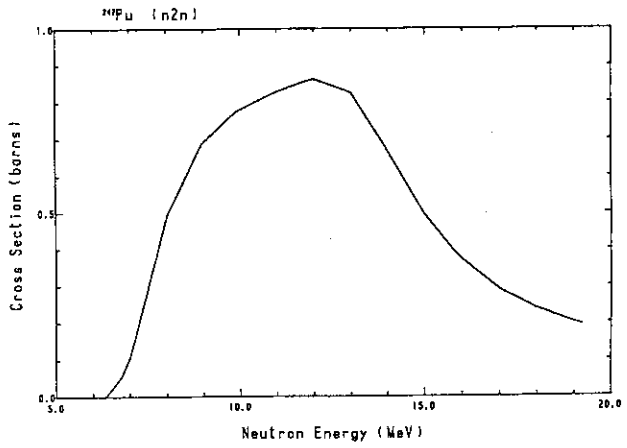

Fig. 107 The (n,2n)-reaction cross-section of ^{242}Pu.

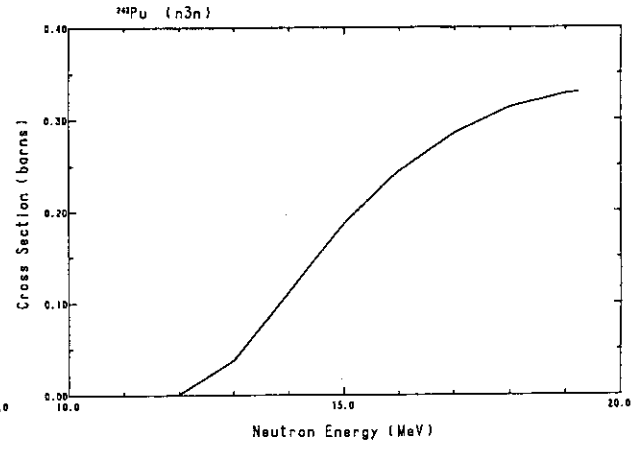

Fig. 108 The (n,3n)-reaction cross-section of ^{242}Pu.

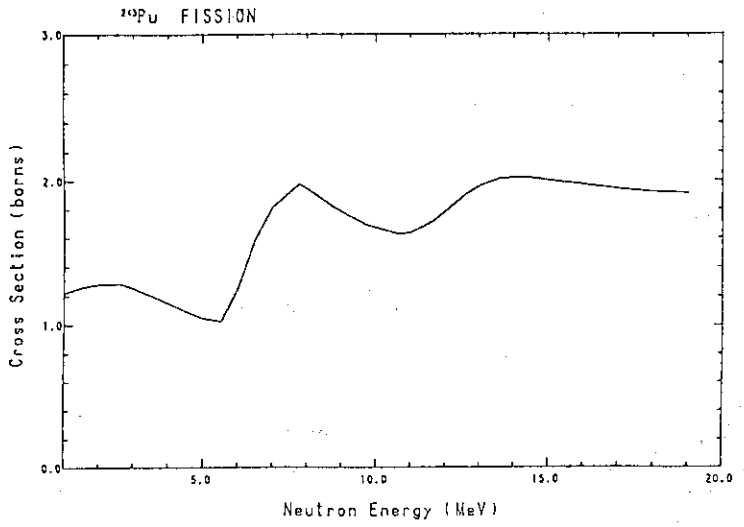

Fig. 109 The fission cross-section of ^{243}Pu.

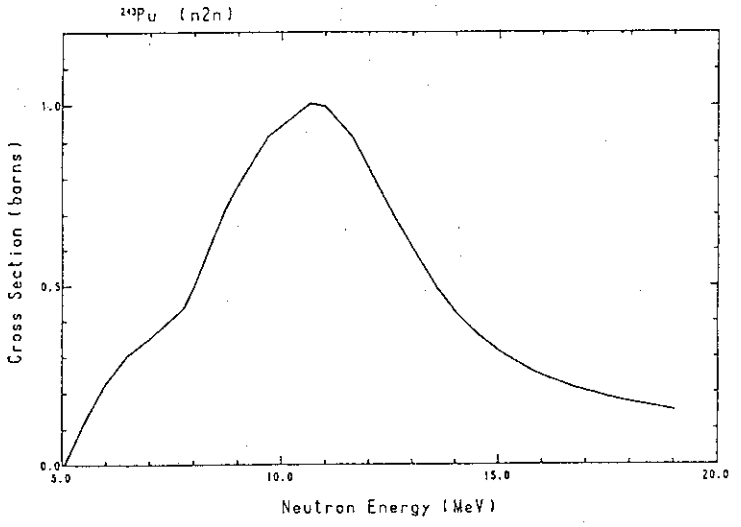

Fig. 110 The (n,2n)-reaction cross-section of ^{243}Pu.

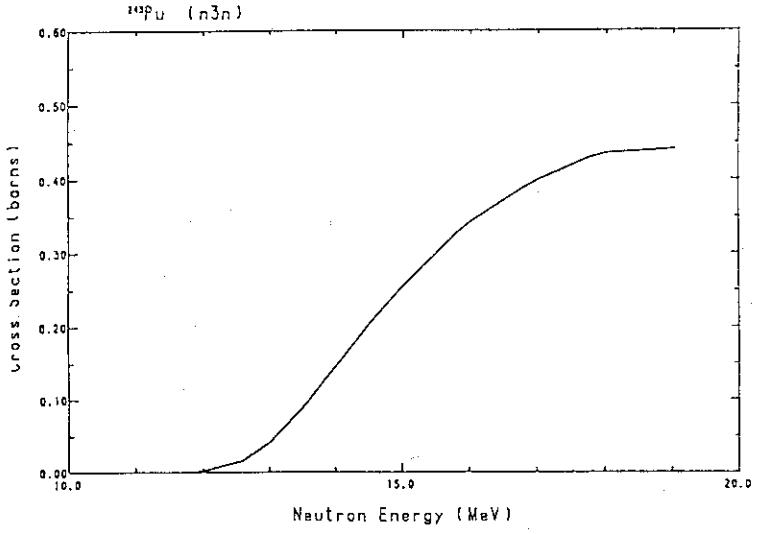

Fig. 111 The (n,3n)-reaction cross-section of ^{243}Pu.

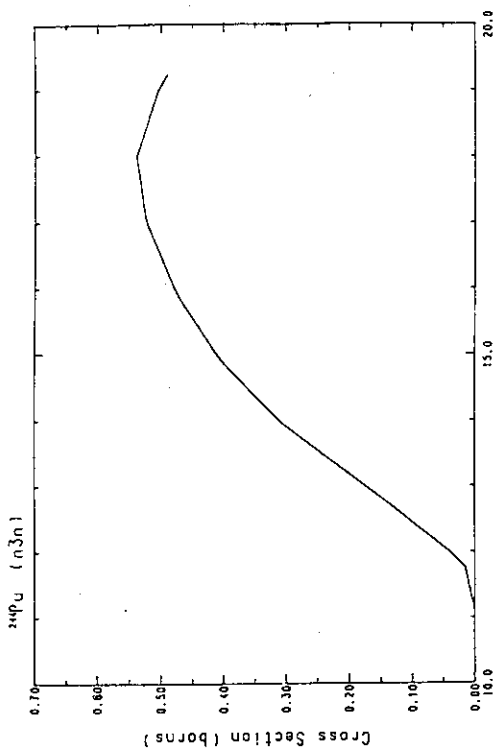

Fig. 114 The (n,3n)-reaction cross-section of ^{244}Pu.

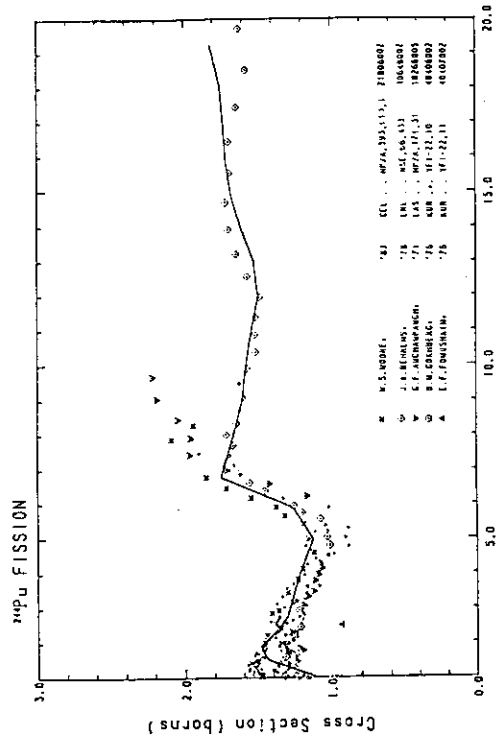

Fig. 112 The fission cross-section of ^{244}Pu.

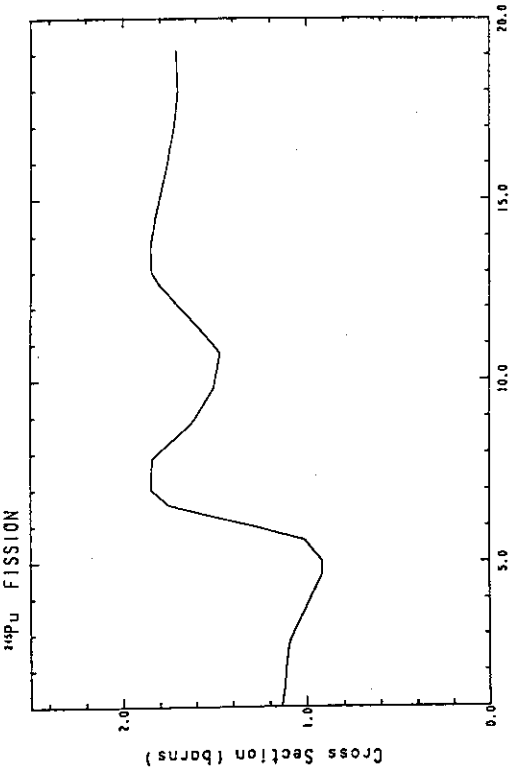

Fig. 115 The fission cross-section of ^{245}Pu.

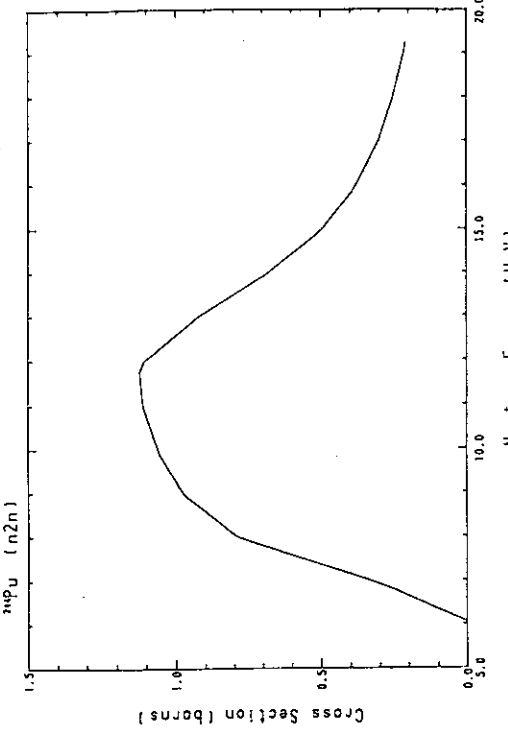

Fig. 113 The (n,2n)-reaction cross-section of ^{244}Pu.

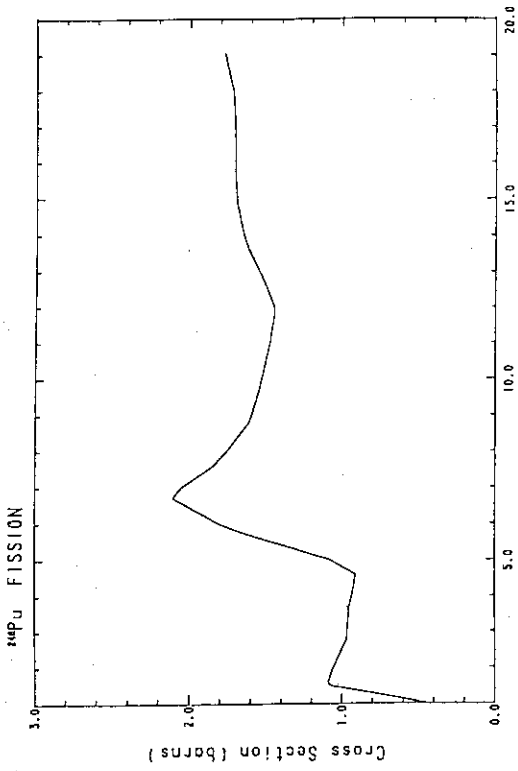

Fig. 116 The (n,2n)-reaction cross-section of ^{245}Pu.

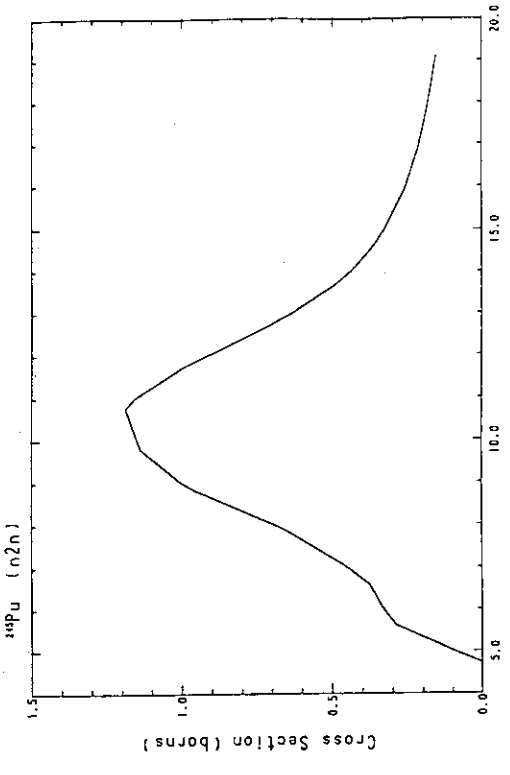

Fig. 117 The (n,3n)-reaction cross-section of ^{245}Pu.

Fig. 118 The fission cross-section of ^{246}Pu.

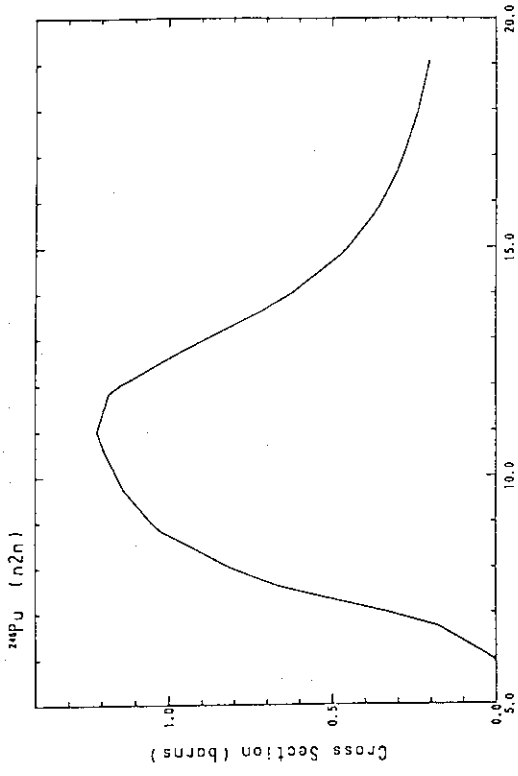

Fig. 119 The (n,2n)-reaction cross-section of ^{246}Pu.

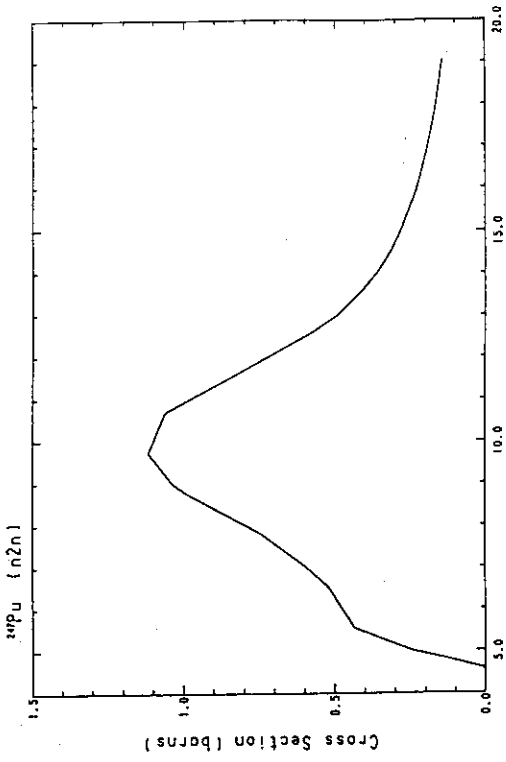

Fig. 122 The (n,2n)-reaction cross-section of ^{247}Pu.

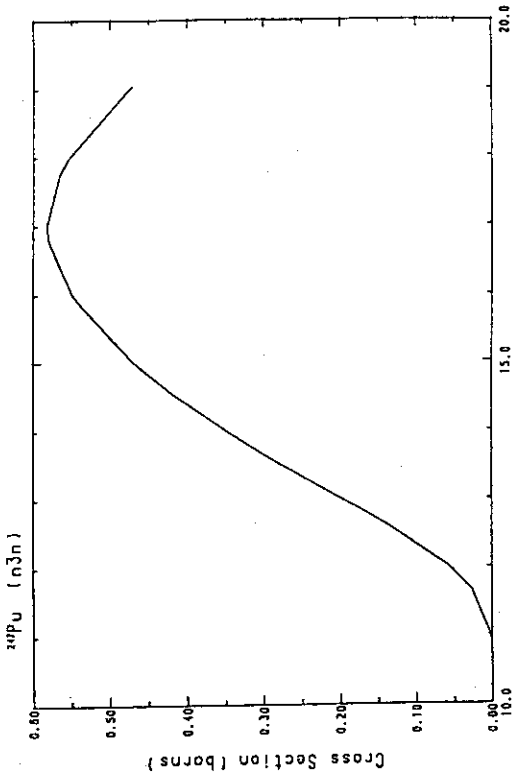

Fig. 123 The (n,3n)-reaction cross-section of ^{247}Pu.

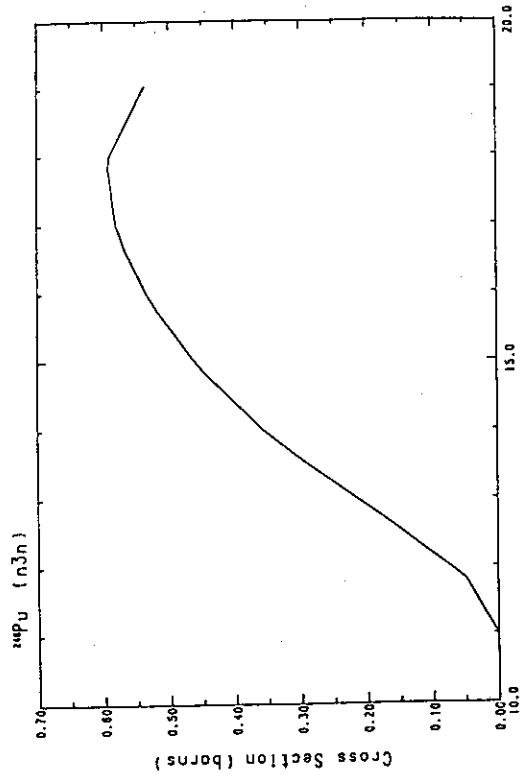

Fig. 120 The (n,3n)-reaction cross-section of ^{246}Pu.

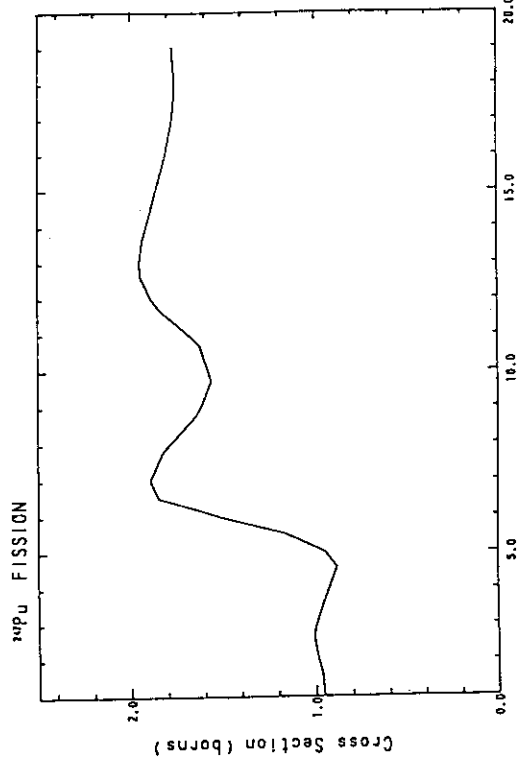

Fig. 121 The fission cross-section of ^{247}Pu.

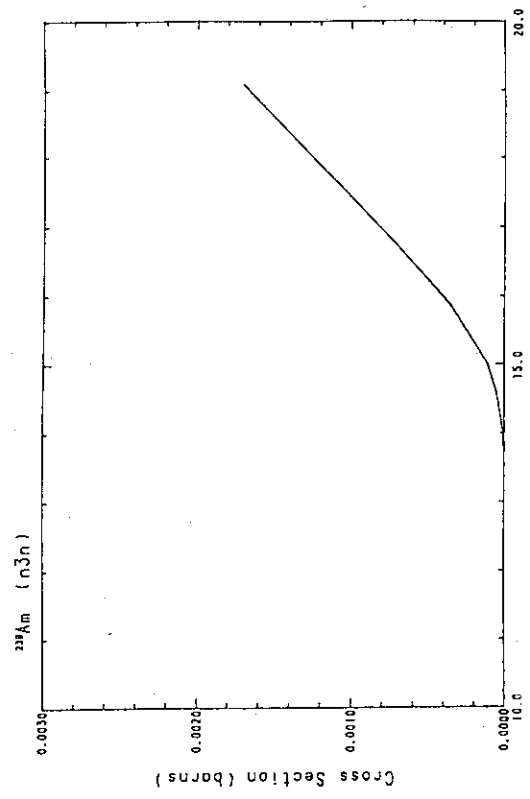

Fig. 126 The (n,3n)-reaction cross-section of ^{239}Am.

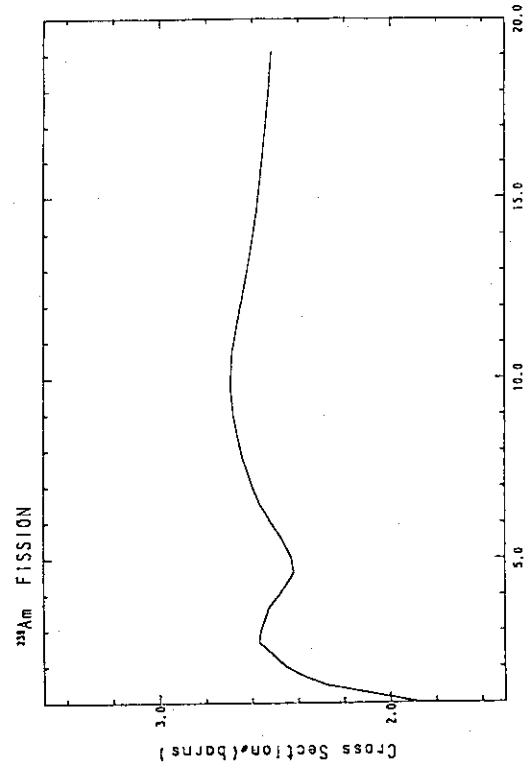

Fig. 124 The fission cross-section of ^{239}Am.

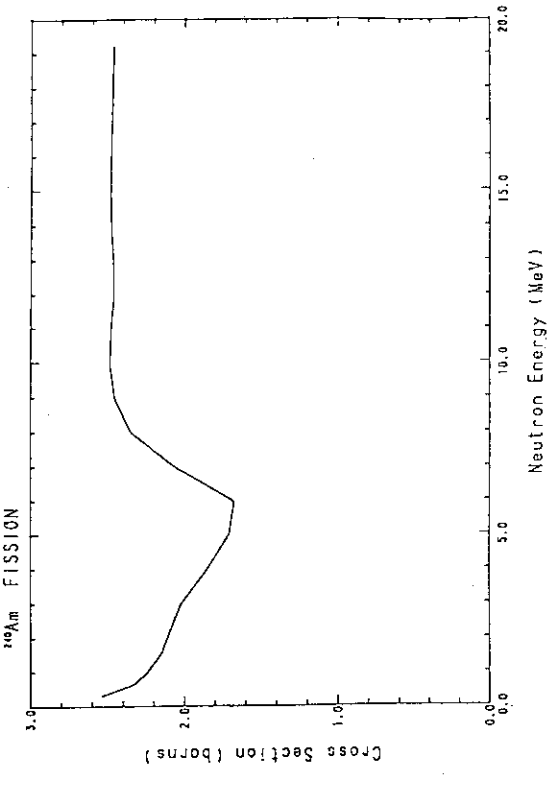

Fig. 127 The fission cross-section of ^{240}Am.

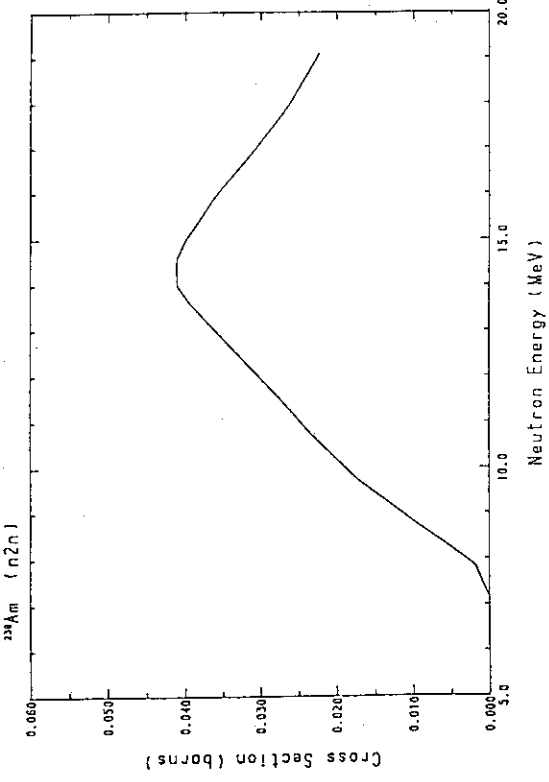

Fig. 125 The (n,2n)-reaction cross-section of ^{239}Am.

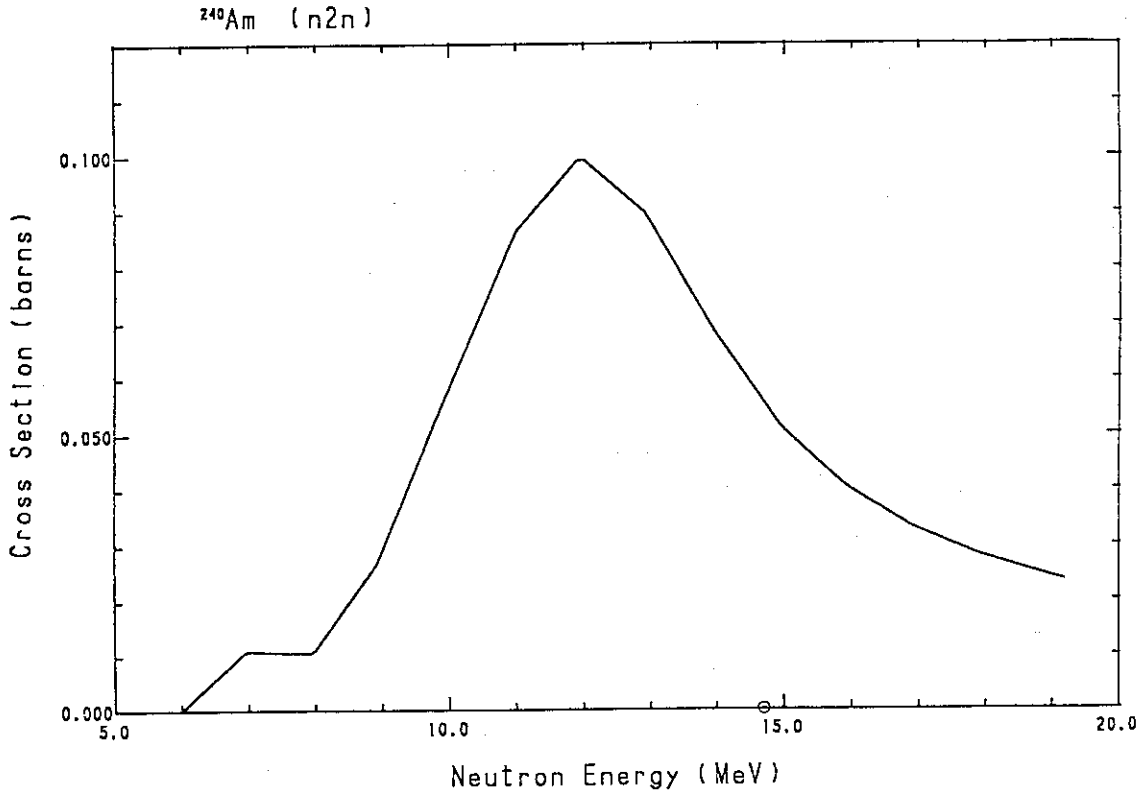

Fig. 128 The (n,2n)-reaction cross-section of ^{240}Am.

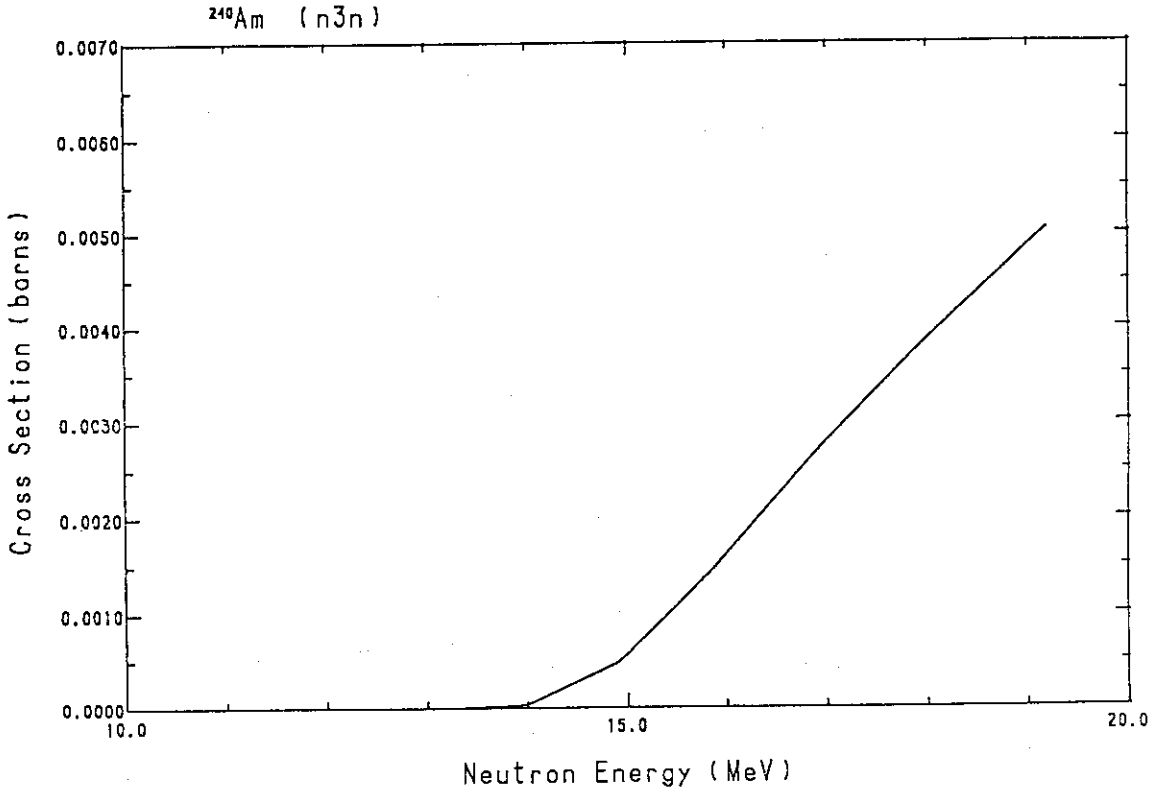

Fig. 129 The (n,3n)-reaction cross-section of ^{240}Am.

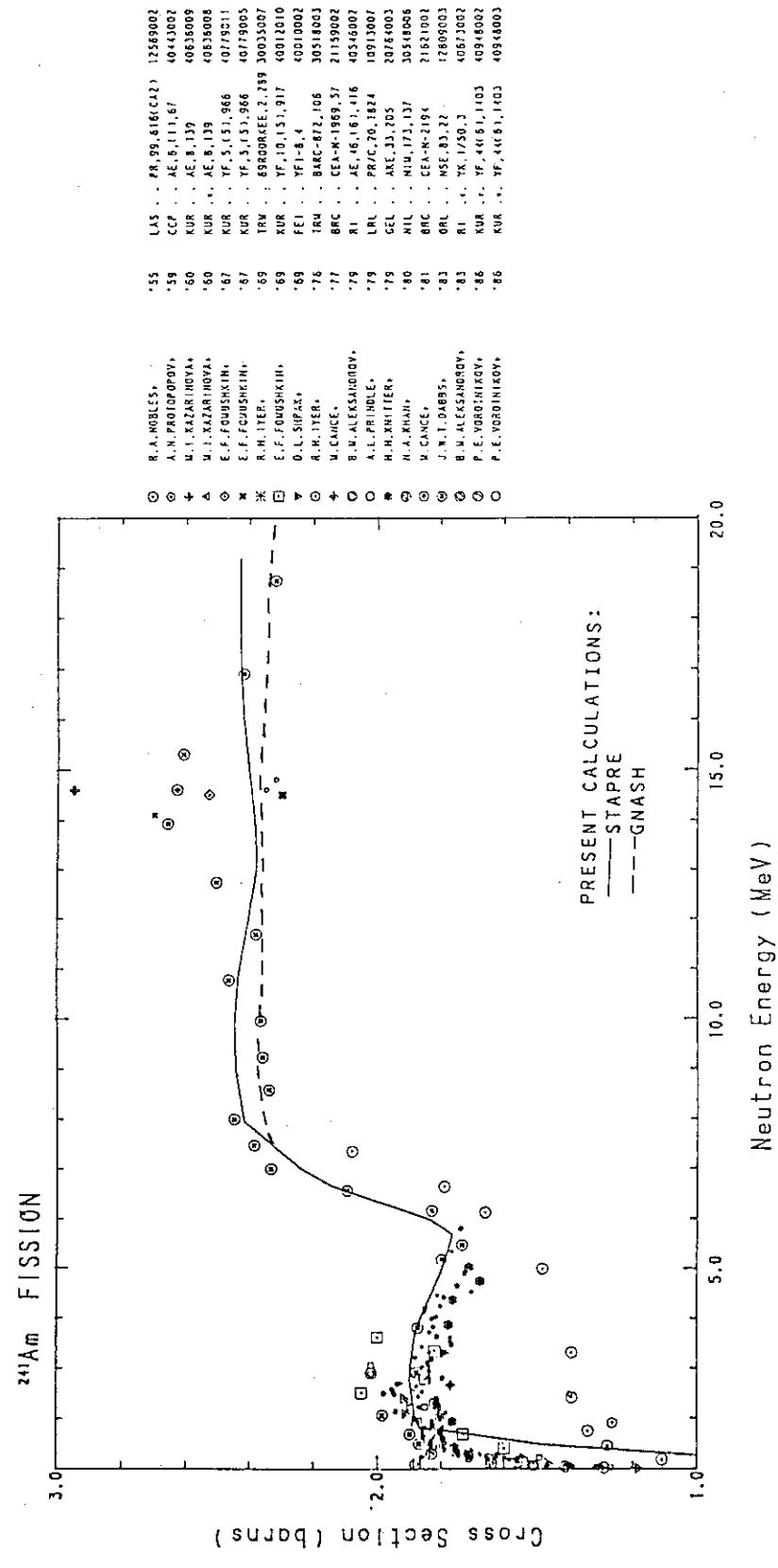

Fig. 130 The fission cross-section of ^{241}Am.

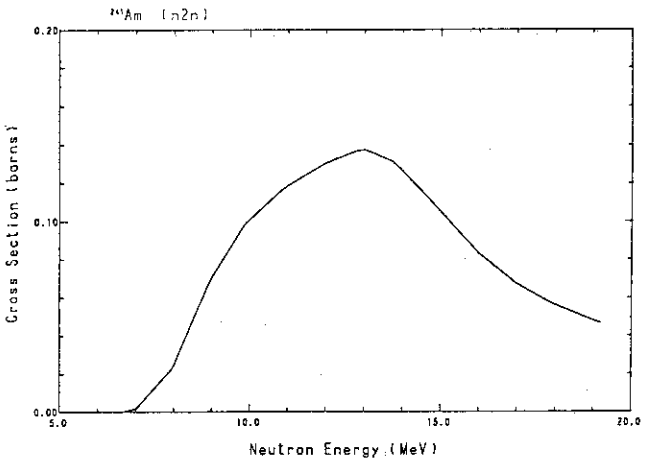

Fig. 131 The (n,2n)-reaction cross-section of ^{241}Am.

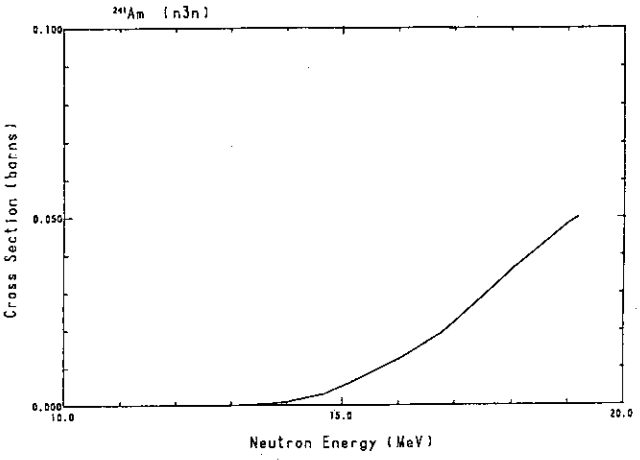

Fig. 132 The (n,3n)-reaction cross-section of ^{241}Am.

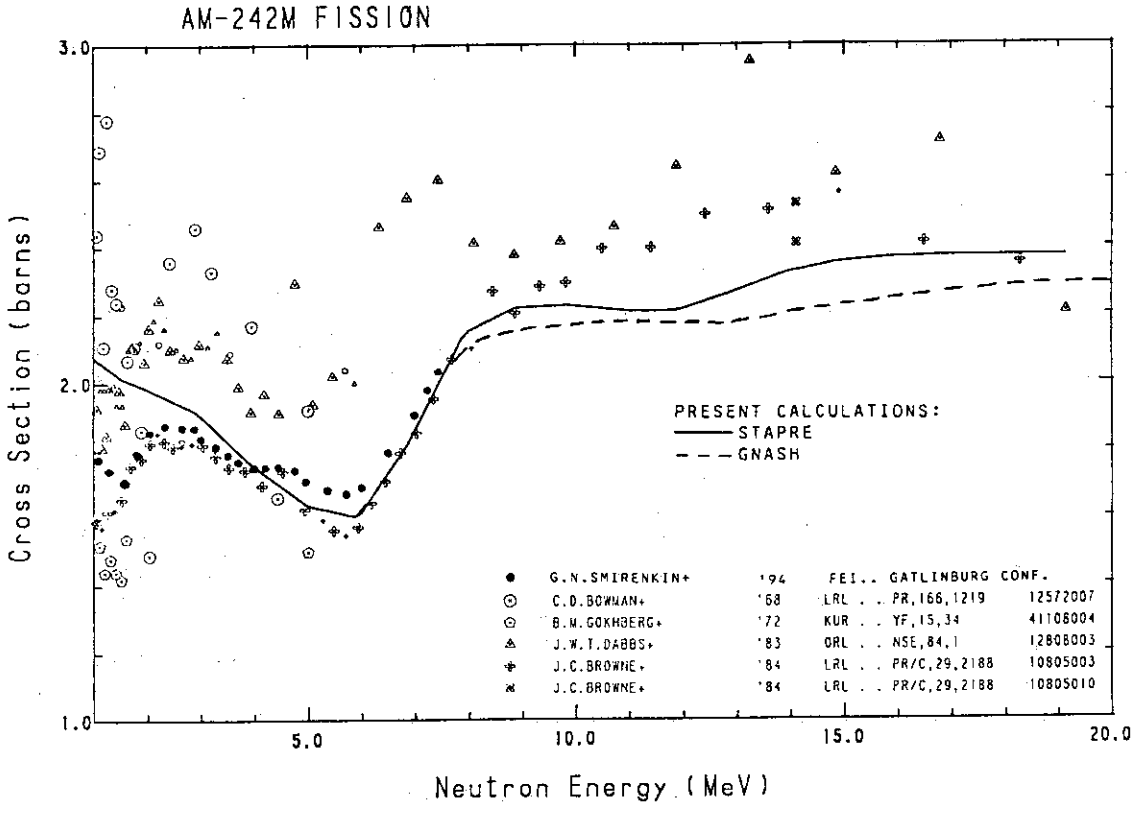

Fig. 133 The fission cross-section of ^{242}Am.

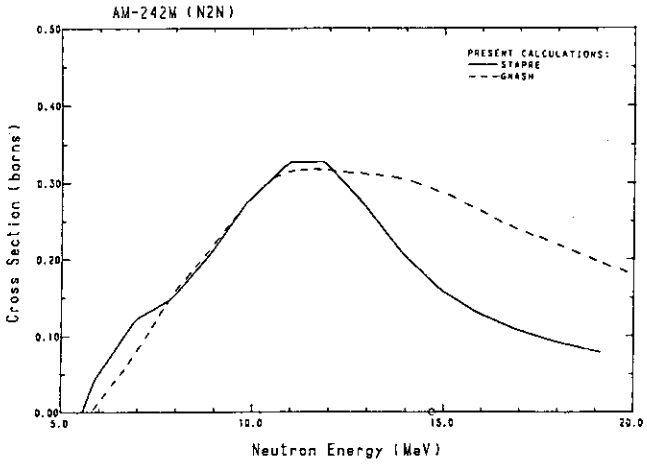

Fig. 134 The (n,2n)-reaction cross-section of ^{242m}Am.

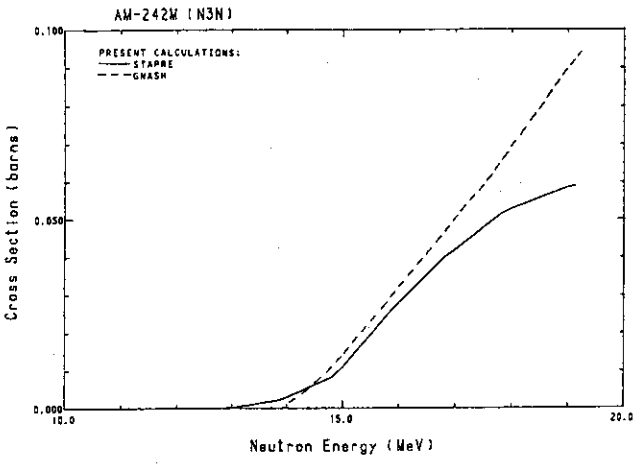

Fig. 135 The (n,3n)-reaction cross-section of ^{242m}Am.

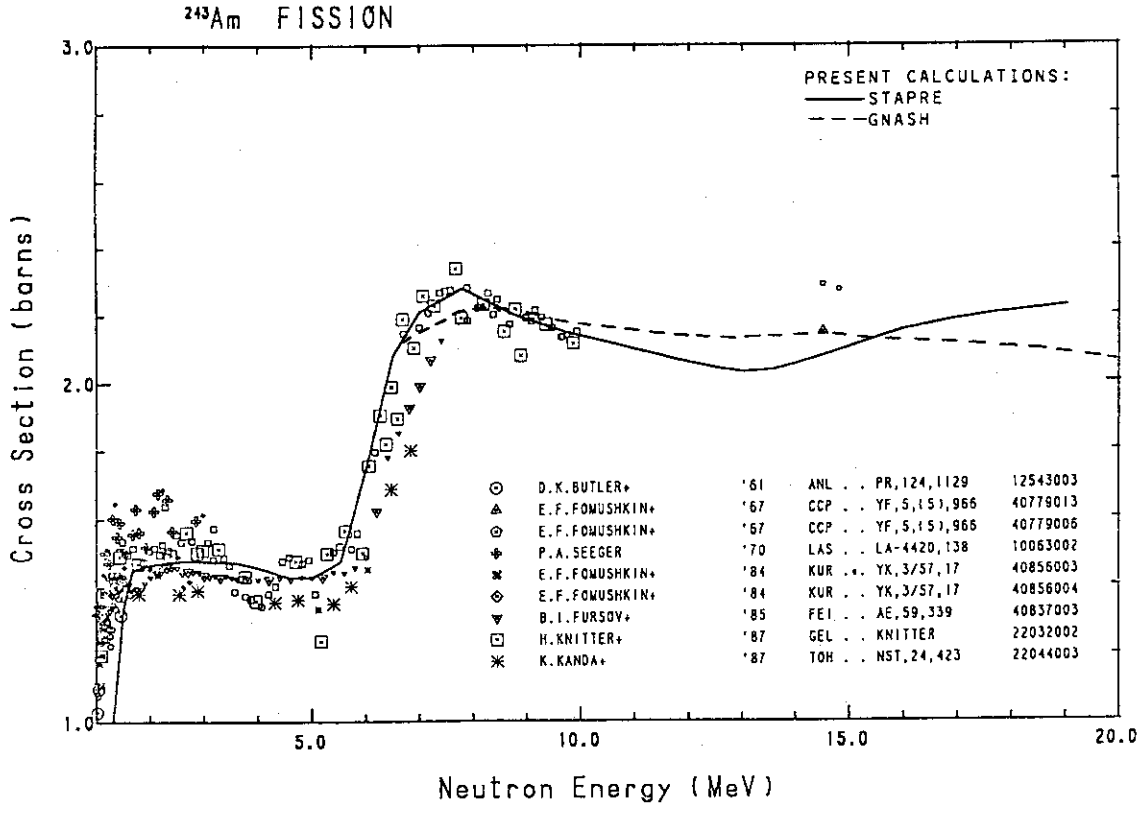

Fig. 136 The fission cross-section of ^{243}Am.

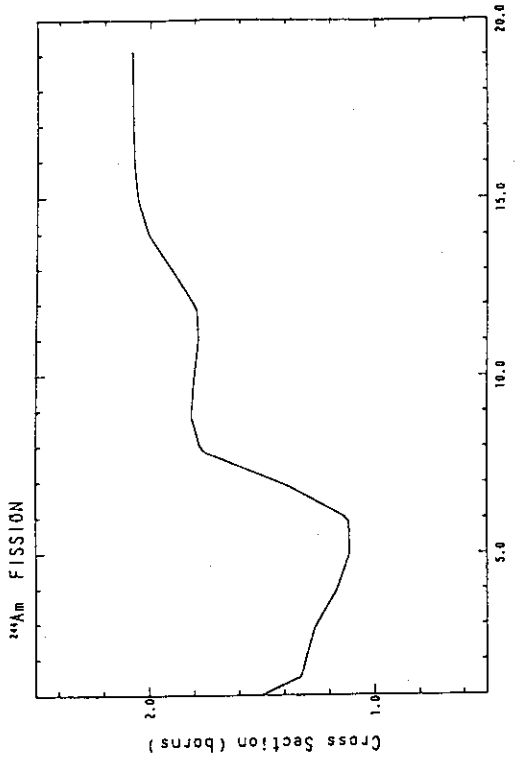

Fig. 139 The fission cross-section of ^{244}Am.

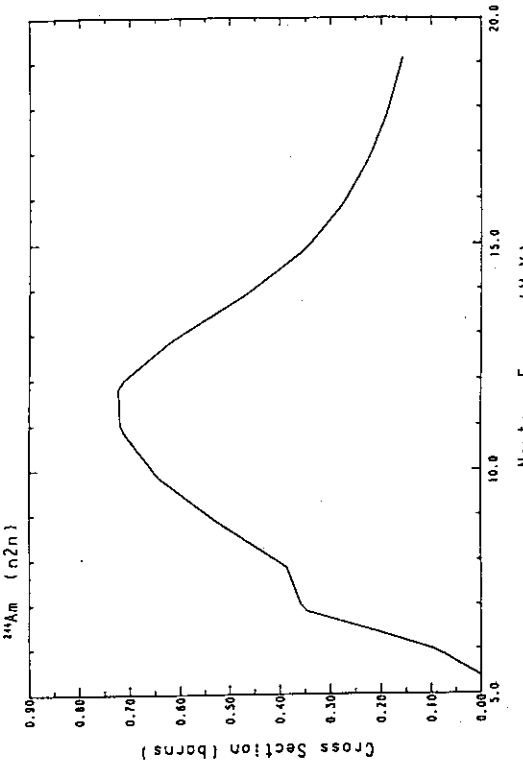

Fig. 140 The (n,2n)-reaction cross-section of ^{244}Am.

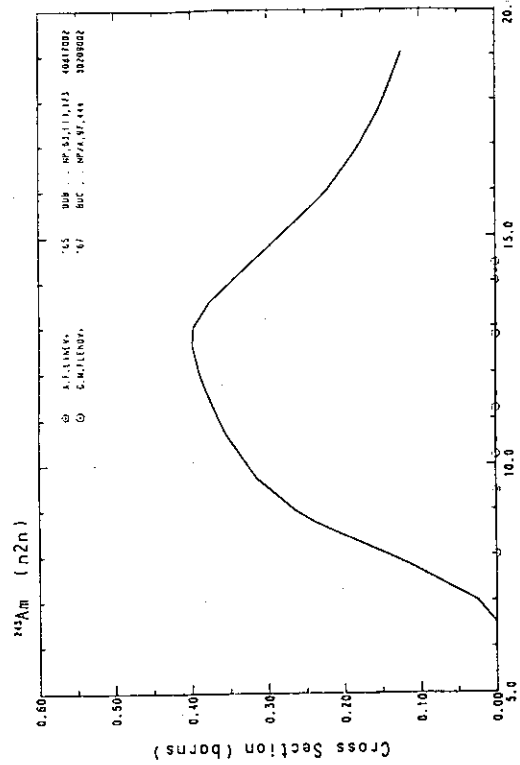

Fig. 137 The (n,2n)-reaction cross-section of ^{243}Am.

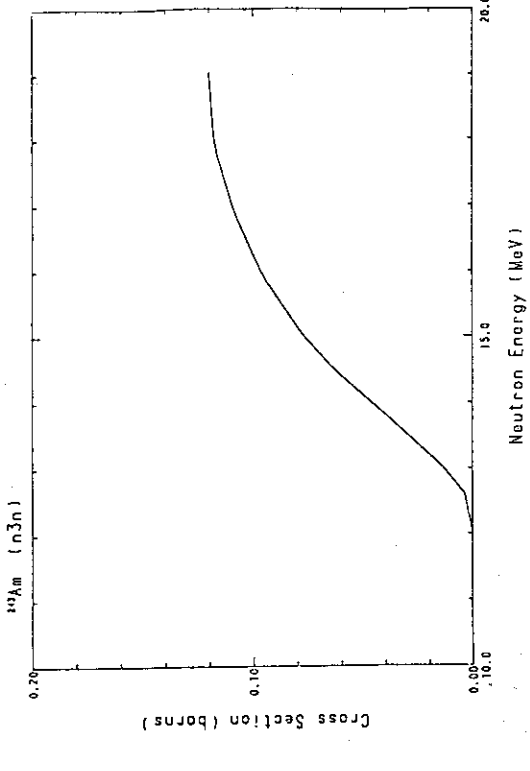

Fig. 138 The (n,3n)-reaction cross-section of ^{243}Am.

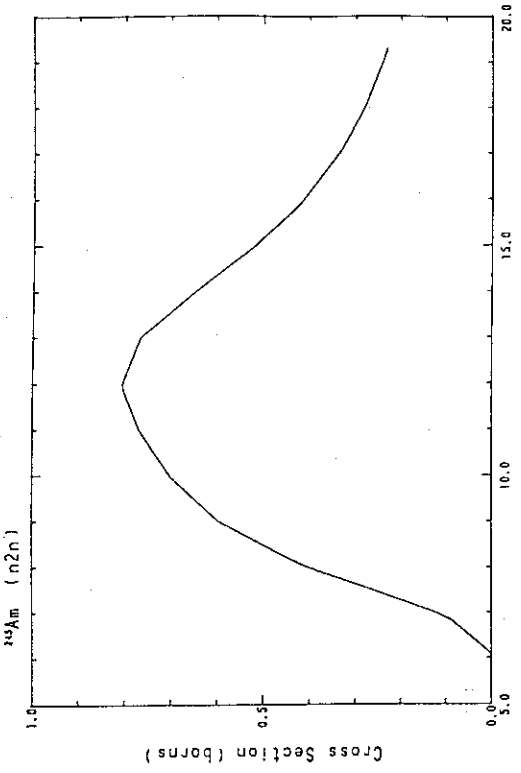

Fig. 143 The (n,2n)-reaction cross-section of ^{245}Am.

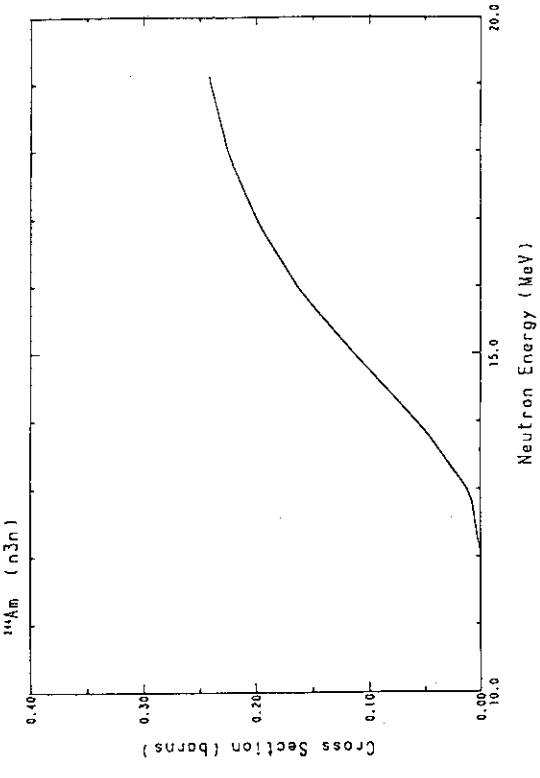

Fig. 141 The (n,3n)-reaction cross-section of ^{244}Am.

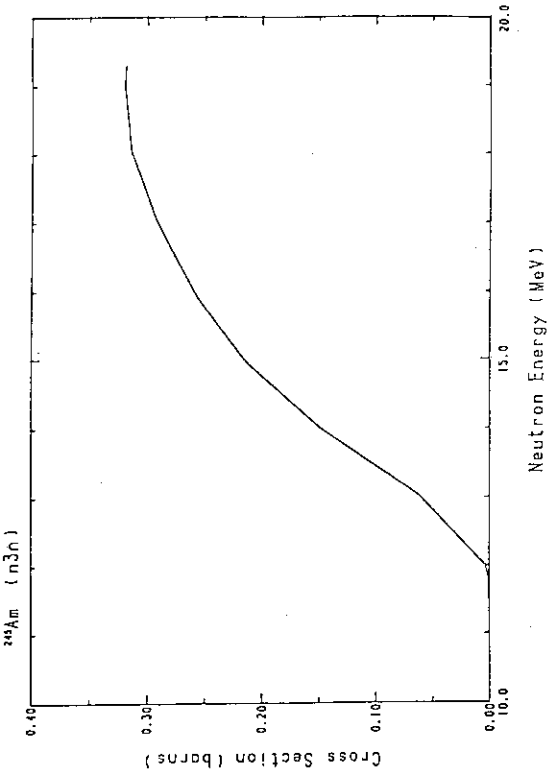

Fig. 144 The (n,3n)-reaction cross-section of ^{245}Am.

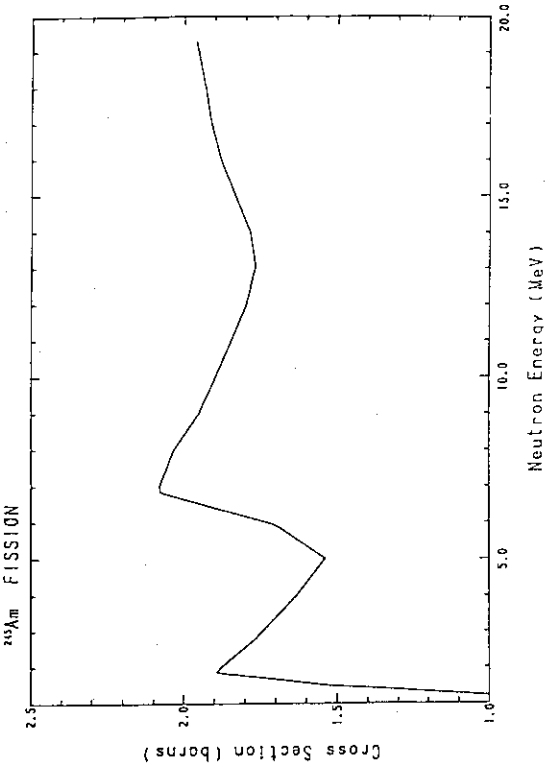

Fig. 142 The fission cross-section of ^{245}Am.

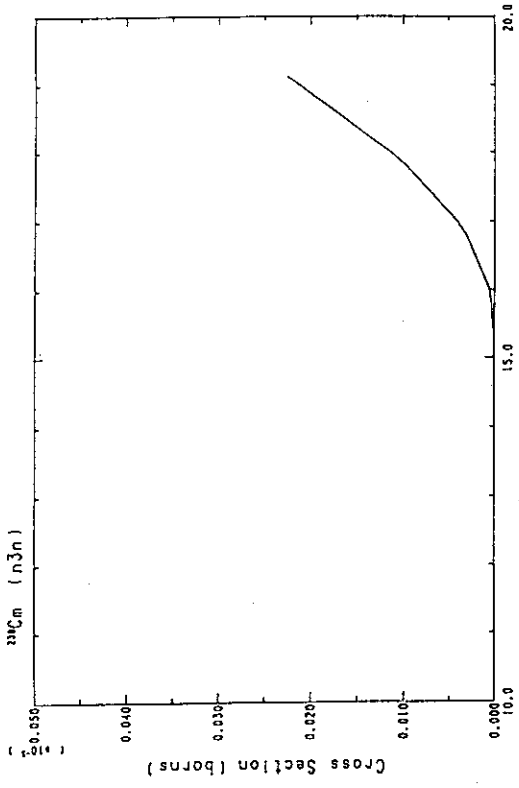

Fig. 147 The (n,3n)-reaction cross-section of ^{238}Cm.

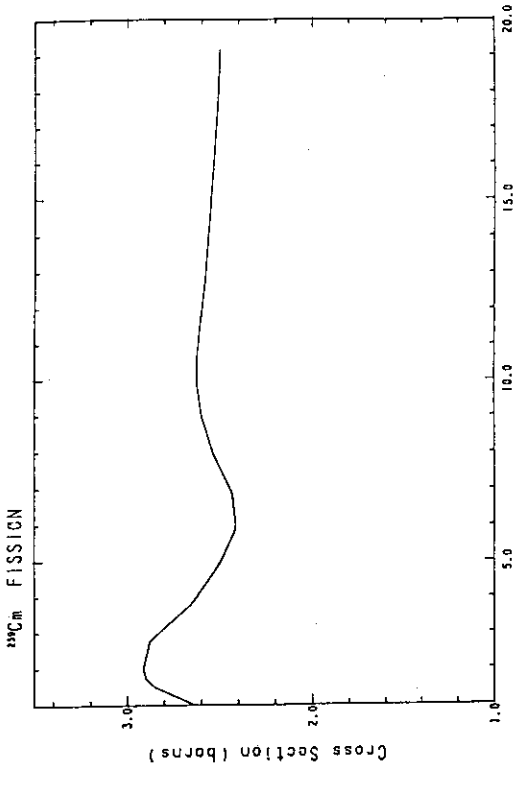

Fig. 148 The fission cross-section of ^{239}Cm.

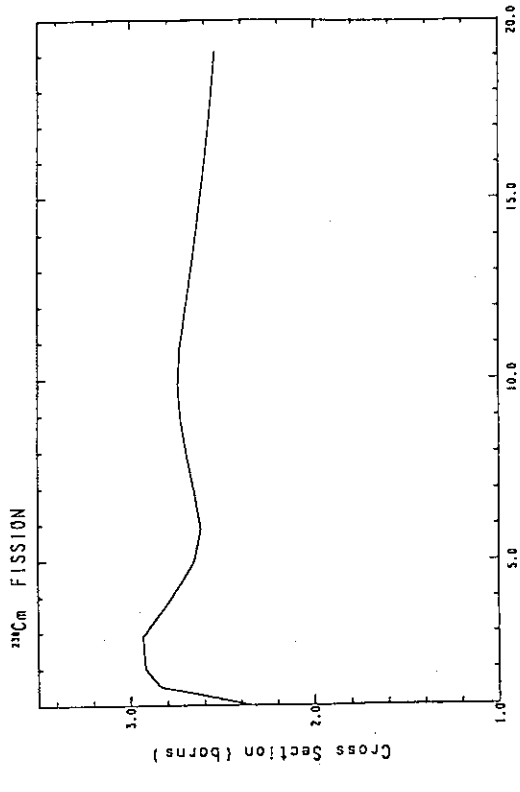

Fig. 145 The fission cross-section of ^{238}Cm.

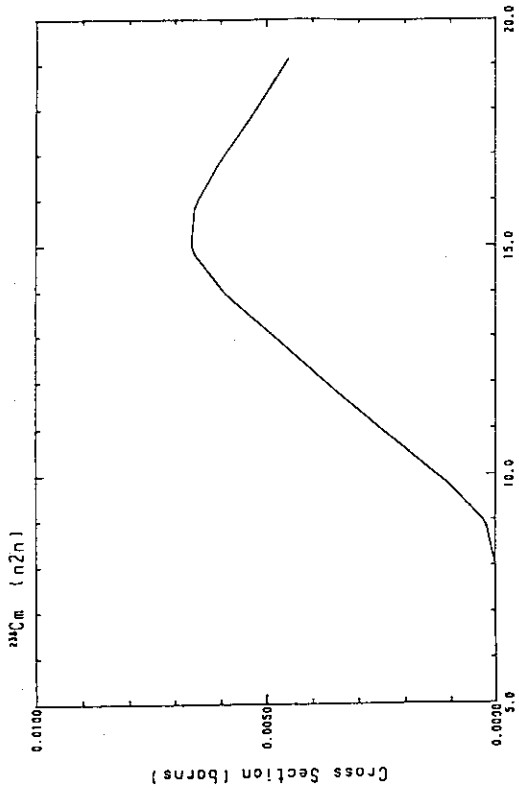

Fig. 146 The (n,2n)-reaction cross-section of ^{238}Cm.

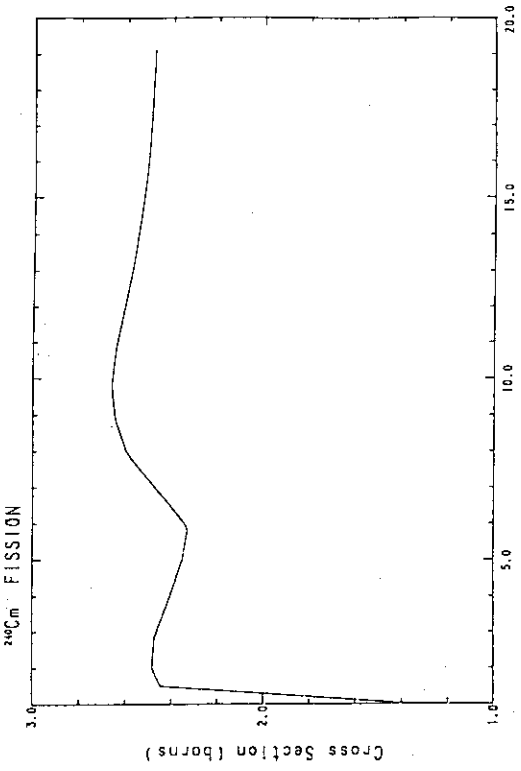

Fig. 151 The fission cross-section of ^{240}Cm.

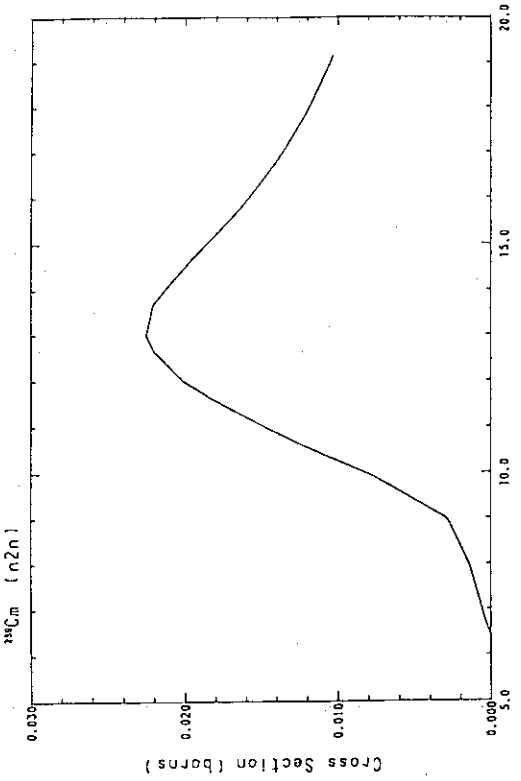

Fig. 149 The (n,2n)-reaction cross-section of ^{239}Cm.

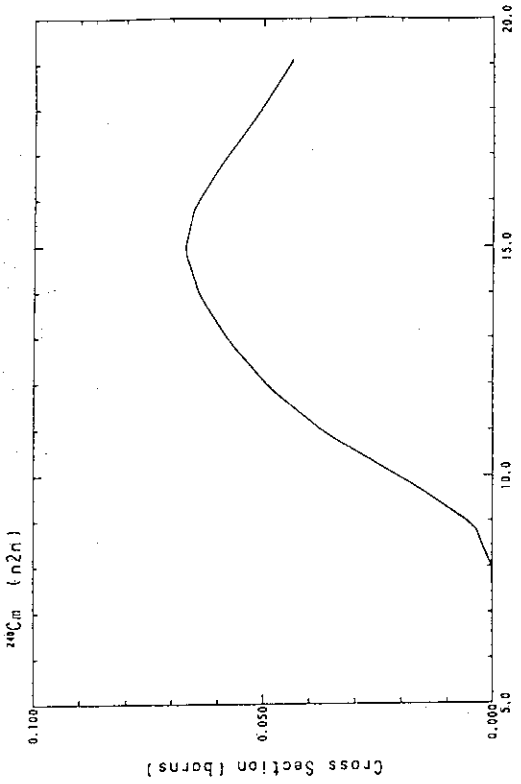

Fig. 152 The (n,2n)-reaction cross-section of ^{240}Cm.

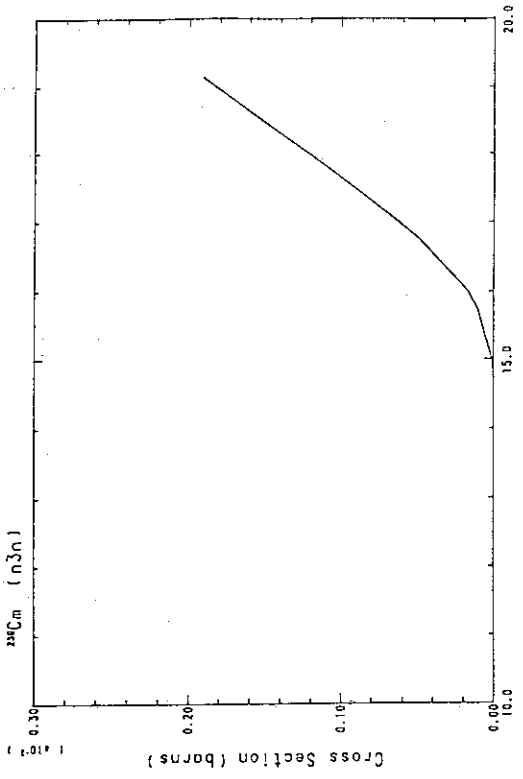

Fig. 150 The (n,3n)-reaction cross-section of ^{239}Cm.

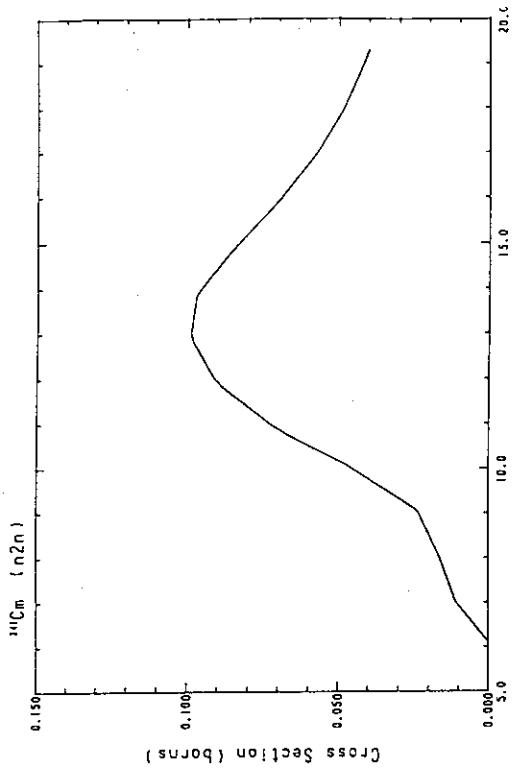

Fig. 155 The (n,2n)-reaction cross-section of ^{241}Cm.

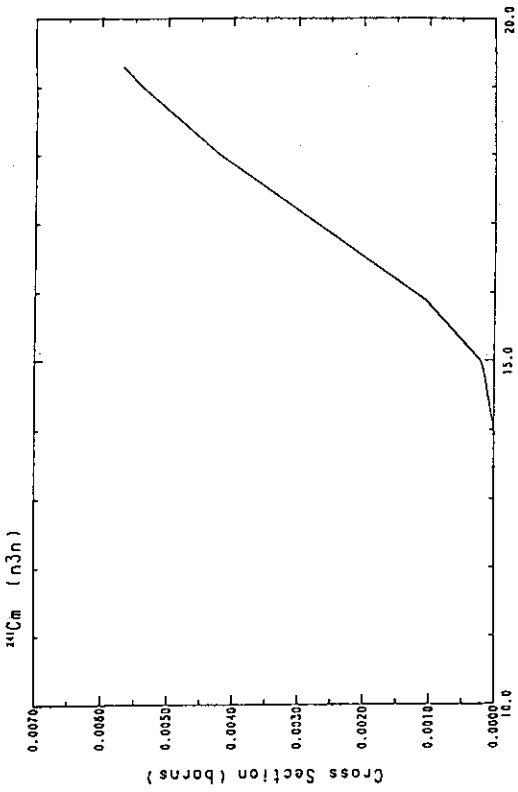

Fig. 156 The (n,3n)-reaction cross-section of ^{241}Cm.

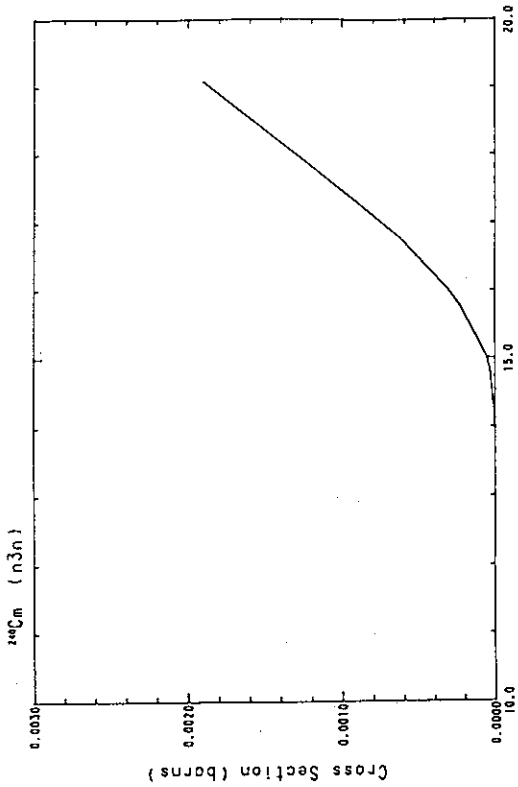

Fig. 153 The (n,3n)-reaction cross-section of ^{240}Cm.

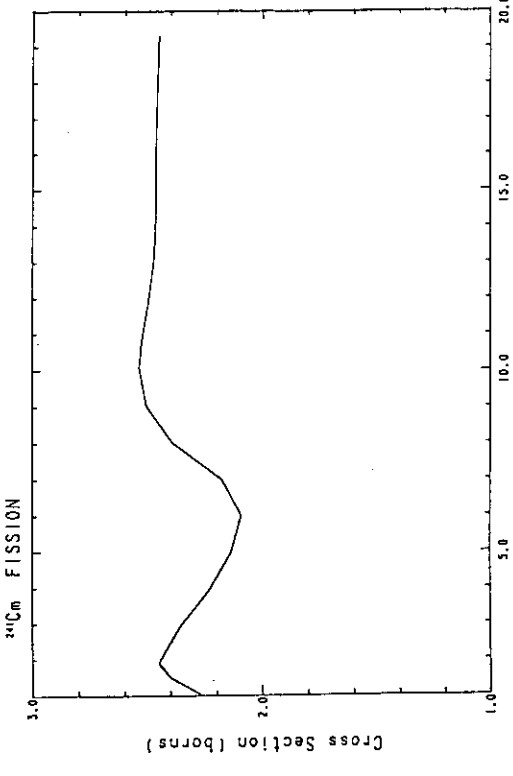

Fig. 154 The fission cross-section of ^{241}Cm.

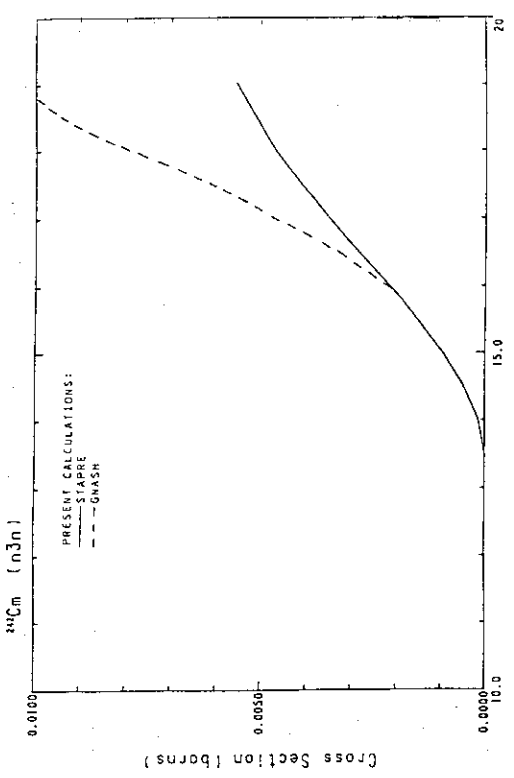

Fig. 159 The (n,3n)-reaction cross-section of ^{242}Cm.

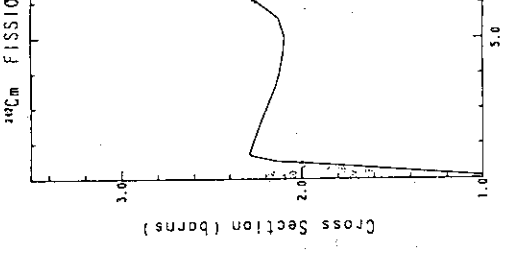

Fig. 157 The fission cross-section of ^{242}Cm.

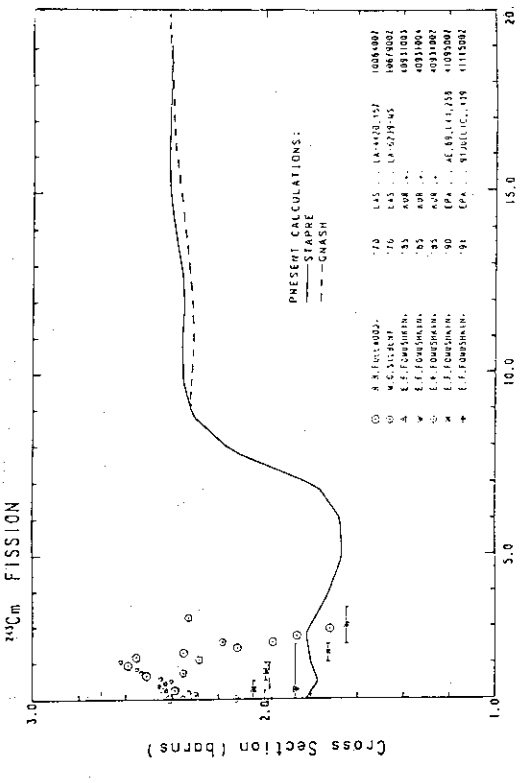

Fig. 160 The fission cross-section of ^{243}Cm.

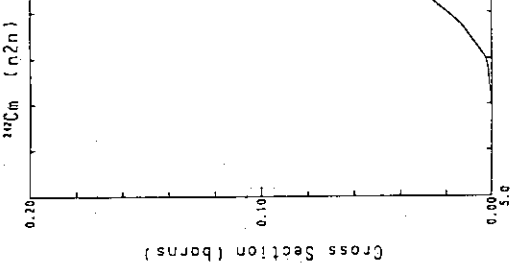

Fig. 158 The (n,2n)-reaction cross-section of ^{242}Cm.

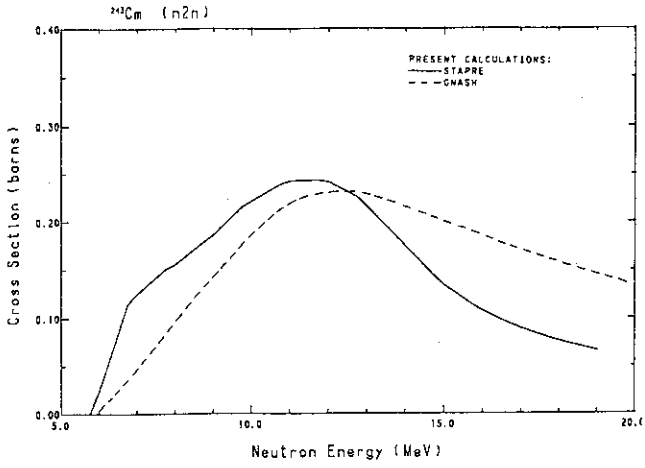

Fig. 162 The (n,3n)-reaction cross-section of ^{243}Cm.

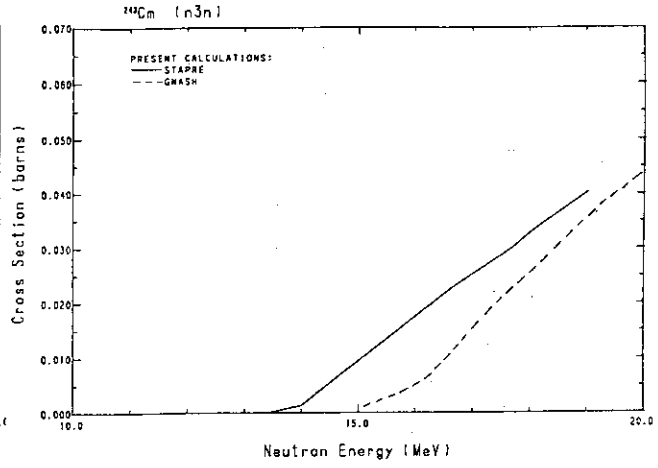

Fig. 161 The (n,2n)-reaction cross-section of ^{243}Cm.

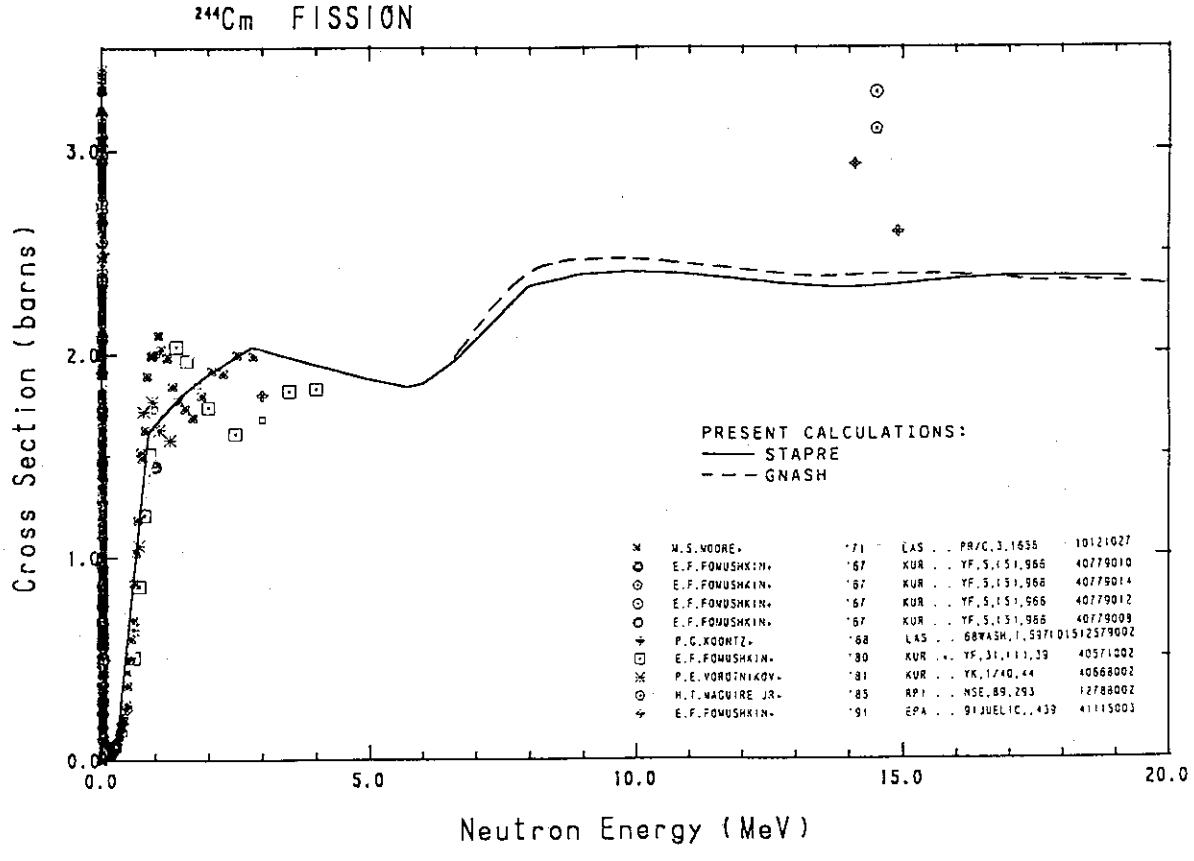

Fig. 163 The fission cross-section of ^{244}Cm.

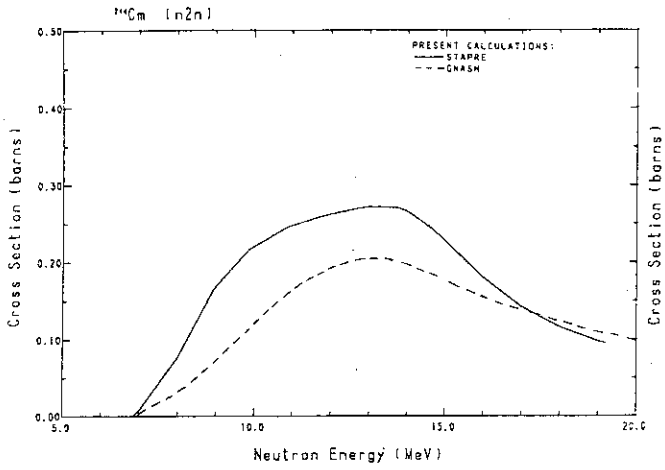

Fig. 164 The (n,2n)-reaction cross-section of ^{244}Cm.

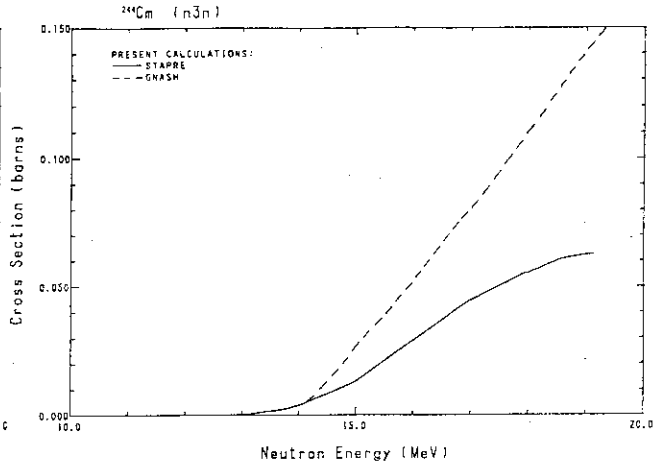

Fig. 165 The (n,3n)-reaction cross-section of ^{244}Cm.

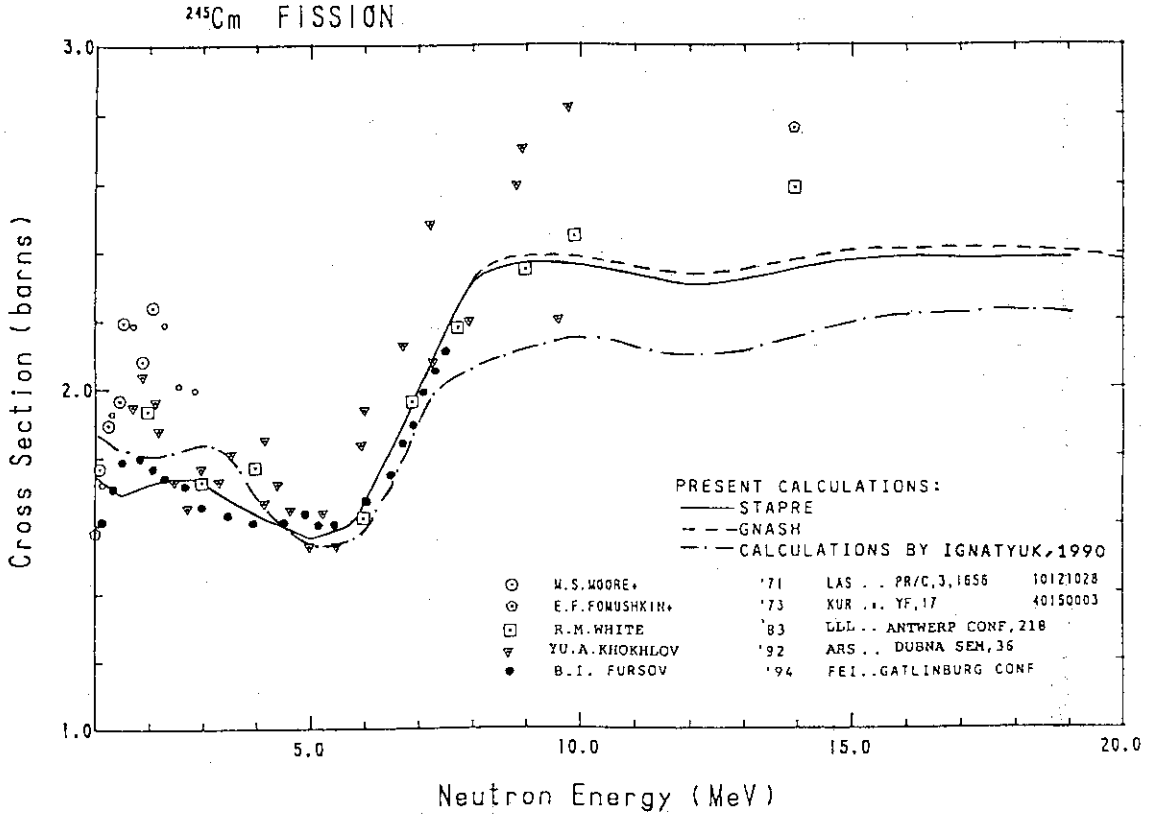

Fig. 166 The fission cross-section of ^{245}Cm.

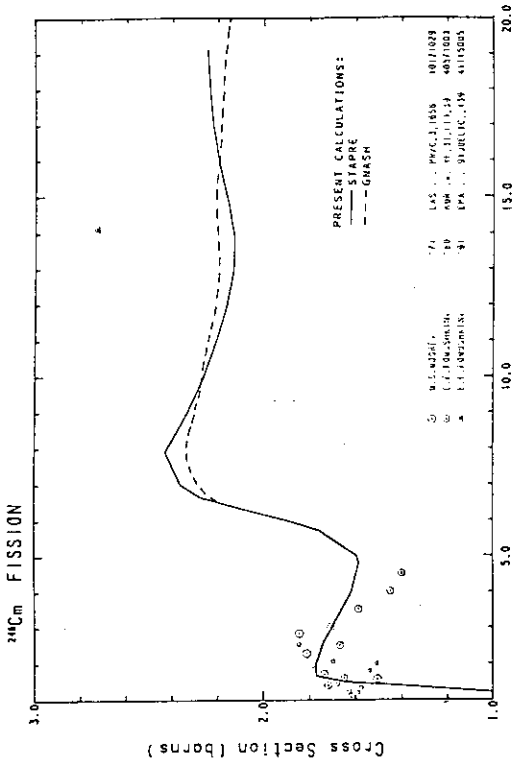

Fig. 169 The fission cross-section of ^{245}Cm.

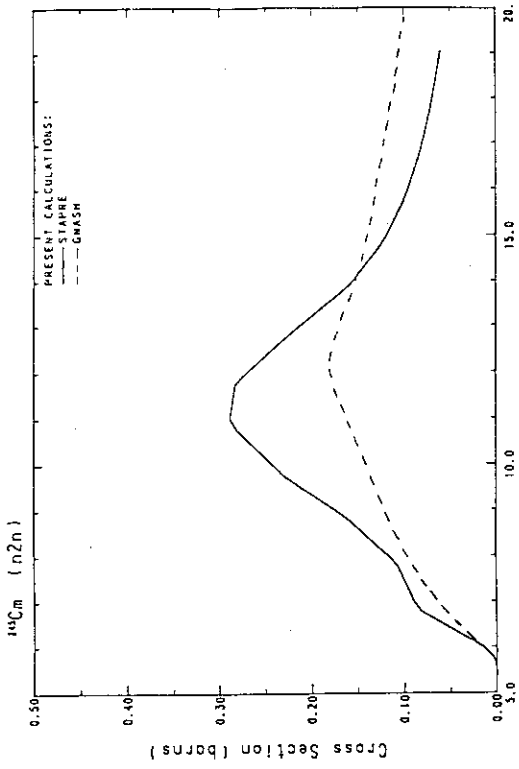

Fig. 167 The (n,2n)-reaction cross-section of ^{245}Cm.

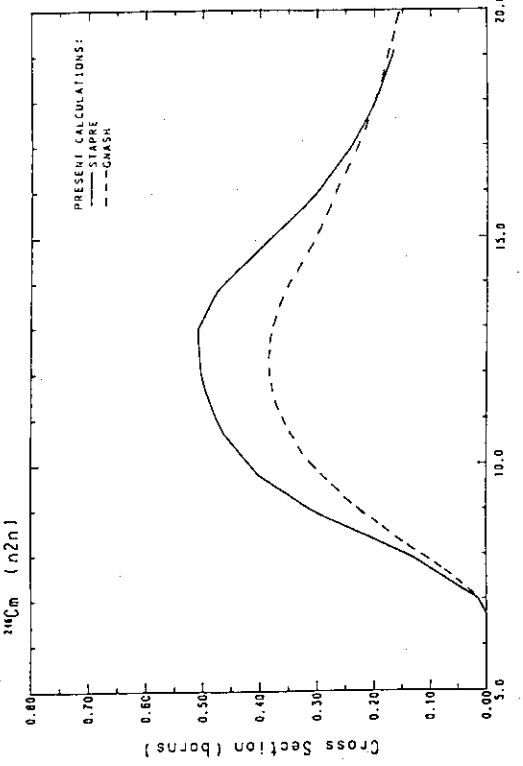

Fig. 170 The (n,2n)-reaction cross-section of ^{246}Cm.

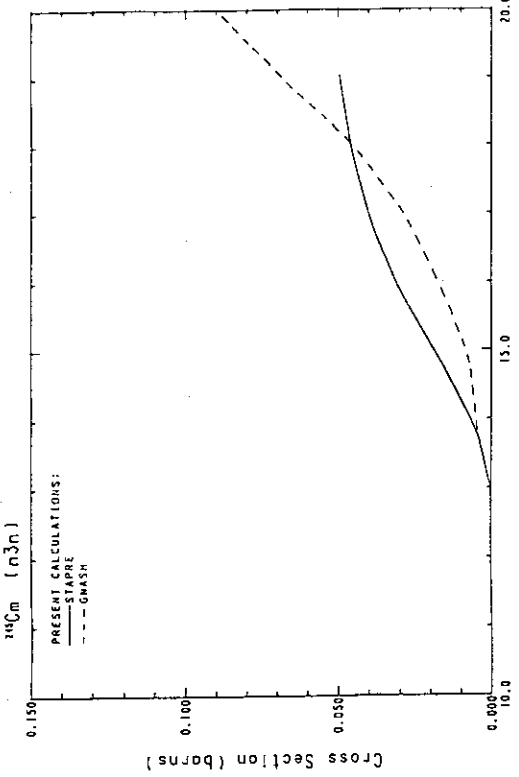

Fig. 168 The (n,3n)-reaction cross-section of ^{245}Cm.

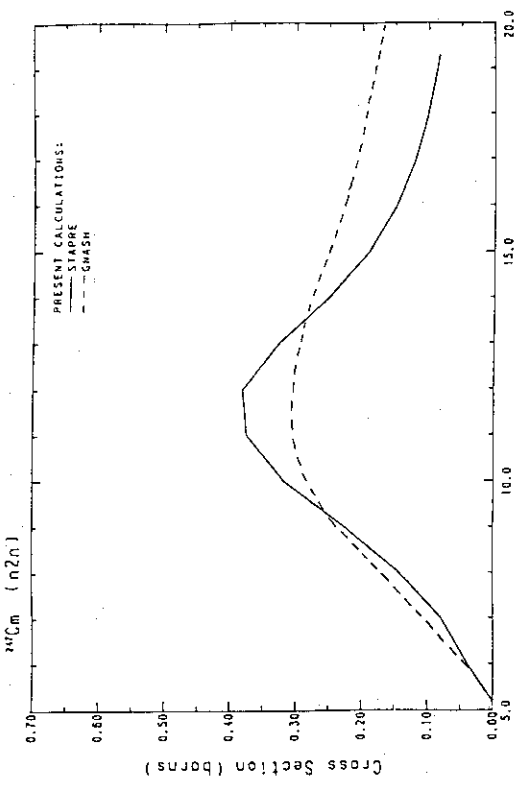

Fig. 171 The (n,3n)-reaction cross-section of ^{246}Cm.

Fig. 173 The (n,2n)-reaction cross-section of ^{247}Cm.

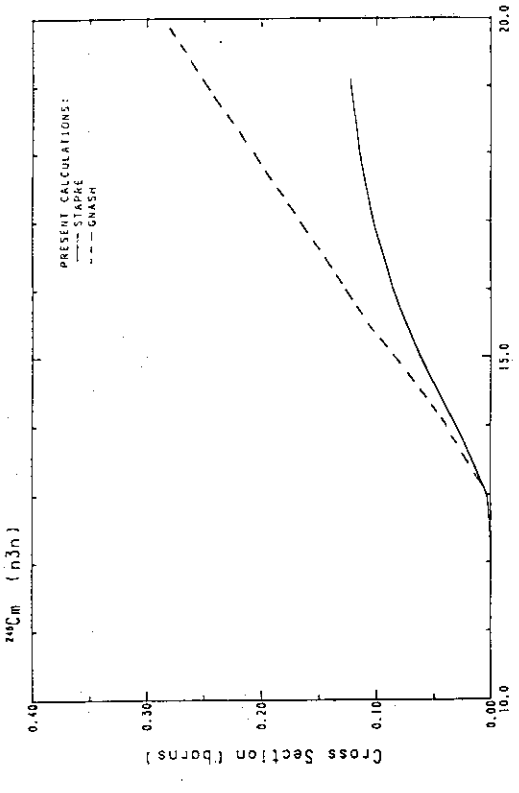

Fig. 172 The fission cross-section of ^{247}Cm.

Fig. 174 The (n,3n)-reaction cross-section of ^{247}Cm.

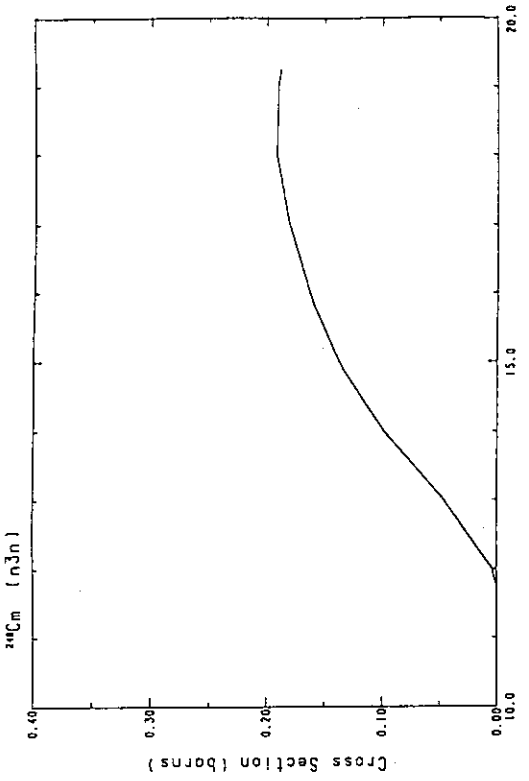

Fig. 177 The (n,3n)-reaction cross-section of ^{248}Cm.

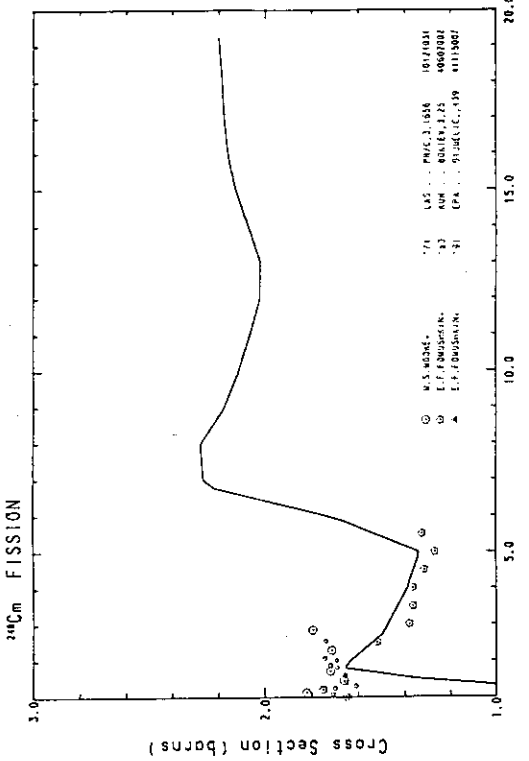

Fig. 175 The fission cross-section of ^{248}Cm.

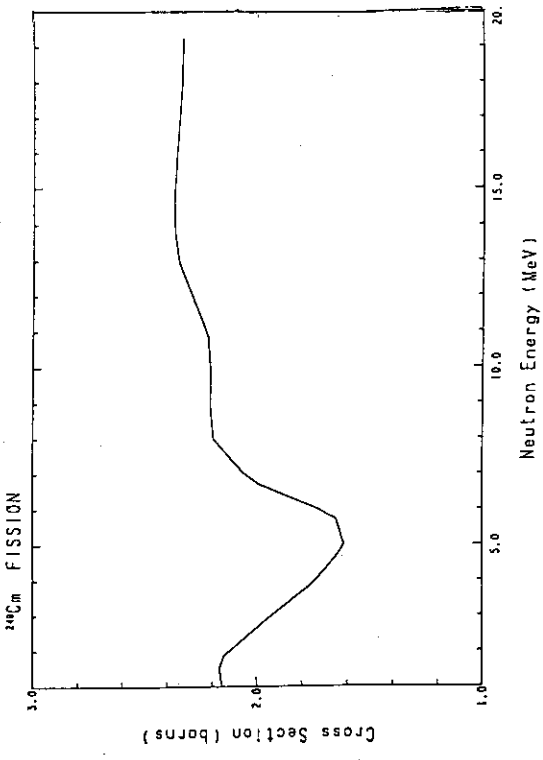

Fig. 178 The fission cross-section of ^{249}Cm.

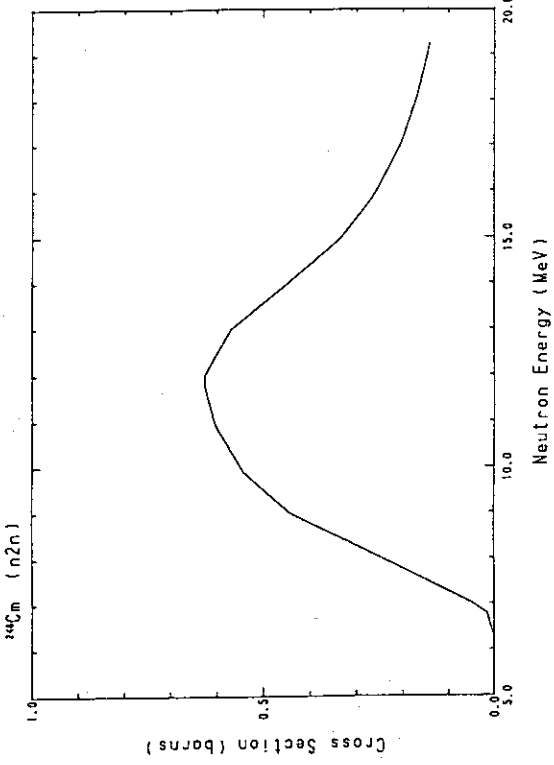

Fig. 176 The (n,2n)-reaction cross-section of ^{248}Cm.

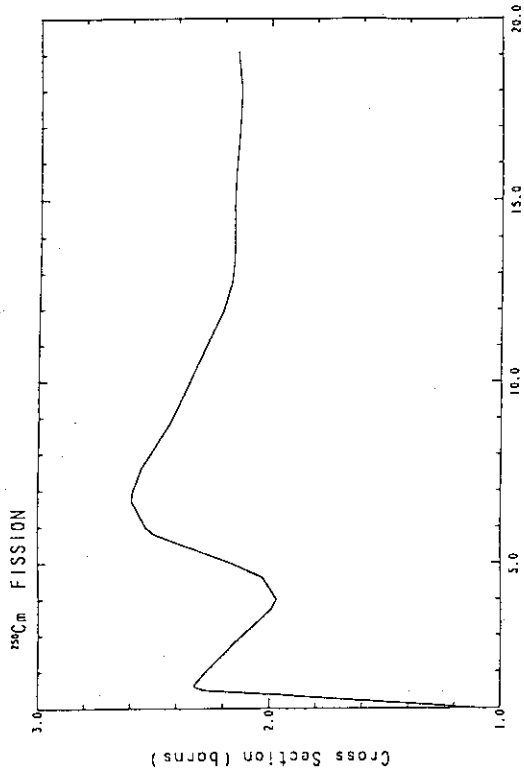

Fig. 181 The fission cross-section of ^{250}Cm.

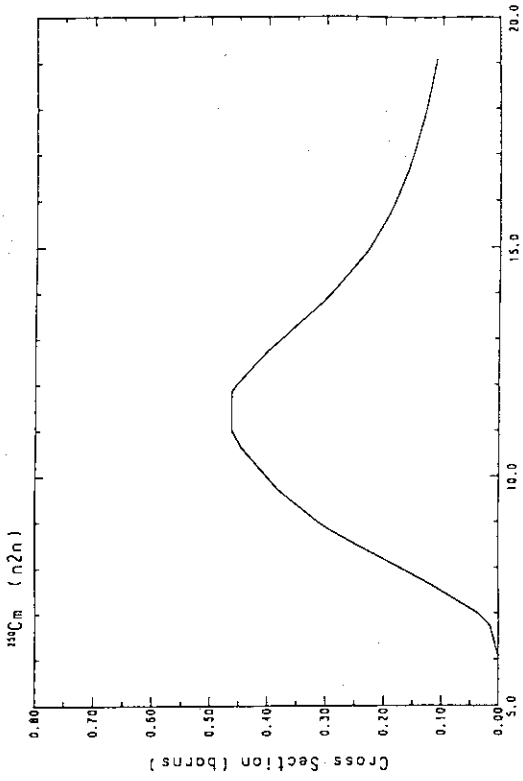

Fig. 182 The (n,2n)-reaction cross-section of ^{250}Cm.

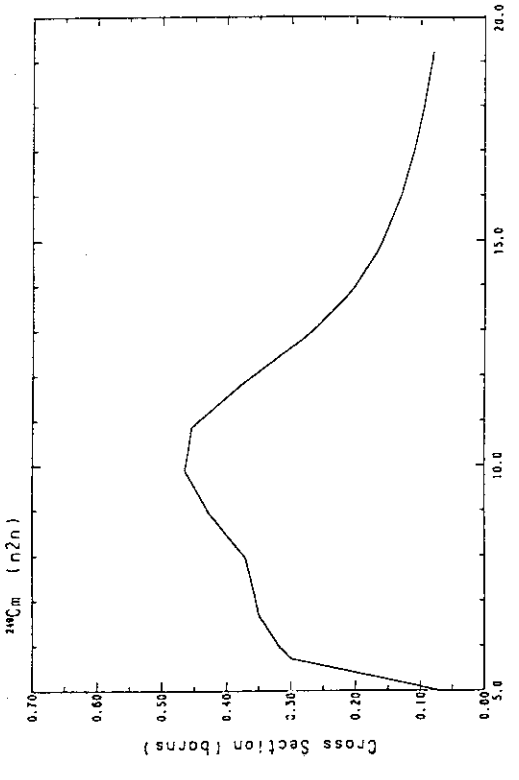

Fig. 179 The (n,2n)-reaction cross-section of ^{249}Cm.

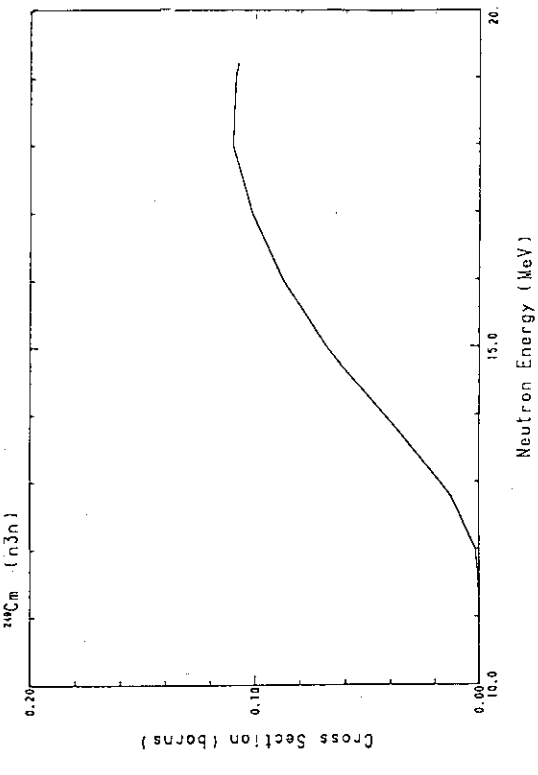

Fig. 180 The (n,3n)-reaction cross-section of ^{249}Cm.

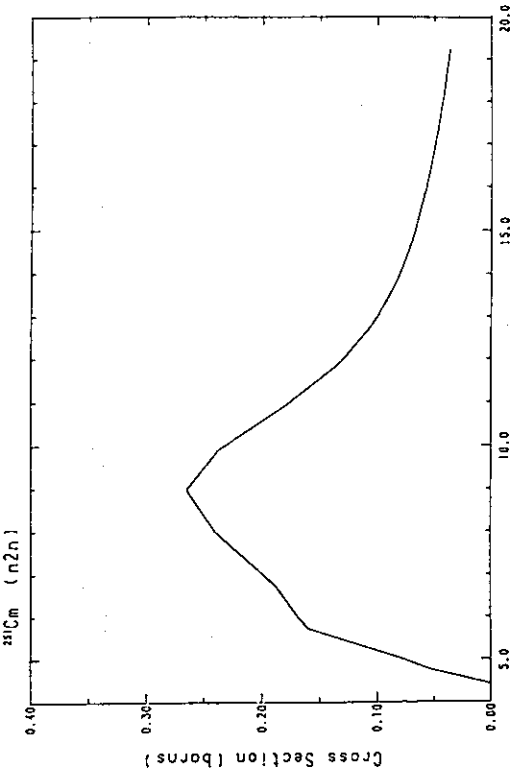

Fig. 183 The (n,3n)-reaction cross-section of ^{250}Cm.

Fig. 185 The (n,2n)-reaction cross-section of ^{251}Cm.

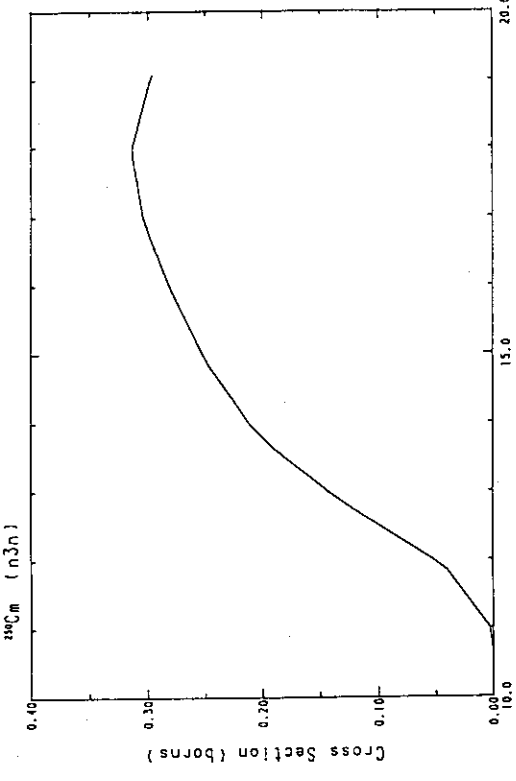

Fig. 184 The fission cross-section of ^{251}Cm.

Fig. 186 The (n,3n)-reaction cross-section of ^{251}Cm.

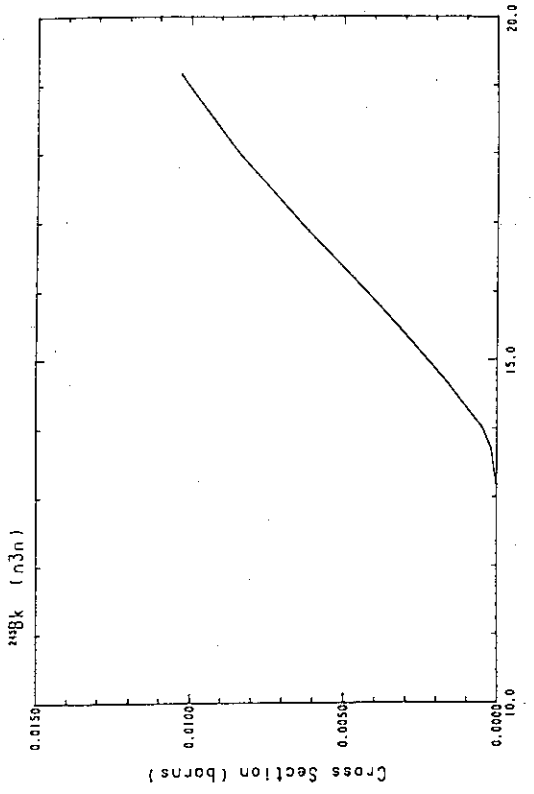

Fig. 189 The (n,3n)-reaction cross-section of ^{245}Bk.

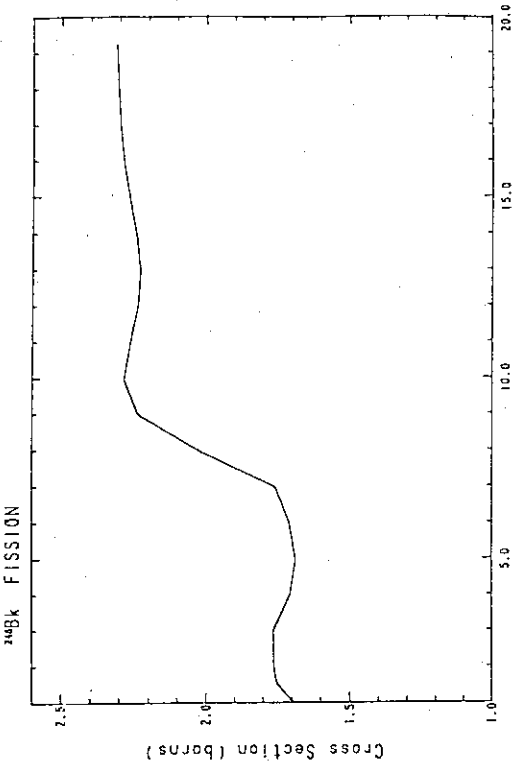

Fig. 190 The fission cross-section of ^{246}Bk.

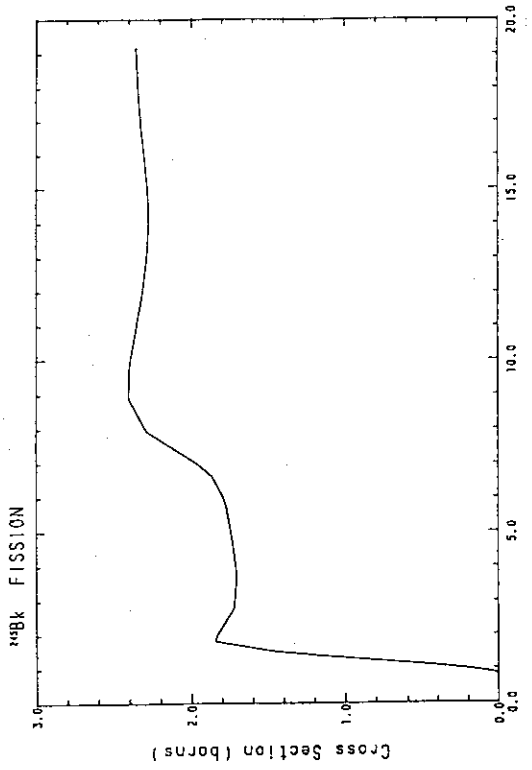

Fig. 187 The fission cross-section of ^{245}Bk.

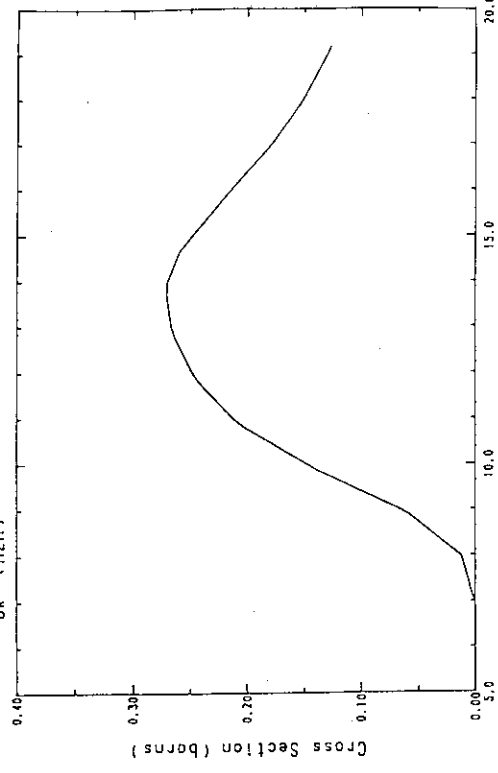

Fig. 188 The (n,2n)-reaction cross-section of ^{245}Bk.

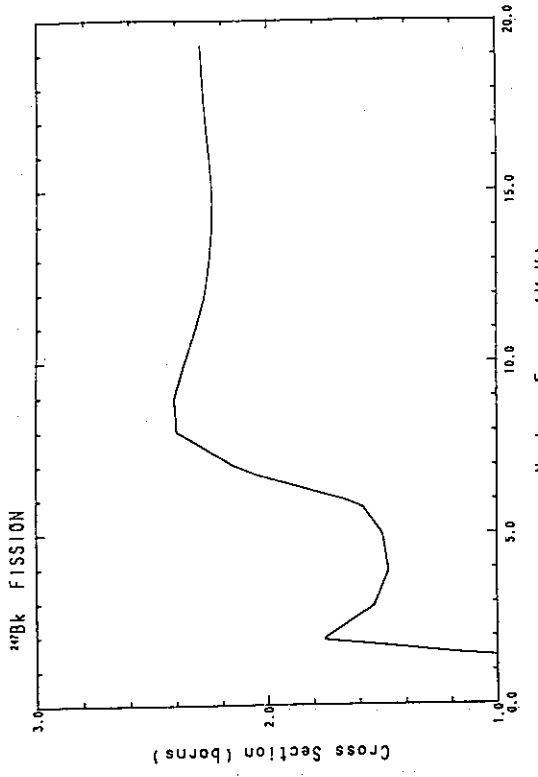

Fig. 193 The fission cross-section of ^{247}Bk.

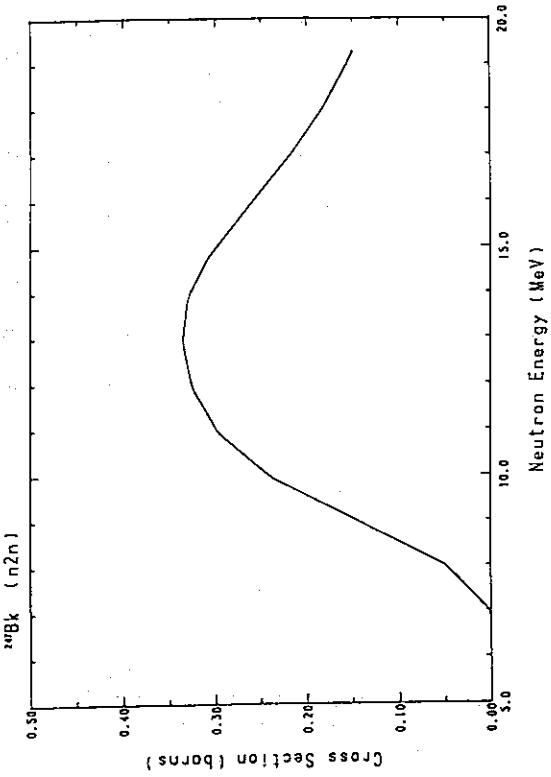

Fig. 194 The (n,2n)-reaction cross-section of ^{247}Bk.

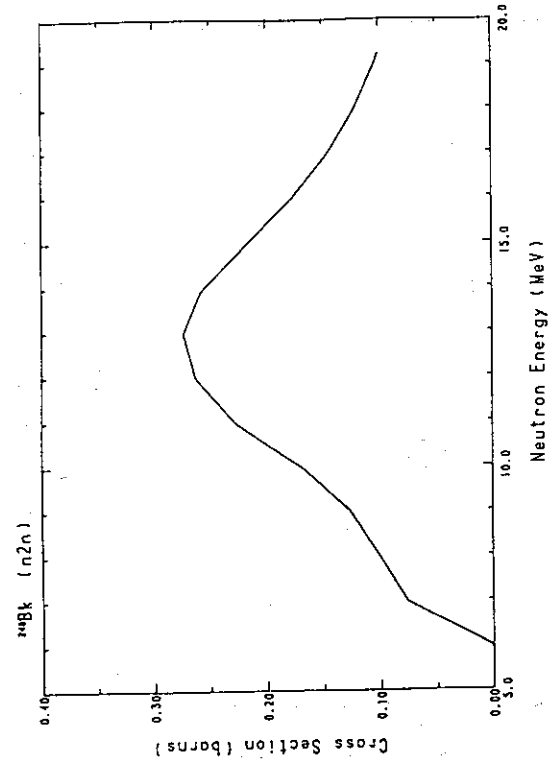

Fig. 191 The (n,2n)-reaction cross-section of ^{246}Bk.

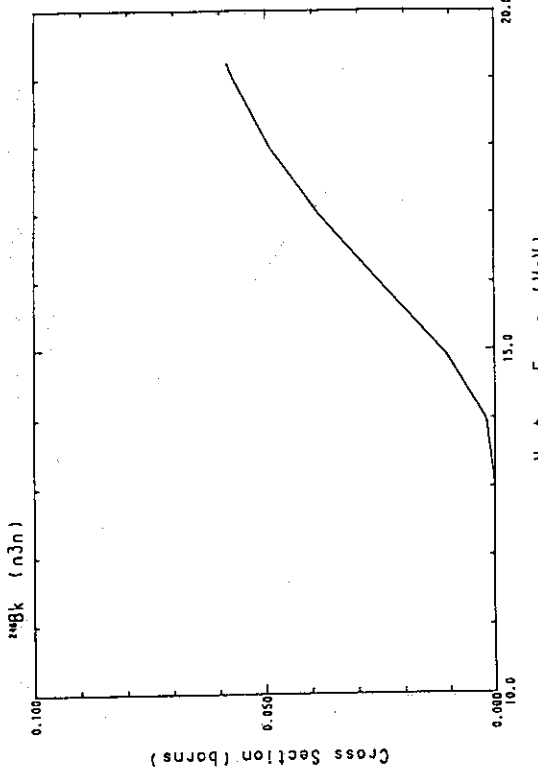

Fig. 192 The (n,3n)-reaction cross-section of ^{246}Bk.

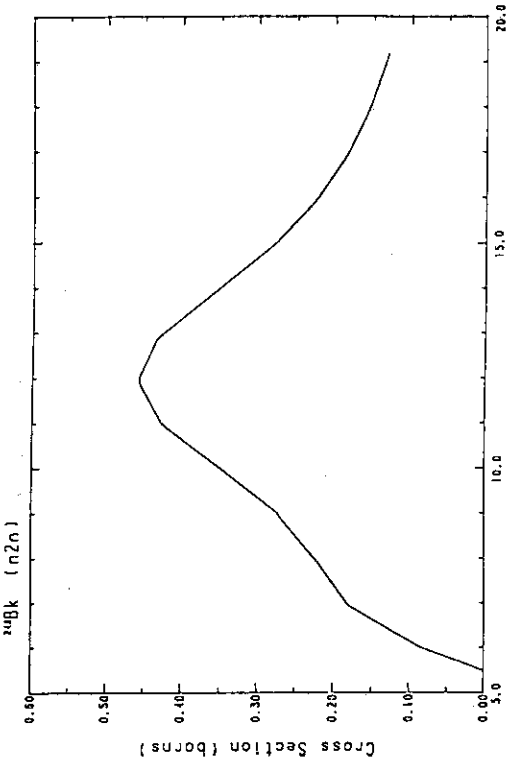

Fig. 197 The (n,2n)-reaction cross-section of ^{249}Bk.

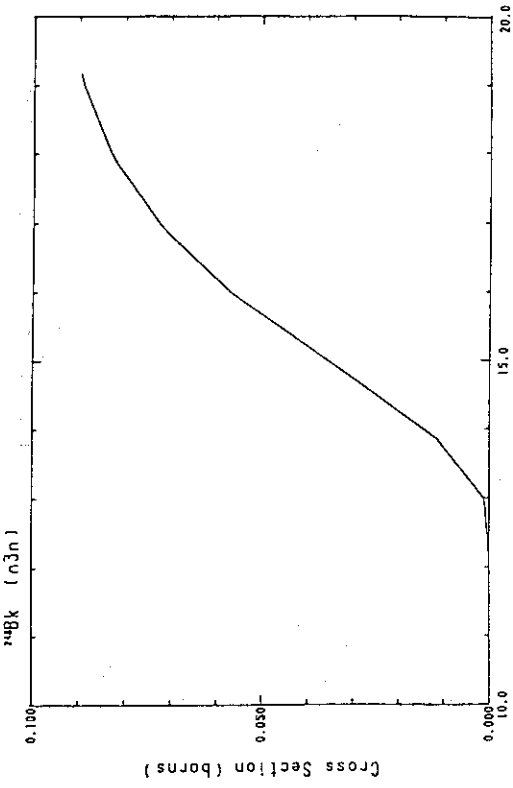

Fig. 198 The (n,3n)-reaction cross-section of ^{249}Bk.

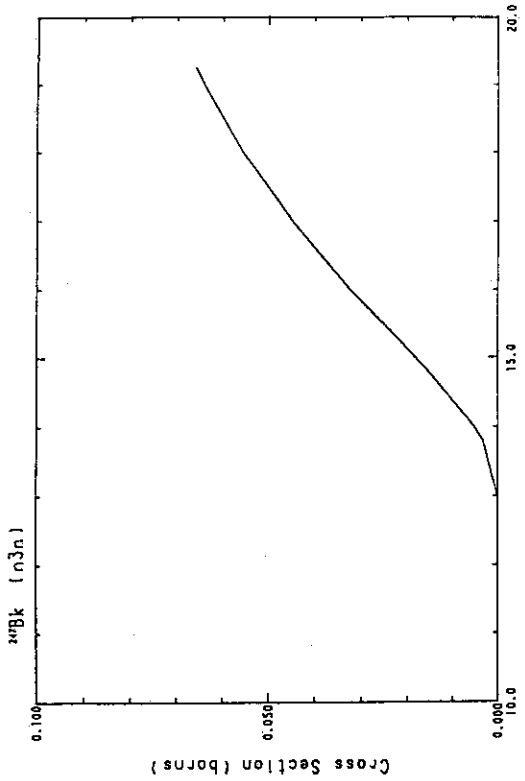

Fig. 195 The (n,3n)-reaction cross-section of ^{247}Bk.

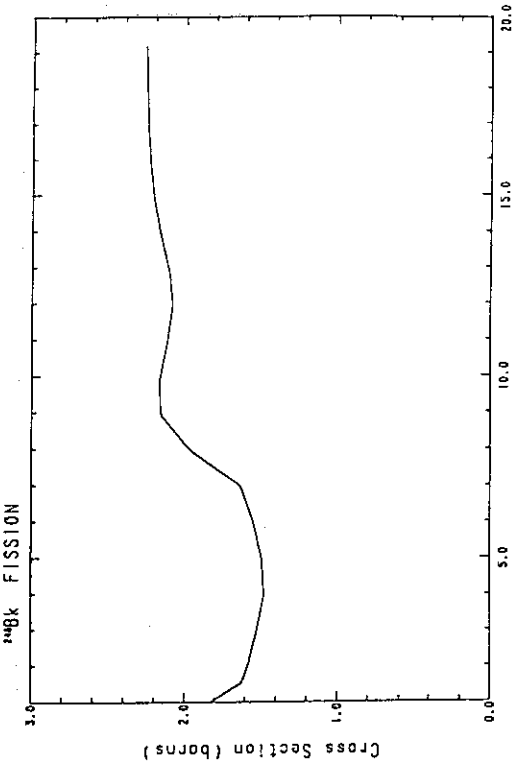

Fig. 196 The fission cross-section of ^{249}Bk.

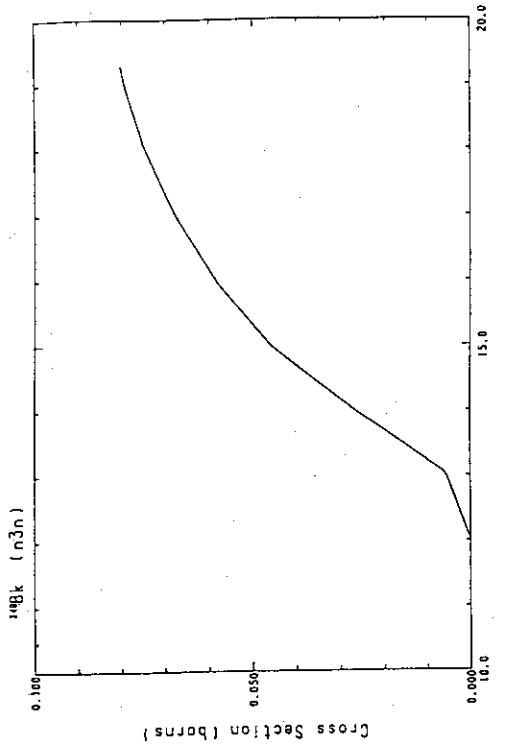

Fig. 201 The (n,3n)-reaction cross-section of ^{249}Bk.

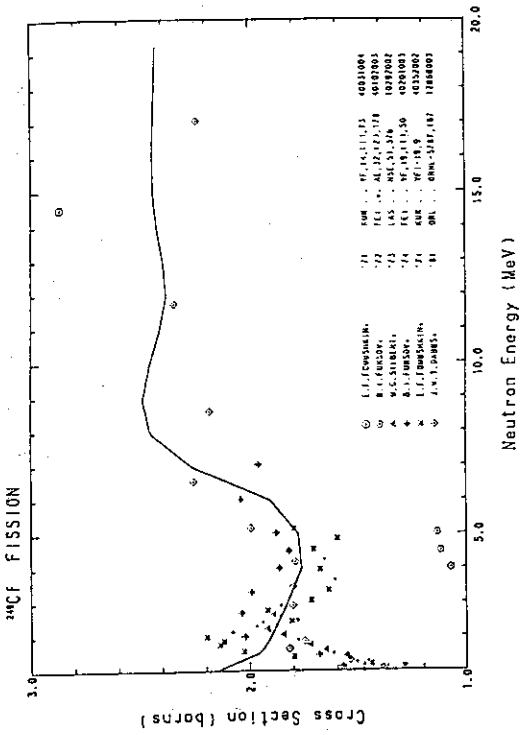

Fig. 202 The fission cross-section of ^{249}Cf.

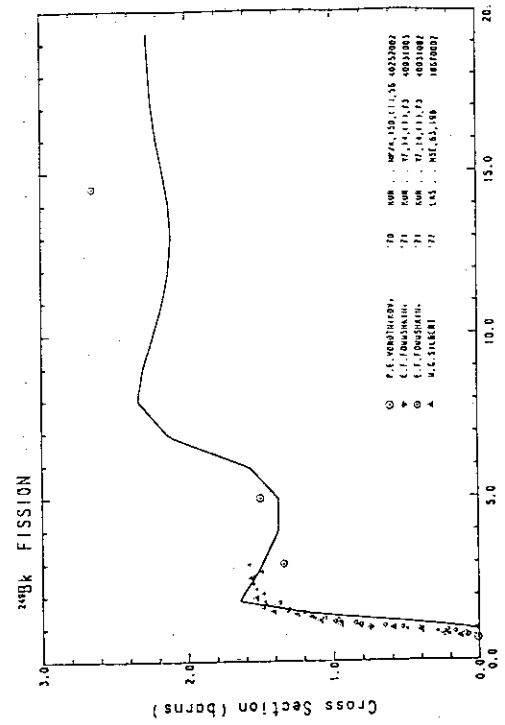

Fig. 199 The fission cross-section of ^{249}Bk.

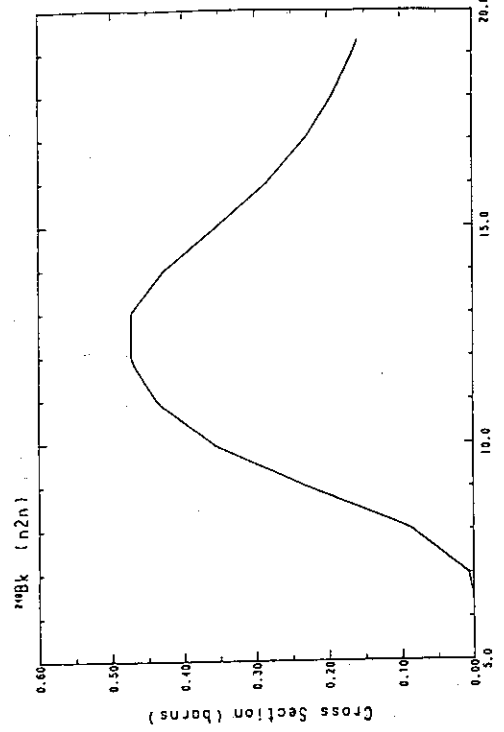

Fig. 200 The (n,2n)-reaction cross-section of ^{249}Bk.

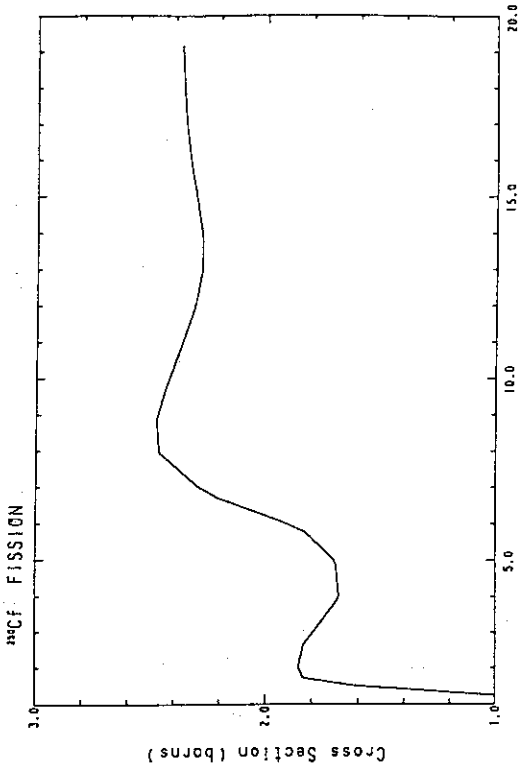

Fig. 205 The fission cross-section of ^{250}Cf.

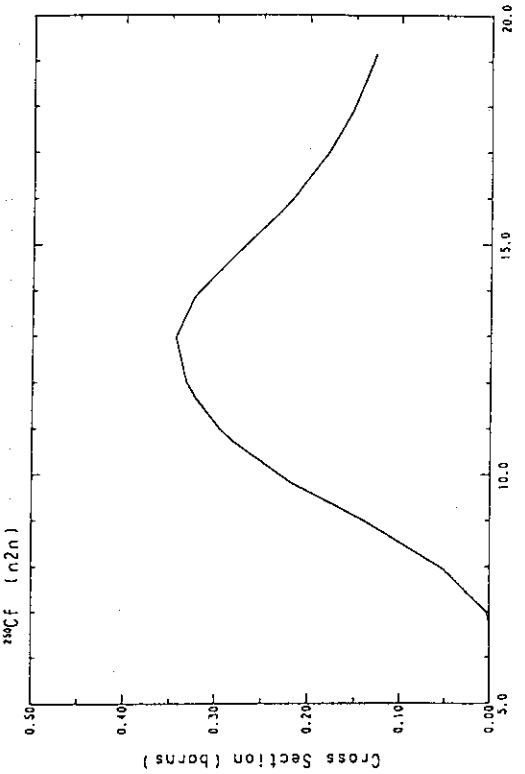

Fig. 206 The (n,2n)-reaction cross-section of ^{250}Cf.

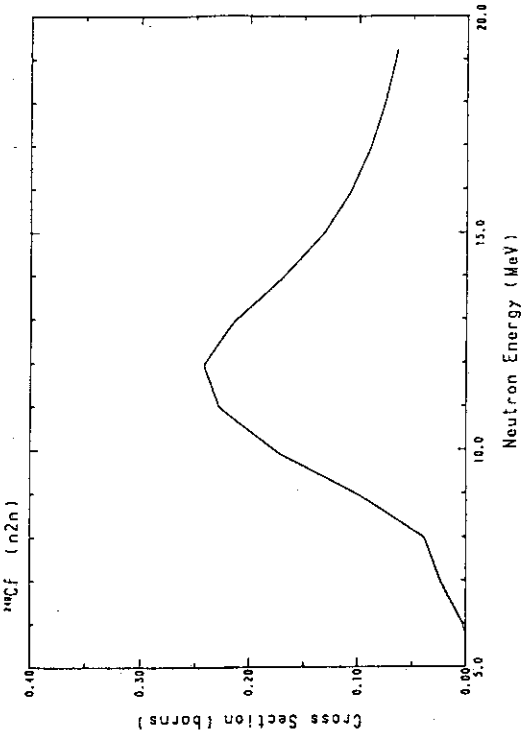

Fig. 203 The (n,2n)-reaction cross-section of ^{249}Cf.

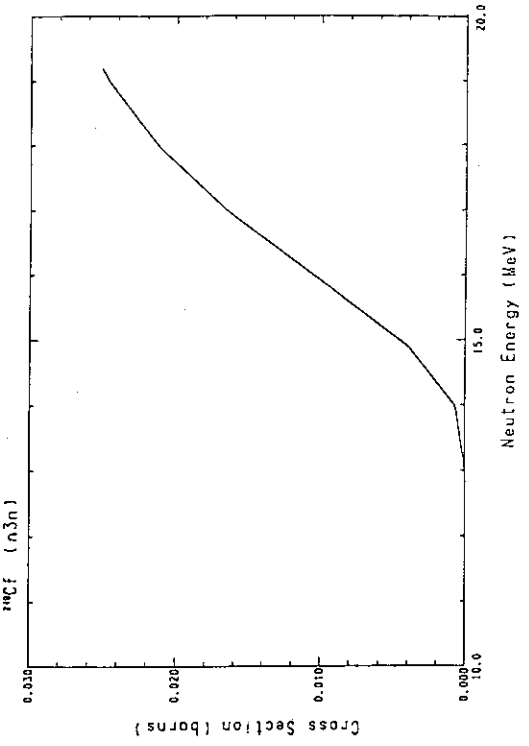

Fig. 204 The (n,3n)-reaction cross-section of ^{249}Cf.

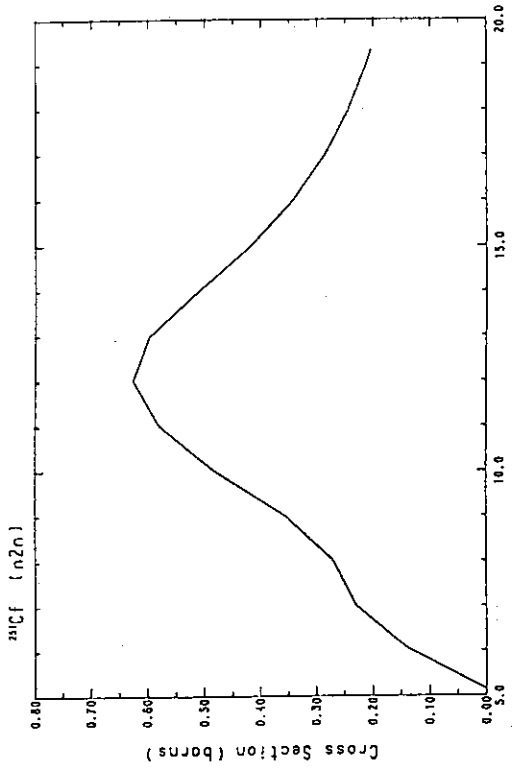

Fig. 207 The (n,3n)-reaction cross-section of ^{250}Cf.

Fig. 209 The (n,2n)-reaction cross-section of ^{251}Cf.

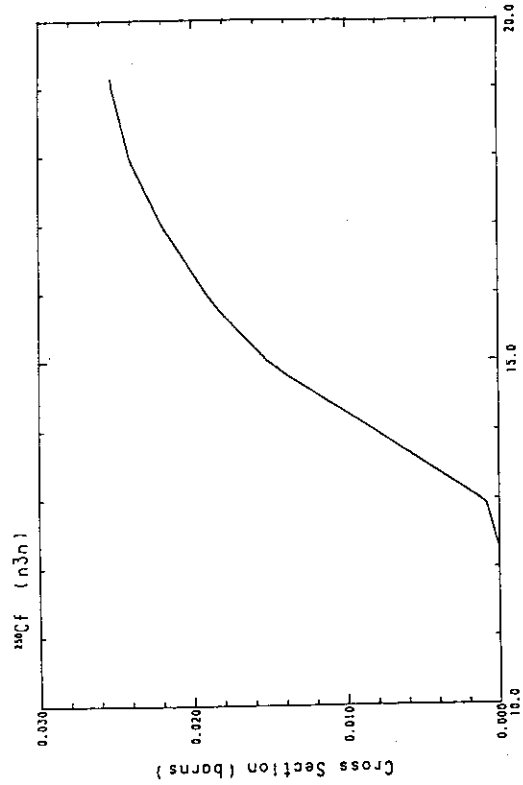

Fig. 208 The fission cross-section of ^{251}Cf.

Fig. 210 The (n,3n)-reaction cross-section of ^{251}Cf.

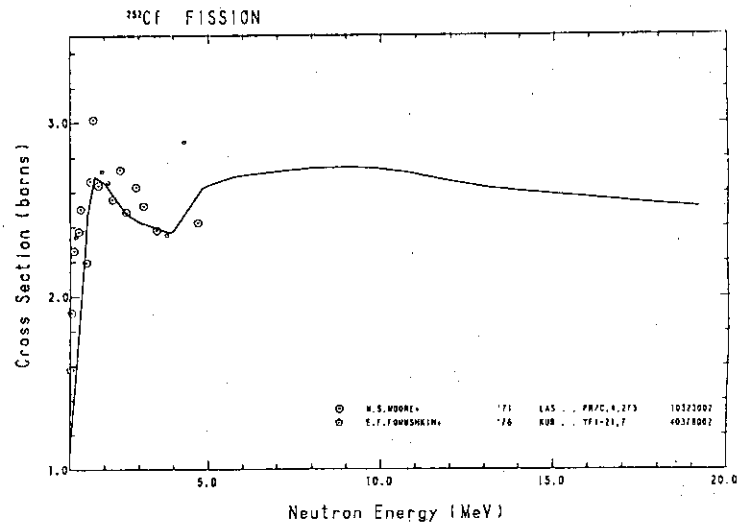

Fig. 211 The fission cross-section of ^{252}Cf.

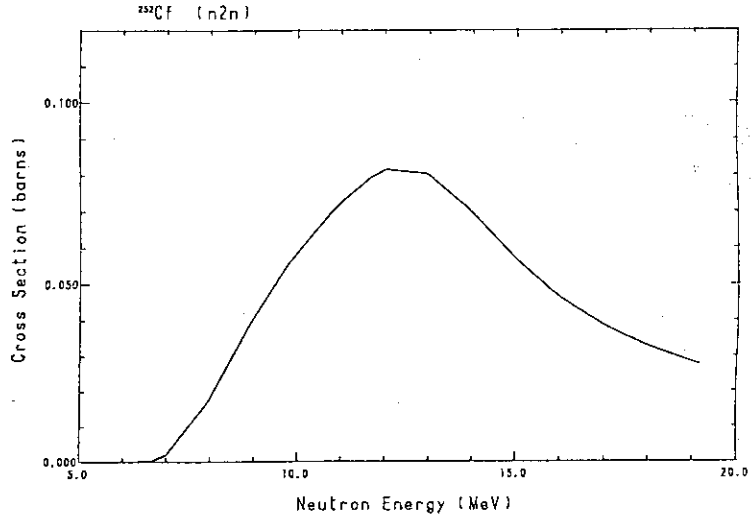

Fig. 212 The (n,2n)-reaction cross-section of ^{252}Cf.

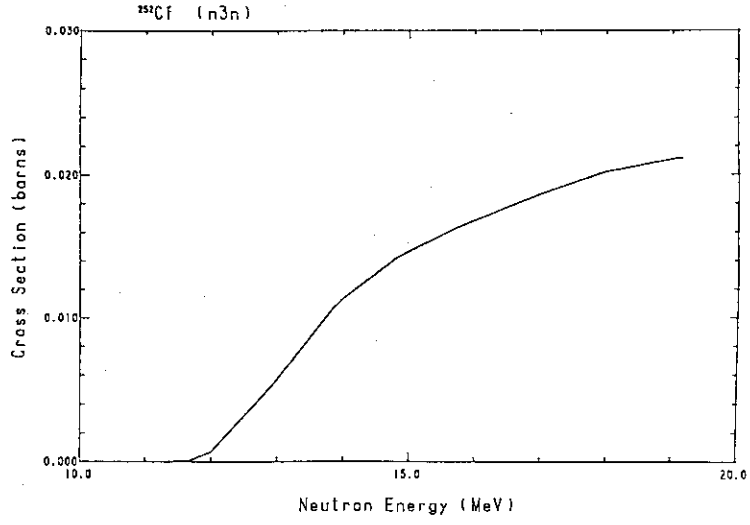

Fig. 213 The (n,3n)-reaction cross-section of ^{252}Cf.

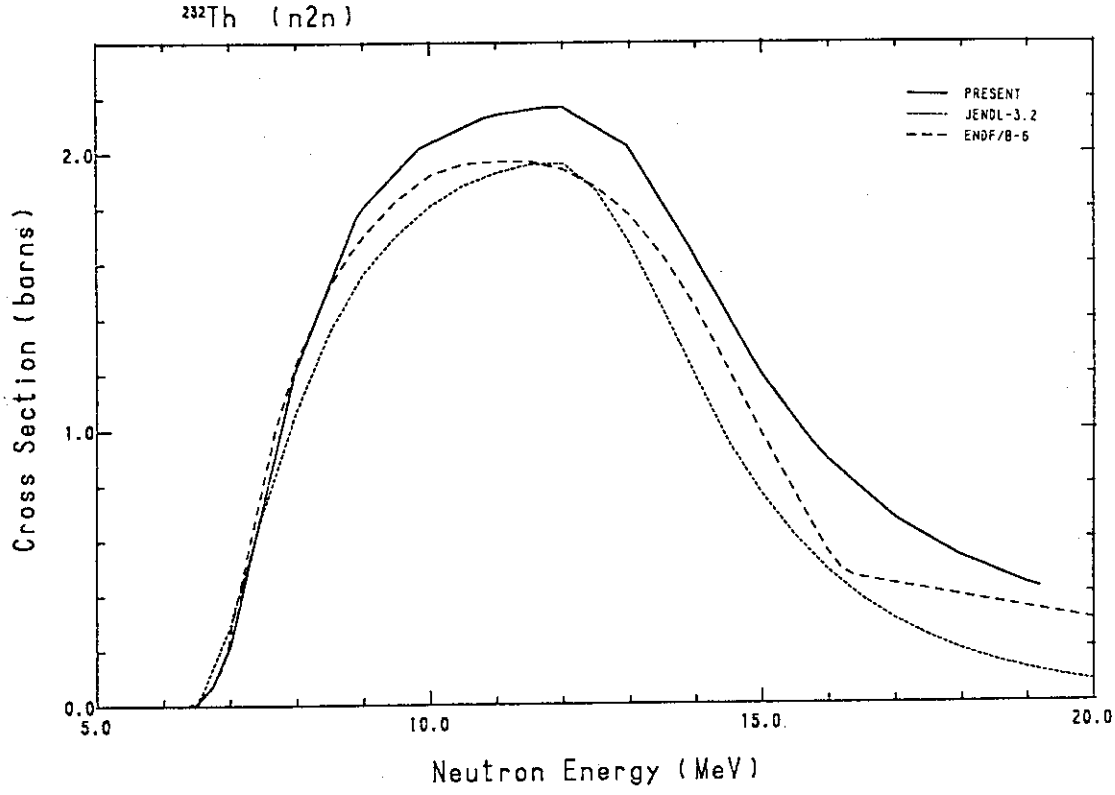

Fig. 214 Comparison of the (n,2n)-cross-section for ^{232}Th.

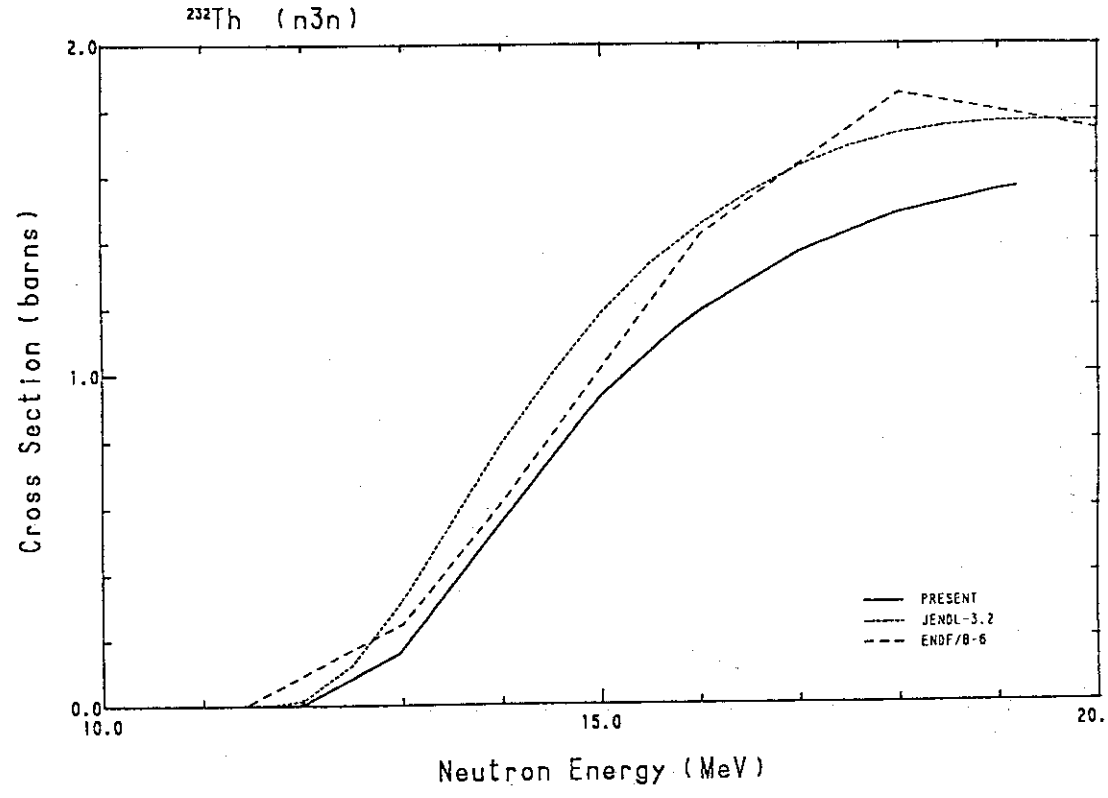

Fig. 215 Comparison of the (n,3n)-cross-section for ^{232}Th.

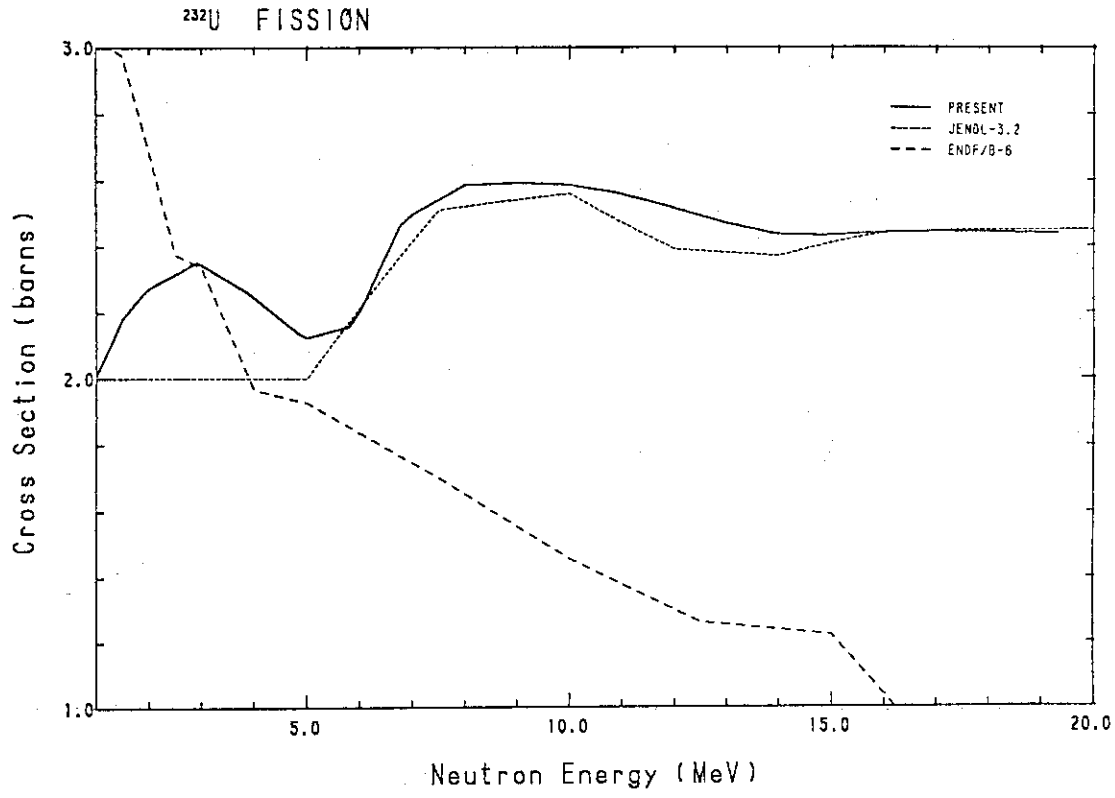

Fig. 216 Comparison of the fission cross-section for ^{232}U.

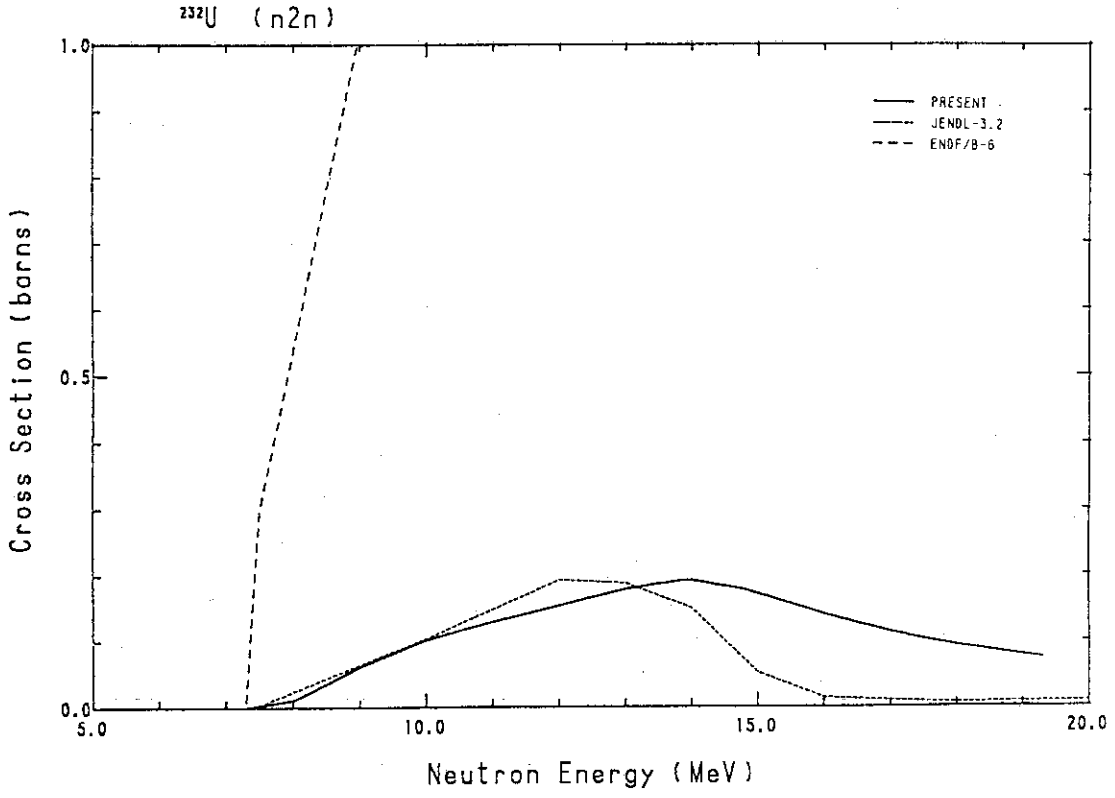

Fig. 217 Comparison of the (n,2n)-cross-section for ^{232}U.

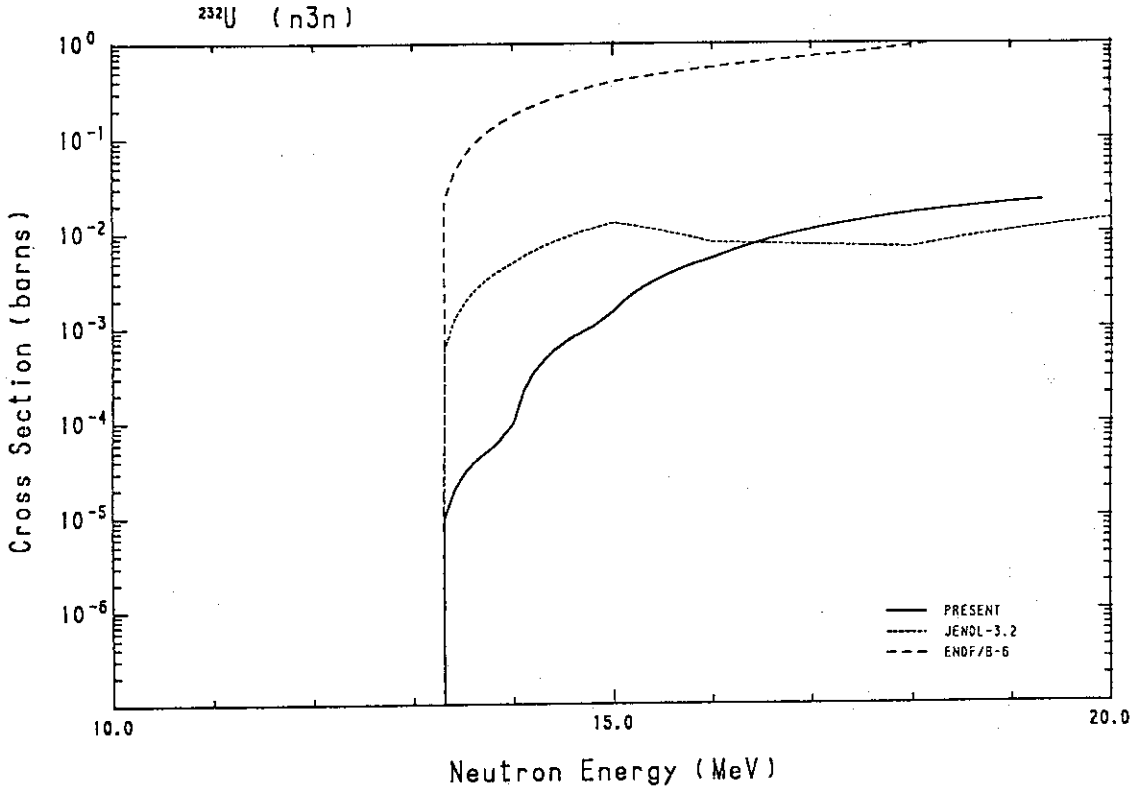

Fig. 218 Comparison of the (n,3n)-cross-section for ^{232}U.

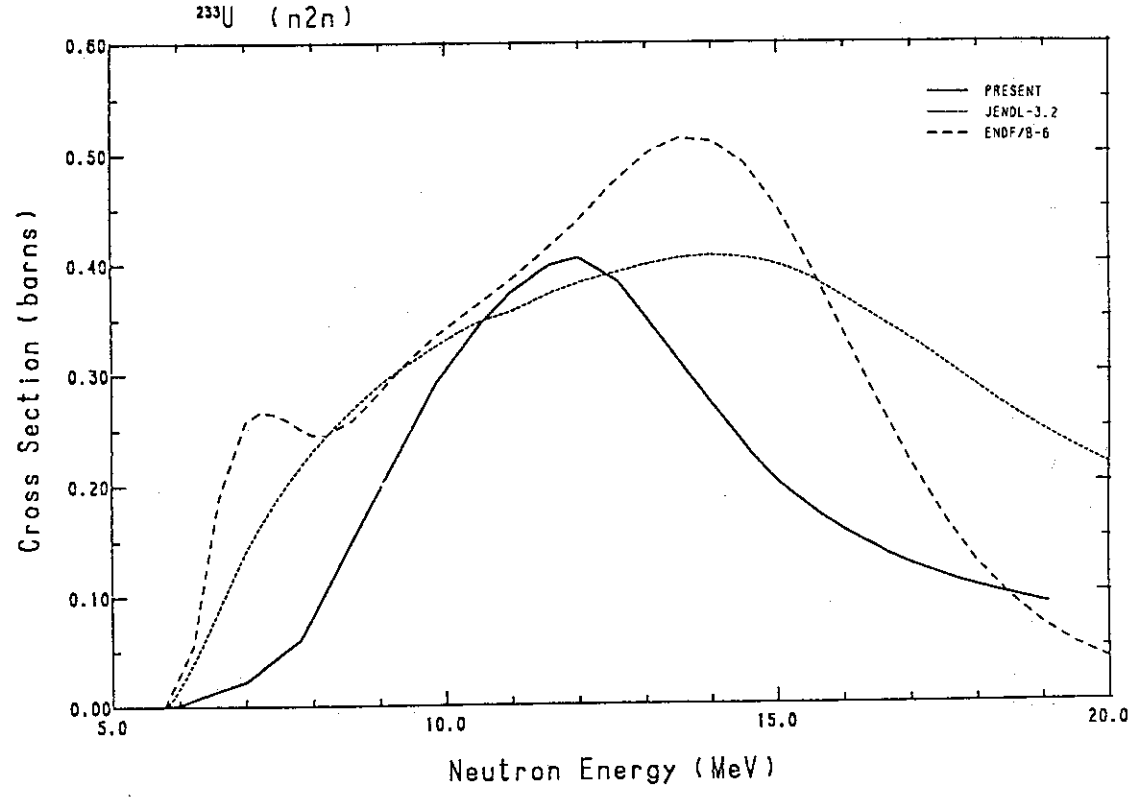

Fig. 219 Comparison of the (n,2n)-cross-section for ^{233}U.

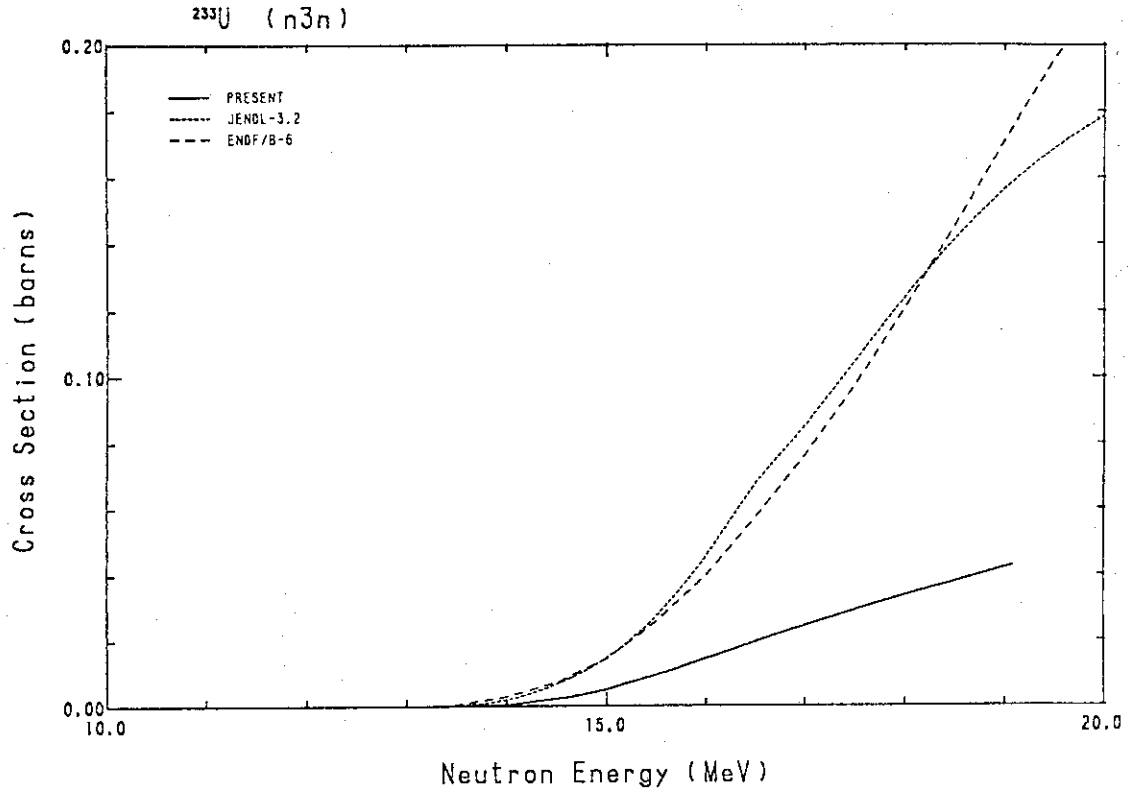

Fig. 220 Comparison of the (n,3n)-cross-section for ^{233}U.

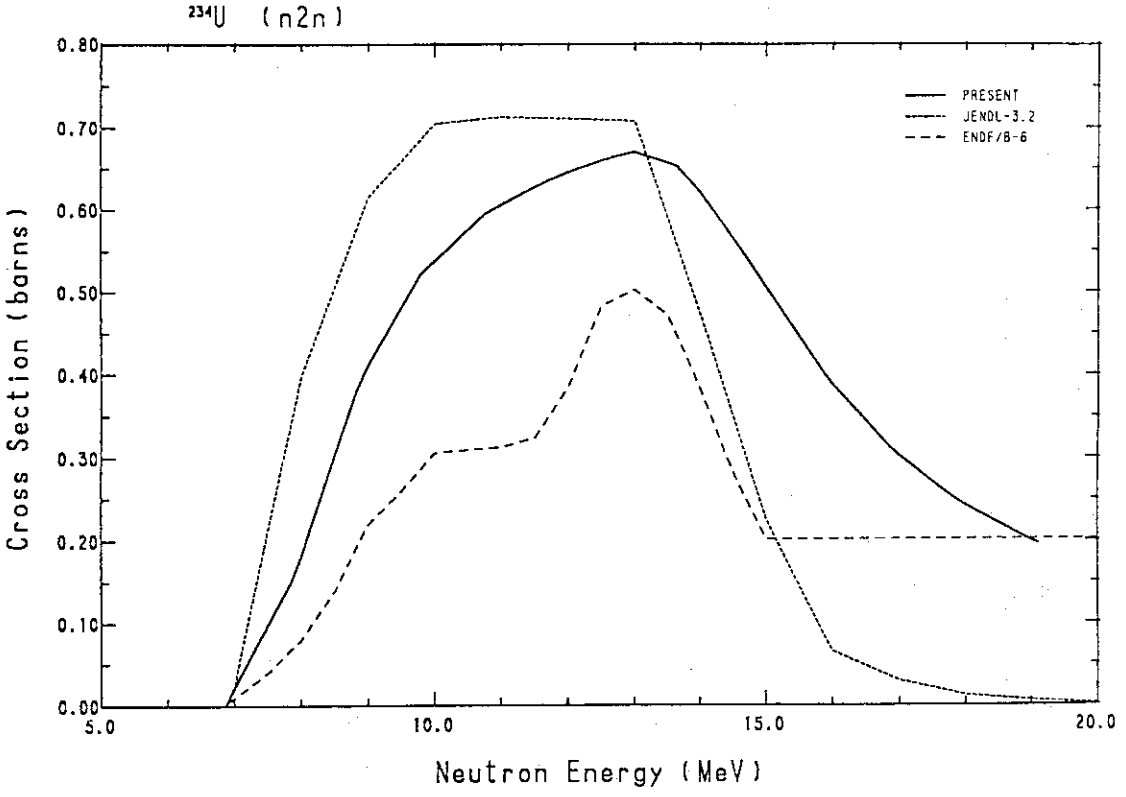

Fig. 221 Comparison of the (n,2n)-cross-section for ^{234}U.

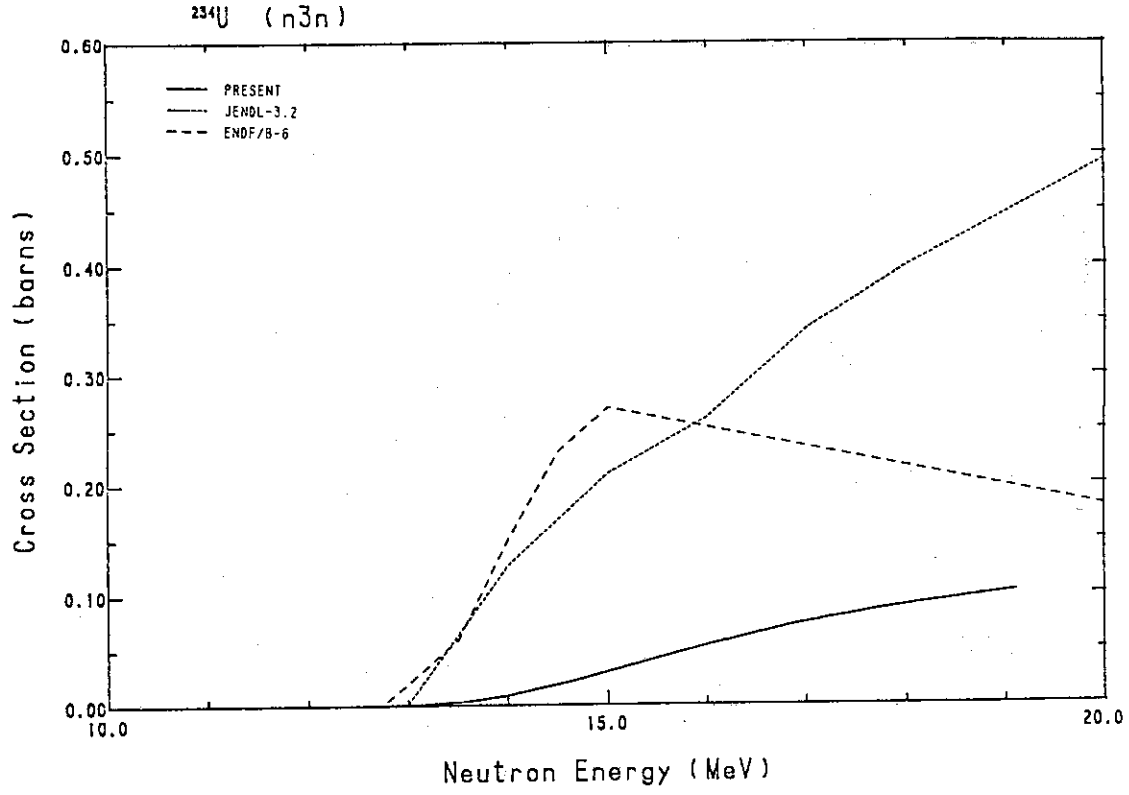

Fig. 222 Comparison of the (n,3n)-cross-section for ^{234}U.

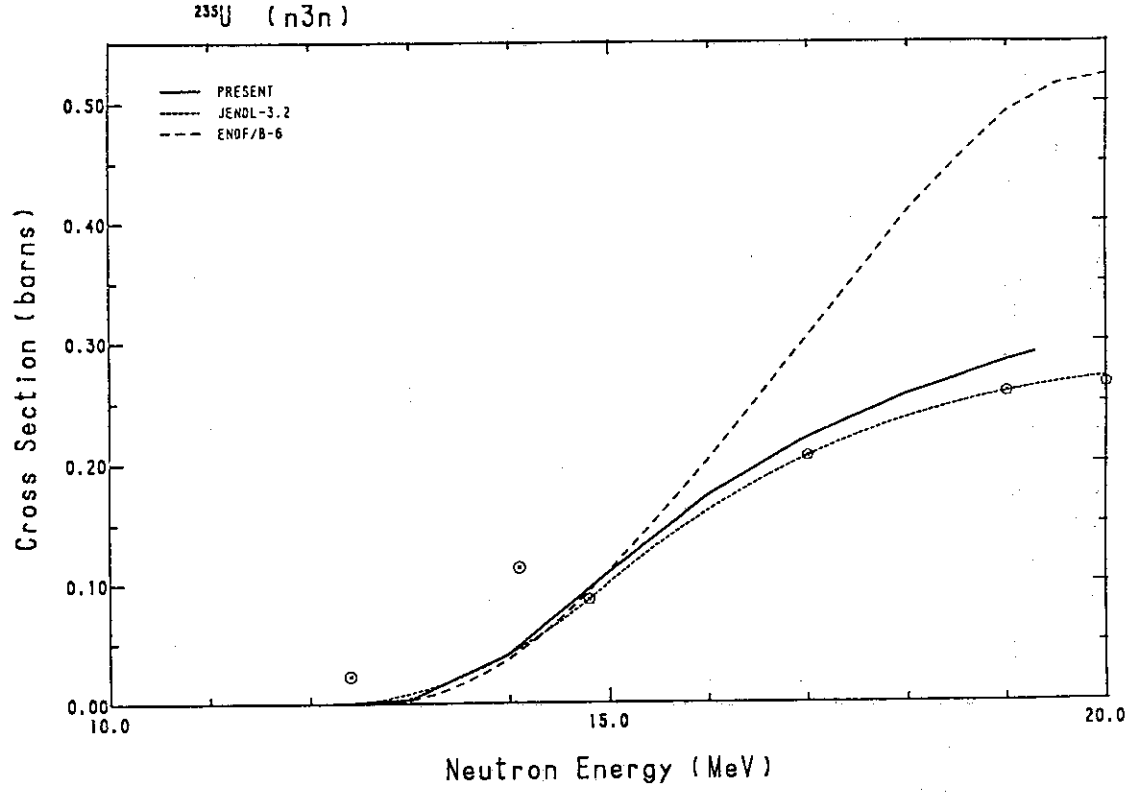

Fig. 223 Comparison of the (n,3n)-cross-section for ^{235}U.

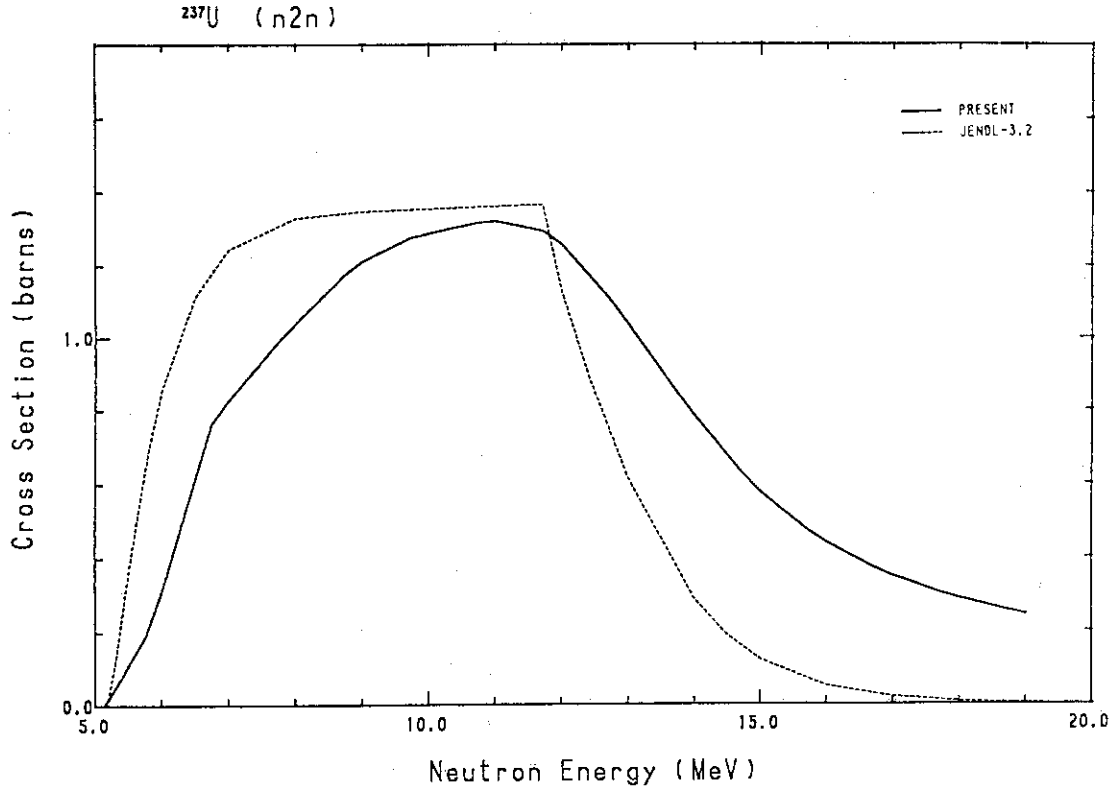

Fig. 224 Comparison of the (n,2n)-cross-section for ^{237}U.

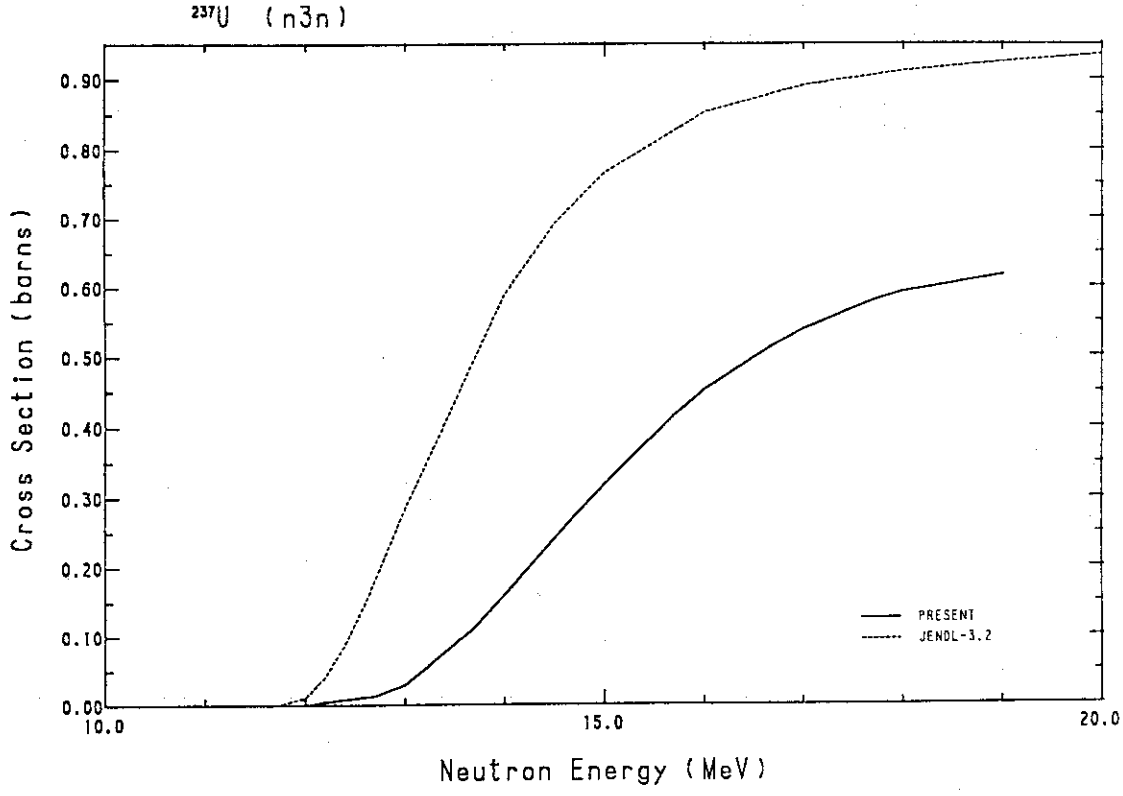

Fig. 225 Comparison of the (n,3n)-cross-section for ^{237}U.

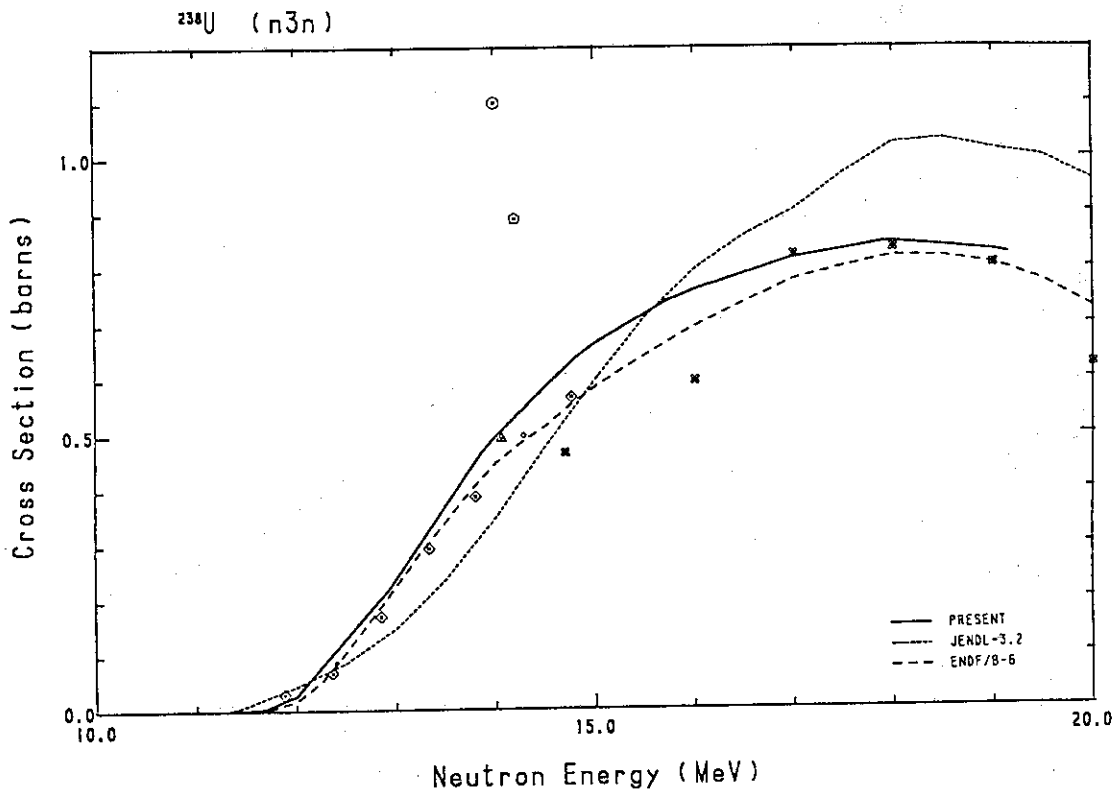

Fig. 226 Comparison of the (n,3n)-cross-section for ^{238}U.

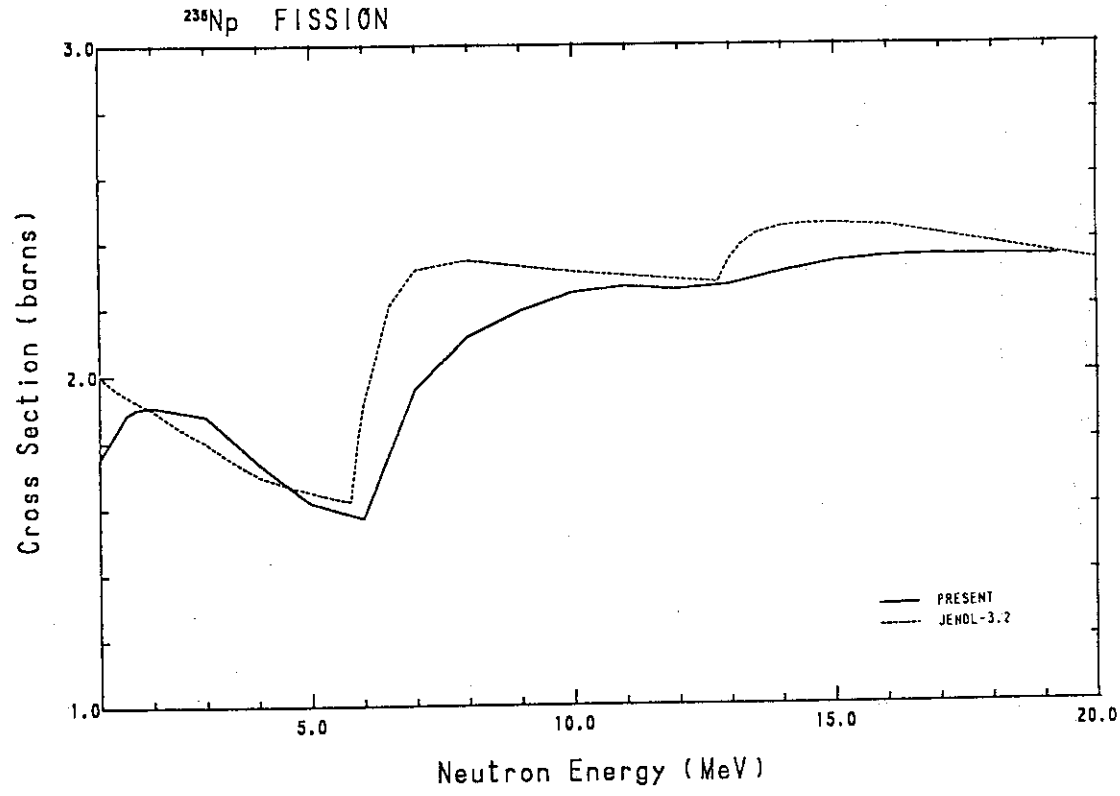

Fig. 227 Comparison of the fission cross-section for ^{236}Np.

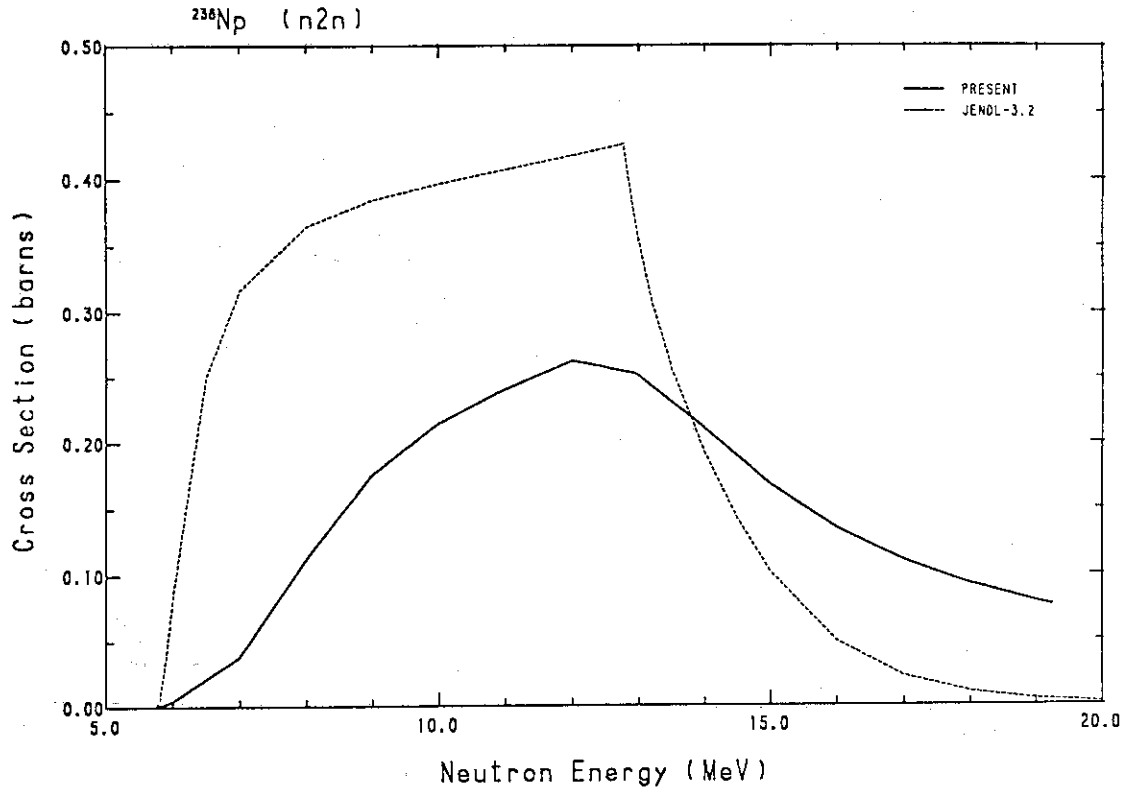

Fig. 228 Comparison of the (n,2n)-cross-section for ^{236}Np.

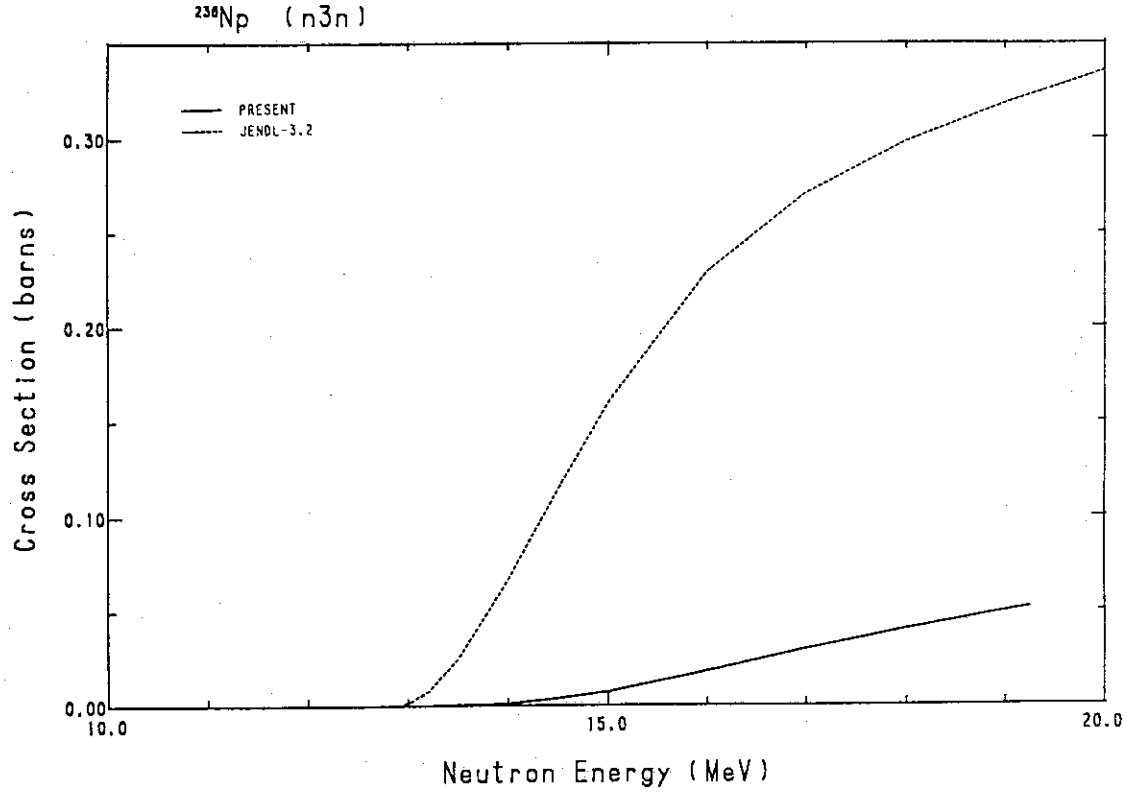

Fig. 229 Comparison of the (n,3n)-cross-section for ^{236}Np.

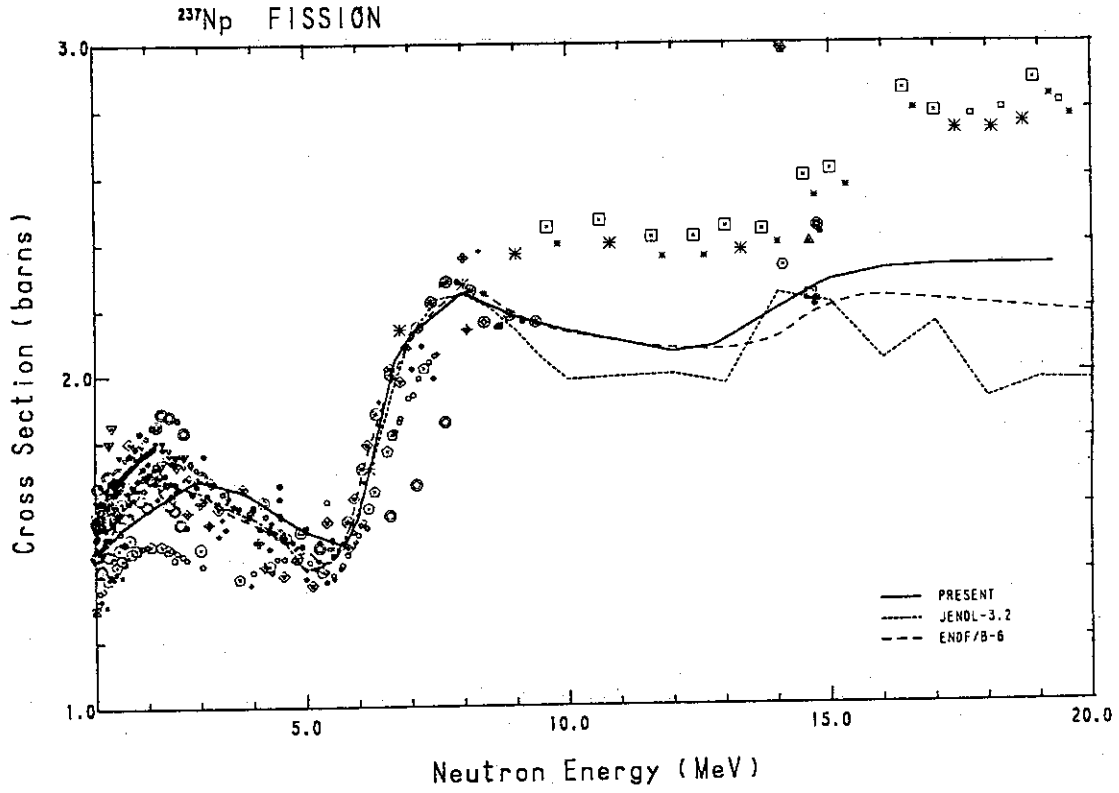

Fig. 230 Comparison of the fission cross-section for ^{237}Np.

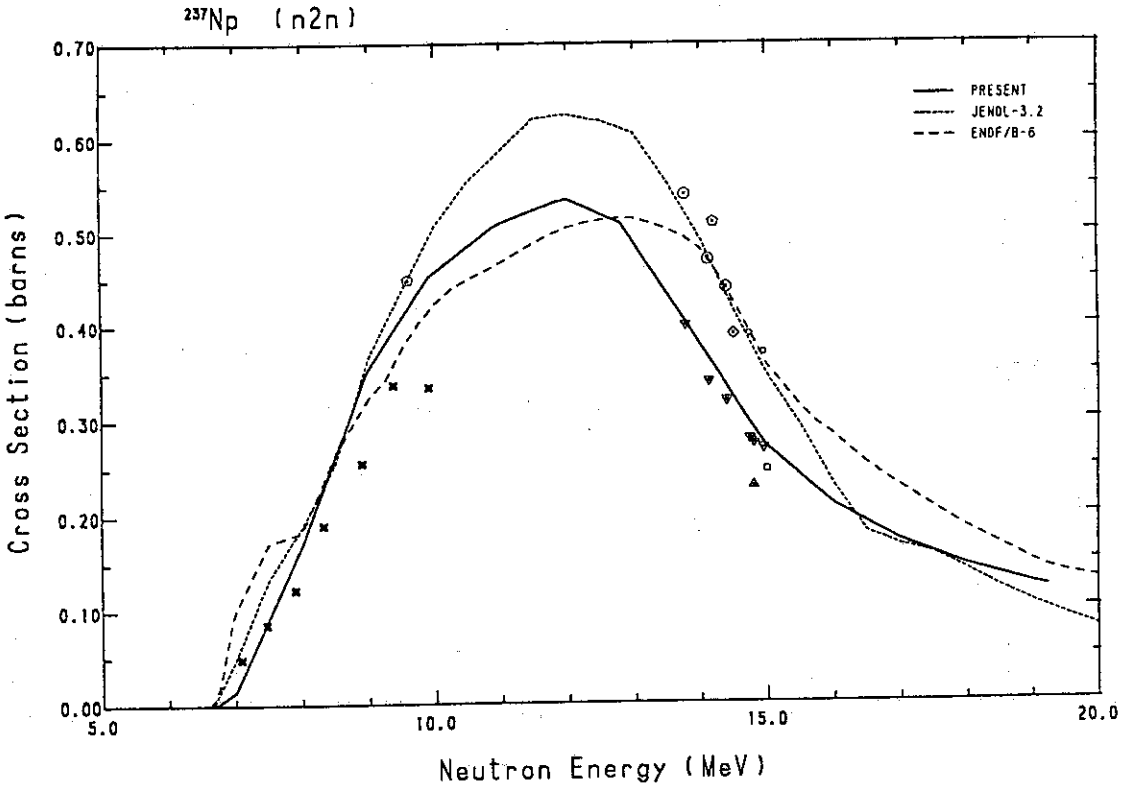

Fig. 231 Comparison of the (n,2n)-cross-section for ^{237}Np.

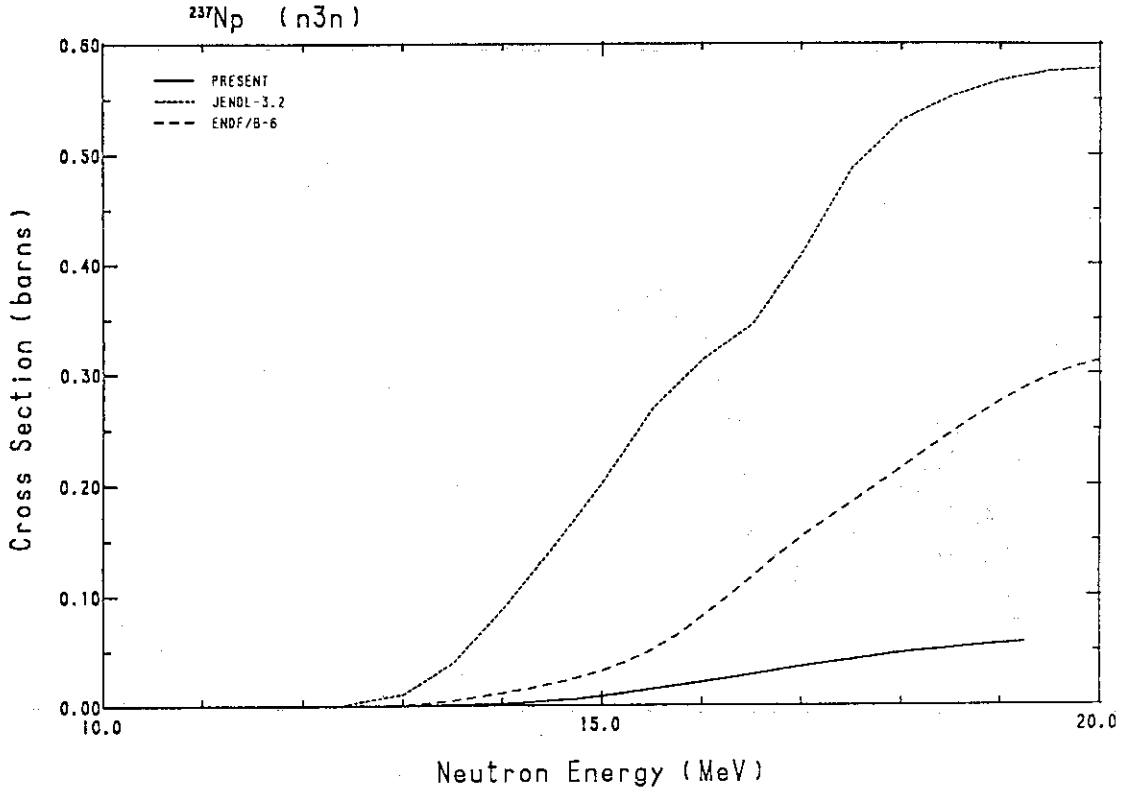

Fig. 232 Comparison of the (n,3n)-cross-section for ^{237}Np.

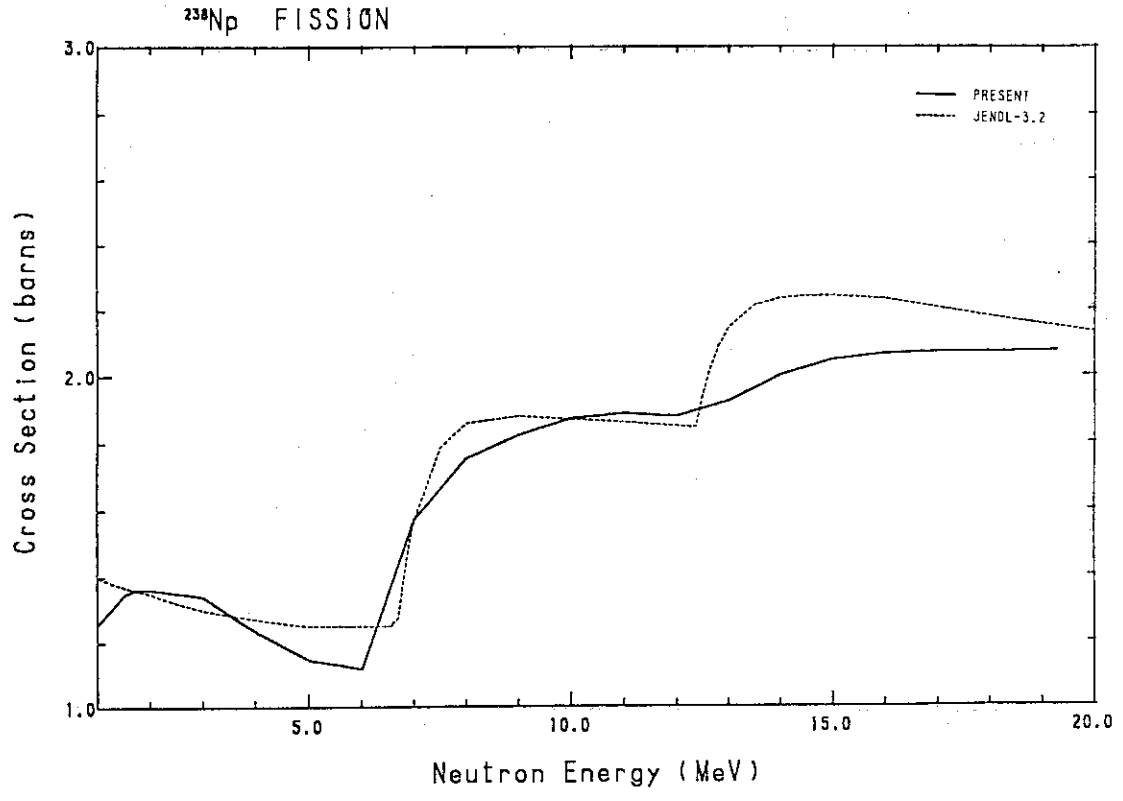

Fig. 233 Comparison of the fission cross-section for ^{238}Np.

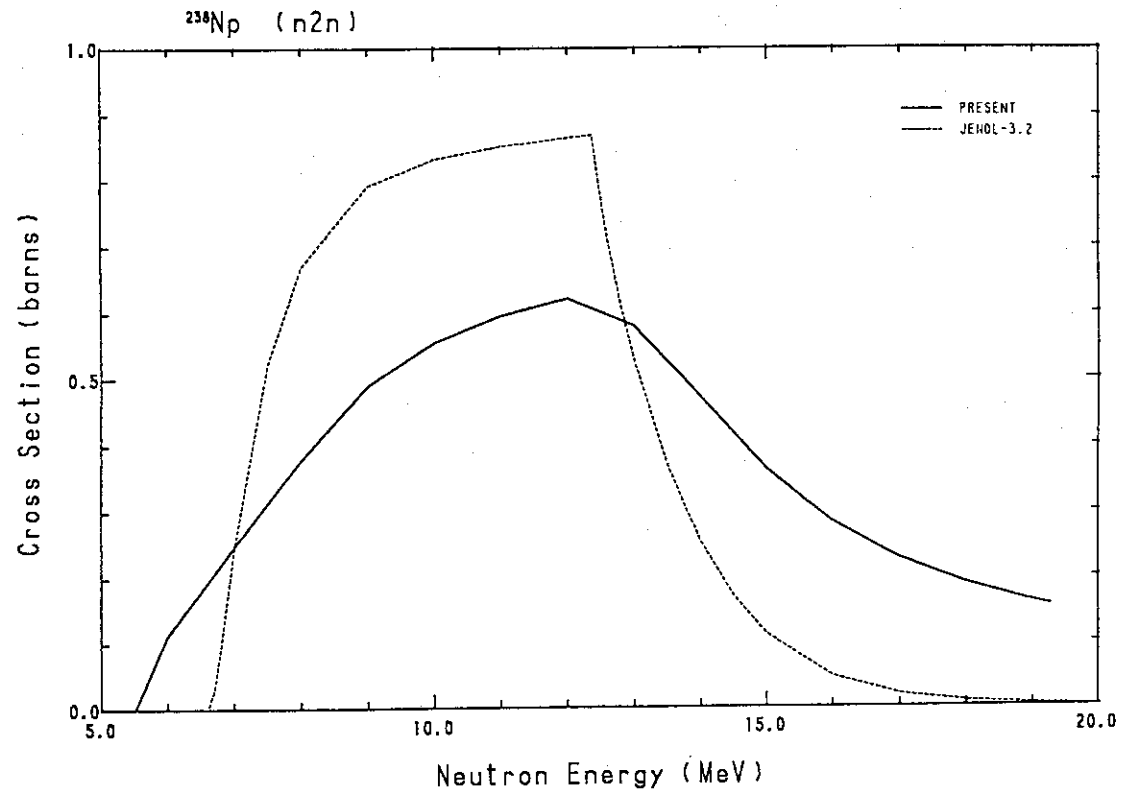

Fig. 234 Comparison of the (n,2n)-cross-section for ^{238}Np.

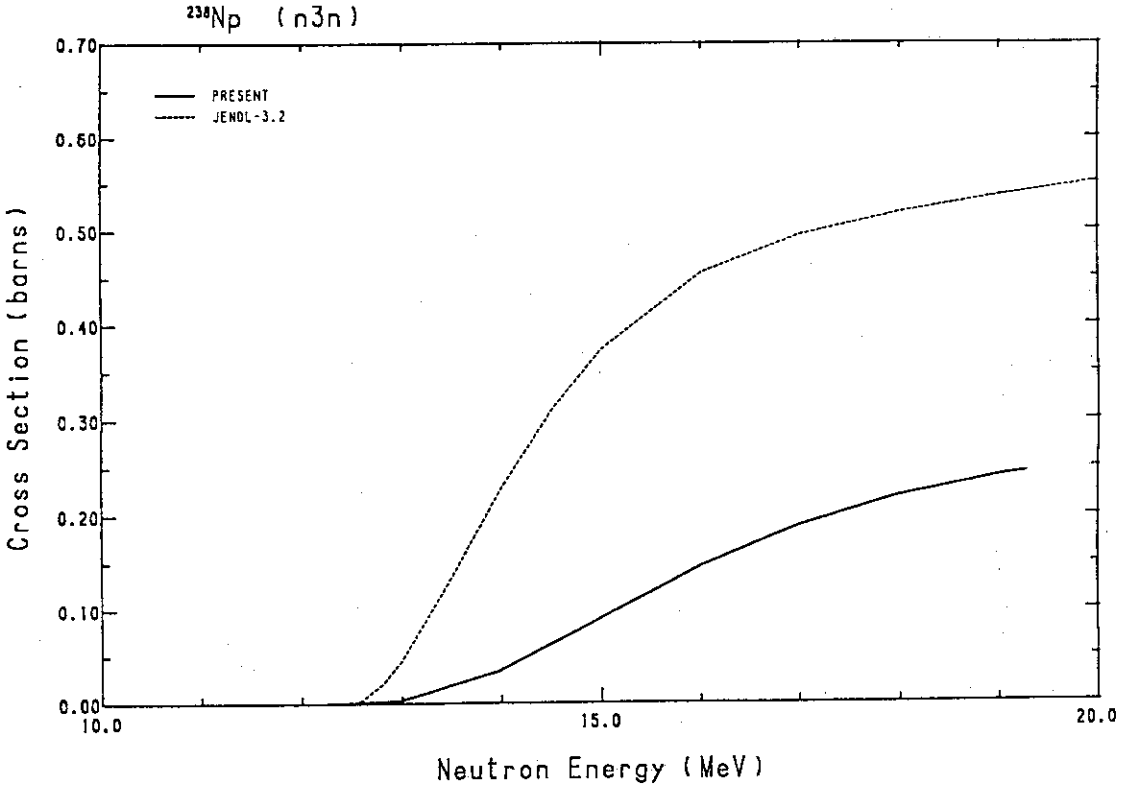

Fig. 235 Comparison of the (n,3n)-cross-section for ^{238}Np.

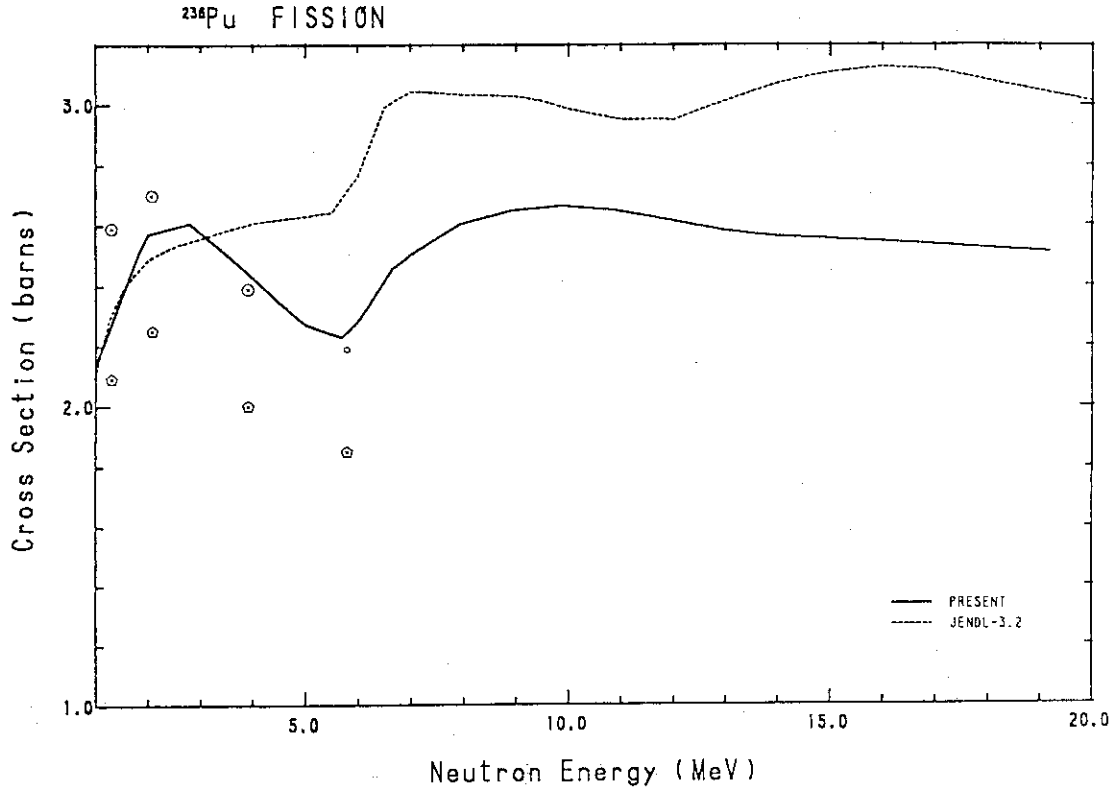

Fig. 236 Comparison of the fission cross-section for ^{236}Pu.

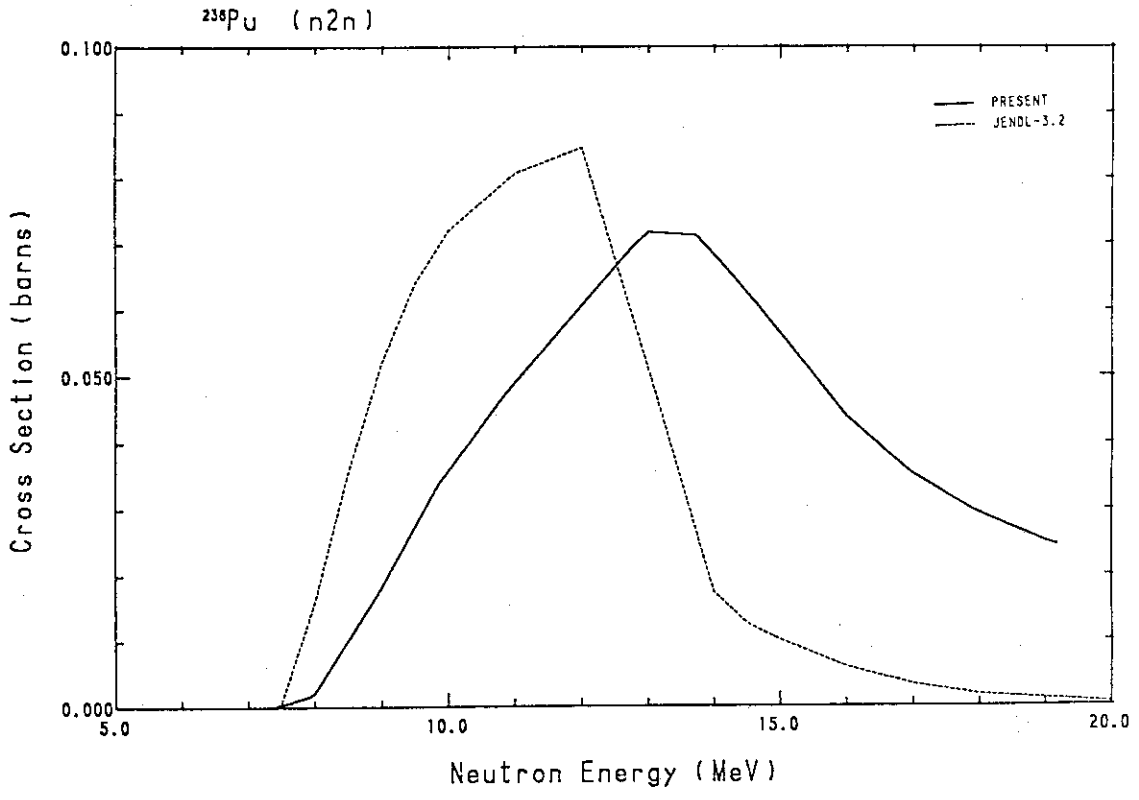

Fig. 237 Comparison of the (n,2n)-cross-section for ^{236}Pu.

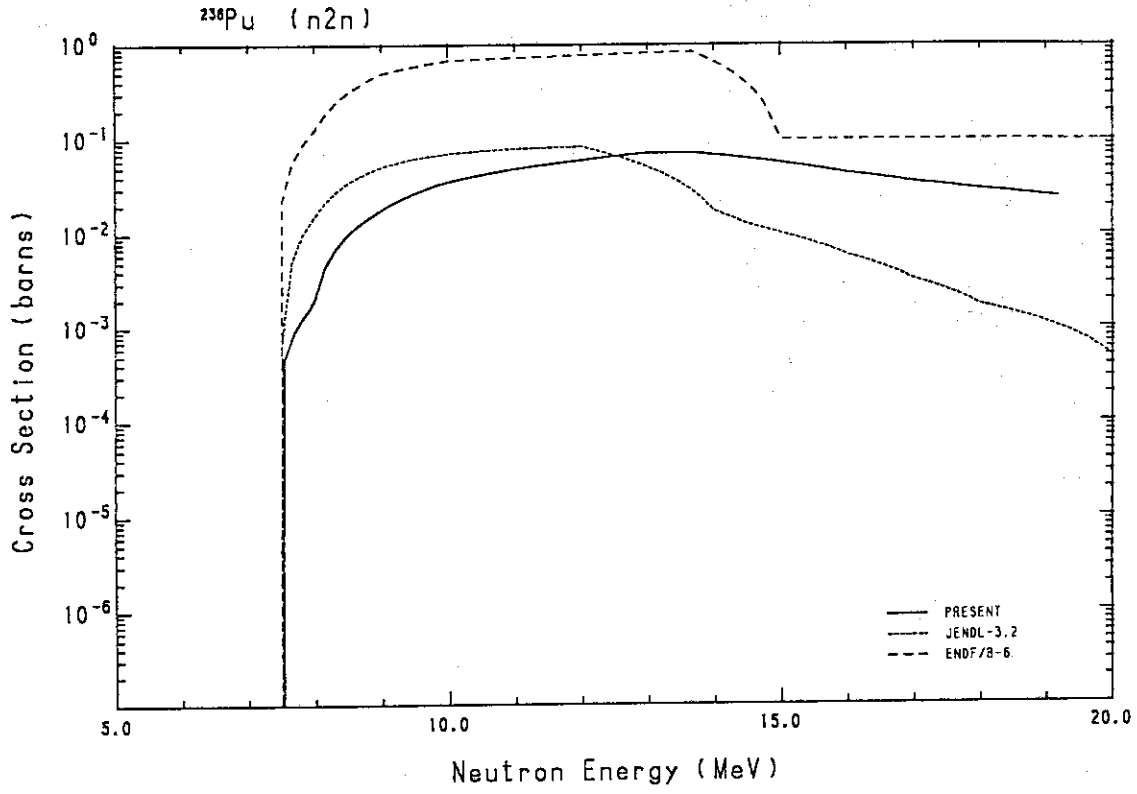

Fig. 238 Comparison of the (n,2n)-cross-section for ^{236}Pu.

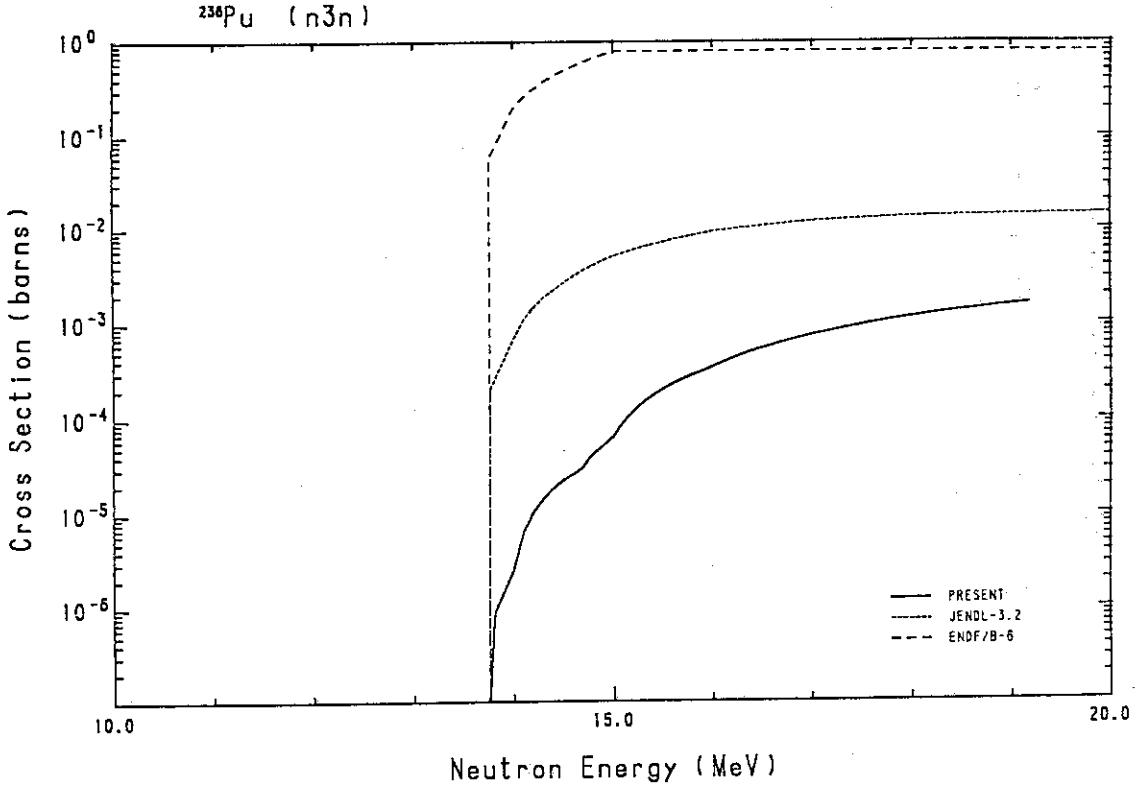

Fig. 239 Comparison of the (n,3n)-cross-section for ^{236}Pu.

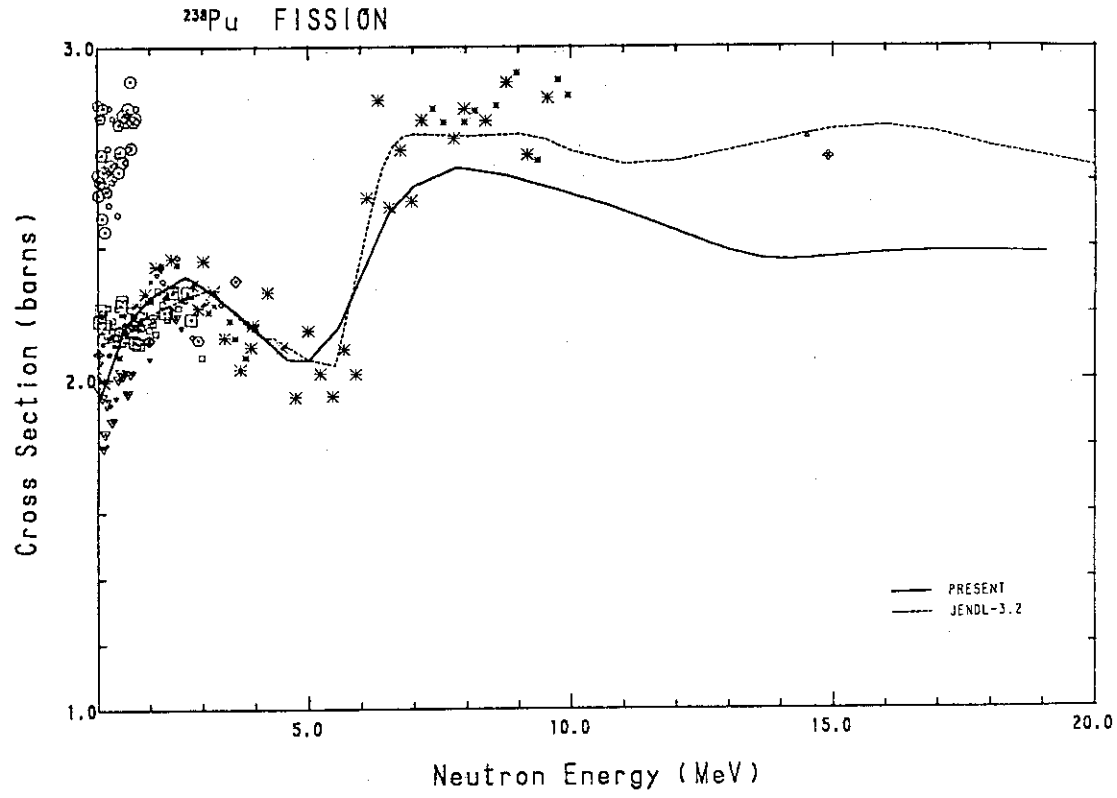

Fig. 240 Comparison of the fission cross-section for ^{238}Pu.

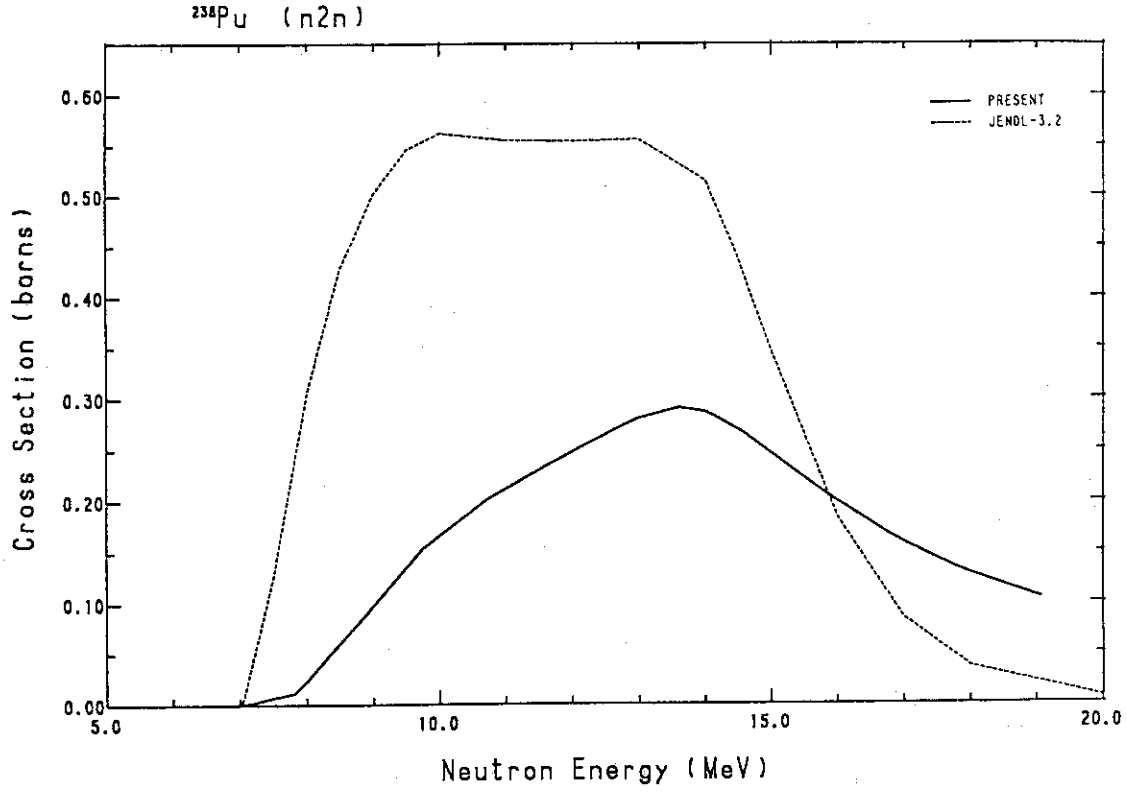

Fig. 241 Comparison of the (n,2n)-cross-section for ^{238}Pu.

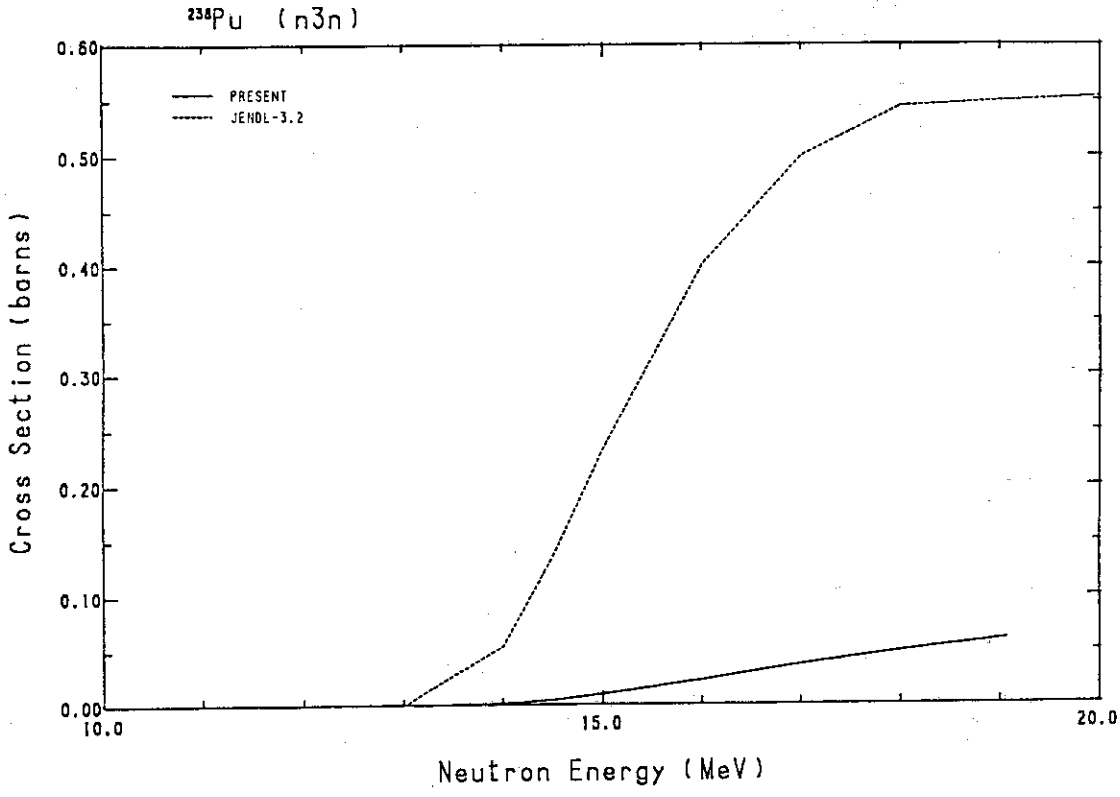

Fig. 242 Comparison of the (n,3n)-cross-section for ^{238}Pu.

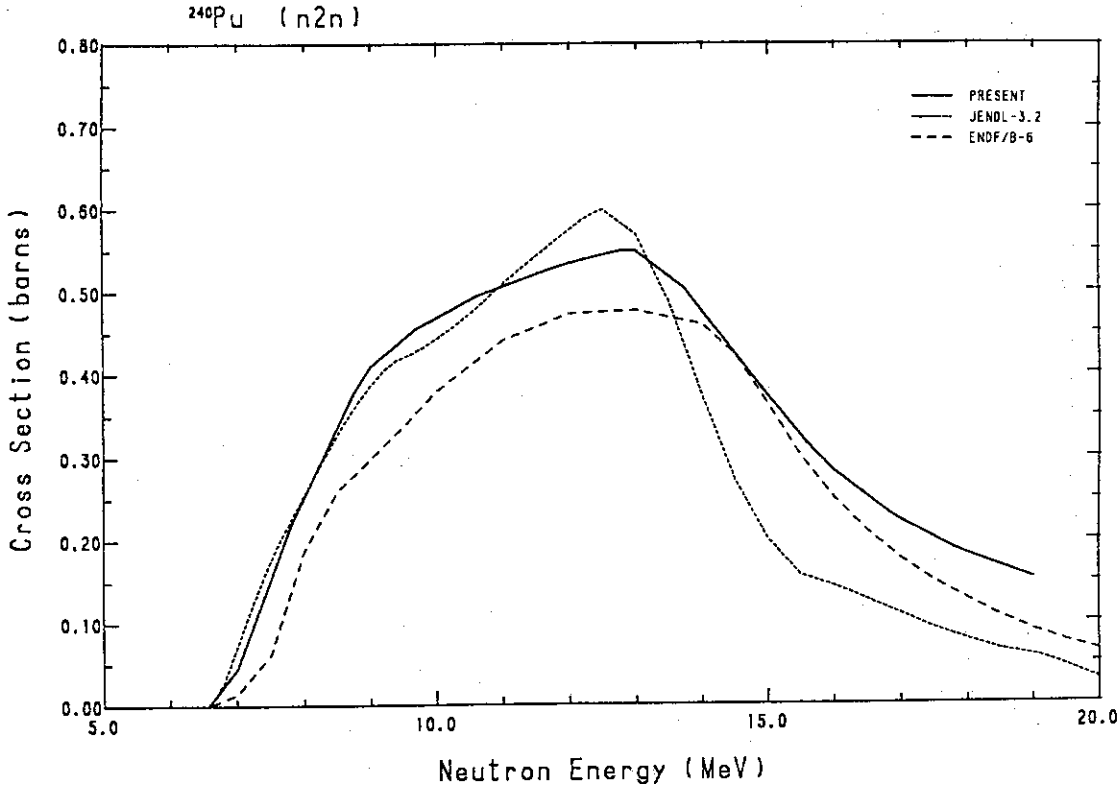

Fig. 243 Comparison of the (n,2n)-cross-section for ^{240}Pu.

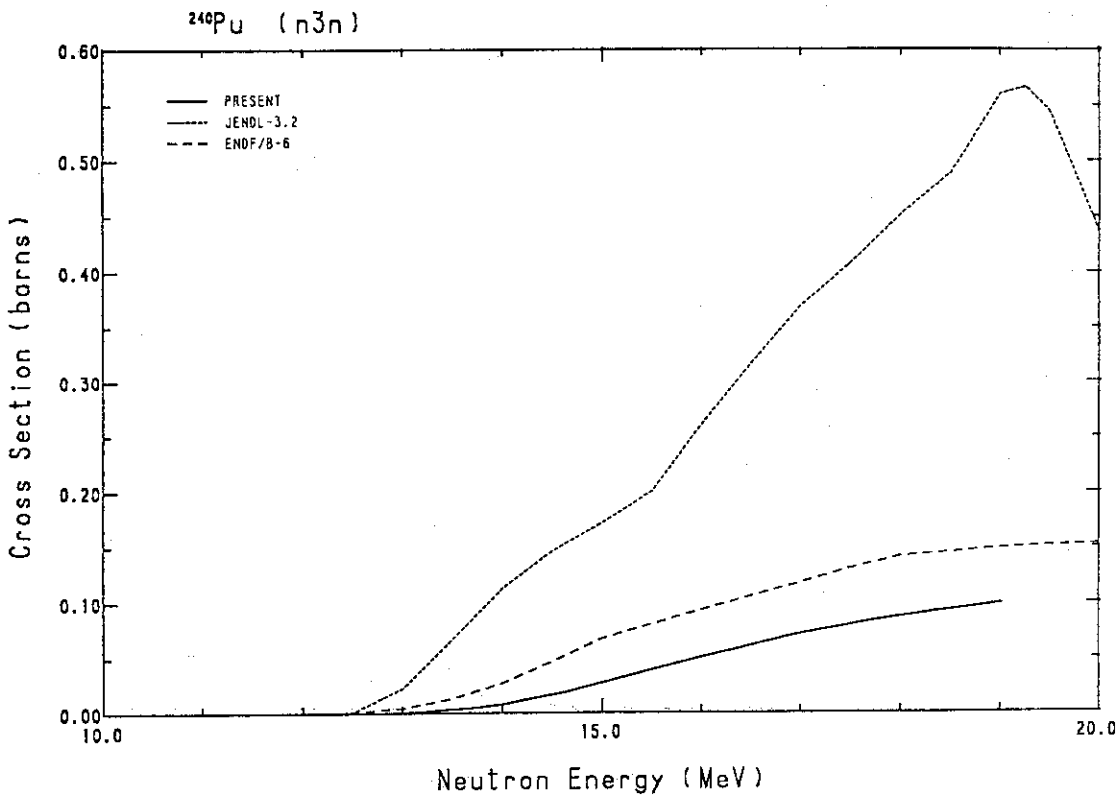

Fig. 244 Comparison of the (n,3n)-cross-section for ^{240}Pu.

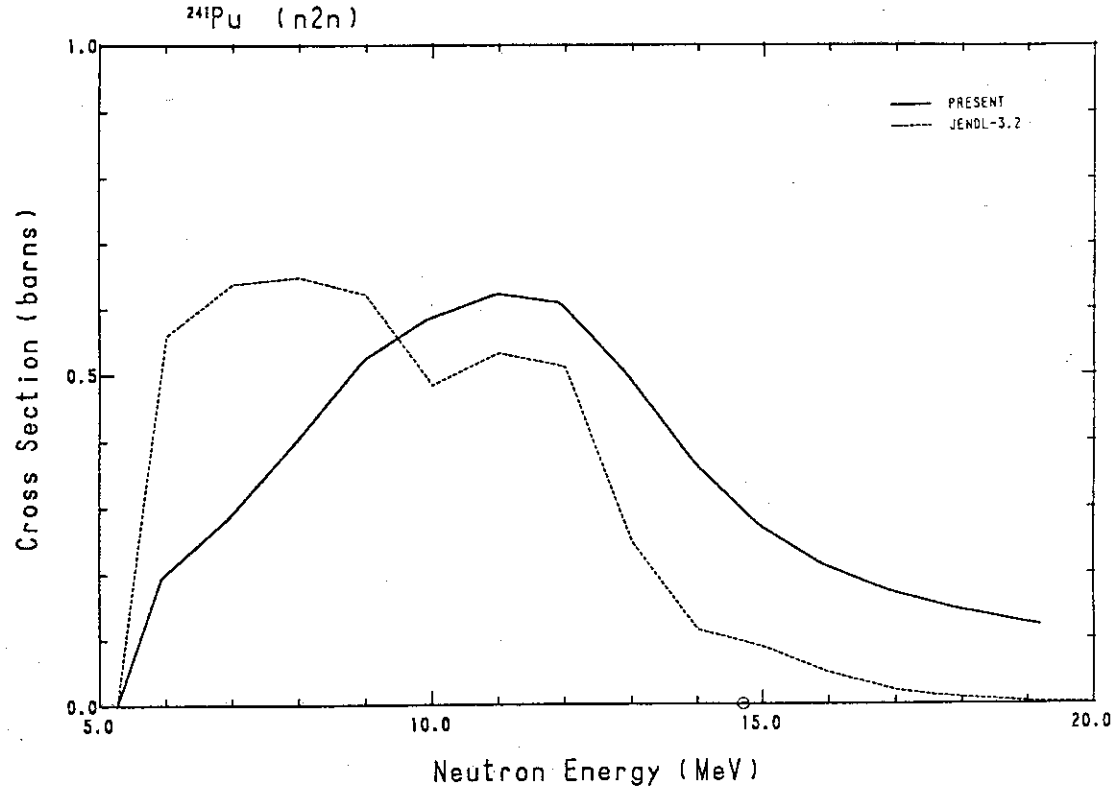

Fig. 245 Comparison of the (n,2n)-cross-section for ^{241}Pu.

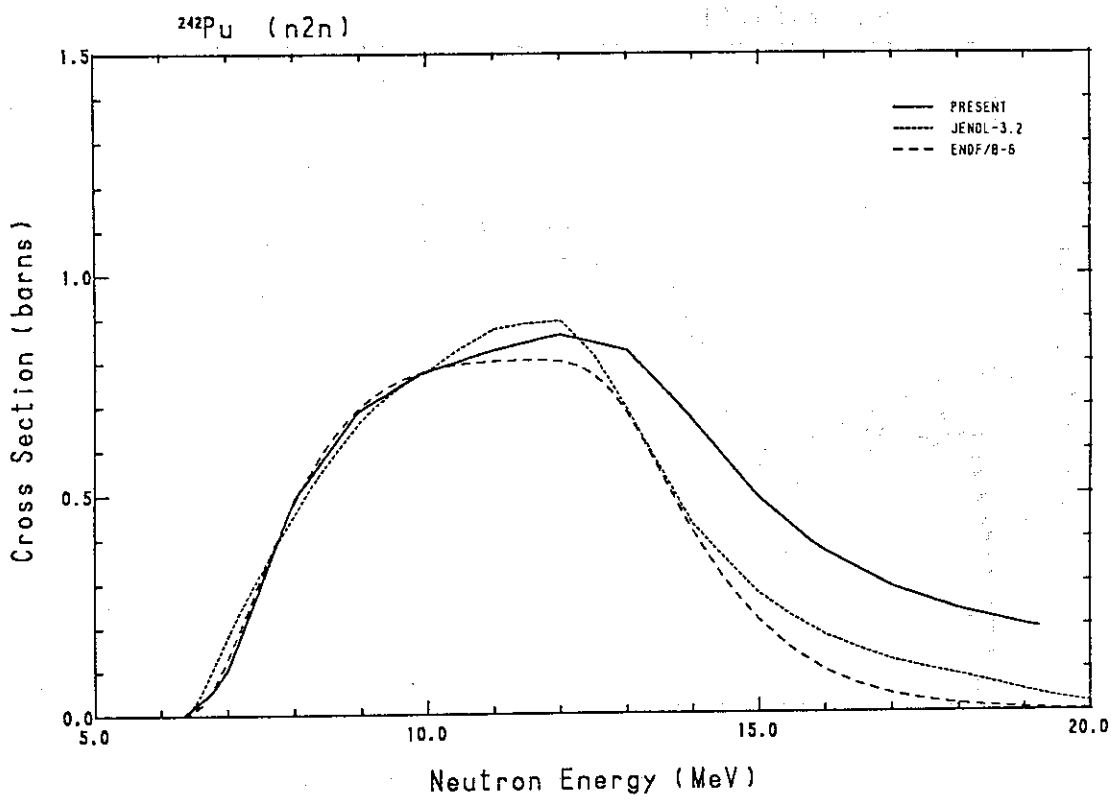

Fig. 246 Comparison of the (n,2n)-cross-section for ^{242}Pu.

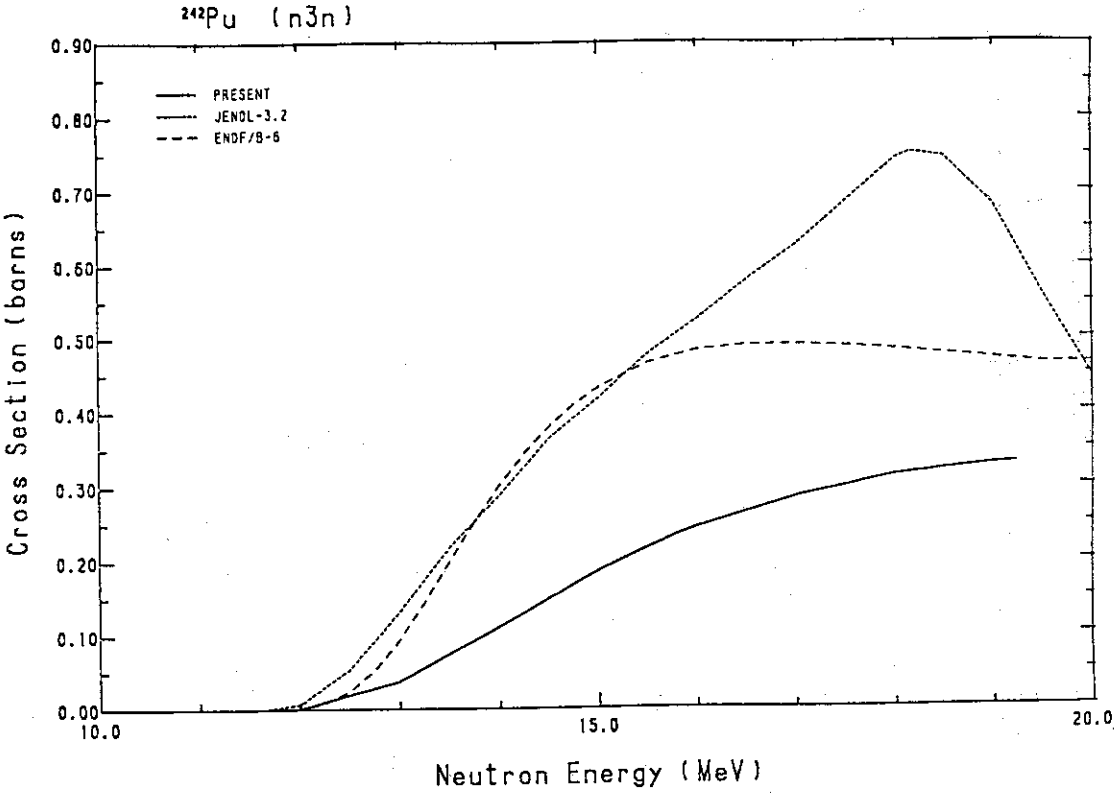

Fig. 247 Comparison of the (n,3n)-cross-section for ^{243}Pu.

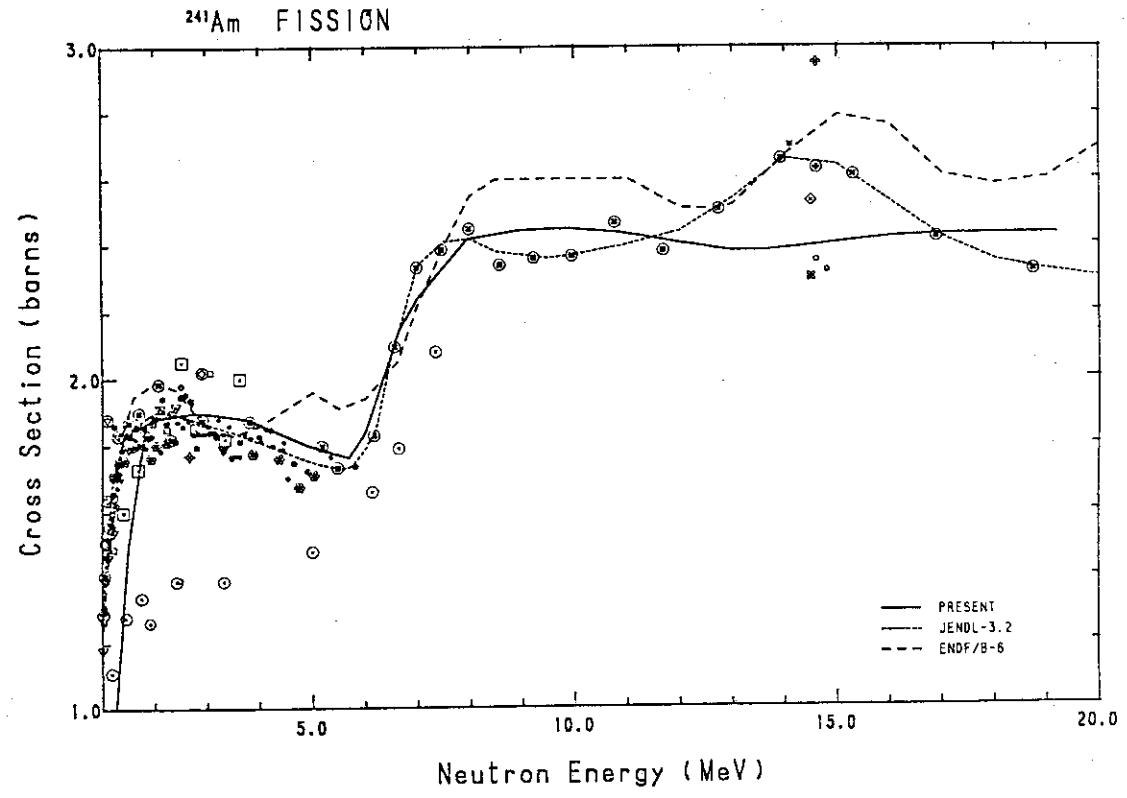

Fig. 248 Comparison of the fission cross-section for ^{241}Am.

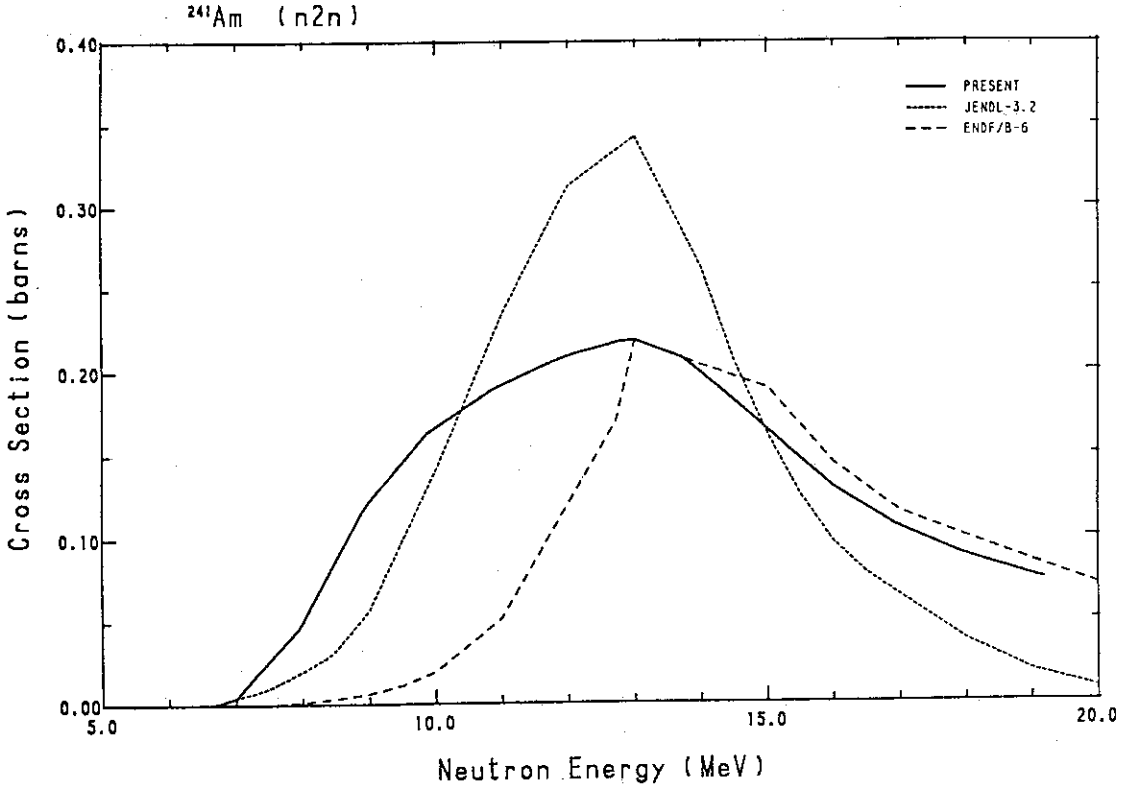

Fig. 249 Comparison of the (n,2n)-cross-section for ^{241}Am.

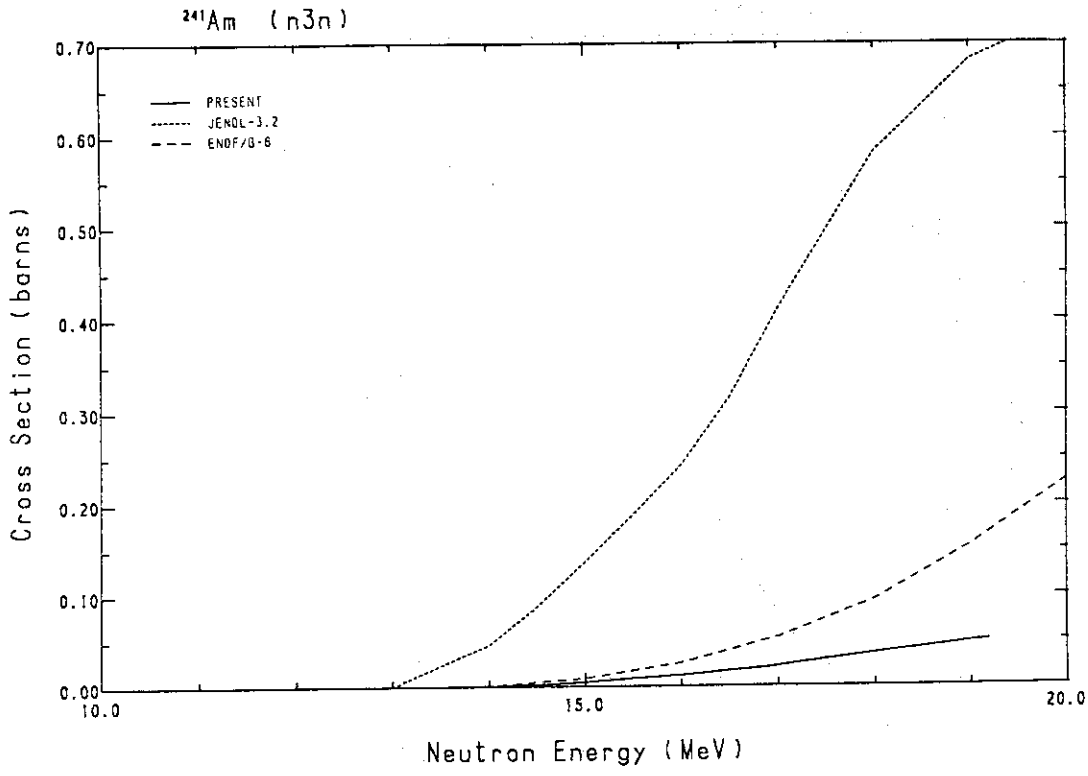

Fig. 250 Comparison of the (n,3n)-cross-section for ^{241}Am.

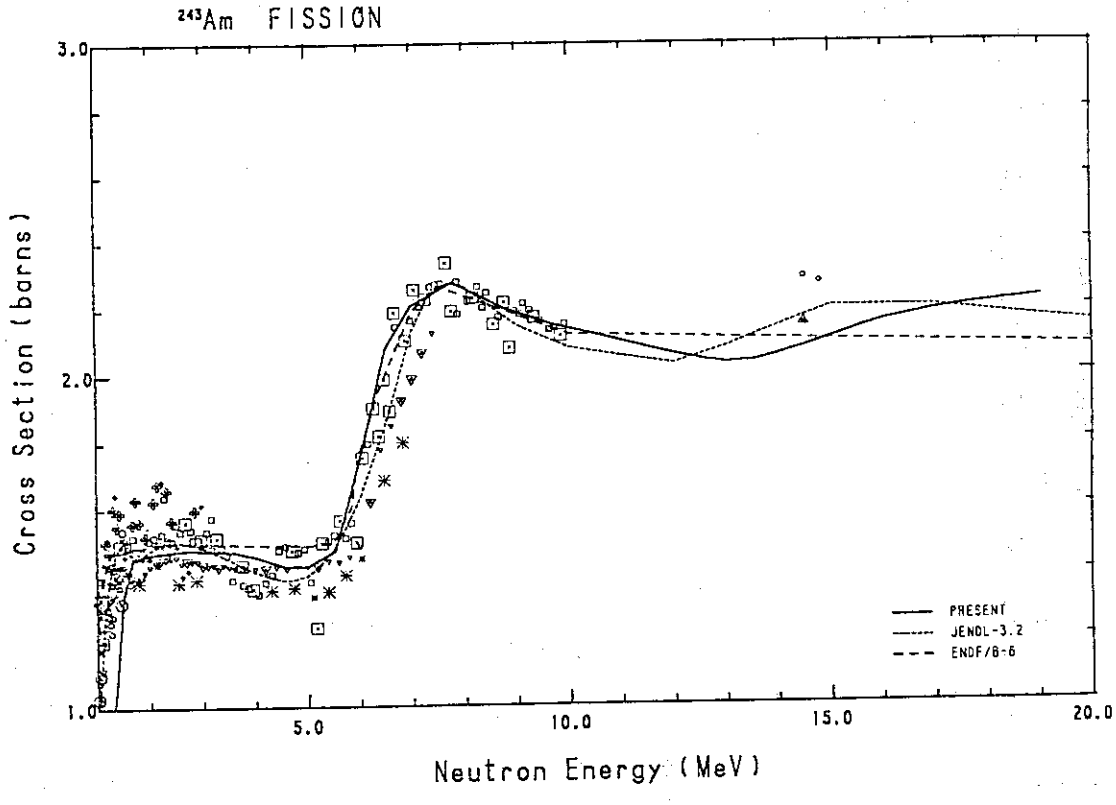

Fig. 251 Comparison of the fission cross-section for ^{243}Am.

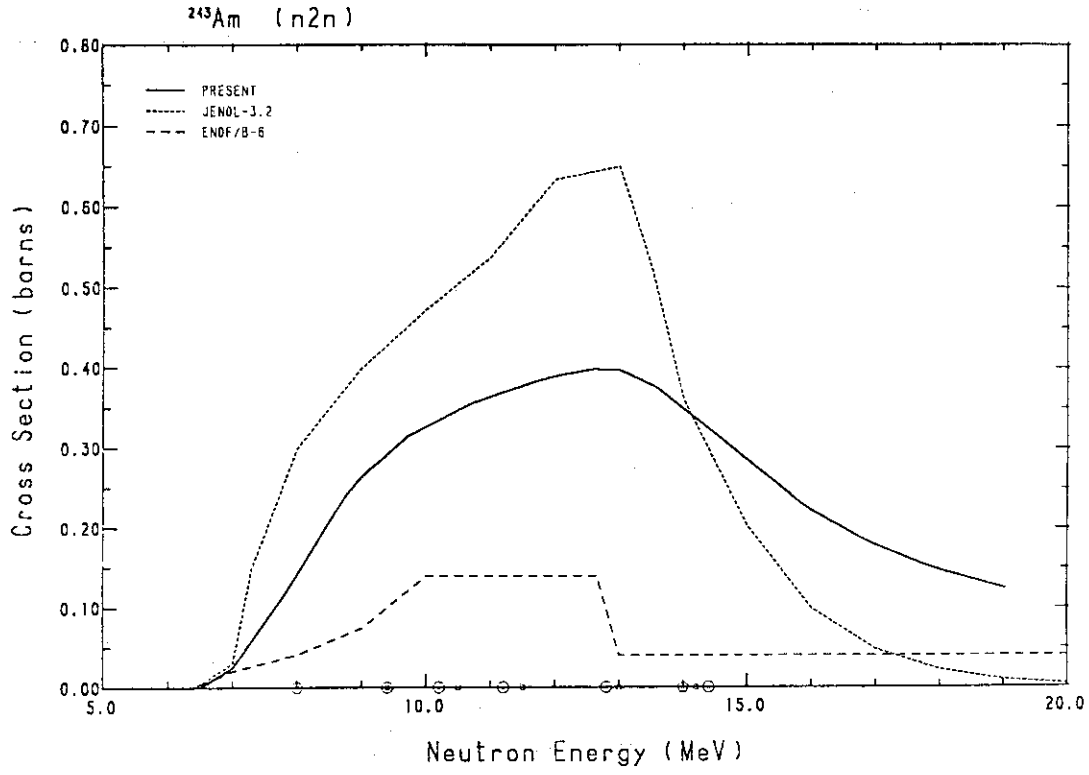

Fig. 252 Comparison of the (n,2n)-cross-section for ^{243}Am.

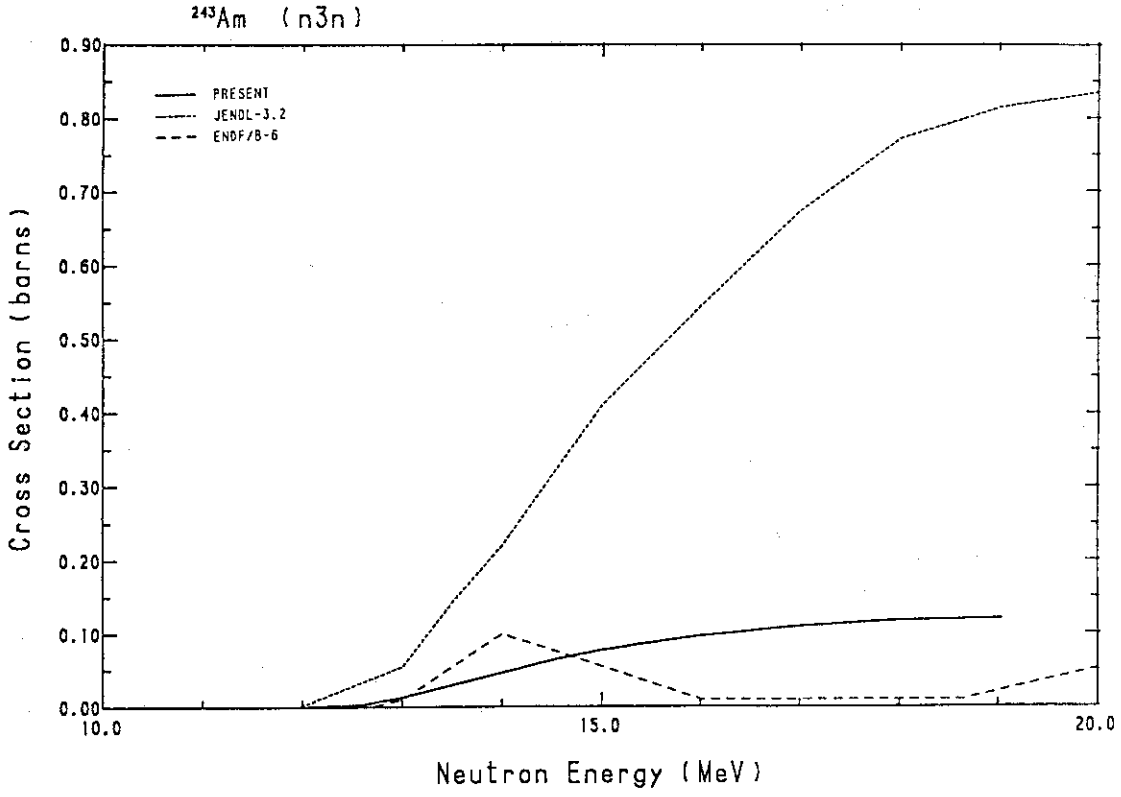

Fig. 253 Comparison of the (n,3n)-cross-section for ^{243}Am.

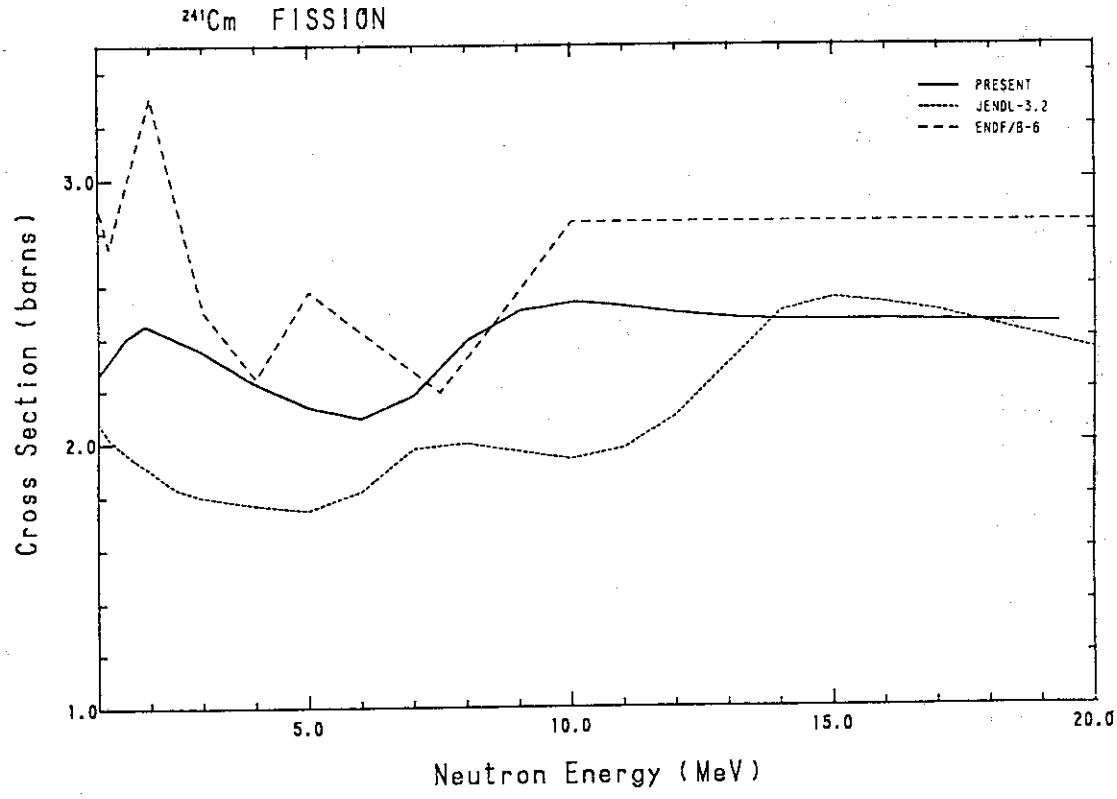

Fig. 254 Comparison of the fission cross-section for ^{241}Cm.

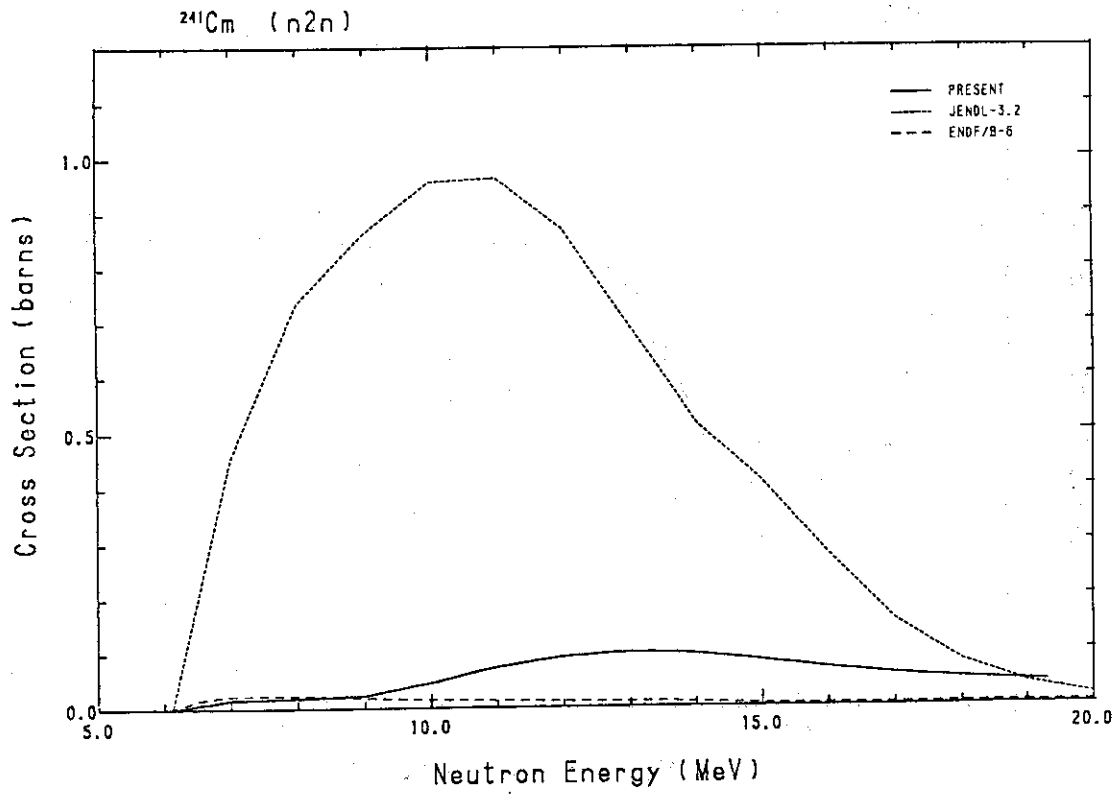

Fig. 255 Comparison of the (n,2n)-cross-section for ^{241}Cm.

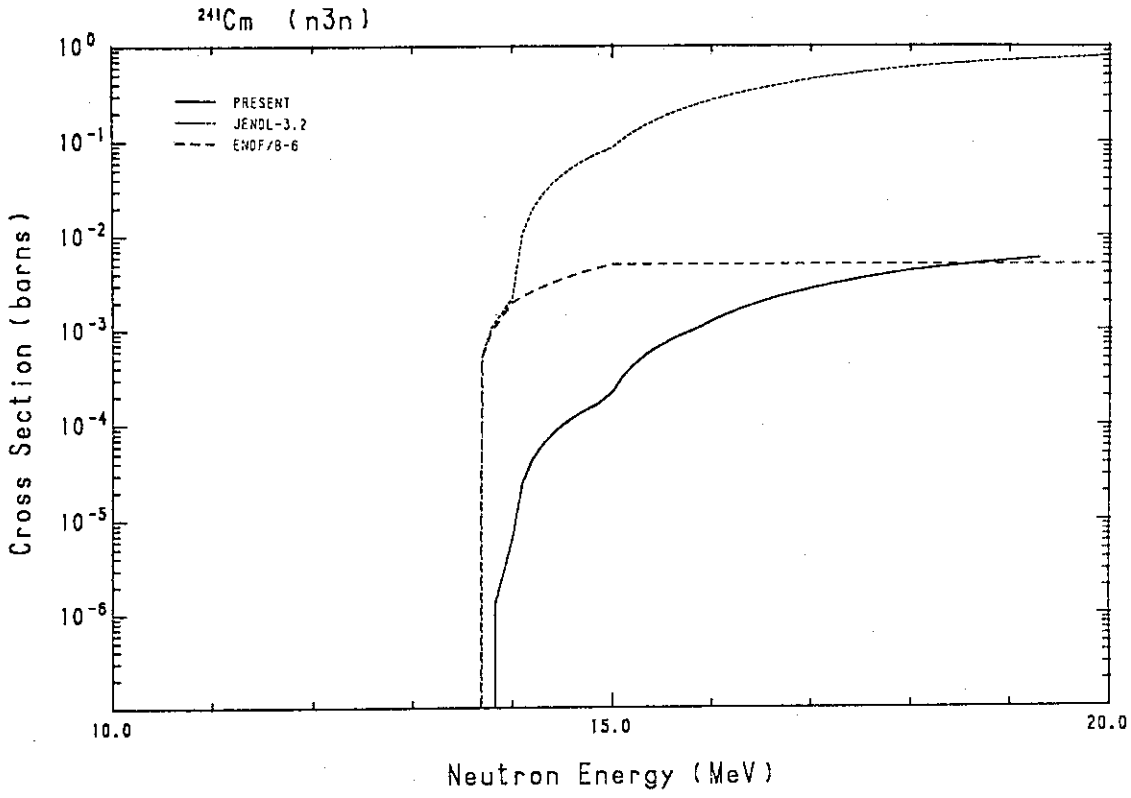

Fig. 256 Comparison of the (n,3n)-cross-section for ^{241}Cm.

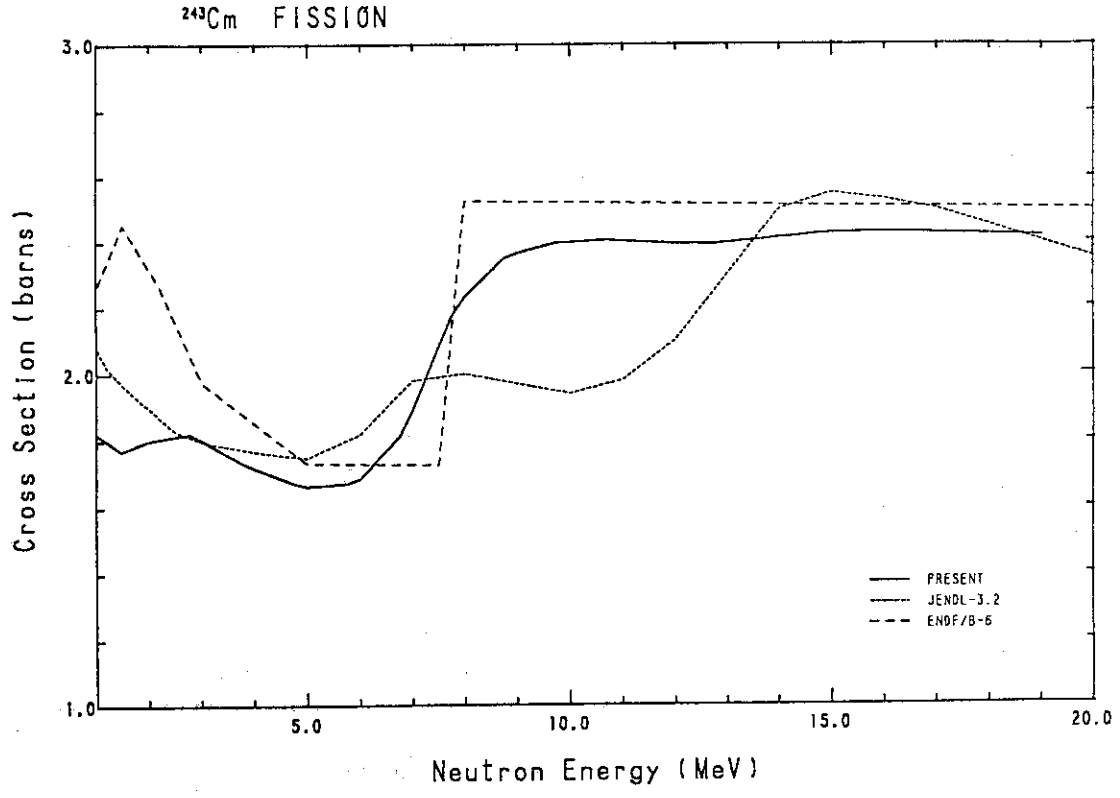

Fig. 257 Comparison of the fission cross-section for ^{243}Cm.

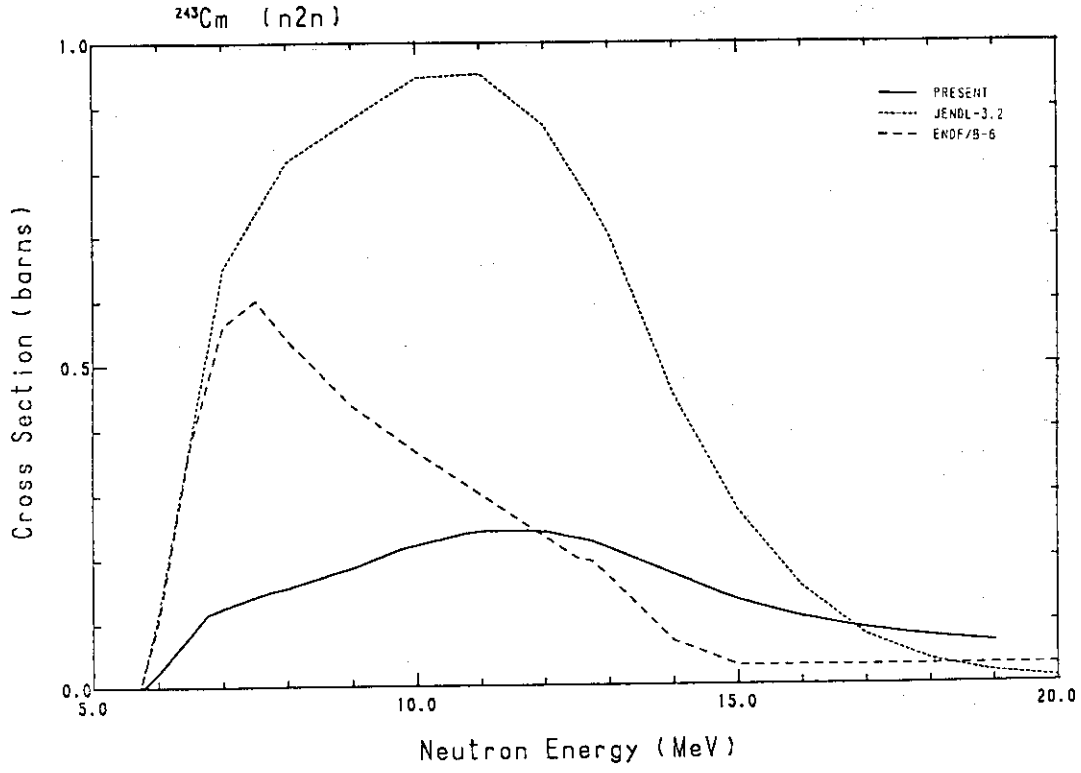

Fig. 258 Comparison of the (n,2n)-cross-section for ^{243}Cm.

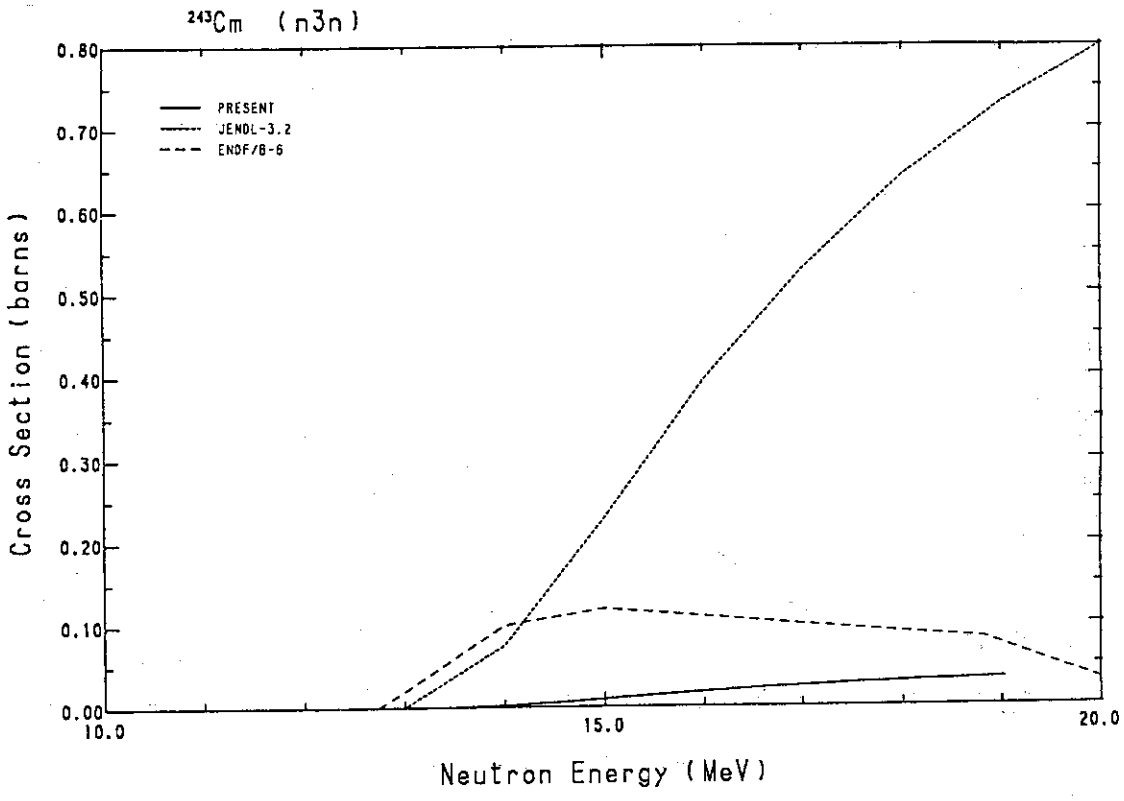

Fig. 259 Comparison of the (n,3n)-cross-section for ^{243}Cm.

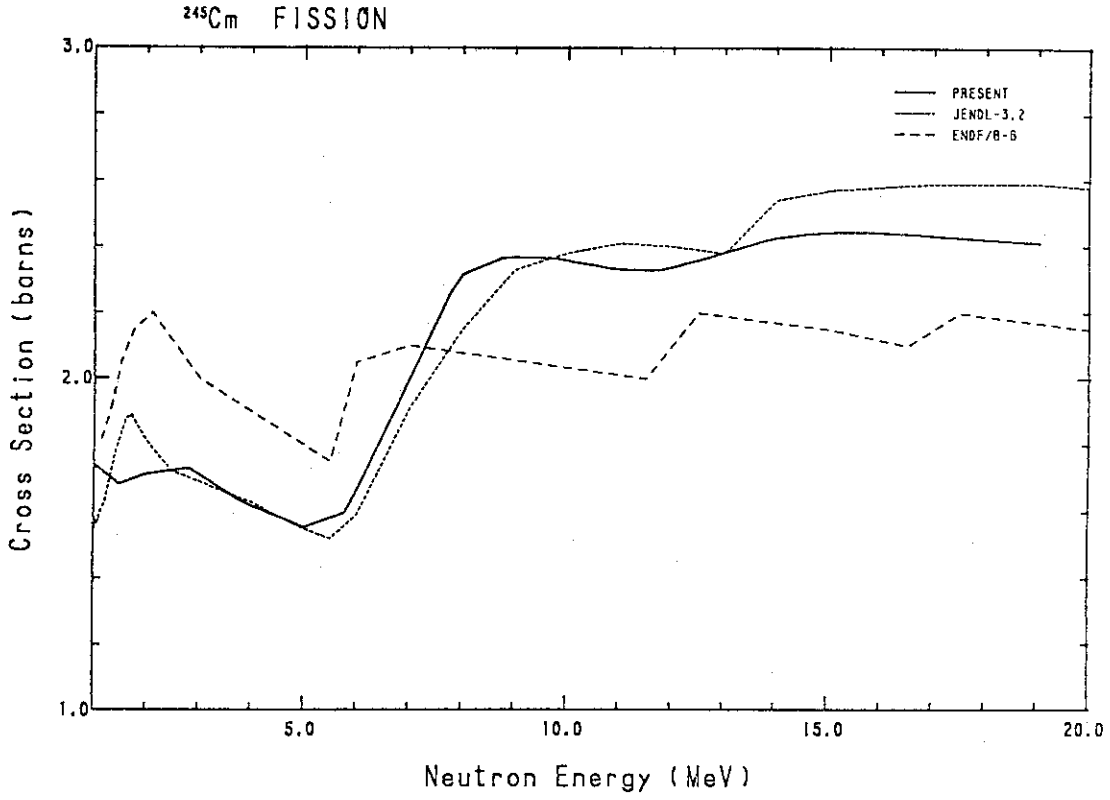

Fig. 260 Comparison of the fission cross-section for ^{245}Cm.

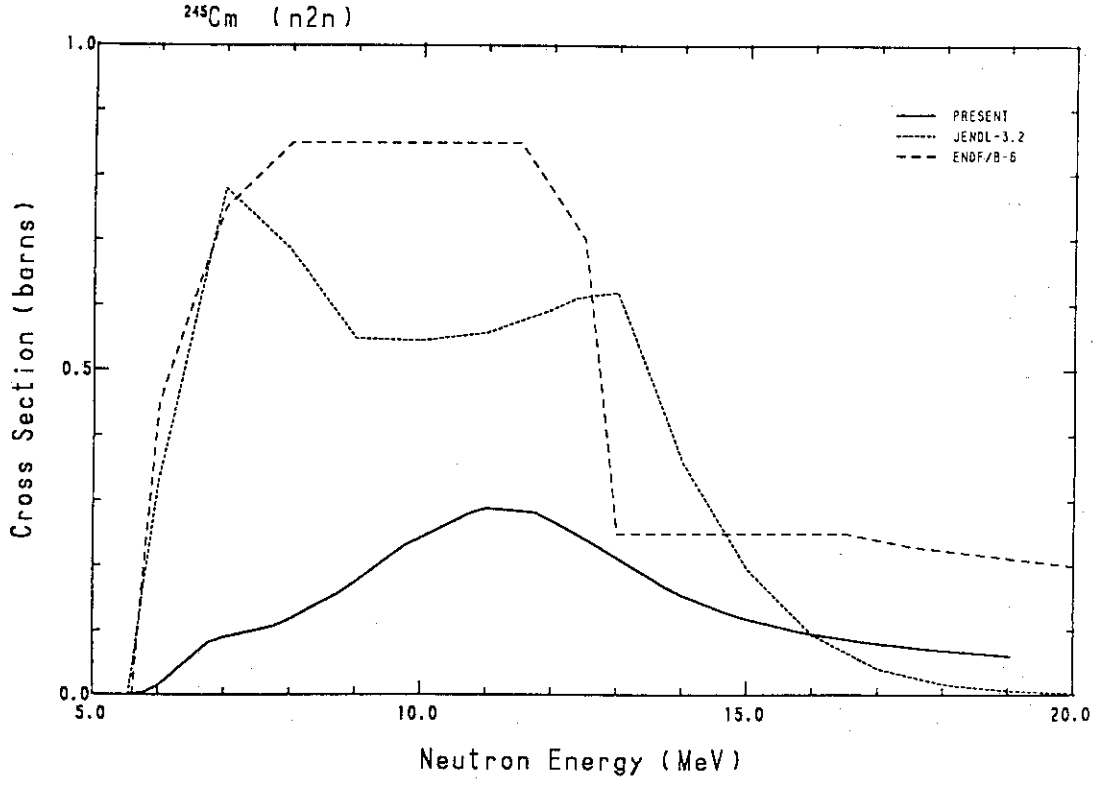

Fig. 261 Comparison of the (n,2n)-cross-section for ^{245}Cm.

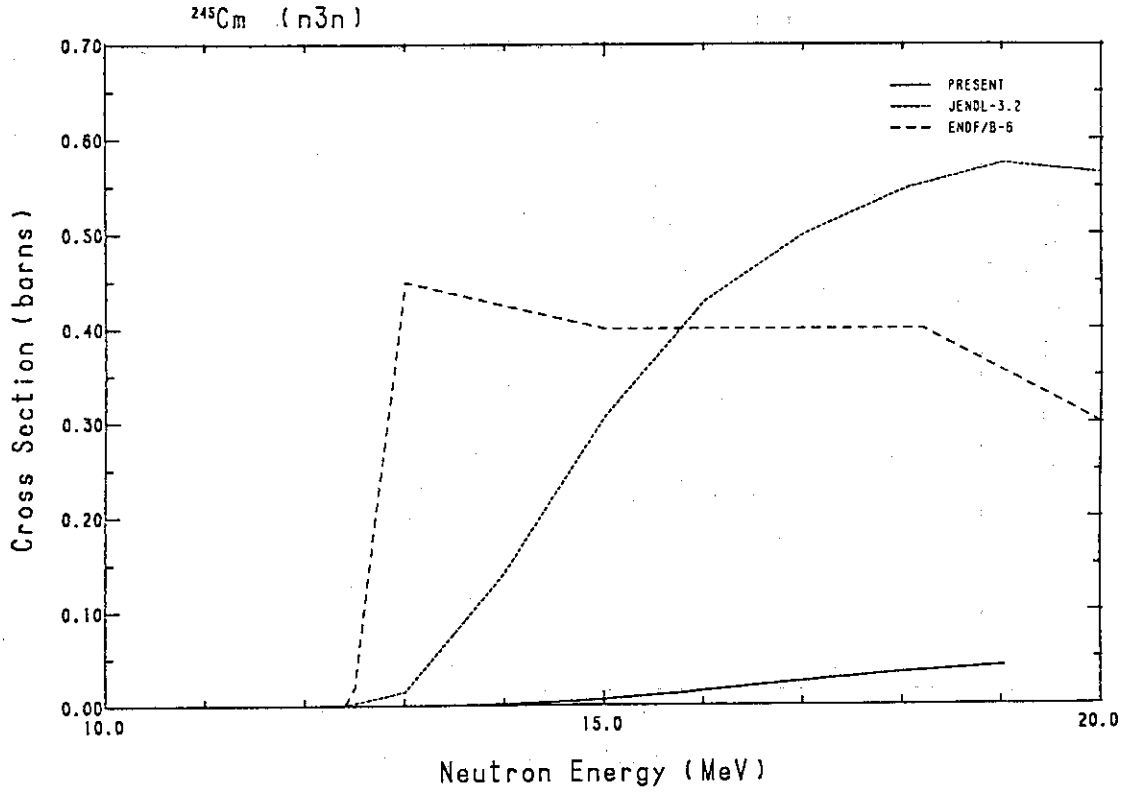

Fig. 262 Comparison of the (n,3n)-cross-section for ^{245}Cm.

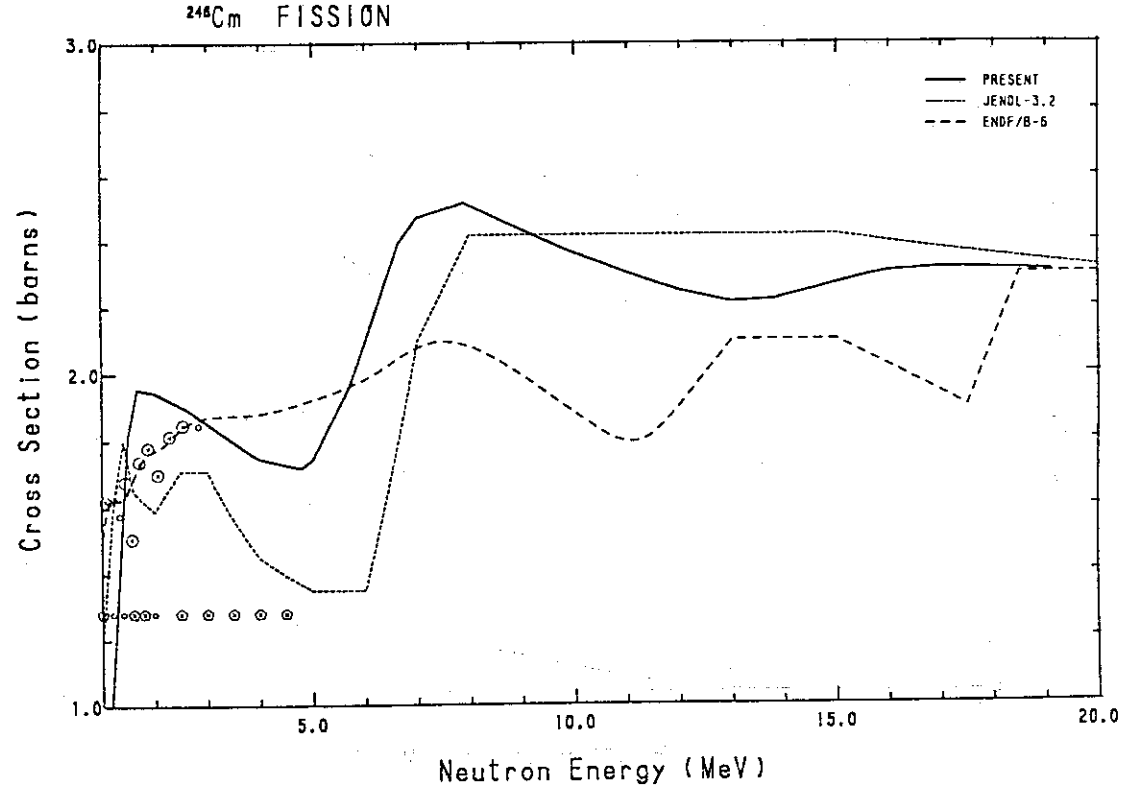

Fig. 263 Comparison of the fission cross-section for ^{246}Cm.

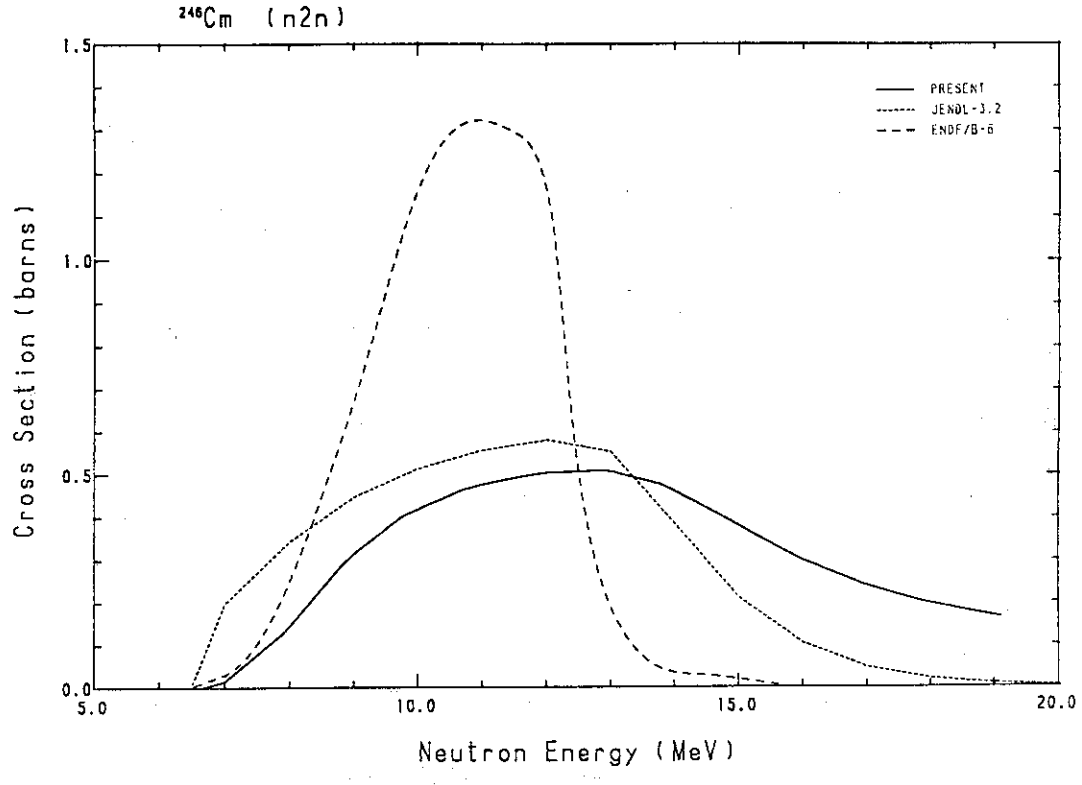

Fig. 264 Comparison of the (n,2n)-cross-section for ^{246}Cm.

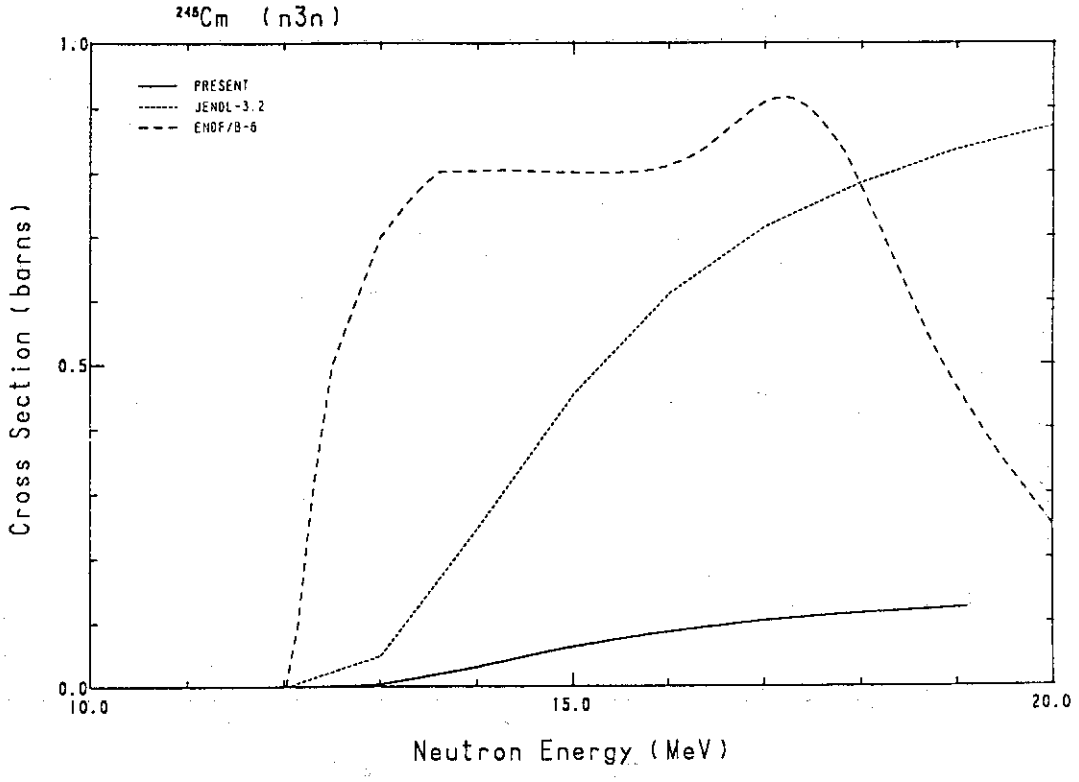

Fig. 265 Comparison of the (n,3n)-cross-section for ^{246}Cm.

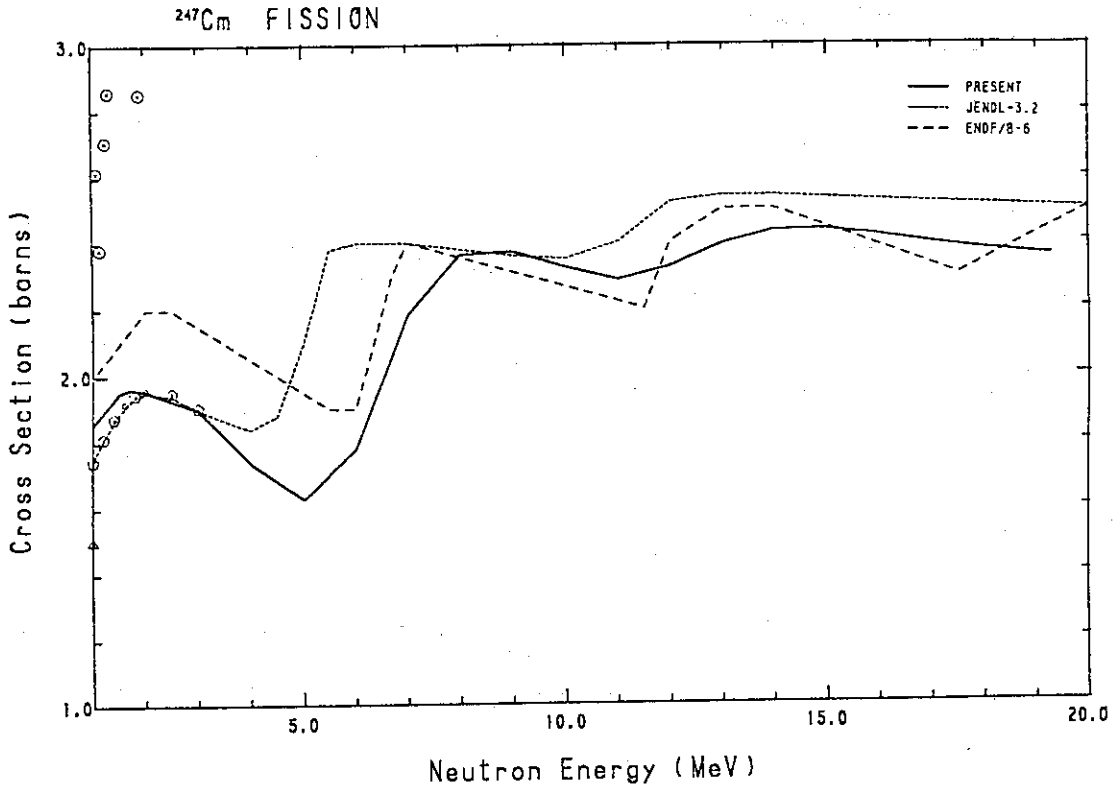

Fig. 266 Comparison of the fission cross-section for ^{247}Cm.

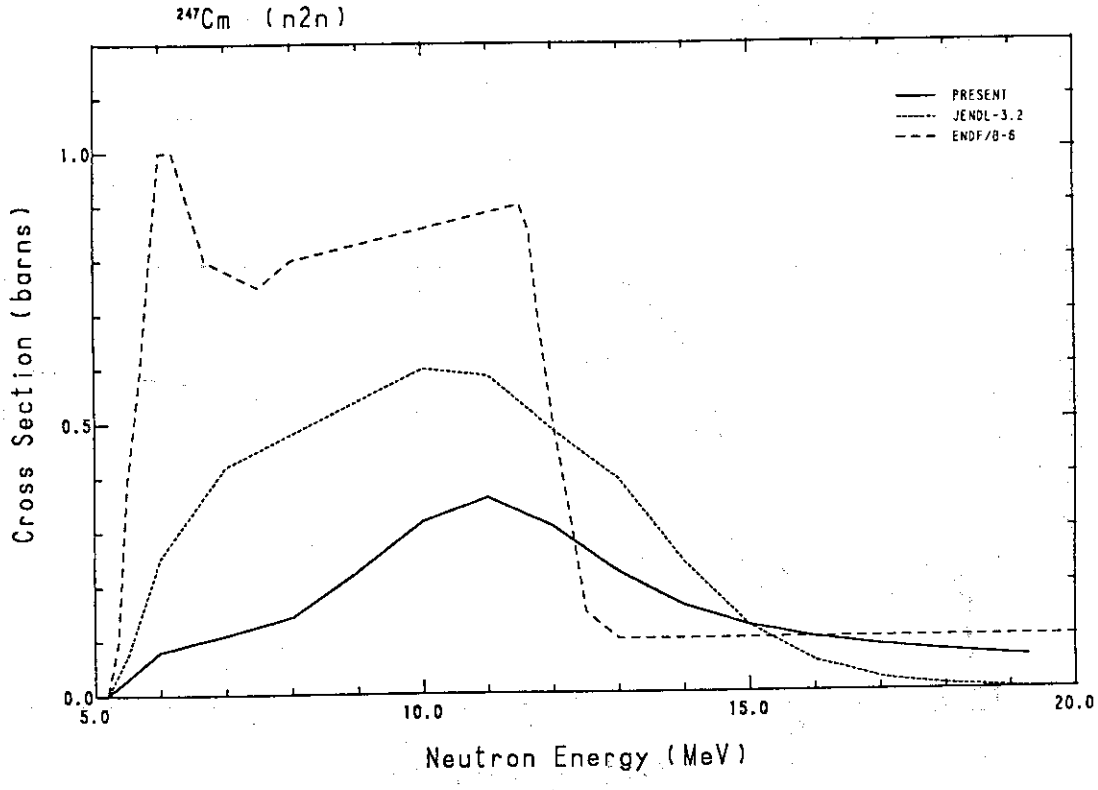

Fig. 267 Comparison of the (n,2n)-cross-section for ^{247}Cm.

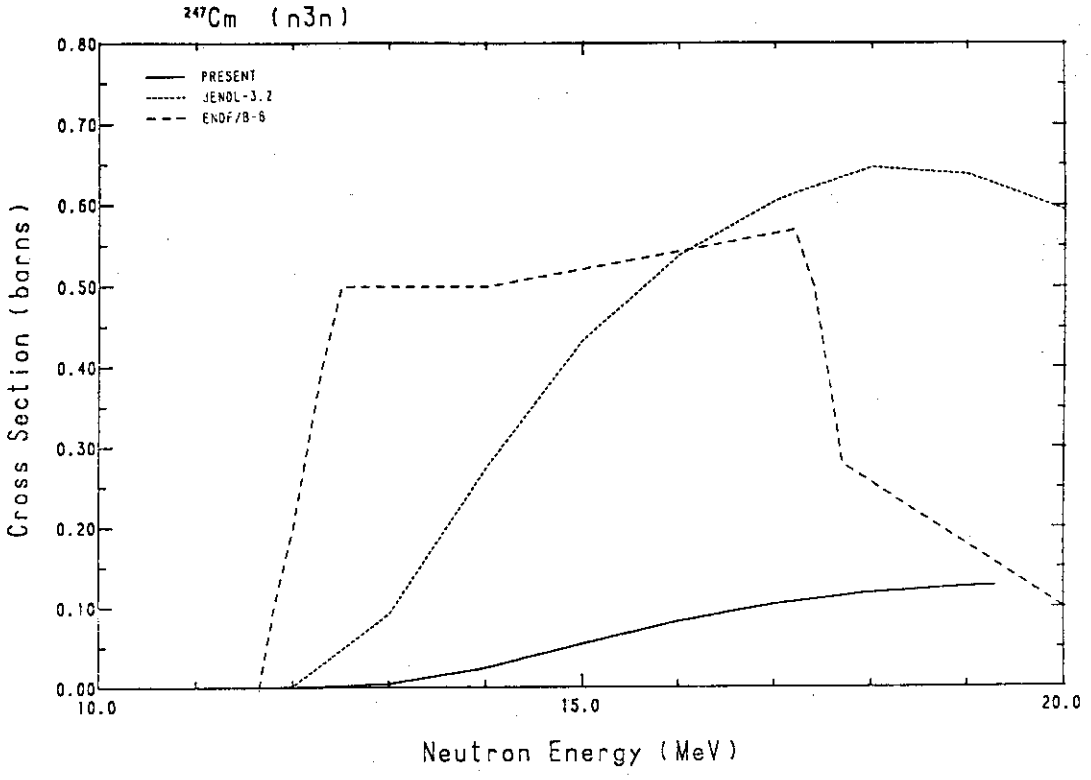

Fig. 268 Comparison of the (n,3n)-cross-section for ^{247}Cm.

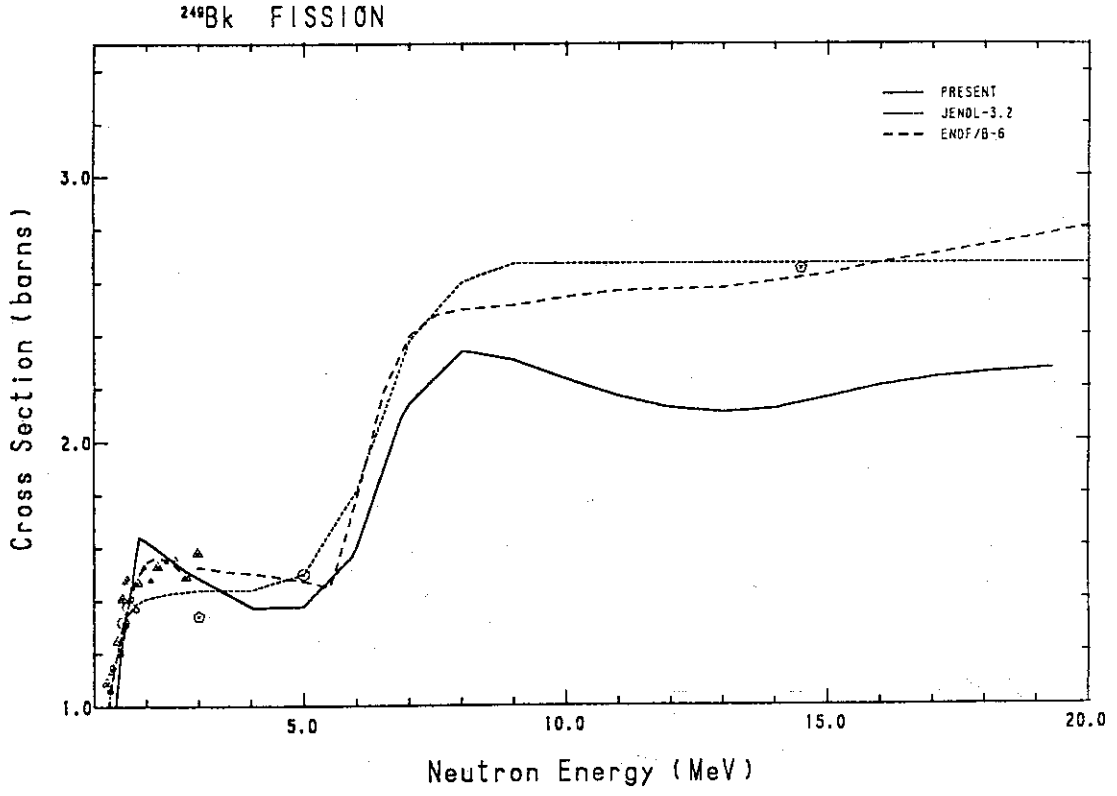

Fig. 269 Comparison of the fission cross-section for ^{249}Bk.

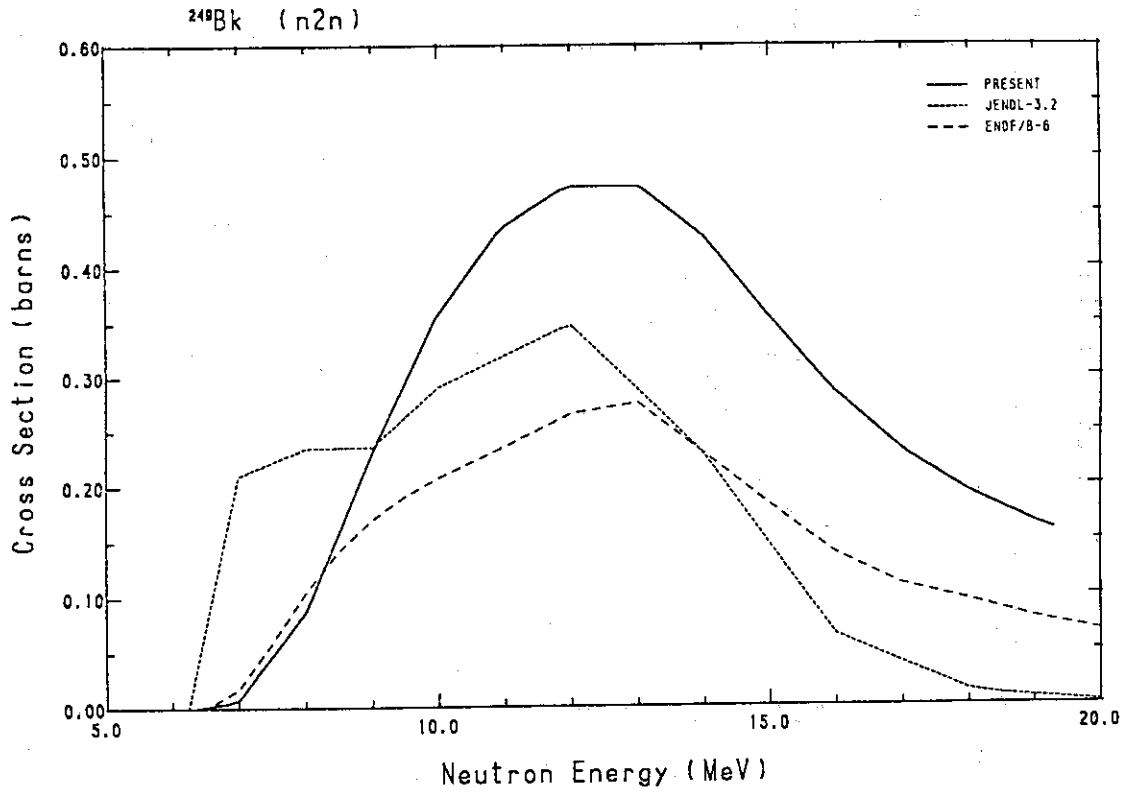

Fig. 270 Comparison of the (n,2n)-cross-section for ^{249}Bk.

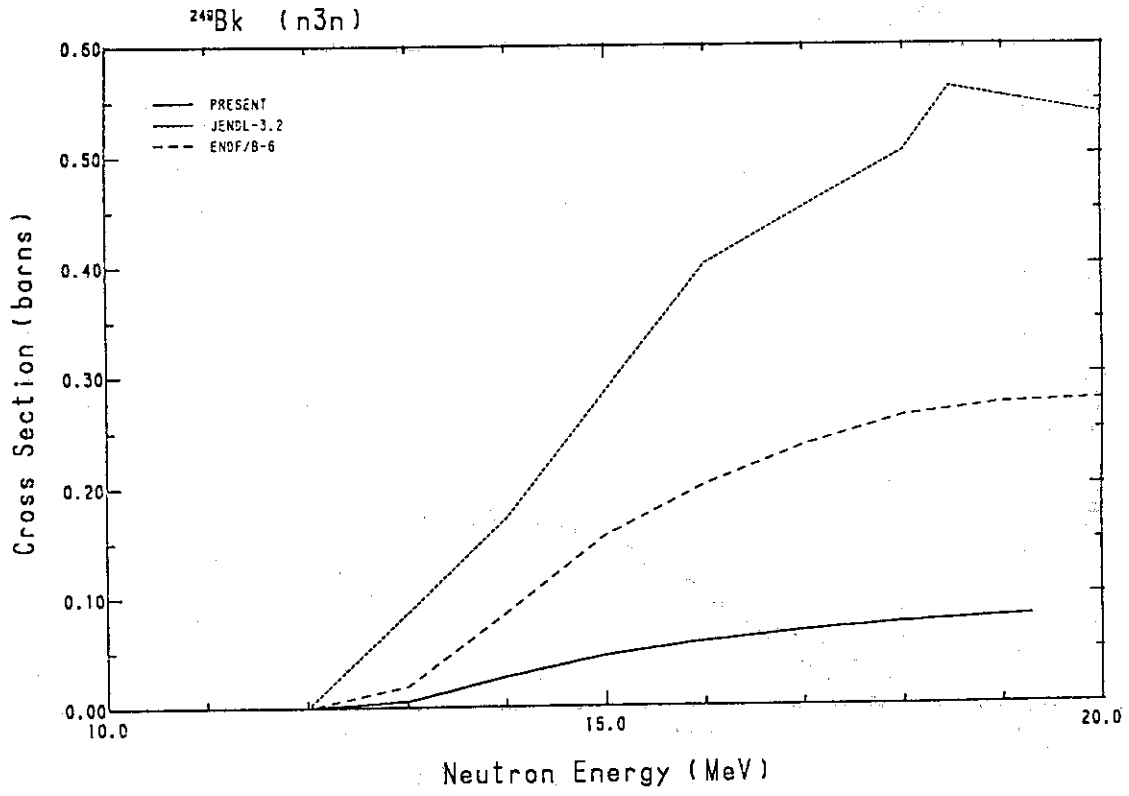

Fig. 271 Comparison of the (n,3n)-cross-section for ^{249}Bk.

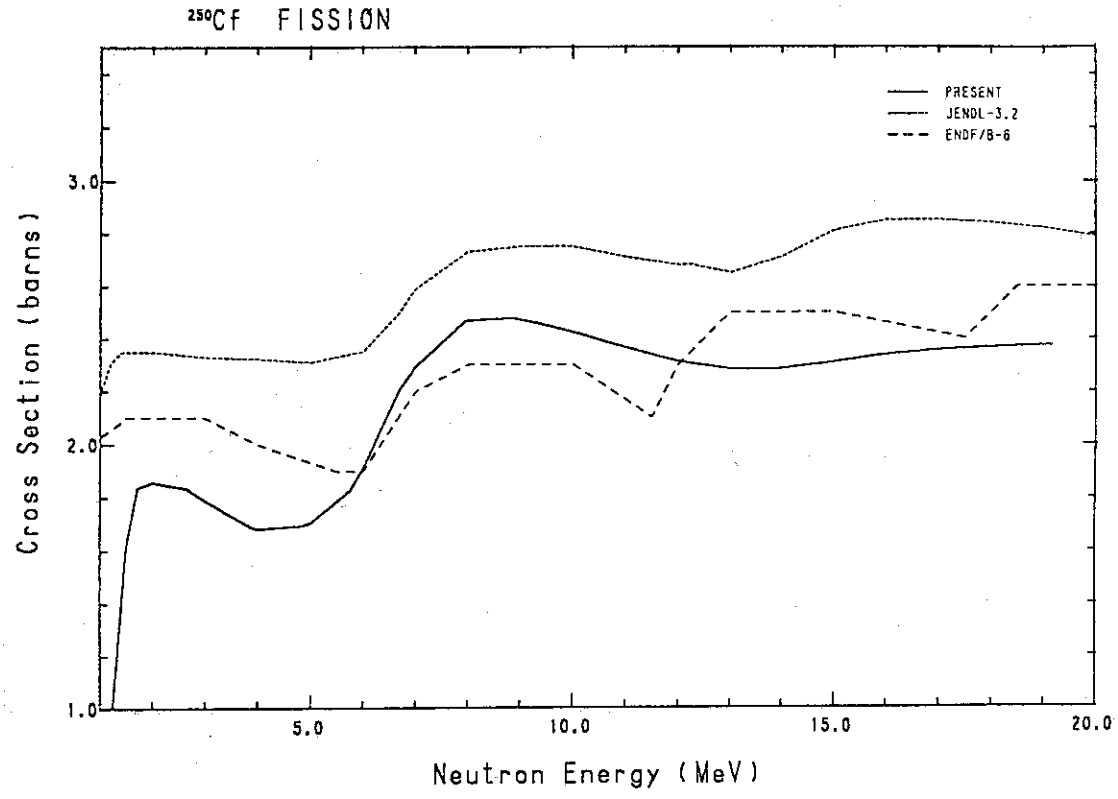

Fig. 272 Comparison of the fission cross-section for ^{250}Cf.

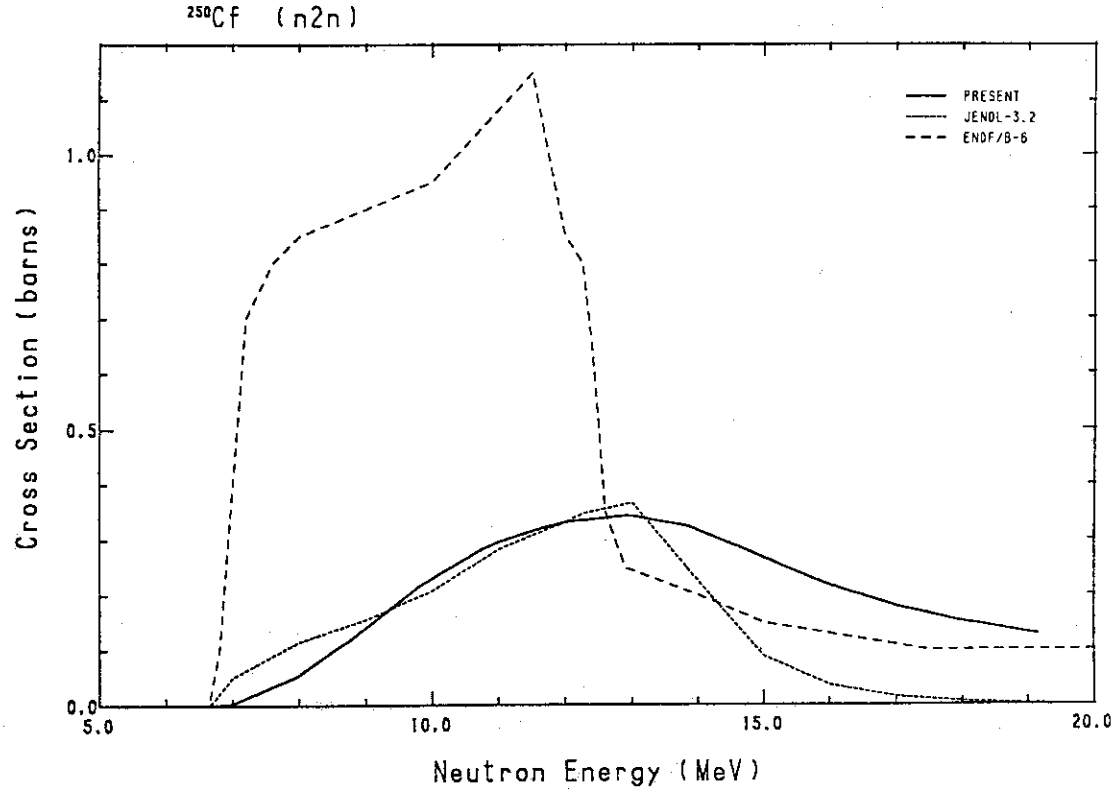

Fig. 273 Comparison of the (n,2n)-cross-section for ^{250}Cf.

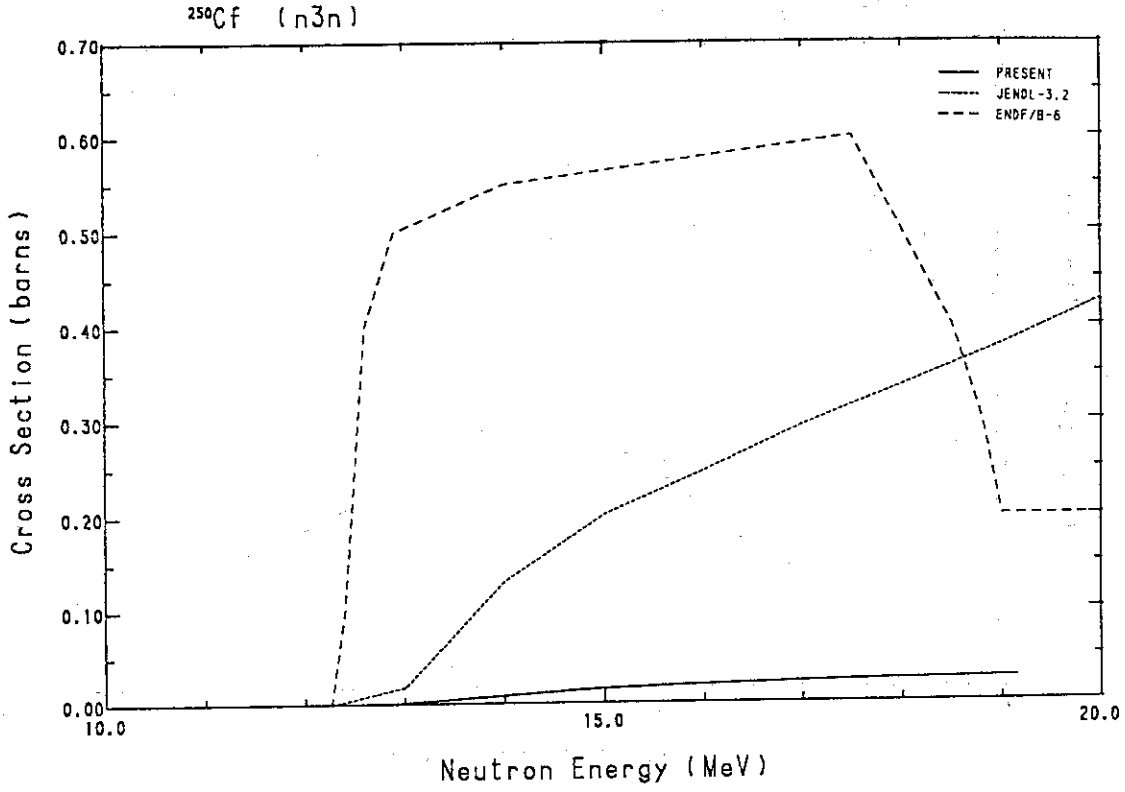

Fig. 274 Comparison of the (n,3n)-cross-section for ^{250}Cf.

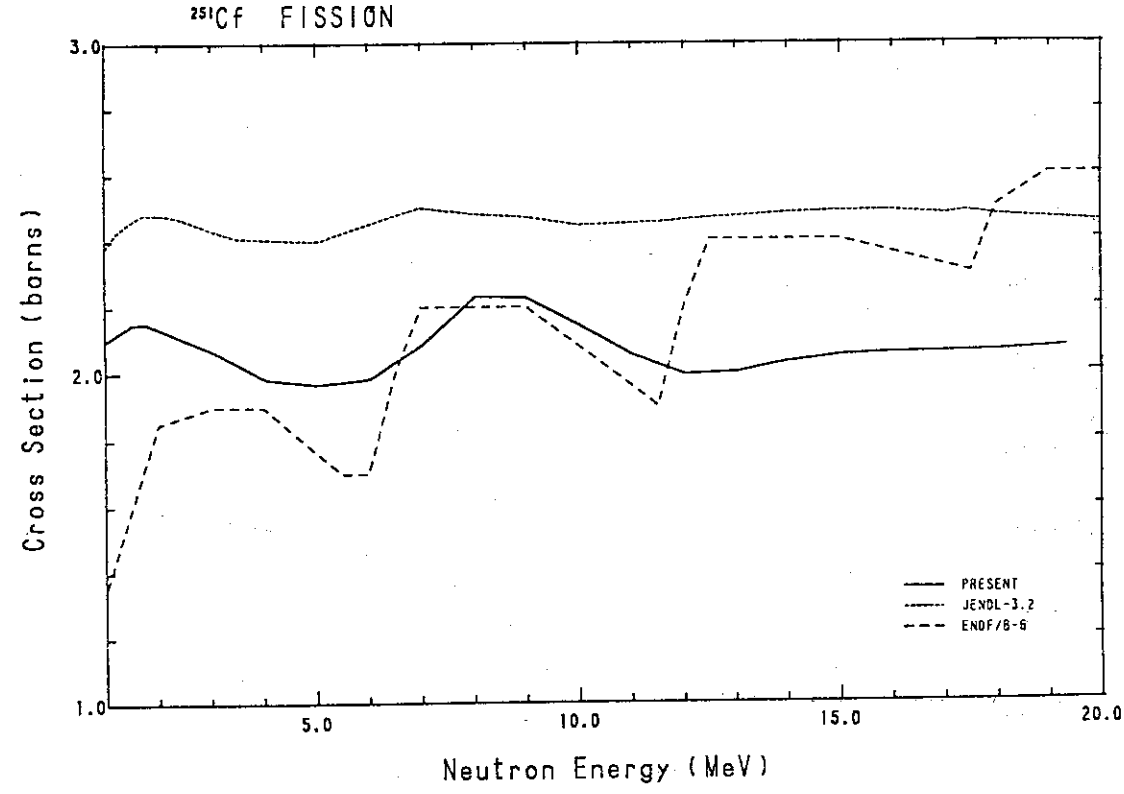

Fig. 275 Comparison of the fission cross-section for ^{251}Cf.

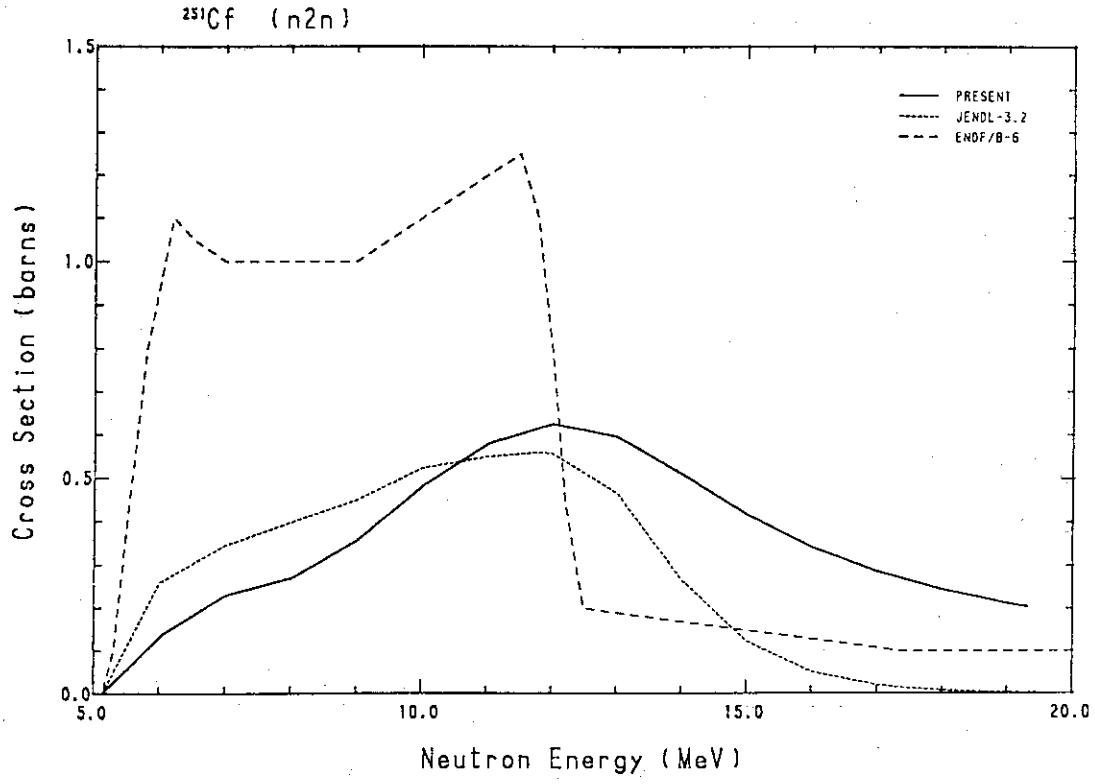

Fig. 276 Comparison of the (n,2n)-cross-section for ^{251}Cf.

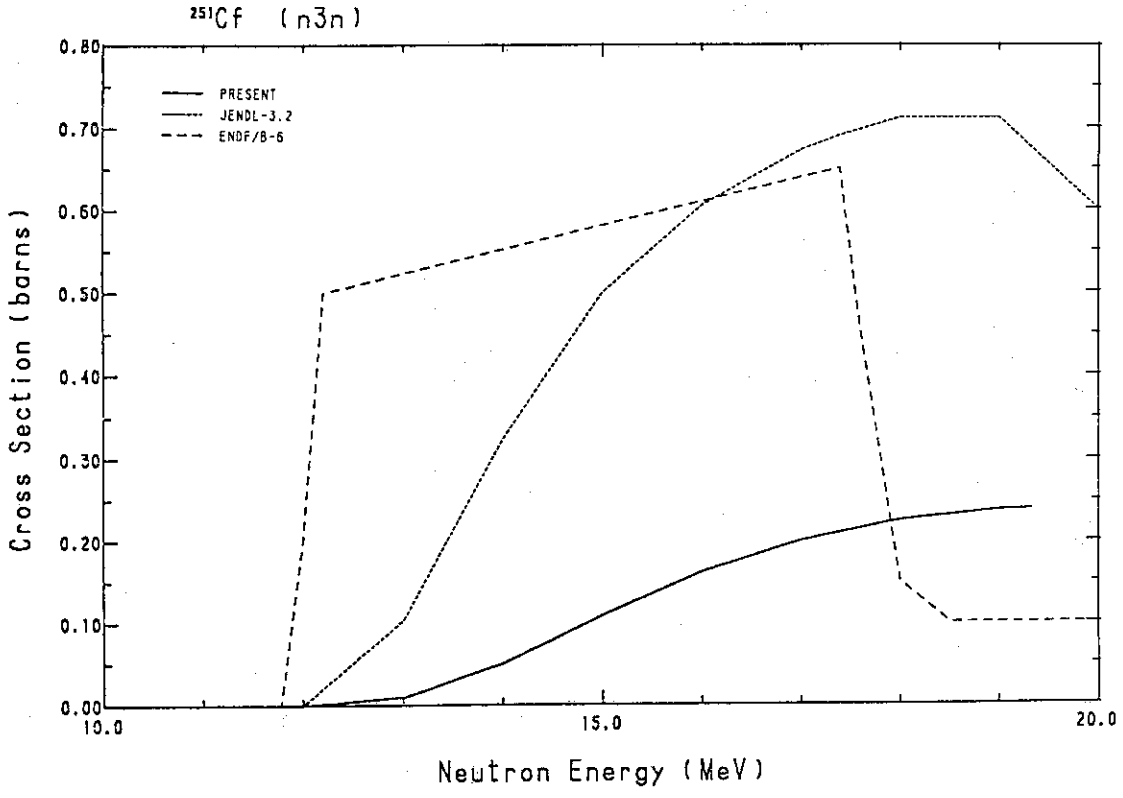

Fig. 277 Comparison of the (n,3n)-cross-section for ^{251}Cf.